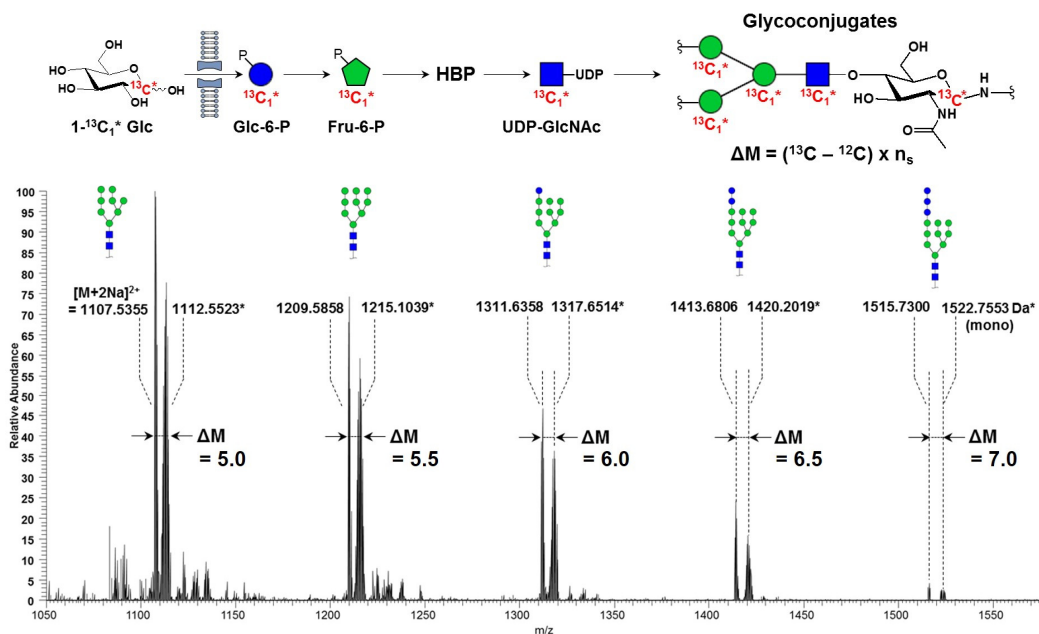




Mass Spectrometry Letters

Relative Quantification of Glycans by Metabolic Isotope Labeling with Isotope Glucose in *Aspergillus niger*



Mass Spectrometry Letters

Editor-in-Chief

Jeongkwon Kim

Chungnam National University, Republic of Korea

E-mail: jkkim48105@cnu.ac.kr

Associate Editors

Stephen J. Blanksby

University of Wollongong, Australia

E-mail: blanksby@uow.edu.au

Sang Won Cha

Dongguk University, Republic of Korea

E-mail: chasw@dongguk.edu

Yu-Ju Chen

Institute of Chemistry, Academia Sinica, Taiwan

E-mail: yjchen@chem.sinica.edu.twan

Ki Hwan Choi

Korea Research Institute of Standards and Science, Republic of Korea

E-mail: kihwan.choi@kriss.re.kr

Yong Seok Choi

Dankook University, Republic of Korea

E-mail: analysc@dankook.ac.kr

Ivan Keung Chu

The University of Hong Kong, Hong Kong, China

E-mail: ivankchu@hku.hk

Fumitaka Esaka

Japan Atomic Energy Agency, Japan

E-mail: esaka.fumitaka@jaea.go.jp

Sang Beom Han

Chungang University, Republic of Korea

E-mail: hansb@cau.ac.kr

Sang Yun Han

Gachon University, Republic of Korea

E-mail: sanghan@gachon.ac.kr

Han Bin Oh

Sogang University, Republic of Korea

E-mail: hanbinoh@sogang.ac.kr

Ki Hun Kim

Korea Institute of Science and Technology, Republic of Korea

E-mail: kihun.kim@kist.re.kr

(Manuscript Editor)

Hookeun Lee

Lee Gil Ya Cancer and Diabetes Institute, Republic of Korea

E-mail: hkleee@gachon.ac.kr

Hyesuk Lee

Catholic University, Republic of Korea

E-mail: sianalee@catholic.ac.kr

Jae Ik Lee

Korea Institute of Science and Technology, Republic of Korea

E-mail: jaeicklee@kist.re.kr

Sangkyu Lee

Kyungpook National University, Republic of Korea

E-mail: sangkyu@knu.ac.kr

David M. Lubman

University of Michigan, USA

E-mail: dmlubman@umich.edu

Jong-Ho Park

Chonbuk National University, Republic of Korea

E-mail: proton@jbnu.ac.kr

Yasushi Shigeri

Department of Chemistry Wakayama Medical University

E-mail: yshigeri@wakayama-med.ac.jp

So Young Shin

Wonkwang University, Republic of Korea

E-mail: shins@wku.ac.kr

Jongcheol Seo

Pohang University of Science and Technology, Republic of Korea

E-mail: jongcheol.seo@postech.ac.kr

Young Hae Choi

Leiden University, Nederland

E-mail: y.h.choi@biology.leidenuniv.nl

Joonhyuk Suh

University of Georgia, USA

E-mail: J.Suh@uga.edu

Newman Siu Kwan Sze

Nanyang Technological University, Singapore

E-mail: sksze@ntu.edu.sg

Troy D. Wood

The State University of New York at Buffalo, USA

E-mail: twood@buffalo.edu

Hye Hyun Yoo

Hanyang University, Republic of Korea

E-mail: yoooh@hanyang.ac.kr

Lihua Zhang

Dalian Institute of Chemical Physics, China

E-mail: lihuazhang@dicp.ac.cn

Advisory Board

Bong Cheol Jeong

Korea Institute of Science and Technology, Republic of Korea

E-mail: bcc0319@kist.re.kr

Hyun Sik Kim

Korea Basic Science Institute-Ochang, Republic of Korea

E-mail: fticr@kbsi.re.kr

Young Hwan Kim

Korea Basic Science Institute-Ochang, Republic of Korea

E-mail: yhkim@kbsi.re.kr

Yong-Il Lee

Changwon National University, Republic of Korea

E-mail: yilee@changwon.ac.kr

Myeong Hee Moon

Yonsei University, Republic of Korea

E-mail: mhmoon@yonsei.ac.kr

Seung Koo Shin

POSTECH, Republic of Korea

E-mail: skshin@postech.ac.kr

Hun-Young So

Korea Research Institute of Standards and Science, Republic of Korea

E-mail: hys@kriss.re.kr

Kuseok Song

Korea Atomic Energy Research Institute, Republic of Korea

E-mail: sks@kaeri.re.kr

Yong-Hyeon Yim

Korea Research Institute of Standards and Science, Republic of Korea

E-mail: yhyim@kriss.re.kr

Jong Shin Yoo

Korea Basic Science Institute-Ochang, Republic of Korea

E-mail: jongshin@kbsi.re.kr

Editorial Board

Suresh K. Aggarwal

Bhabha Atomic Research Centre, India

E-mail: skaggr2002@rediffmail.com

Yoon-Seok Chang

POSTECH, Republic of Korea

E-mail: yschang@postech.ac.kr

Yu Bai

College of Chemistry and Molecular Engineering Peking University, China

E-mail: yu.bai@pku.edu.cn

Jongki Hong

Kyung Hee University, Republic of Korea

E-mail: jhong@khu.ac.kr

Taegeol Lee

Korea Research Institute of Standards and Science, Republic of Korea

E-mail: tglee@kriss.re.kr

Hongli Li

U.S. Food & Drug Administration, USA

E-mail: hongli@fda.hhs.gov

Jinying Li

China Institute of Atomic Energy, China

E-mail: lijinying@vip.163.com

Heung-bin Lim

Dankook University, Republic of Korea

E-mail: plasma@dankook.ac.kr

Kwang-Hyeon Liu

Kyungpook National University, Republic of Korea

E-mail: dstlkh@knu.ac.kr

Seungun Myeong

Kyunggi University, Republic of Korea

E-mail: swmyung@kgu.ac.kr

Zeeyong Park

Gwangju Institute of Science and Technology, Republic of Korea

E-mail: zeeyong@gist.ac.kr

Jentaie Shiea

National Chung-Hsing University, Taiwan

E-mail: jetea@mail.nsysu.edu.tw

ISO Abbreviation: *Mass Spectrom. Lett.*

Websites: www.msletters.org; msletters.koar.kr

Editorial Office

Administration office of the Korean Society for Mass Spectrometry

78 Daejeon Dunsan P.O.Box, 111 Dunsan-ro, Seo-gu, Daejeon, 35239, Republic of Korea

Contact: Yae Jin Joo

Homepage: www.ksms.org

E-mail: ksms@ksms.org

Tel: 82-70-8688-1696

Fax: 82-43-240-5159

Editor-in-Chief: Jeongkwon Kim, Ph.D.

E-mail: jkim48105@cnu.ac.kr

Phone: 82-42-821-5477

Department of Chemistry

Chungnam National University

Republic of Korea

Manuscript Editor: Ki Hun Kim, Ph.D.

E-mail: kihun.kim@kist.re.kr

Phone: 82-2-958-5085

Korea Institute of Science and Technology, Republic of Korea

MASS SPECTROMETRY LETTERS is indexed in Academic Society Village (<http://society.kisti.re.kr>), NDSL (National Discovery for Science Leaders, <http://www.ndsl.kr>), KSCI (Korea Science Citation Index, <http://ksci.kisti.re.kr>), KCI (Korea Citation Index, <http://www.kci.go.kr>), Chemical Abstracts (<http://cas.org>), and Scopus (www.scopus.com).

The journal hardcopy is distributed free to all the KSMS members who pay the membership fee in the corresponding year or at the cost of 20 US dollars/year to non-members.

All Mass Spectrometry Letters content is published and distributed under the terms of the Creative Commons Attribution License (<http://creativecommons.org/licenses/by/3.0>).

Subscription information

Mass Spectrometry Letters follows 'OPEN ACCESS' policy. One who wants to have an access to the full text is recommended to visit the Mass Spectrometry Letters official website (<http://www.msletters.org/>).

The printed material is sent to all the members of the KSMS for free and anyone who wants to receive the printed journal in Korea is strongly recommended to enroll in the KSMS. The membership fee information can be found in the KSMS homepage (www.ksms.org). One who wants to receive the printed journal abroad should contact Yae Jin Joo for more information.

Printed on December 25, 2022

Published on December 31, 2022

Publisher: Young Hwan Kim, President of KSMS

Publication Office: The Korean Society for Mass Spectrometry

Published since December 2010

Frequency of publication: 4 issues/year

The number of circulation of the printed journal: 400 copies/issue

Printed by Hanrimwon, Seoul, Korea, Tel: 82-2-2273-4201

ISSN 2233-4203 (print)

e-ISSN 2093-8950

©Korean Society for Mass Spectrometry

Aims and Scope

Mass Spectrometry Letters publishes brief letters (maximum length of 4 pages), technical notes, articles, reviews, and tutorials on fundamental research and applications in all areas of mass spectrometry. The manuscripts can be either invited by the editors or submitted directly by authors to the journal editors. Mass Spectrometry Letters topical sections are diverse, covering ion chemistry in a broad sense; gas-phase thermodynamics or kinetics; theory and calculations related with mass spectrometry or ions in vacuum; ion-optics; analytical aspects of mass spectrometry; instrumentations; methodology developments; ionization methods; proteomics and its related research; metabolomics and its related research; bioinformatics; software developments; database development; biological research using mass spectrometry; pharmaceutical research by mass spectrometry; food sciences using mass spectrometry; forensic results using mass spectrometry; environmental mass spectrometry; inorganic mass spectrometry; chromatography-mass spectrometry; tandem mass spectrometry; small molecule research using mass spectrometry; TOF-SIMS, etc. The scope of Mass Spectrometry Letters is not limited to the above-mentioned areas, but includes ever-expanding areas related directly or indirectly to mass spectrometry. Criteria for publication are originality, urgency, and reportable values. Short preliminary or proof-of-concept results, which will be further detailed by the following submission to other journals, are recommended for submission.

CONTENTS

Volume 13, Number 4
December 2022

REVIEW

- Mass Spectrometry-Based Analytical Methods of Amatoxins in Biological Fluids to Monitor Amatoxin-Induced Mushroom Poisoning**
*Jin-Sung Choi and Hye Suk Lee** 95
- High-Throughput Screening Technique for Microbiome using MALDI-TOF Mass Spectrometry: A Review**
*Abhik Mojumdar, Hee-Jin Yoo, Duck-Hyun Kim, and Kun Cho** 106
- Combining the Power of Advanced Proteome-wide Sample Preparation Methods and Mass Spectrometry for defining the RNA-Protein Interactions**
Tong Liu, Chaoshuang Xia, Xianyu Li, and Hongjun Yang** 115

ARTICLE

- Headspace GC-MS Analysis of Spring Blossom Fragrance at Chungnam National University Daedeok Campus**
*Yeonwoo Choi[†], Sanghyun Lee[†], Young-Mi Kim, Huu-Quang Nguyen, Jeongkwon Kim, and Jaebeom Lee** 125
- The Advanced Analytical Method Through the Quantitative Comparative Study of Taurine in Feed Using LC-MS/MS**
Yeong Jun Seon[†], Hyung Ju Seo[†], Jiye Yoon, Hyunjeong Cho, Sunghie Hong, Seung Hwa Lee, and Tae Woong Na** 133
- Relative Quantification of Glycans by Metabolic Isotope Labeling with Isotope Glucose in *Aspergillus niger***
*Soo-Hyun Choi[†], Ye-Eun Cho[†], Do-Hyun Kim, Jin-il Kim, Jihee Yun, Jae-Yoon Jo, and Jae-Min Lim** 139
- A Sensitive, Efficient, and Cost-Effective Method to Determine Rotigotine in Rat Plasma Using Liquid-Liquid Extraction (LLE) and LC-MRM**
Ji Seong Kim[†], Yong Jin Jang[†], Jin Hee Kim, Jin Hwan Kim, Jae Hee Seo, Il-Ho Park, Myung Joo Kang, and Yong Seok Choi** 146
- Inhibitory Effects of Dietary Schisandra Supplements on CYP3A Activity in Human Liver Microsomes**
*Bae-Gon Kang, Eun-Ji Park, So-Young Park, and Kwang-Hyeon Liu** 152
- Simultaneous Liquid Chromatography Tandem Mass Spectrometric Determination of 35 Prohibited Substances in Equine Plasma for Doping Control**
Young Beom Kwak, Jundong Yu, and Hye Hyun Yoo** 158
- Comparative Analysis of the Phyto-compounds Present in the Control and Experimental Peels of *Musa paradisiaca* used for the Remediation of Chromium Contaminated Water**
Vidhya Kaniyappan, Regina Mary Rathinasamy, and Job Gopinath Manivanan* 166

CONTENTS

Volume 13, Number 4
December 2022

**Analysis of Amyloid Beta 1-16 (A β 16) Monomer and Dimer Using Electrospray Ionization
Mass Spectrometry with Collision-Induced Dissociation**

*Kyoung Min Kim and Ho-Tae Kim** 177

TUTORIAL

Comparative Sample Preparation Methods for a Label-Free Proteomic Analysis

*Thy N. C. Nguyen[†], Jung Hyun Lee, Nayeon Kim, Jae Rim Choi, Hung M. Vu, and Min-Sik Kim** 184

Mass Spectrometry-Based Analytical Methods of Amatoxins in Biological Fluids to Monitor Amatoxin-Induced Mushroom Poisoning

Jin-Sung Choi and Hye Suk Lee*

College of Pharmacy, The Catholic University of Korea, Bucheon 14662, Republic of Korea

Received November 15, 2022, Revised November 24, 2022, Accepted November 25, 2022

First published on the web December 31, 2022; DOI: 10.5478/MSL.2022.13.4.95

Abstract : Amatoxin-induced mushroom poisoning starts with nonspecific symptoms of toxicity but hepatic damage may follow, resulting in the rapid development of liver insufficiency and, ultimately, coma and death. Accurate detection of amatoxins, such as α -, β -, and γ -amanitin, within the first few hours after presentation is necessary to improve the therapeutic outcomes of patients. Therefore, analytical methods for the identification and quantification of α -, β -, and γ -amanitin in biological samples are necessary for clinical and forensic toxicology. This study presents a literature review of the analytical techniques available for amatoxin detection in biological matrices, and established an inventory of liquid chromatography (LC) techniques with mass spectrometry (MS), ultraviolet (UV) detection, and electrochemical detection (ECD). LC-MS methods using quadrupole tandem mass spectrometry, time-of-flight mass spectrometry, and orbitrap MS are powerful analytical techniques for the identification and determination of amatoxins in plasma, urine, serum, and tissue samples, with high sensitivity, specificity, and reproducibility compared to LC with UV and ECD, enzyme-linked immunoassay, and capillary electrophoresis methods.

Keywords : amatoxin-induced mushroom poisoning, α -amanitin, β -amanitin, γ -amanitin, LC-MS/MS, biological samples

Introduction

Mushrooms are consumed worldwide as an ingredient of many meals, but severe syndromes and even death can be caused by the misidentification of wild poisonous mushrooms as edible.¹⁻⁶ Mushrooms such as *Psilocybe* species and *Amantia muscaria* are intentionally abused because of their psychoactive activities.⁷ There is some evidence that mushroom poisoning may be increasing, and that exotic species are entering new areas and countries, thereby expanding the range of mushroom poisoning symptoms observed in presenting patients.⁸ White et al.⁹ classified mushroom toxins based on the clinical types of mushroom poisoning, as follows: primary hepatotoxicity (amatoxins), primary nephrotoxicity (AHDA, orellanine), neurotoxicity (psilocybins, muscarines, ibotenic acid, muscimol), mytotoxicity (saponaceolide B), metabolic/endocrine toxicity

(gyromitrins, coprines, trichothecenes, polyporic acid), gastrointestinal irritants, and miscellaneous (entinan, acromelic acid).

Although global data are not available, the absolute number and incidence of mushroom poisoning cases may be increasing based on local studies.⁹⁻¹² An emerging mushroom poisoning risk in Europe may be the result of the large migrant influx, a subset of whom forage for food because of poor economic circumstances. This results in the consumption of mushrooms not known to the migrants and an increased incidence of amatoxin-type mushroom poisoning.^{3,10} Because most toxic syndromes caused by mushroom toxins start with unspecific symptoms, diagnostic difficulties are most common during the critical first hours after presentation.³ Therefore, suspected poisonings should be confirmed or excluded to ensure that therapy starts as soon as possible, and to prevent an inappropriate therapy being implemented. The analytical strategies used to identify poisonous mushroom toxins include spore analysis (if mushroom leftovers or gastric content are available) and the identification of various toxins and their metabolites in human biological samples.^{3,14,15} It is therefore necessary to develop sensitive, selective, and rapid analytical methods for the identification and quantification of mushroom toxins and their metabolites in the human biological matrix.

The purpose of this study was to review the bioanalytical methods used for the diagnosis of amatoxin-induced mushroom poisoning, which is the main cause of fatal mushroom poisoning.^{3,10,13}

Open Access

*Reprint requests to Hye Suk Lee

<https://orcid.org/0000-0003-1055-9628>

E-mail: sianalee@catholic.ac.kr

All the content in Mass Spectrometry Letters (MSL) is Open Access, meaning it is accessible online to everyone, without fee and authors' permission. All MSL content is published and distributed under the terms of the Creative Commons Attribution License (<http://creativecommons.org/licenses/by/3.0/>). Under this license, authors reserve the copyright for their content; however, they permit anyone to unrestrictedly use, distribute, and reproduce the content in any medium as far as the original authors and source are cited. For any reuse, redistribution, or reproduction of a work, users must clarify the license terms under which the work was produced.

Amatoxins

Amatoxins are highly toxic bicyclic octapeptides (Figure 1). They are the most toxic compounds among mushroom toxins, and are found in the *Amanita*, *Galerina*, and *Lepiota* mushroom species.^{4,6} Among these species, *Amanita phalloides* has the most toxin components/weight and is responsible for most cases of fatal poisoning.¹⁵⁻¹⁸ These toxins are classified as neutral substances (α -amanitin, γ -amanitin, amaninamide, amanullin, and proamanullin) or acidic substances (β -amanitin, ε -amanitin, amanine, and amanullic acid), which differ in terms of the number of hydroxyl groups and amide carboxyl exchange (Figure 1).^{19,20} Amatoxins are water-soluble, heat-stable, and resistant to enzyme and acid degradation. Therefore, these substances remain unchanged during freezing, drying, and cooking (including frying, grilling, boiling, steaming, and other processing operations, such as digestive processing), and are resistant to gastrointestinal inactivation and metabolic processes.^{18,21-23} However, amatoxins can be degraded slowly when stored in an open and aqueous solution, or exposed to sun or neon light for periods of about 7–8 months, which could potentiate the toxicity of amatoxins upon exposure in vivo.^{17,20} The content of amatoxins varies among *Amanita* species, but α - and β -amanitin are the most abundant substances. For example, an amatoxin content of 9.3 mg/g was observed in dried mushrooms, while α - and β -amanitin accounted for 56% of the toxins found in dried powder from *A. phalloides*.²⁴ It has been reported that α - and β -amanitin account for 82% of toxins (2.87 mg of amanitin/3.49 mg peptide toxins/g dried powder) in *A. exitialis*.^{25,26} According to Yilmaz et al.,²⁷ an oral intake of approximately 50 g of fresh *A. phalloides*, equivalent to a dose of 0.32 mg/kg of amatoxins, can be lethal.

The LD₅₀ value of α -amanitin was reported to be 0.3–

0.6 mg/kg in mice and 4.0 mg/kg in rats (intraperitoneal injection), 0.1 mg/kg in humans (oral administration), and 0.1 mg/kg in dogs (intravenous injection).^{17,28,29} The LD₅₀ values of β -amanitin, γ -amanitin, ε -amanitin, amanitin, and amaninamide were reported to be 0.5, 0.2–0.5, 0.3–0.6, 0.5, and 0.5 mg/kg, respectively, in mice following intraperitoneal injection.¹⁷ The LD₅₀ values for orally administered amanullin, amanullinic acid, and proamanullin in mice were > 20 mg/kg, but these levels are not toxic to humans.^{17,28}

Amanita phalloides poisoning can cause acute hepatitis, leading to the rapid development of liver insufficiency and, ultimately, coma and death.^{5,15,17} However, nephrotoxicity has been less frequently reported.³⁰ The main toxicity mechanism of amatoxins is the inhibition of RNA polymerase II, which leads to the inhibition of messenger RNA synthesis and protein synthesis.³¹⁻³³ Other toxic mechanisms have been suggested, including oxidative stress-related damage via the increased formation of reactive oxygen species induced by an increase in superoxide dismutase activity and inhibition of catalase activity,^{18,34,35} and amatoxin-induced apoptosis caused by the translocation of p53 to the mitochondria, leading to alteration of mitochondrial membrane permeability through the formation of a complex with Bcl-xL and Bcl-2.^{17,18,36-39} The cytotoxicity of α -amanitin is 10-fold greater than that of β -amanitin in MCF-7 cells.⁴⁰ The main toxicological studies of amatoxins have focused on α - and β -amanitin; therefore, no conclusions have been drawn regarding potential toxicity differences between neutral and acid amatoxins.^{15,17}

Toxicokinetic studies of α - and β -amanitin after the intravenous, intraperitoneal, and oral administration of amatoxin in rats and mice have been reported.^{14,18,20,21,41,42} Low absolute bioavailability of α -amanitin (3.5–4.8%) and β -amanitin (7.3–9.4%), and substantial transport thereof to

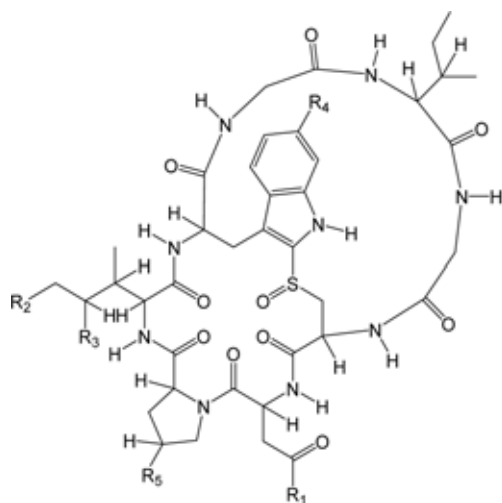


Figure 1. Chemical structures of amatoxins.

Compound	R ₁	R ₂	R ₃	R ₄	R ₅
α -amanitin	NH ₂	OH	OH	OH	OH
β -amanitin	OH	OH	OH	OH	OH
γ -amanitin	NH ₂	H	OH	OH	OH
ε -amanitin	OH	H	OH	OH	OH
amanullin	NH ₂	H	H	OH	OH
amaninamide	NH ₂	OH	OH	H	OH
proamanullin	NH ₂	H	H	OH	H
amanin	OH	OH	OH	H	OH
amanullic acid	OH	H	H	OH	OH

the intestines, kidneys, and liver, were observed after they were orally administered to mice at doses of 2, 5, or 10 mg/kg.^{41,42} α - and β -amanitin show similarities in terms of the elimination process; they are both eliminated in urine without significant metabolism.^{21,41,42} α - and β -amanitin show OATP1B1- and OATP1B3-mediated hepatic uptake, but only β -amanitin shows OAT3-mediated kidney uptake.⁴² α - and β -amanitin were detected in serum, plasma, urine, liver, and fecal samples of amatoxin poisoning patients.^{15,43–46} Among 43 amatoxin-intoxicated patients, 11 showed plasma concentrations of 8–190 ng/mL for α -amanitin and 23.5–162 ng/mL for β -amanitin.⁴⁶ In total, 35 urine, 12 feces, and 4 liver and kidney samples were obtained from 43 amatoxin-intoxicated patients, with ranges of 0.03–3.29 mg for α -amanitin and 0.05–5.21 mg for β -amanitin in 24 of the urine samples; 8.4–152 μ g for α -amanitin and 4.2–6270 μ g for β -amanitin in 10 fecal samples; and 10–19 ng/g and 122–1719 ng/g for α -amanitin, and 170.8–3298 ng/g and 1017–1391 ng/g for β -amanitin, in liver and kidney samples, respectively, for three of patients.⁴⁶ Although cellular uptake (mediated by hepatic or renal transporters) is approximately two-fold higher for β -amanitin than α -amanitin, as is liver and kidney accumulation, the contribution of β -amanitin to in vivo amatoxin toxicity may be lower than that of α -amanitin because of differences in their cytotoxicity.⁴⁰

Benzylpenicillin, silibinin, and *N*-acetylcysteine have been used for the treatment of amatoxin-induced mushroom poisoning.^{3,17} The therapeutic effects may be attributed to the hepatoprotective and anti-oxidative activities of silibinin and *N*-acetylcysteine, and the reduced hepatic distribution of α - and β -amanitin resulting from the inhibition of OATP1B3 by benzylpenicillin, silibinin, and cyclosporine.^{17,40,47–49}

Analytical methods of amatoxins in biological fluids

Confirmation of the intake of mushrooms containing amatoxins is needed by detecting amatoxins such as α -, β -, and γ -amanitin in biological fluids to avoid expensive and time-consuming treatment for every suspected intoxication case.¹⁵ Sufficient analytical sensitivity is also necessary because hospitalization often occurs late after intake such that only trace amounts of toxins can be found.^{15,44,46} Several methods have been reported for the qualification and quantification of amatoxins in biological fluids using liquid chromatography (LC) combined with mass spectrometry (MS),^{41–45,50–70} ultraviolet (UV) detection,^{71,72,75,77,78} or electrochemical detection (ECD),^{71,73,74,76} as well as capillary zone electrophoresis (CZE),^{79,80} radioimmunoassay (RIA),^{81,82} enzyme-linked immunosorbent assay (ELISA),^{83,84} and lateral flow immunoassay (LFA).⁸⁵ However, each method has drawbacks. The ELISA and LFA methods have been used for the screening of α -, β -, or γ -amanitin in clinical toxicology, but compared to LC-MS methods they have the

disadvantages of low sensitivity (3–10 ng/mL), high workload, false-negative and -positive results, and the requirement for additional confirmation in forensic cases.

The LC-MS methods have the advantages of high specificity, sensitivity, resolution, and rapidity relative to other analytical methods, making them suitable for routine clinical and forensic toxicological analysis of amatoxins. The LC-MS methods that have been developed for the analysis of α -, β -, and γ -amanitin in various biological fluids are summarized in Table 1. High-performance liquid chromatography (HPLC) with UV detection and ECD methods for the quantification of α - and β -amanitin in plasma, urine, liver, and kidney are summarized in Table 2; these methods have drawbacks such as low sensitivity and laborious sample preparation.

Sample preparation

Blood, plasma, serum, urine, bile, and tissue samples have been used for clinical purposes, forensic toxicology, and toxicokinetics of amatoxins.^{41–45,51–80} Because the amatoxin concentrations in urine are usually higher than those in serum and plasma,^{26,45,46} urine is considered as the biological sample of choice. However, major drawbacks of urine sampling include reduced output in the case of decreased renal function and acute renal failure, which can occur in some amatoxin and other mushroom poisoning cases, and the greater intra- and interindividual variability in the urine as a biomatrix. If therapeutic measures like fluid replacement or forced diuresis are applied, the low amounts of amatoxins in urine could be further diluted. Therefore, blood, plasma, and serum samples are more commonly used in clinics than urine samples for the determination of amatoxins.

For the determination of α -, β -, and γ -amanitin in human and animal plasma, serum, urine, and tissue samples using HPLC, LC-MS, liquid chromatography-tandem mass spectrometry (LC-MS/MS), matrix-assisted laser desorption ionization-time of flight mass spectrometry (MALDI-TOF MS), and CZE, several sample preparation techniques have been developed, including protein precipitation with acetonitrile, methanol, or perchloric acid,^{41,42,51,52,59,64,71} liquid-liquid extraction (LLE),⁷⁸ solid-phase extraction (SPE) with reverse-phase, cation exchange or immunoaffinity cartridges,^{43,50,54,56,58,60–62,66–68,70,71,73,74,76} SPE of the aqueous phase obtained after LLE with dichloromethane or chloroform,⁵⁵ SPE of the aqueous phase obtained after protein precipitation of the biomatrix with acetonitrile and LLE of the supernatant with chloroform,^{44,45,65,69,72,77} and online column switching technique,^{63,75} and simple dilution in CZE^{79,80} (Tables 1 and 2). These methods use different volumes of biological matrix samples, as follows: serum, 100–5000 μ L,^{54,60,67,69,72,76–78} plasma, 5–3000 μ L,^{41,42,44,50–53,57–60,67,68,74,75} and urine, 50–10000 μ L.^{41,42,43,45,50,54–58,60–67,70,73,76–80} (Tables 1 and 2). Two or three sample preparation procedures have

Table 1. The LC-MS and LC-MS/MS methods used for the determination of amatoxins in various biological matrices.

Toxin	Matrix	Sample preparation	Column	Mobile phase	Ionization (mode)	Linearity (LOD)	Transitions	Ref
β -Amanitin	Mouse plasma (5 μ L), urine (50 μ L), tissues	Protein precipitation with methanol	Atlantis dC18	Gradient elution of 0.1% formic acid and methanol	Negative ESI (PRM)	Plasma: 0.5–200 ng/mL Urine: 2–500 ng/mL; Liver: 50–50000 ng/g; Kidney: 25–5000 ng/g	β -amanitin: m/z 918.33185>900.32123, 4'-hydroxydiclofenac (IS): m/z 310.00443>266.01450	42
α -Amanitin	Human urine	SPE (immunoaffinity column)	Kinetex	Gradient elution of methanol and 0.005% formic acid	Negative ESI (MRM)	1–200 ng/mL (Plasma: 0.004 ng/mL; Urine: 0.002 ng/mL)	α -amanitin: m/z 917.4>899.3, β -amanitin: m/z 918.4>900.3, γ -amanitin: m/z 901.4>883.3	50
α -Amanitin	Rat plasma (50 μ L)	Protein precipitation with methanol and dilution	Acquity BEH C18	Gradient elution of water and acetonitrile	Negative ESI (MRM)	0.9–600 ng/mL	α -amanitin: m/z 917.4>205.0, roxithromycin (IS): m/z 835.8>484.7	51
α -Amanitin	Mouse plasma (5 μ L), urine (50 μ L), tissues	Protein precipitation with methanol	Atlantis dC18	Gradient elution of 0.1% formic acid and methanol	Negative ESI (PRM)	0.5–500 ng/mL plasma & urine	α -amanitin: m/z 917.34747>899.33710, verproside (IS): m/z 497.12936>153.01897	41
α -Amanitin	Mouse plasma (5 μ L)	Protein precipitation with methanol	Atlantis dC18	Gradient elution of 0.1% formic acid and methanol	Negative ESI (PRM)	0.5–500 ng/mL	α -amanitin: m/z 917.34747>899.33710, β -amanitin: m/z 918.33185>900.32123, 4'-hydroxydiclofenac (IS): m/z 310.00443>266.01450	52
α -Amanitin	Human plasma (100 μ L)	Protein precipitation with acetonitrile, LLE, online SPE (ODS cartridge)	XBridge BEH C18	Gradient elution of methanol and water	Negative ESI (MRM)	0.05–20 ng/mL (0.02 ng/mL)	α -amanitin: m/z 917.4>205.1, β -amanitin: m/z 918.4>205.1	45
α -Amanitin	Human serum (500 μ L) & urine (1000 μ L), pig liver (5 g)	SPE (β -cyclodextrin column) & laborated molecularly imprinted polymers	Acquity BEH C18	Gradient elution of 0.2% formic acid and methanol	Positive ESI (SRM)	Serum: 1.0–30 ng/mL (0.33–0.42 ng/mL) Urine: 0.5–30 ng/mL (0.16–0.33 ng/mL) Liver: 0.1–30 ng/g (0.035–0.056 ng/g)	α -amanitin: m/z 460.33>259.19, β -amanitin: m/z 461.22>259.19, γ -amanitin: m/z 452.29>243.11, phalloidin: m/z 847.54>157.1, phalloicidin: m/z 789.29>330.2	54
α -Amanitin	Human plasma (2500 μ L)	Protein precipitation with acetonitrile, LLE, and SPE (polymeric SCX cartridge)	Accucore C18	Gradient elution of 8 mM ammonium acetate containing 0.05% acetic acid and acetonitrile-methanol	Positive ESI (Orbitrap)	20–2000 pg/mL	α -amanitin: m/z 919.3614 β -amanitin: m/z 920.3614 identification: m/z 259.1275	44
α -Amanitin	Human urine	Protein precipitation with formic acid in acetonitrile-methanol (5:1, v/v), LLE, online SPE (ODS cartridge)	XBridge BEH C18	Gradient elution of methanol and water	Negative ESI (MRM)	0.1–50 μ g/L (LOD, 0.03 μ g/L)	α -amanitin: m/z 917.4>205.1	53

Table 1. Continued.

Toxin	Matrix	Sample preparation	Column	Mobile phase	Ionization (mode)	Linearity (LOD)	Transitions	Ref
α -Amanitin, β -Amanitin, Ricinine, Psilocin, Bufotenine, Muscarine, Muscimol, Ibotenic acid	Human urine (1500 μ L)	Liquid-liquid extraction and SPE (Polymeric SCX cartridge)	Nucleodur HILIC	Gradient elution of methanol, acetonitrile, water, and 120 mM ammonium formate	Positive ESI (Orbitrap)	Limit of identification: α -amanitin, β -amanitin: 1 ng/mL; ricinine, psilocin bufotenine, muscarine: 5 ng/mL muscimol: 2000 ng/mL ibotenic acid: 1500 ng/mL	α -amanitin: m/z 919.3614, β -amanitin: m/z 920.3455, ricinine: m/z 165.0659, muscarine: m/z 174.1489, muscimol: m/z 115.0502, psilocin/bufotenine: m/z 205.1335, ibotenic acid: m/z 159.0400, l-tryptophan (IS): m/z 210.1285, psilocin-d ₁₀ (IS): m/z 215.1963	55
α -Amanitin, β -Amanitin, γ -Amanitin	Human urine (300 μ L)	SPE (Oasis® Hydrophilic- Lipophilic Balance)	Acquity BEH HILIC	Gradient elution of acetonitrile and 20 mM ammonium formate with 0.2% formic acid	Positive ESI (SRM)	α - & γ -amanitin: 1–200 ng/mL, β -amanitin: 2.5–200 ng/mL (LOD: α :- 0.458 ng/mL, β :- 0.930 ng/mL; γ :- 0.169 ng/mL)	α -amanitin: m/z 919.3>338.9, β -amanitin: m/z 920.3>644.3, γ -amanitin: m/z 903.2>855.3, ¹⁵ N ₁₀ - α -amanitin (IS): m/z 929.3>911.4, Methionine sulfoxide (IS): m/z 889.4>871.4	56
α -Amanitin, β -Amanitin, Phallacin, Phallisin, Phalloacidin	Rat plasma & urine (200 μ L), mushroom	Protein precipitation with acetonitrile	Inertsil ODS-3	Gradient elution of 20 mM ammonium acetate containing 0.1% formic acid and acetonitrile	positive ESI (IT-TOF)	Qualitative identification	α -amanitin: m/z 919.3600, β -amanitin: m/z 920.3400, phallacin: m/z 849.3000, phallisin: m/z 863.3200, phalloacidin: m/z 847.3300	57
α -Amanitin, β -Amanitin, γ -Amanitin, Phalloacidin	Dog plasma, urine (1000 μ L)	Plasma: dilution and sonication Urine: SPE (Oasis WAX 1cc)	Acquity UPLC HSS T3	Gradient elution of 20 mM ammonium acetate and acetonitrile	positive ESI (MRM)	0.1–100 mg/kg (LOD: 0.01 mg/kg in urine and plasma: LOQ: 0.05 mg/kg)	α -amanitin: m/z 919.0>259.1, β -amanitin: m/z 920.0>259.1, γ -amanitin: m/z 903.0>86.1, phalloacidin: m/z 848.0>157.1	58
α -Amanitin	Rat plasma (100 μ L)	Protein precipitation with 1% formic acid in acetonitrile	Hypersil GOLD C18	Gradient elution of 20 mM ammonium acetate with 0.1% formic acid and acetonitrile	Positive ESI (MRM)	10–1500 ng/mL (LOD, 3.0 ng/mL)	α -amanitin: m/z 919.45>259.20, colchicine (IS): m/z 400.20>358.20	59
α -Amanitin, β -Amanitin, γ -Amanitin, Phalloidin, Phalloacidin	Human plasma, serum, urine (100 μ L)	SPE (PRIME HLB μ Elution 96-well plate)	CORTECS UPLC C18+	Gradient elution of 0.2 formic acid and 0.2% formic acid in methanol	Positive ESI (MRM)	1–100 ng/mL (LOD: α -, β -, γ -amanitin in plasma: 0.5 ng/mL, α -, γ -amanitin in urine: 1 ng/mL, phalloidin, phalloacidin: 0.5 ng/mL)	α -amanitin: m/z 919.5>86.0, β -amanitin: m/z 920.5>86.0, γ -amanitin: m/z 903.0>86.0, phalloidin: m/z 789.4>157.0, phalloacidin: m/z 847.0>157.0	60
α -Amanitin, β -Amanitin, Muscarine	Human urine (1000 μ L)	SPE (weak cation phase (Strata-X-CW))	Acclaim RS 120 C18	Gradient elution of 2 mM ammonium formate with 0.1% formic acid and acetonitrile	Positive ESI (TOF)	α -, β -amanitin: 1–1000 ng/mL (LOD, 1 ng/mL), muscarine: 0.1–100 ng/mL (LOD, 0.1 ng/mL)	α -amanitin: m/z 919.3614, β -amanitin: m/z 920.3454, muscarine: m/z 174.1489, phalloacidin (IS): m/z 847.3263	61

Table 1. Continued.

Toxin	Matrix	Sample preparation	Column	Mobile phase	Ionization (mode)	Linearity (LOD)	Transitions	Ref
α -Amanitin, β -Amanitin, Phalloidin	Human urine (500 μ L)	SPE (Bond Elut Agilent C18)	C18 Accucore	Gradient elution of 10 mM ammonium acetate with 0.1% formic acid and 0.1% formic acid in acetonitrile	Positive ESI (Orbitrap)	1–100 ng/mL (LOD: α -amanitin, phalloidin: 0.25 ng/mL, β -amanitin: 0.5 ng/mL)	α -amanitin: m/z 919.3614, β -amanitin: m/z 920.3455, phalloidin: m/z 789.3257, flurazepam (IS): m/z 388.1586	62
α -Amanitin, β -Amanitin	Human urine (100 μ L)	On-line turbulent flow chromatography	Accucore Phenyl-hexyl	Gradient elution of 10 mM ammonium acetate with 0.01% formic acid and acetonitrile with 0.1% formic acid	Negative ESI (Orbitrap)	1–100 ng/mL	α -amanitin: m/z 917.3458; β -amanitin: m/z 918.3298; γ -amanitin methyl ether (IS): m/z 915.3665	63
α -Amanitin, β -Amanitin	Human urine (200 μ L)	Protein precipitation with acetonitrile and dilution with water	Schzero SM-C18	Gradient elution of 5 mM ammonium formate and methanol	Positive ESI (Q-TOF) MS/MS	α -: 0.01–5 μ g/mL β -: 0.005–5 μ g/mL	α -amanitin: m/z 919.361>259.1289, β -amanitin: m/z 920.345>259.1287	64
α -Amanitin, β -Amanitin	Human urine (1000 μ L), liver (1 g)	Protein precipitation with acetonitrile, LLE, and SPE (Oasis HLB 6 cc cartridge)	Acquity UPLC HSS T3	Gradient elution of 20 mM ammonium acetate (pH 5) and acetonitrile	Positive ESI (MRM)	10–200 ng/mL or ng/g (LOD: α -: 0.22 ng/mL urine, 10.9 ng/g liver; β -: 0.2 ng/mL urine, 9.7 ng/g liver)	α -amanitin: m/z 919.48>901.53, β -amanitin: m/z 920.48>902.44, tilmicosin (IS): m/z 869.60>696.50	65
α -Amanitin, β -Amanitin, Phalloidin	Human urine (400 μ L)	SPE (Oasis HLB 1 cc cartridge)	-	-	MALDI (TOF)	10–500 ng/mL (LOD: 5 ng/mL)	α -amanitin: m/z 941, β -amanitin: m/z 942, phalloidin: m/z 811, microcystin (IS): m/z 1038	66
α -Amanitin, β -Amanitin, Phalloidin	Human serum, plasma, urine, rat urine (500 μ L)	SPE (Oasis HLB 3 cc cartridge)	Acquity UPLC BEH Shield RP18	Gradient elution of 0.1% formic acid in water and methanol	Positive ESI (MRM)	2–420 ng/mL (LOD: 1 ng/mL in human plasma, 1.5 ng/mL in human serum, 0.5 ng/mL human urine, 1.5 ng/mL rat urine)	α -amanitin: m/z 919.6>919.6, β -amanitin: m/z 920.6>920.6, phalloidin: m/z 788.9>616, virginiamycin B (IS): m/z 868>663	67
α -Amanitin, β -Amanitin	Human plasma (1000 μ L)	SPE (Discovery DSC-18, 500 mg)	Capcell Pak C18 UG120	Gradient elution of 0.1% formic acid in water and 0.1% formic acid in acetonitrile	Positive ESI (SIM)	10–500 ng/mL (LOD: 0.5 ng/mL)	α -amanitin: m/z 919-921, β -amanitin: m/z 920-922	68
α -Amanitin	Human serum (1000 μ L), dog liver	Protein precipitation (acetonitrile), LLE, and SPE (Xtract XRDH C18/ benzenesulfonic acid)	Synergi RP-Polar	Gradient elution of 10 mM ammonium acetate with 0.1% formic acid and acetonitrile	Positive ESI (MS/MS/MS mode)	LOD: 0.26 ng/g serum, 0.5 ng/g liver	α -amanitin: m/z 941>746>300	69

Table 1. Continued.

Toxin	Matrix	Sample preparation	Column	Mobile phase	Ionization (mode)	Linearity (LOD)	Transitions	Ref
α -Amanitin, β -Amanitin	Human urine (5000 μ L)	SPE (immunoaffinity column)	Hypersil RP-18	Gradient elution of 10 mM ammonium acetate (pH 5) and methanol	Positive ESI (SIM)	5–75 ng/mL (LOD: 2.5 ng/mL)	α -amanitin: m/z 919, 920, 921, β -amanitin: m/z 920, 921, 922, γ -amanitin methyl ether (IS): m/z 917, 918, 919	43
α -Amanitin, β -Amanitin	Human urine (5000 μ L)	SPE (LiChrolut RP-18)	Kromasil RP-18	Methanol : 20 mM ammonium acetate (pH 5) (22:78, v/v)	Positive ESI (SIM)	50–500 ng/mL (LOD, 10 ng/mL)	α -amanitin: m/z 919, β -amanitin: m/z 920	70

LL: liquid-liquid extraction; SPE: solid-phase extraction; SCX: strong cation exchange; LOD: limit of detection; ESI: electrospray ionization; PRM: parallel reaction monitoring; SIM: selected ion monitoring; SRM: selected reaction monitoring; MRM: multiple reaction monitoring; TOF: time of flight; IS: internal standard.

Table 2. The HPLC and capillary zone electrophoresis methods for the determination of amatoxins in various biological matrices.

Toxins	Matrix	Sample preparation	Column	Mobile phase	detection	Linearity (LOD)	Ref
HPLC							
α -Amanitin	Rat liver, kidney (1 g)	Protein precipitation with perchloric acid	Spherisorb RP-18	20% methanol in 50 mM citric acid, 0.46 mM octanesulfonic acid (pH 5.5 adjusted with 10 mM NaOH)	DAD 305 nm; Electrochemical detection	UV: 0.33–10 μ g/g liver; 0.5–10 μ g/g kidney (LOD: 0.05 μ g/g liver; 0.125 μ g/g kidney) ECD: 0.21–10 μ g/g liver; 0.11–10 μ g/g kidney (LOD: 0.015 μ g/g liver; 0.05 μ g/g kidney)	71
α -Amanitin	Human serum (500 μ L)	Protein precipitation with 1% acetic acid-acetonitrile, aqueous LLE, and SPE (SCX or C18/polymetric SCX)	Diamonsil C18	30% methanol in 10 mM ammonium acetate with 0.1% formic acid	UV 302 nm	SPE with polymetric SCX: 20–500 ng/mL (LOD 6.0 ng/mL) SPE with C18/polymetric SCX: 10–500 ng/mL (LOD 3.0 ng/mL)	72
α -Amanitin	Human urine (10000 μ L)	SPE (Bond Elut Certify containing C8 and SCX)	Supelcosil LC18	10% acetonitrile in 5 mM bisodic phosphate (pH 7.2)	Coulometric detection	10–200 ng/mL (LOD, 10 ng/mL)	73
α -Amanitin	Human plasma (2000 μ L)	SPE (SepPak C18)	Polystyrene-divinyl benzene	9% acetonitrile in 50 mM phosphate buffer	Ampherometric detection	3–200 ng/mL (LOD, 2 ng/mL)	74
α -Amanitin, Phalloidin	Human plasma (3000 μ L)	Column-switching (precolumn: MPLC cartridge RP-8 Spheri-5)	MPLC cartridge RP-8 Spheri-5	acetonitrile-water (16.67 : 83.33, v/v)	UV 303 nm	10–100 ng/mL (LOD: 10 ng/mL)	75
α -Amanitin, β -Amanitin, γ -Amanitin	Human serum (2000 μ L) & urine (1000 μ L)	SPE (serum: SepPak C18 and silica; urine: immunoaffinity sorbent)	Hypersil WP300 butyl	8% acetonitrile in 20 mM ammonium acetate (pH 5) containing 0.5 mM EDTA	Ampherometric detection	20–200 ng/mL (LOD 2.5 ng/mL urine)	76
α -Amanitin, β -Amanitin	Human serum (5000 μ L) & urine (100 μ L), stomach washings (250 μ L)	Protein precipitation with acetonitrile, LLE, and SPE (SepPak C18)	Ultrasphere ODS	12% acetonitrile in 20 mM ammonium acetate (pH 5)	UV 280 nm	20–500 ng/mL serum	77
α -Amanitin, β -Amanitin, Phalloidin	Human serum & urine (1000 μ L); mushroom (2 g)	Aqueous phase after LLE with methanol-chloroform	Lichrosorb RP18	Gradient elution of 10 mM ammonium acetate (pH 5) and acetonitrile	UV 302 nm	0.5–20 μ g/mL (LOD: 10 ng for α -, β - amanitin; 5 ng for phalloidin)	78
capillary zone electrophoresis							
α -Amanitin, β -Amanitin	Human urine (10 μ L)	Dilution with BGE (1:20)	Fused-silica capillary	5 mM borate buffer (pH 10)	UV 214 nm	5–100 ng/mL (LOD: 2.5 ng/mL)	79
α -Amanitin, β -Amanitin	Human urine, mushroom	Dilution with water (urine, 1:1; mushroom extract, 1:2500)	Capillary	100 mM phosphate (pH 2.4)	UV 214 nm	1–1000 μ g/mL mushroom; urine: qualification	80

LLE: liquid-liquid extraction; SPE: solid-phase extraction; SCX: strong cation exchanger; LOD: limit of detection

been combined in an attempt to avoid the matrix effect, but this has disadvantages such as high labor requirements and a long turnaround time (~24 h).

LC-MS methods

Reverse-phase chromatography using C₁₈, C₈, C₄, or phenylhexyl columns is the most common technique for chromatographic analysis of α -, β -, and γ -amanitin in biological fluids. Gradient elution of mobile phase A (ammonium acetate or formic acid) and mobile phase B (acetonitrile or methanol) has been used as the mobile phase for LC-MS methods (Table 1), whereas isocratic elution is used in HPLC methods (Table 2). Hydrophilic interaction chromatography has been used for the simultaneous determination of α -, β -, and γ -amanitin, and six mushroom toxins in human urine, to increase the retention and ionization efficiency.^{55,56}

Positive and negative electrospray ionization (ESI) modes have been used for the ionization of amatoxins when applying LC-MS methods (Table 1). Negative ESI mode has higher sensitivity and smaller matrix effects compared to positive ESI mode.^{41,42,45,50-53,64} MALDI-TOF MS has been used for qualitative analysis of α -amanitin, β -amanitin, and phalloidin in human urine.⁶⁶

For the quantification of α -, β -, and γ -amanitin, selective ion monitoring mode with quadrupole MS,^{43,68,70} multiple reaction monitoring (MRM) or selected reaction monitoring (SRM) mode with triple quadrupole tandem MS (MS/MS),^{45,50,51,53,54,56,58-60,65,67} and parallel reaction monitoring (PRM) mode using orbitrap MS^{41,42,44,55,62,63} have been used (Table 1). LC-MS/MS methods using quadrupole MS/MS and orbitrap MS are powerful techniques with high sensitivity (lower limit of quantification [LLOQ] = 0.02–50 ng/mL plasma for α -, β -, and γ -amanitin), reproducibility, and specificity. Recently, LC-MS/MS methods performed in PRM mode and protein precipitation of plasma samples (5 mL) for sample clean-up showed good sensitivity (LLOQ 0.5 ng/mL for α - and β -amanitin), selectivity, and speed.^{41,42,52}

Conclusions

Because the incidence of amatoxin-induced mushroom poisoning has increased globally, early detection of amatoxins in cases of suspected mushroom poisoning is necessary to improve patient outcomes through aggressive and immediate supportive care among other potential therapies. Early diagnosis of amatoxins has been achieved using LC-MS/MS methods. These methods may be suitable for routine clinical and forensic toxicological analysis of amatoxins in plasma, serum, urine, and tissue samples due to the high specificity, sensitivity, and reproducibility relative to other analytical methods. However, protein precipitation, LLE, and SPE have been

combined for sample preparation, to minimize matrix effects and achieve high sensitivity, but with high labor requirements and a long turnaround time. There is a need to improve sample preparation procedures for rapid clinical and forensic toxicological analyses.

Acknowledgements

This work was supported by the National Research Foundation of Korea (NRF) grant funded by the Korea government (MSIT) (NRF-2020R1A2C2008461).

References

- Govorushko, S.; Rezaee, R.; Dumanov, J.; Tsatsakis, A. *Food Chem. Toxicol.* **2019**, 128, 267, DOI: 10.1016/j.fct.2019.04.016.
- Brandenburg, W. E.; Ward, K. J. *Mycologia* **2018**, 110, 637, DOI: 10.1080/00275514.2018.1479561.
- White, J.; Weinstein, S. A.; De Haro, L.; Bédry, R.; Schaper, A.; Rumack, B. H.; Zilker, T. *Toxicicon* **2019**, 157, 53, DOI: 10.1016/j.toxicicon.2018.11.007.
- Clarke, D.; Crews, C. *Encyclopedia of Food Safety* **2014**, 2, 269.
- Karlson-Stiber, C.; Persson, H. *Toxicicon* **2003**, 42, 339, DOI: 10.1016/s0041-0101(03)00238-1.
- Diaz, J. H.; James, H. *Wilderness Environ. Med.* **2018**, 29, 111, DOI: 10.1016/j.wem.2017.10.002.
- Stebelska, K. *Ther. Drug Monit.* **2013**, 35, 420, DOI: 10.1097/FTD.0b013e31828741a5.
- Flammer, R.; Schenk-Jäger, K. M. *Ther. Umsch.* **2009**, 66, 357, DOI: 10.1024/0040-5930.66.5.357.
- Diaz, J. H. *Wilderness Environ. Med.* **2018**, 29, 111, DOI: 10.1016/j.wem.2018.06.008.
- Latha, S. S.; Naveen, S.; Pradeep, C. K.; Sivaraj, C.; Dinesh, M. G.; Anilakumar, K. R. *Front. Pharmacol.* **2018**, 9, 90, DOI: 10.3389/fphar.2018.00090.
- Schenk-Jäger, K. M.; Egli, S.; Hanimann, D.; Senn-Iriet, B.; Kupferschmidt, H.; Buntgen, U. *PLoS One* **2016**, 11, e0162314, DOI: 10.1371/journal.pone.0162314.
- Vo, K.T.; Montgomery, M. E.; Mitchell, S. T.; Scheerlinck, P. H.; Colby, D. K.; Meier, K. H.; Kim-Katz, S.; Anderson, I. B.; Offerman, S. R.; Olson, K. R.; Smollin, C. G. *Morb. Mortal. Wkly. Rep.* **2017**, 66, 549, DOI: 10.15585/mmwr.mm6621a1.
- Carlvik, B.; Lindeman, E. *Clin. Toxicol.* **2017**, 55, 374, DOI: 10.1080/15563650.2017.1309792.
- Beuhler, M. C. Overview of mushroom poisoning, in: Brent, J.; Burkhart, K.; Dargan, P.; Hatten, B.; Megarbane, B.; Palmer, R.; White, J. (Eds.), *Critical Care Toxicology: Diagnosis and Management of the Critically Poisoned Patient*, **2017**, 2103–2128.
- Plament, E.; Guitton, J.; Gaulier, J. M.; Gaillard, Y. *Pharmaceuticals* **2020**, 13, 454, DOI: 10.3390/ph13120454.
- Poucheret, P.; Fons, F.; Dore, J. C.; Michelot, D.; Rapior, S. *Toxicicon* **2010**, 55, 1338, DOI: 10.1016/j.toxicicon.2010.02.005.

17. Garcia, J.; Costa, V. M.; Carvalho, A.; Baptista, P.; de Pinho, P. G.; de Lourdes Bastos, M.; Carvalho, F. *Food Chem. Toxicol.* **2015**, *86*, 41, DOI: 10.1016/j.fct.2015.09.008.
18. Le Dare, B.; Ferron, P.-J.; Gicquel, T. *Toxins* **2021**, *13*, 417, DOI: 10.3390/toxins1306417.
19. Hallen, H. E.; Luo, H.; Scott-Craig, J. S.; Walton, J. D. *Proc. Natl. Acad. Sci. USA* **2007**, *104*, 19097, DOI: 10.1073/pnas.0707340104.
20. Escoda, O.; Reverter, E.; To-Figueras, J.; Casals, G.; Fernández, J.; Nogué, S. *Liver Int.* **2019**, *39*, 1128, DOI: 10.1111/liv.14028.
21. Le Daré, B.; Ferron, P.-J.; Couette, A.; Ribault, C.; Morel, I.; Gicquel, T. *Toxicol. Lett.* **2021**, *346*, 1, DOI: 10.1016/j.toxlet.2021.04.006.
22. Brandenburg, W. E.; Ward, K. J. *Mycologia* **2018**, *110*, 637, DOI: 10.1080/00275514.2018.1479561.
23. Nicholson, F. B.; Korman, M. G. *Aust. N. Z. J. Med.* **1997**, *27*, 448, DOI: 10.1111/j.1445-5994.1997.tb02212.x.
24. Kaya, E.; Karahan, S.; Bayram, R.; Yaykasli, K.O.; Colakoglu, S.; Saritas, A. *Toxicol. Ind. Health* **2015**, *31*, 1172, DOI: 10.1177/0748233713491809.
25. Sun, J.; Niu, Y.-M.; Zhang, Y.-T.; Li, H.-J.; Yin, Y.; Zhang, Y.-Z.; Ma, P.-B.; Zhou, J.; Huang, L.; Zhang, H.-S. *Toxicon* **2018**, *143*, 59, DOI: 10.1016/j.toxicon.2018.01.008.
26. Sun, J.; Zhang, Y.-T.; Niu, Y.-M.; Li, H.-J.; Yin, Y.; Zhang, Y.-Z.; Ma, P.-B.; Zhou, J.; Lu, J.-J.; Zhang, H.-S. *Toxins* **2018**, *10*, 215, DOI: 10.3390/toxins10060215.
27. Yilmaz, I.; Ermis, F.; Akata, I.; Kaya, E. *Wilderness Environ. Med.* **2015**, *26*, 491, DOI: 10.1016/j.wem.2015.08.002.
28. Wieland, T.; Faulstich, H.; Fiume, L. *CRC Crit. Rev. Biochem.* **1978**, *5*, 185, DOI: 10.3109/10409237809149870.
29. Vetter, J. *Toxicon* **1998**, *36*, 13, DOI: 10.1016/s0041-0101(97)00074-3.
30. Mydlík, M.; Derzsiová, K.; Frank, K. *Przegl. Lek.* **2013**, *70*, 381.
31. Wieland, T. *Int. J. Pept. Protein Res.* **1983**, *22*, 257, DOI: 10.1111/j.1399-3011.1983.tb02093.x.
32. Rodrigues, D. F.; Pires das Neves, R.; Carvalho, A. T. P.; Lourdes Bastos, M.; Costa, V. M.; Carvalho, F. *Arch. Toxicol.* **2020**, *94*, 2079, DOI: 10.1007/s00204-020-02735-0.
33. Steurer, B.; Janssens, R. C.; Geverts, B.; Geijer, M. E.; Wienholz, F.; Theil, A. F.; Chang, J.; Dealy, S.; Pothof, J.; van Cappellen, W. A.; Houtsmuller, A. B.; Marteiijn, J. A. *Proc. Natl. Acad. Sci. USA* **2018**, *115*, E4368, DOI: 10.1073/pnas.1717920115.
34. Zheleva, A.; Tolekova, A.; Zhelev, M.; Uzunova, V.; Platikanova, M.; Gadzheva, V. *Med. Hypotheses* **2007**, *69*, 361, DOI: 10.1016/j.mehy.2006.10.066.
35. Dündar, Z. D.; Ergin, M.; Kiliç, İ.; Çolak, T.; Oltulu, P.; Cander, B. *Turk. J. Med. Sci.* **2017**, *47*, 318, DOI: 10.3906/sag-1503-163.
36. Arima, Y.; Nitta, M.; Kuninaka, S.; Zhang, D.; Fujiwara, T.; Taya, Y.; Nakao, M.; Saya, H. *J. Biol. Chem.* **2005**, *280*, 19166, DOI: 10.1074/jbc.M410691200.
37. Wang, M.; Chen, Y.; Guo, Z.; Yang, C.; Qi, J.; Fu, Y.; Chen, Z.; Chen, P.; Wang, Y. *Toxicon* **2018**, *156*, 34, DOI: 10.1016/j.toxicon.2018.11.002.
38. Kim, D.; Kim, S.; Na, A. Y.; Sohn, C. H.; Lee, S.; Lee, H. S. *Toxins* **2021**, *13*, 197, DOI: 10.3390/toxins13030197.
39. Kim, D.; Lee, M.S.; Sung, E.; Lee, S.; Lee, H. S. *Int. J. Mol. Sci.* **2022**, *23*, 12294, DOI: 10.3390/ijms232012294.
40. Kaya, E.; Bayram, R.; Yaykasli, K. O.; Yilmaz, I.; Bayram, S.; Yaykasli, E.; Yavuz, M. Z.; Gepdiremen, A. *A. Turk. J. Med. Sci.* **2014**, *44*, 728.
41. Park, R.; Choi, W.-G.; Lee, M. S.; Cho, Y.-Y.; Lee, J.Y.; Kang, H.C.; Sohn, C. H.; Song, I.-S.; Lee, H. S. *J. Toxicol. Environ. Health A* **2021**, *84*, 821, DOI: 10.1080/15287394.2021.1944942.
42. Bang, Y. Y.; Song, I.-S.; Lee, M. S.; Lim, C. H.; Cho, Y.-Y.; Lee, J. Y.; Kang, H. C.; Lee, H. S. *Pharmaceutics* **2022**, *14*, 774, DOI: 10.3390/pharmaceutics14040774.
43. Maurer, H. H.; Schmitt, C. J.; Weber, A. A.; Kraemer, T. *J. Chromatogr. B* **2000**, *748*, 125, DOI: 10.1016/s0378-4347(00)00270-x.
44. Bambauer, T. P.; Waggmann, L.; Weber, A. A.; Meyer, M. R. *Toxins* **2020**, *12*, 671, DOI: 10.3390/toxins12110671.
45. Xu, X. M.; Meng, Z.; Zhang, J. S.; Chen, Q.; Han, J. L. *J. Pharm. Biomed. Anal.* **2020**, *190*, 113523, DOI: 10.1016/j.jpba.2020.113523.
46. Jaeger, A.; Jehl, F.; Flesch, F.; Sauder, P.; Kopferschmitt, J. *J. Toxicol. Clin. Toxicol.* **1993**, *31*, 63, DOI: 10.3109/15563659309000374.
47. Letschert, K.; Faulstich, H.; Keller, D.; Keppler, D. *Toxicol. Sci.* **2006**, *91*, 140, DOI: 10.1093/toxsci/kfj141.
48. Wlcek, K.; Koller, F.; Ferenci, P.; Stieger, B. *Drug Metab. Dispos.* **2013**, *41*, 1522, DOI: 10.1124/dmd.113.051037.
49. Garcia, J.; Carvalho, A.; das Neves, R. P.; Malheiro, R.; Rodrigues, D. F.; Figueiredo, P. R.; Bovolini, A.; Duarte, J. A.; Costa, V. M.; Carvalho, F. *Food Chem. Toxicol.* **2022**, *166*, 113198, DOI: 10.1016/j.fct.2022.113198.
50. Zhang, X.; Cai, X.; Zhang, X.; Li, R.; Zhao, Y. *Se Pu* **2022**, *40*, 443, DOI: 10.3724/SP.J.1123.2021.08018.
51. Mao, Z.; Yu, Y.; Sun, H.; Cao, Y.; Jiang, Q.; Chu, C.; Sun, Y.; Huang, S.; Zhang, J.; Chen, F. *Rapid Commun. Mass Spectrom.* **2021**, *35*, e9184, DOI: 10.1002/rcm.9184.
52. Bang, Y. Y.; Lee, M. S.; Lim, C. H.; Lee, H. S. *Mass Spectro. Lett.* **2021**, *12*, 112, DOI: 10.5478/MSL.2021.12.3.112.
53. Xu, X.; Zhang, J.; Cai, Z.; Meng, Z.; Huang, B.; Chen, Q. *Se Pu* **2020**, *38*, 1281, DOI: 10.3724/SP.J.1123.2020.03010.
54. Tan, L.; Li, Y.; Deng, F.; Pan, X.; Yu, H.; Marina, M. L.; Jiang, Z. *J. Chromatogr. A* **2020**, *1630*, 461514, DOI: 10.1016/j.chroma.2020.461514.
55. Bambauer, T. P.; Waggmann, L.; Maurer, H. H.; Weber, A. A.; Meyer, M. R. *Talanta* **2020**, *213*, 120847, DOI: 10.1016/j.talanta.2020.120847.
56. Abbott, N. L.; Hill, K. L.; Garrett, A.; Carter, M. D.; Hamelin, E. I.; Johnson, R. C. *Toxicon* **2018**, *152*, 71, DOI: 10.1016/j.toxicon.2018.07.025.
57. Li, C.; Qian, H.; Bao, T.; Yang, G.; Wang, S.; Liu, X. *Toxicol. Lett.* **2018**, *296*, 95, DOI: 10.1016/j.toxlet.2018.08.005.
58. Sun, J.; Niu, Y. M.; Zhang, Y. T.; Li, H. J.; Yin, Y. Zhang,

- Y. Z.; Ma, P. B.; Zhou, J.; Huang, L.; Zhang, H. S.; Sun, C. Y. *Toxicon* **2018**, 143, 59, DOI: 10.1016/j.toxicon.2018.01.008.
59. Li, C.; Wei, F.; Muhammad, S.; Yang, G.; Wang, S.; Liu, X. *J. Chromatogr. B* **2017**, 1064, 36, DOI: 10.1016/j.jchromb.2017.08.042.
60. Zhang, S.; Zhao, Y.; Li, H.; Zhou, S.; Chen, D.; Zhang, Y.; Yao, Q.; Sun, C. *Toxins* **2016**, 8, 128, DOI: 10.3390/toxins8050128.
61. Tomková, J.; Ondra, P.; Válka, I. *Forensic Sci. Int.* **2015**, 251, 209, DOI: 10.1016/j.forsciint.2015.04.007.
62. Gicquel, T.; Lepage, S.; Fradin, M.; Tribut, O.; Duret, B.; Morel, I. *J. Anal. Toxicol.* **2014**, 38, 335, DOI: 10.1093/jat/bku035.
63. Helfer, A. G.; Meyer, M. R.; Michely, J. A.; Maurer, H. H. *J. Chromatogr. A* **2014**, 1325, 92, DOI: 10.1016/j.chroma.2013.11.054.
64. Ishii, A.; Tada, M.; Kusano, M.; Ogawa, T.; Hattori, H.; Seno, H.; Zaitzu, K. *Forensic Toxicol.* **2014**, 32, 342, DOI: 10.1007/s11419-014-0241-x
65. Leite, M.; Freitas, A.; Azul, A. M.; Barbosa, J.; Costa, S.; Ramos, F. *Anal. Chim. Acta* **2013**, 799, 77, DOI: 10.1016/j.aca.2013.08.044
66. Gonmori, K.; Minakata, K.; Suzuki, M.; Yamagishi, I.; Nozawa, H.; Hasegawa, K.; Wurita, A.; Watanabe, K.; Suzuki, O. *Forensic Toxicol.* **2012**, 30, 179, DOI: 10.1007/s11419-012-0145-6.
67. Nomura, M.; Suzuki, Y.; Kaneko, R.; Ogawa, T.; Hattori, H.; Seno, H.; Ishii, A. *Forensic Toxicol.* **2012**, 30, 185, DOI: 10.1007/s11419-012-0146-5 -92.
68. Tanahashi, M.; Kaneko, R.; Hirata, Y.; Hamajima, M.; Arinobu, T.; Ogawa, T.; Ishii, A. *Forensic Toxicol.* **2010**, 28, 110, DOI: 10.1007/s11419-010-0098-6.
69. Filigenzi, M. S.; Poppenga, R. H.; Tiwary, A. K.; Puschner, B. *J. Agric. Food Chem.* **2007**, 55, 2784, DOI: 10.1021/jf063194w.
70. Maurer, H. H.; Kraemer, T.; Ledvinka, O.; Schmitt, C. J.; Weber, A. A. *J. Chromatogr. B* **1997**, 689, 81, DOI: 10.1016/s0378-4347(96)00348-9.
71. Garcia, J.; Costa, V. M.; Baptista, P.; Bastos Mde, L.; Carvalho, F. *J. Chromatogr. B* **2015**, 997, 85, DOI: 10.1016/j.jchromb.2015.06.001.
72. Tang, Y.; Zhou, L.; Zhou, Z.; Zuo, X.; Cao, M. *LCGC North America*, **2011**, 29, 672.
73. Defendenti, C.; Bonacina, E.; Mauroni, M.; Gelosa, L. *Forensic Sci. Int.* **1998**, 92, 59, DOI: 10.1016/s0379-0738(98)00006-1.
74. Tagliaro, F.; Schiavon, G.; Bontempelli, G.; Carli, G.; Marigo, M. *J. Chromatogr.* **1991**, 563, 299, DOI: 10.1016/0378-4347(91)80036-c.
75. Rieck, W.; Platt, D. *J. Chromatogr.* **1988**, 425, 121, DOI: 10.1016/0378-4347(88)80012-4.
76. Tagliaro, F.; Chiminazzo, S.; Maschio, S. *Chromatographia* **1987**, 24, 482, DOI: 10.1007/BF02688530.
77. Jehl, F.; Gallion, C.; Birckel, P.; Jaeger, A.; Flesch, F.; Minck, R. *Anal. Biochem.* **1985**, 149, 35, DOI: 10.1016/0003-2697(85)90474-9
78. Caccialanza, G.; Gandini, C.; Ponci, R. *J. Pharm. Biomed. Anal.* **1985**, 3, 179, DOI: 10.1016/0731-7085(85)80021-2.
79. Robinson-Fuentes, V. A.; Jaime-Sánchez, J. L.; García-Aguilar, L.; Gómez-Peralta, M.; Vázquez-Garcidueñas, M. S.; Vázquez-Marrufo, G. *J. Pharm. Biomed. Anal.* **2008**, 47, 913, DOI: 10.1016/j.jpba.2008.03.032.
80. Brüggemann, O.; Meder, M.; Freitag, R. *J. Chromatogr. A* **1996**, 744, 167, DOI: 10.1016/0021-9673(96)00173-2.
81. Faulstich, H.; Zobeley, S.; Trischmann, H. *Toxicon*. 1982, 20, 913, DOI: 10.1016/0041-0101(82)90079-4.
82. Andres, R. Y.; Frei, W.; Gautschi, K.; Vonderschmitt, D. *J. Clin. Chem.* **1986**, 32, 1751.
83. Parant, F.; Peltier, L.; Lardet, G.; Pulce, C.; Descotes, J.; Moulisma, M. *Acta Clin. Belg.* **2006**, 61 Suppl. 1, 11, DOI: 10.1179/acb.2006.063.
84. Abuknesha, R. A.; Maragkou, A. *Anal. Bioanal. Chem.* **2004**, 379, 853, DOI: 10.1007/s00216-004-2663-5.
85. Bever, C. S.; Swanson, K. D.; Hamelin, E. I.; Filigenzi, M.; Poppenga, R. H.; Kaae, J.; Cheng, L. W.; Stanker, L. H. *Toxins* **2020**, 12, 123, DOI: 10.3390/toxins12020123.

High-Throughput Screening Technique for Microbiome using MALDI-TOF Mass Spectrometry: A Review

Abhik Mojumdar^{1,2}, Hee-Jin Yoo^{1,3}, Duck-Hyun Kim¹, and Kun Cho^{1,2*}

¹Biochemical analysis team, center for research equipment, Korea Basic Science Institute (KBSI), Ochang Center, Cheongju-si, Chungcheongbuk-do, Republic of Korea

²Department of Bio-Analytical Sciences, University of Science and Technology (UST), Daejeon 34113, Republic of Korea

³Department of Chemistry, Sogang University, Seoul, Republic of Korea

Received November 29, 2022, Revised December 14, 2022, Accepted December 15, 2022

First published on the web December 31, 2022; DOI: 10.5478/MSL.2022.13.4.106

Abstract : A rapid and reliable approach to the identification of microorganisms is a critical requirement for large-scale culturomics analysis. MALDI-TOF MS is a suitable technique that can be a better alternative to conventional biochemical and gene sequencing methods as it is economical both in terms of cost and labor. In this review, the applications of MALDI-TOF MS for the comprehensive identification of microorganisms and bacterial strain typing for culturomics-based approaches for various environmental studies including bioremediation, plant sciences, agriculture and food microbiology have been widely explored. However, the restriction of this technique is attributed to insufficient coverage of the mass spectral database. To improve the applications of this technique for the identification of novel isolates, the spectral database should be updated with the peptide mass fingerprint (PMF) of type strains with not only microbes with clinical relevance but also from various environmental sources. Further, the development of enhanced sample processing methods and new algorithms for automation and de-replication of isolates will increase its application in microbial ecology studies.

Keywords : MALDI-TOF, mass spectrometry, microbiome, environment

Introduction

Microorganisms are present throughout the environment and are crucial to a wide range of natural processes. They play a crucial role in the biodegradation of organic matter, detoxification of various pollutants and hence recycling of nutrients in the ecosystem through the biogeochemical cycles which are fundamental to the environment and for the survival of animals, plants and human life. Pathogenic microbes cause diseases in plants and animals, however, there are other groups of beneficial microbes that can prevent the growth of various harmful microbes. Certain microbes participate in the fermentation and production of various food products whereas the presence of certain other

microbes in food causes spoilage. Moreover, the human body is home to various complex communities of bacteria that plays a significant role in various physical and biochemical activities. In conclusion, microorganisms are present throughout the environment and are significant to a wide range of natural processes. Thus, the identification and classification of microorganisms are crucial and cannot be ignored.

Conventional techniques for bacterial identification are culture-dependent morphological, physiological and biochemical assays which are labor-intensive and time-consuming.¹ Although molecular techniques such as 16S rRNA, DNA-DNA hybridization, polymerase chain reaction (PCR)-based methods and fluorescent in-situ hybridization (FISH) are popular, again, they require high expertise and are expensive and time-consuming.² Thus, rapid and unequivocal identification of microbes in real samples is a current important area of focus.

Mass spectrometry is an analytical technique in which compounds are ionized into charged molecules and the mass-to-charge (m/z) ratio is determined. With the development of soft ionization techniques such as electrospray ionization (ESI) and matrix-assisted laser desorption ionization (MALDI), the scope for the analysis of large biomolecules such as proteins has expanded. When compared to ESI-MS, MALDI-TOF-MS has a few

Open Access

*Reprint requests to Kun Cho

<https://orcid.org/0000-0003-1154-4065>

E-mail: chokun@kbsi.re.kr

All the content in Mass Spectrometry Letters (MSL) is Open Access, meaning it is accessible online to everyone, without fee and authors' permission. All MSL content is published and distributed under the terms of the Creative Commons Attribution License (<http://creativecommons.org/licenses/by/3.0/>). Under this license, authors reserve the copyright for their content; however, they permit anyone to unrestrictedly use, distribute, and reproduce the content in any medium as far as the original authors and source are cited. For any reuse, redistribution, or reproduction of a work, users must clarify the license terms under which the work was produced.

advantages such as it creates singly charged ions, making data interpretation simpler and it does not require prior chromatographic separation.³ Consequently, MALDI-TOF MS has emerged as a clear choice for large-scale

proteomics work due to the high throughput and speed associated with complete automation.⁴

For the first time in 1996, the spectral fingerprints from whole bacteria were obtained by using three strains of

Table 1. Microbial detection techniques. Adapted and modified from Singhal et al. 2015.¹⁰

Detection method	Advantages	Disadvantages
Conventional; culture dependent identification by biochemical tests	<ul style="list-style-type: none"> · Sensitive · Inexpensive 	<ul style="list-style-type: none"> · Lengthy and time-consuming process · Might require 24–48h
Immunological-based methods	<ul style="list-style-type: none"> · Faster than conventional methods · Can detect both contaminating organisms and their toxins 	<ul style="list-style-type: none"> · Not as specific, sensitive and rapid as nucleic acid-based detection methods · Require large amounts of antigen · Developed for only a small number of microorganisms
Florescent in situ hybridization (FISH)	<ul style="list-style-type: none"> · Rapid detection and identification directly from slide smears · Fast and ease-of-use of conventional staining methods combined with the specificity of molecular methods 	<ul style="list-style-type: none"> · Test limited by the availability of specific antigens for detection
Molecular based methods	<ul style="list-style-type: none"> · Culturing of the sample is not required 	<ul style="list-style-type: none"> · A highly precise thermal cyclor is needed
(i) Real-time PCR	<ul style="list-style-type: none"> · Specific, sensitive, rapid and accurate 	<ul style="list-style-type: none"> · Trained laboratory personnel required for performing the test
(ii) Multiplex-PCR	<ul style="list-style-type: none"> · Closed-tube system reduces the risk of contamination 	<ul style="list-style-type: none"> · Discriminatory power and reproducibility are lower compared to PFGE and MLST
(iii) Repetitive extragenic palindromic PCR (rep-PCR)	<ul style="list-style-type: none"> · Can detect many pathogens simultaneously 	<ul style="list-style-type: none"> · Labor-intensive and costly
(iv) Random amplification of polymorphic DNA (RAPD)	<ul style="list-style-type: none"> · Easy to perform 	<ul style="list-style-type: none"> · Lack of reproducibility
(v) Amplified fragment length polymorphism (AFLP)	<ul style="list-style-type: none"> · Cheap, rapid, and easy to perform 	<ul style="list-style-type: none"> · Time-consuming and costly
(vi) Variable-number tandem repeat (VNTR)	<ul style="list-style-type: none"> · High discriminatory ability and reproducibility 	<ul style="list-style-type: none"> · Relatively costly and time-consuming
(vii) Multilocus sequence analysis and multilocus sequence typing (MLST)		
(viii) Pulsed-field gel electrophoresis (PFGE)		
DNA sequencing	<ul style="list-style-type: none"> · 16S rDNA and 18S rDNA sequencing is the gold standards · Can identify fastidious and uncultivable microorganisms 	<ul style="list-style-type: none"> · Trained laboratory personnel and powerful interpretation software are required · Expensive · Not suitable for routine clinical use
Microarrays	<ul style="list-style-type: none"> · Large-scale screening system for simultaneous diagnosis and detection of many pathogens 	<ul style="list-style-type: none"> · Expensive · Trained laboratory personnel required
Loop-mediated isothermal amplification (LAMP) assay	<ul style="list-style-type: none"> · Can generate large copies of DNA in less than an hour · Easy to use · No sophisticated equipment is required 	<ul style="list-style-type: none"> · Developed for only a small number of microorganisms yet
Metagenomic assay	<ul style="list-style-type: none"> · Useful for random detection of pathogens 	<ul style="list-style-type: none"> · Data acquisition and data analysis are time-consuming · Trained laboratory personnel required
MALDI-TOF MS	<ul style="list-style-type: none"> · Fast · Accurate · Less expensive than molecular and immunological-based detection methods · Trained laboratory personnel are not required 	<ul style="list-style-type: none"> · The high initial cost of the MALDI-TOF equipment · The limited resolution, and database discordances

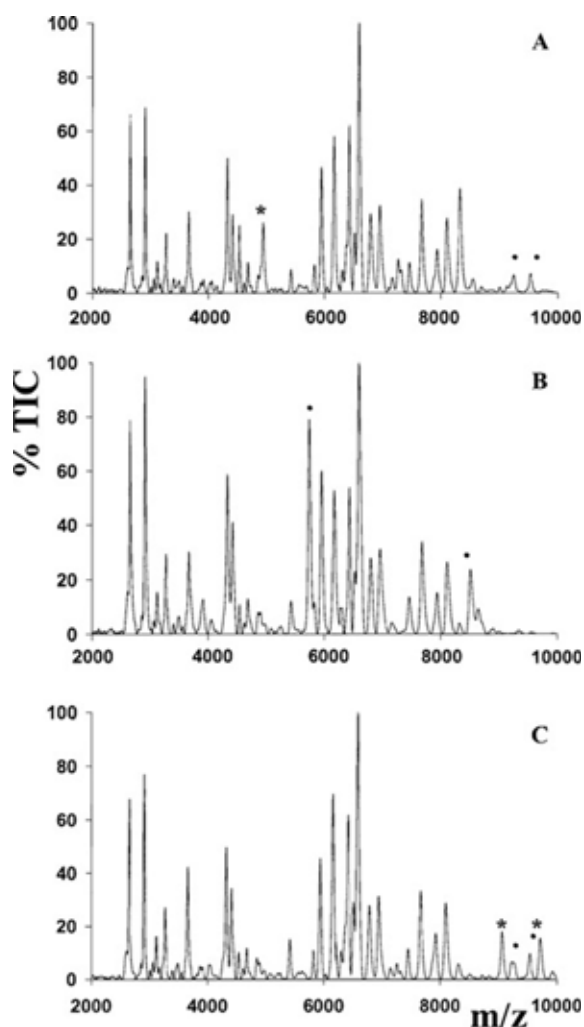


Figure 1. MALDI spectra of (A) *Salmonella* 2B5, (B) *Acinetobacter* 14B5 and (C) *Escherichia coli* 1B1 showing the potential genus- (•) and strain- (*) specific biomarkers. Reprinted with permission from Ruelle et al.¹² (2004). Copyright 2004 John Wiley & Sons.

*Pseudomonas*⁵ and in the same year, spectral fingerprints of various *Bacillus* species were also acquired by using MALDI-TOF-MS.⁶ Since then, a lot of focus has been placed on using MALDI-TOF to identify not only bacteria but also yeast and mold.⁷ However, since the last decade, the technology has been utilized for routine analysis of microbes as it is rapid, reliable, cost-effective and has various other advantages over conventional techniques.⁸ Some of the advantages and disadvantages of various microbial detection techniques have been shown in Table 1. Further, the technology has the potential to replace current identification methods in microbiology labs because it can identify a wide variety of microorganisms.⁹ Thus, this review focuses on the comprehensive illustration

of the use of MALDI-TOF-MS for microbial identification in various environmental fields.

To comprehend the microbial population, monitor the environment, and find potential pathogenic bacteria, it is essential to identify microorganisms from environmental sources. The ability to identify each microbe by its unique protein fingerprint has made MALDI-TOF-MS a significant advancement in the field of environmental proteomics. The identification of unknown microbe is carried out either by matching the abundance of the biomarkers with the proteome database or by comparing the PMF with the PMFs present in the database. Several conserved signals under various experimental conditions that can be used as potential biomarkers were observed by Wang et al.¹¹ Several other studies also reveal the specific conserved biomarkers which are unaffected by environmental factors can be used for bacterial identification as shown in the work by Ruelle et al.¹² (Figure 1). Although several in-house databases have been created,¹³ however, the currently the two major databases are the MALDI BioTyper library by Bruker Daltonics, Inc. which uses Bruker Main Spectrum analysis (MSP) and the SARAMIS by bioMérieux which uses the bioMérieux SuperSpectrum approaches.^{14, 15} The accuracy of identification of unknown microbes using MALDI-TOF MS depends on the database. Generally, the identification accuracy up to the species level is 90%,¹⁶ however, the database should be regularly updated in order to enhance the identification of novel microbes.¹⁷ Additionally, the sample culture, preparation, storage, and the type of matrix used affect the reproducibility of MS spectra obtained with MALDI.⁸

MALDI-TOF MS in microbial identification

Ecological and environmental studies

Commonly used methods for identification and classification involve 16S rRNA sequencing, gel electrophoresis techniques, rep-PCR and multilocus sequence typing (MLST).¹⁸ However, such techniques are expensive, time taking and laborious. As an alternative, MALDI-TOF MS has been utilized for exploring the biodiversity of microorganisms by identifying and characterizing novel strains in different environments. For taxonomic classification, microorganisms are separated into genera, species and strains. MALDI-TOF MS has been proven to resolve intra- and inter-species classifications and distinguish very closely related species with high reliability. Dieckmann et al.¹⁹ reported the difference in 1 bp out of 400 bp or 3-4 bp out of 1500 bp of the 16S rRNA gene sequence of *Pseudoalteromonas* sp. by their MALDI-TOF-MS spectra. Investigating the variety and composition of microbes requires careful observation of various habitats, diets, and surfaces. It is carried out sometimes to constantly check on the spread of harmful pathogens or occasionally to find the source of bacterial contamination. MALDI-TOF MS has

proven that it can be used to continuously monitor these settings and offer insightful data on the richness and composition of bacterial species. Zeng et al.²⁰ utilized a culturomics technique involving MALDI-TOF MS-based high-throughput colony screening technique and genome sequencing to identify one novel strain of Gemmatimonadetes out of 330 isolates from the streams in Northern Greenland. Another study reported that 8 biosurfactant-producing bacteria out of 234 isolates were characterized by MALDI-TOF MS and identified as *Proteus mirabilis*, *Alcaligenes faecalis*, and *Providencia alcalifaciens*.²¹ Environmental water isolates of *Aeromonas* were also isolated and identified using MALDI-TOF MS by comparing m/z signatures with known strains. It was suggested in the work that this technique is useful for environmental monitoring due to its speed and capacity to handle a large number of samples.²²

Some researchers are interested in learning more about the microbiota connected to distinct metal ores since bacteria play a significant role in the biogeochemical cycle of various elements. Nosalova et al.²³ conducted one such study to look at the microbiota of gold ore. Colony-forming units (CFU) within the range of 2.18×10^5 to 3.16×10^5 bacteria per 1 g of dry ore material were detected in cultivation studies. Results revealed that 89% of the 473 isolates from gold ore belonged to the genus *Acinetobacter*, *Microbacterium*, *Pseudomonas*, and *Rhizobium*. Another study conducted in the Rozalia gold mine in Hodrusa-Hamre revealed that the gold ores mainly consisted of bacteria from 18 different species including *Aerococcus*, *Pseudomonas*, *Rhizobium*, *Acinetobacter*, *Microbacterium*, *Acidovorax*, *Staphylococcus* and others.²⁴

Environmental biotechnology and bioremediation

Environmental pollution is a major problem, and today eco-friendly remedial methods are a necessity. A potential strategy is a bioremediation, which uses microorganisms to decrease or remove toxic substances from the environment.²⁵ As a high-throughput method, MALDI-TOF MS is a useful tool for bioremediation research. With the use of this approach, site-specific microorganisms found in polluted settings may be quickly identified. A study conducted by Garcia Lara et al.²⁶ identified 25 bacterial strains using Bruker BioTyper (Bruker Daltonics) from DDT-contaminated sites. Among 25 strains, 4 were identified at the genus level whereas rest 21 strains were identified at the species level.

A category of environmental contaminants is hydrocarbons, and for successful biodegradation, it is crucial to isolate and characterize novel microorganisms with the capability to break down these pollutants. The diversity of the bacterial population in highly weathered oil-contaminated sites was studied using MALDI-TOF MS (Figure 2) and differentiation of the isolates was done by principal component analysis (PCA) and dendrogram analysis (Figure 3).²⁷ Microorganisms belonging to *Bacillus* species

were identified with high extracellular biosurfactant activities capable of biodegrading weather hydrocarbons. Silva et al.²⁸ reported isolation and identification of 44 bacteria were isolated from compost and identified using the 16S rRNA gene sequencing and MALDI-TOF MS techniques. 36 bacteria were discovered using MALDI-TOF MS at the species level such as *Bacillus shackletonii* and *Klebsiella pneumoniae* or genus levels such as *Gordonia*, *Acinetobacter*, *Stenotrophomonas* and *Pseudomonas*. Silva-Jimenez et al.²⁹ also studied the bacterial diversity of seawater, surface water and marine sediments and identified 52 bacteria using Bruker BioTyper (Bruker Daltonics) that has a high potential to degrade and utilize pyrene as the sole energy source. The bacteria identified belonged to *Actinobacteria*, *Proteobacteria* and *Firmicutes*.

Additionally, without the necessity for culture, it is also feasible to identify the enzymes responsible for the degradation of chemical hazards. In research published in 2015, Lovecka et al.³⁰ gathered isolates from polluted areas in the Czech Republic where they were able to break down lindane, hexachlorobenzene, and DDT (dichlorodiphenyl-trichloroethane). The amplification of the pesticide degradation genes *linA* and *bphA1* allowed researchers to analyze the degradation processes carried out by microorganisms. MALDI-TOF MS was used to identify six out of seven isolates which were *Rhodococcus* sp., *Aeromonas* sp., *Stenotrophomonas* sp. and three *Bacillus* sp. which was also cross-checked with 16S rRNA sequencing results. Furthermore, the in-situ monitoring of the bioremediation approach may also be done using MALDI-TOF MS. Undoubtedly, this technique can be utilized for more exploration.

Agriculture and plant pathology

In order to protect crops and boost agricultural productivity, several researchers have used MALDI-TOF MS to identify plant growth-promoting bacteria and pathogenic fungi. Researchers at the Federal University of Lavras, Brazil, have identified endophytic bacteria from garlic roots as potential plant growth promoters for commercial use.³¹ MALDI-TOF MS was used to analyze the microbial activities of 48 microorganisms, which included nitrogen fixation, phosphate production and siderophores production. The garlic roots contained *Burkholderia cepacia* and *Enterobacter cloacae*. Whereas Muthuri et al.³² isolated a total of 43 endophytic bacteria with potential plant growth-promoting activities from bananas and analyzed them using MALDI-TOF MS. The identified isolates belong to *Bacillus*, *Enterobacter*, *Ewingella*, *Klebsiella*, *Pseudomonas*, *Rahnella*, *Raoultella*, *Serratia*, *Yersinia* and *Yokenella*.

MALDI-TOF MS has been utilized to isolate and identify plant growth-promoting rhizobacteria (PGPR) in order to reduce heavy metal stress in plants. Pramanik et al.³³ reported the identification of *Klebsiella pneumoniae* K5 which has been reported to be highly resistant to

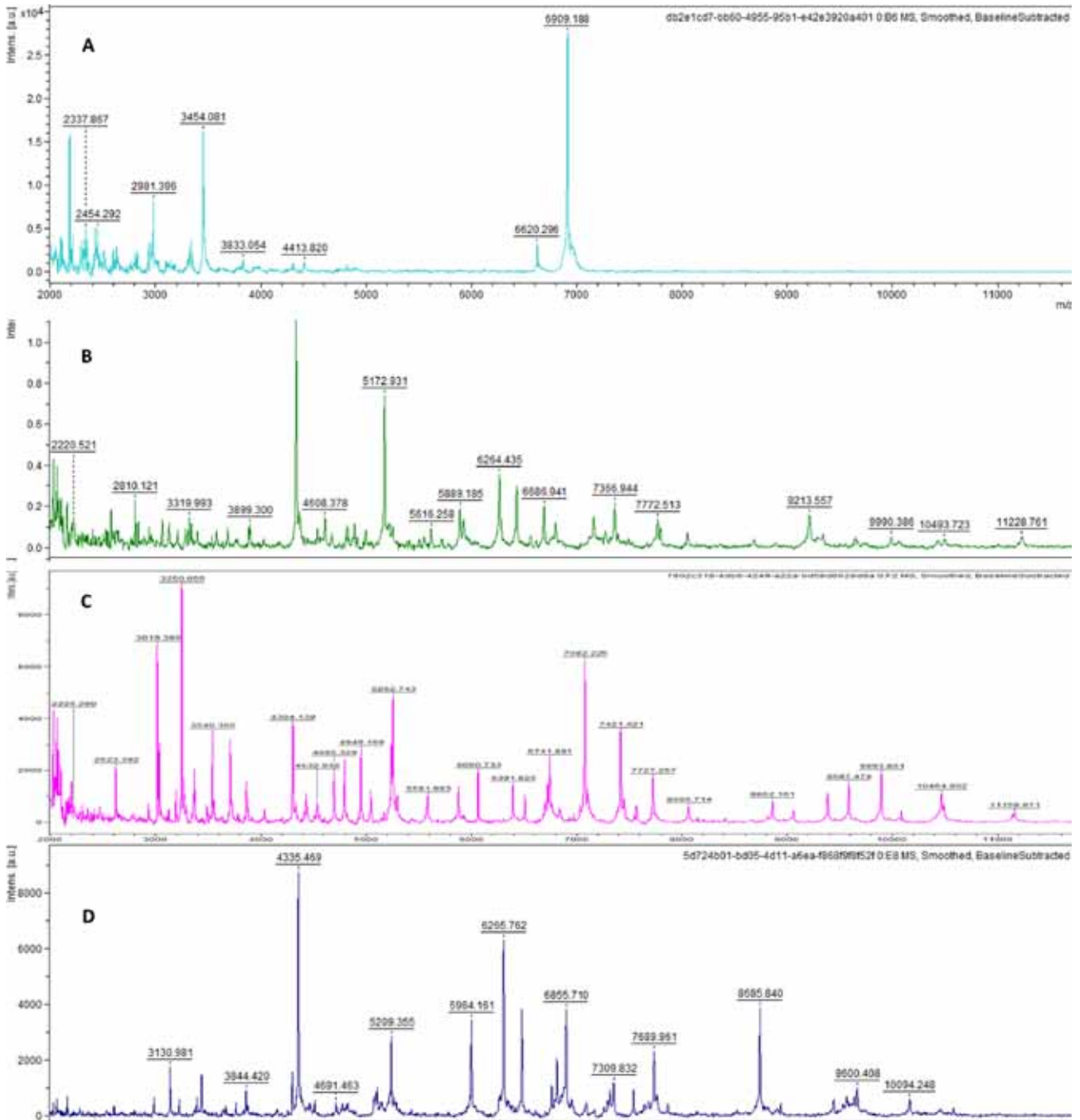


Figure 2. MALDI-TOF MS spectra of A) *Bacillus subtilis* (SA28), B) *Bacillus cereus* (SA17), C) *Bacillus licheniformis* (S33) and D) *Lysinibacillus boronitolerans* (SA3). Reprinted with from Alsayegh et al.²⁷ (2021).

cadmium stress with a value of 4 mg/ml. An easy MALDI-TOF MS-based novel method to identify and characterize zinc-solubilizing bacteria was also proposed by Costerousse et al.³⁴ Further salt-tolerant PGPR have been identified using MALDI-TOF MS for their use in agriculture to reduce stress in plants and promote growth.³⁵

The identification of plant pathogens using MALDI-TOF

MS technology has been established in several research. Plant pathogens infecting rice seedlings such as *Burkholderia gladioli* pv. *Gladioli*, *B. glumae* and *Erwinia chrysanthemi* pv. *Zae* have been identified using MALDI-TOF MS directly from sample extracts. Despite small spectral changes, MALDI-TOF MS analysis revealed that the extracts of infected rice seedlings generated peaks

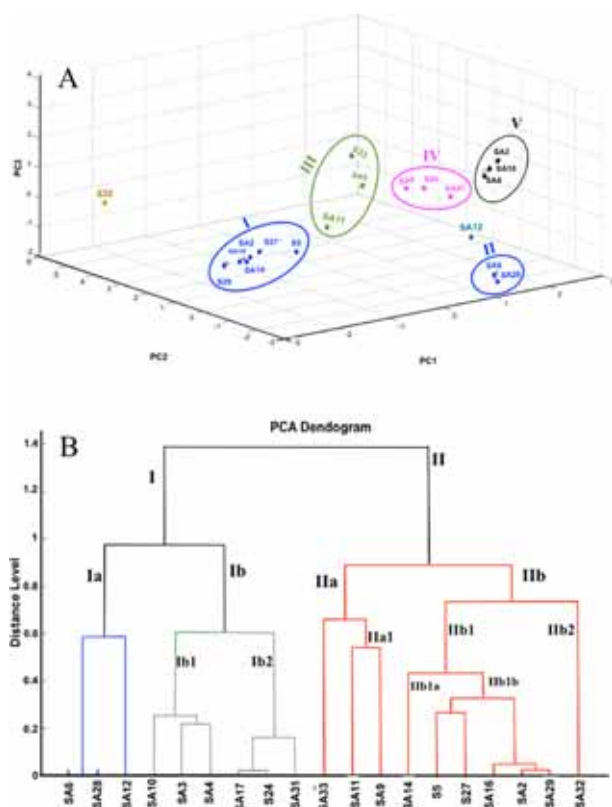


Figure 3. (A) Classification of studied strains using PCA plot (B) PCA dendrogram of the studied strains. Reprinted from Alsayegh et al.²⁷ (2021).

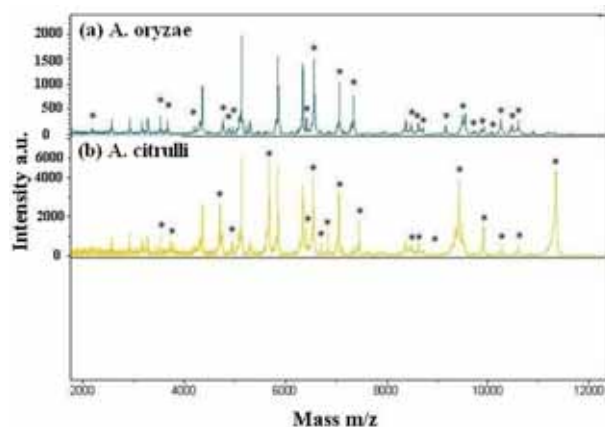


Figure 4. PMF obtains using MALDI-TOF MS for *A. oryzae* and *Acidovorax citrulli*. Reprinted from Wang et al.³⁸ (2012).

originating from bacteria with spectral peaks that had considerably high scores.³⁶ A novel strain *Pseudomonas grimontii*, which is potential pathogenic bacteria causing rot disease was identified using MALDI-TOF MS.³⁷ Wang et al.³⁸ differentiated two closely related plant pathogens which is even more difficult using the carbon source

utilization process and ELISA. The two strains were identified as *Acidovorax citrulli* and *A. oryzae* using MALDI-TOF MS (Figure 4). Similarly, two closely related pathovars of *Xanthomonas oryzae* have also been identified in the same process.³⁹ These citations from the literature highlight the potential and broad application of MALDI-TOF MS in the study of plant growth-promoting and growth-inhibiting bacteria.

Food microbiology and water treatment

It is crucial to rapidly detect pathogenic microorganisms in order to maintain the safety and quality of food and drink items. There are several different ways that microorganisms are connected to food. They may be included in the production of food items, they might cause food to spoil, and they might even spread through food. By recognizing and separating distinct lactic acid bacteria, fermentative bacteria and foodborne pathogenic bacteria, MALDI-TOF MS technology can contribute to the study of food microbiology. *Brochothrix thermosphacta* is one of the major strains responsible for seafood and meat spoilage and has been characterized using MALDI-TOF MS.⁴⁰ The quality of raw milk has a significant role in influencing the quality of dairy products that are made. In order to understand the impact of protracted refrigeration on the changes in raw milk microbial ecology, Zhang et al.⁴¹ investigated the quantities and kinds of psychrotrophic in raw milk with and without refrigerated enrichment (5 days at 7°C). *Pseudomonas* was observed to have the highest abundance among 119 isolates from fresh raw milk belonging to 12 genera and 23 species. Whereas, after refrigeration for 5 days, 127 isolates classified as 9 genera and 20 species were identified. This technique has further been used for the characterization of bacteria present in milk, yogurt and probiotics and bacteria responsible for the spoilage of milk and pork, biogenic amine-producing bacteria, and causative agents for seafood-borne bacteria.¹⁰

MALDI-TOF MS has been applied to the bacterial examination of drinking water, wastewater, and natural waterways for environmental monitoring. In a recent study, bacterial components in tap water and mineral water were identified. A total of 10 samples of mineral water from various brands and 11 samples of tap water from various localities were acquired.⁴² *Alphaproteobacteria* were more prevalent in tap water than *Gammaproteobacteria*, which were often isolated from mineral water, resulting in differences in the bacterial diversity found in the two distinct forms of drinking water. Additionally, because some of the bacteria were only found during one season, the season in which the water was bottled also had an impact on the variety and abundance of bacteria. The study demonstrated that the MALDI-TOF MS is an effective approach for frequently checking the quality of water in the water business and may be used to determine the variety of bacteria in the water meant for human consumption.

Challenges and future perspectives

Although MALDI-TOF MS has been shown for its potential and applicability in routine analysis for microbial identification, however, till date it possesses certain limitations. *Bacteroides fragilis* group (BFG) isolated from various environmental samples including human and rat fecal matter, sewage from wastewater treatment plants, etc. were investigated by MALDI-TOF MS. The results showed variation in accuracy for hospital and untreated wastewater (20%), wastewater (40%) and human and rat fecal samples (100%). This could be due to the similarity of strains from various samples for which the MS database was optimized.⁴³ A study was conducted to explore the accuracy of identification by MALDI-TOF MS for 21 globally distributed species of *Burkholderia cepacia*. However, the accuracy for detection and characterization has been reported to be affected due to the high similarity between the species. Based on various studies for clinical as well as environmental samples related to the identification of the *B. cepacia* complex, the accuracy is significantly low for environmental strains as compared to clinical strains.⁴⁴⁻⁴⁶

The most essential step in identifying a species is comparing the PMF of an unknown isolate to reference mass fingerprints in a database, which necessitates a database to contain mass fingerprints of different strains of each species as well as reference mass fingerprints of all species of relevance. To enhance the spectrum depiction of the bacterial species, the sample preparation guidelines and spectral profile analysis (baseline subtraction, normalization, and others) need to be standardized. Insufficient spectral data in the public database is a major challenge today. However, the establishment of a drinking water library by Pinar-Mendez et al. is the most current and top-notch illustration of an internal database which is used as the alternative solution for the insufficient database. The incorporation of in-house databases into the public open-access databases and the development of user-friendly and cheaper software for analyses will further boost the credibility of the technology in near future.

Conclusions

MALDI-TOF MS has been demonstrated to be a workhorse in proteomics and can be a powerful tool in the investigation of environmental microbiology and bioremediation. Through comparison with molecular methods, several studies have proven the effectiveness of MALDI-TOF for the identification of environmental bacteria and concluded that this is an efficient and appropriate approach for environmental bacteria. With future advancements in reference bacteria database libraries, frequent implementation in environmental investigations should be promoted owing to time savings and cost-effectiveness. The method

has been used with great accuracy and precision to identify a variety of bacteria, including those that are important for the environment and biotechnology such as those that degrade pollutants, biomineralize, fermentative, food- and water-borne diseases, produce coliforms and lactic acid, and relate to and promote plant development. Additionally, it also monitors environmental routines that improved in quick identification of bacteria present in water, air, and other surfaces.

There are still unexplored potential uses for MALDI-TOF MS technology. These applications may include the proteins and enzymes detection synthesized by bacteria for a particular environmental purpose, such as the synthesis of biosurfactants, minerals, or pollutants. The approach may be used to identify the relevant proteins/genes utilizing advanced bioinformatics techniques. Ultimately, there is a discrepancy between the taxonomic identity of bacteria and their prospective environmental functions. This gap must be closed through more research and development in order to maximize the technology's potential for environmental investigations and assure quick research breakthroughs through time and money savings.

Conflict of interest

There are no conflicts to declare.

Acknowledgements

This work was supported by the National Research Foundation of Korea Grant funded by the Ministry of Science and ICT (MSIT), Korean Government, (grant no. 2021-DD-RD-0012; P0020819; C230222).

References

1. Franco-Duarte, R., Černáková, L., Kadam, S., S. Kaushik, K., Salehi, B., Bevilacqua, A., Corbo, M.R., Antolak, H., Dybka-Śtepiń, K., Leszczewicz, M., Relison Tintino, S. *Microorganisms* **2019**, *7*, 130. DOI: 10.3390/microorgansms7050130
2. Sauer, S., Kliem, M. *Nature Reviews Microbiology*, **2010**, *8*, 74. DOI: 10.1038/nrmicro2243
3. Everley, R.A.; Mott, T.M.; Wyatt, S.A.; Toney, D.M.; Croley, T.R. *Journal of the American Society for Mass Spectrometry* **2008**, *19*, 1621. DOI: 10.1016/j.jasms.2008.07.003
4. Ekström, S.; Önnarfjord, P.; Nilsson, J.; Bengtsson, M.; Laurell, T.; Marko-Varga, G. *Analytical chemistry* **2000**, *72*, 286. DOI: 10.1021/ac990731l
5. Holland, R.; Wilkes, J.; Rafii, F.; Sutherland, J.; Persons, C.; Voorhees, K.; Lay Jr, J. *Rapid Communications in Mass Spectrometry* **1996**, *10*, 1227. DOI: 10.1002/(SICI)1097-0231(19960731)10:10<1227::AID-RCM659>3.0.CO;2-6

6. Krishnamurthy, T.; Rajamani, U.; Ross, P. *Rapid Communications in Mass Spectrometry* **1996**, *10*, 883. DOI: 10.1002/(SICI)1097-0231(19960610)10:8<883::AID-RCM594>3.0.CO;2-V
7. Kostrzewa, M.; Spärbier, K.; Maier, T.; Schubert, S. *PROTEOMICS—Clinical Applications* **2013**, *7*, 767. DOI: 10.1002/prca.201300042
8. Fenselau, C.C. *Journal of the American Society for Mass Spectrometry* **2013**, *24*, 1161. DOI: 10.1007/s13361-013-0660-7
9. Biswas, S.; Rolain, J.-M. *Journal of microbiological methods* **2013**, *92*, 14. DOI: 10.1016/j.mimet.2012.10.014
10. Singhal, N.; Kumar, M.; Kanaujia, P.K.; Viridi, J.S. *Frontiers in microbiology* **2015**, *6*, 791. DOI: 10.3389/fmicb.2015.00791
11. Wang, Z.; Russon, L.; Li, L.; Roser, D.C.; Long, S.R. *Rapid Communications in Mass Spectrometry* **1998**, *12*, 456. DOI: 10.1002/(SICI)1097-0231(19980430)12:8<456::AID-RCM177>3.0.CO;2-U
12. Ruelle, V.; Moulalij, B.E.; Zorzi, W.; Ledent, P.; Pauw, E.D. *Rapid Communications in Mass Spectrometry* **2004**, *18*, 2013. DOI: 10.1002/rcm.1584
13. Ashfaq, M.Y.; Da'na, D.A.; Al-Ghouti, M.A. *Journal of Environmental Management* **2022**, *305*, 114359. DOI: 10.1016/j.jenvman.2021.114359
14. Havlicek, V.; Lemr, K.; Schug, K.A. *Analytical chemistry* **2013**, *85*, 790. DOI: 10.1021/ac3031866
15. Dingle, T.C.; Butler-Wu, S.M. *Clinics in laboratory medicine* **2013**, *33*, 589. DOI: 10.1016/j.cll.2013.03.001
16. Martiny, D.; Busson, L.; Wybo, I.; El Haj, R.A.; Dediste, A.; Vandenberg, O. *Journal of clinical microbiology* **2012**, *50*, 1313. DOI: 10.1128/JCM.05971-11
17. De Carolis, E.; Vella, A.; Vaccaro, L.; Torelli, R.; Spanu, T.; Fiori, B.; Posteraro, B.; Sanguinetti, M. *The Journal of Infection in Developing Countries* **2014**, *8*, 1081. DOI: 10.3855/jidc.3623
18. Sandrin, T.R.; Goldstein, J.E.; Schumaker, S. *Mass spectrometry reviews* **2013**, *32*, 188. DOI: 10.1002/mas.21359
19. Dieckmann, R.; Graeber, I.; Kaesler, I.; Szewzyk, U.; Von Döhren, H. *Applied microbiology and biotechnology* **2005**, *67*, 539. DOI: 10.1007/s00253-004-1812-2
20. Zeng, Y.; Wu, N.; Madsen, A.M.; Chen, X.; Gardiner, A.T.; Koblížek, M. *Frontiers in microbiology* **2021**, *11*, 606612. DOI: 10.3389/fmicb.2020.606612
21. Powthong, P.; Suntornthiticharoen, P. *Bulgarian Journal of Agricultural Science* **2018**, *24*, 623.
22. Donohue, M.J.; Best, J.M.; Smallwood, A.W.; Kostich, M.; Rodgers, M.; Shoemaker, J.A. *Analytical chemistry* **2007**, *79*, 1939. DOI: 10.1021/ac0611420
23. Nosál'ová, L.; Maliničová, L.; Kisková, J.; Timková, I.; Sedláková-Kaduková, J.; Pristaš, P. *Geomicrobiology Journal* **2021**, *38*, 415. DOI: 10.1080/01490451.2021.1871685
24. Malinicova, L.; Nosal'ova, L.; Timkova, I.; Pristas, P.; Sedlakova-Kadukova, J. *Inžynieria Mineralna* **2020**. . DOI: 10.29227/IM-2020-01-47
25. Vidali, M. *Pure and applied chemistry* **2001**, *73*, 1163. DOI: 10.1351/pac200173071163
26. Garcia Lara, B.; Wrobel, K.; Corrales Escobosa, A.R.; Serrano Torres, O.; Enciso Donis, I.; Wrobel, K. *Folia Microbiologica* **2021**, *66*, 355. DOI: 10.1007/s12223-020-00848-8
27. Alsayegh, S.Y.; Al Disi, Z.; Al-Ghouti, M.A.; Zouari, N. *Biotechnology Reports* **2021**, *31*, e00660. DOI: 10.1016/j.btre.2021.e00660
28. Silva, N.M.; de Oliveira, A.M.S.A.; Pegorin, S.; Giusti, C.E.; Ferrari, V.B.; Barbosa, D.; Martins, L.F.; Morais, C.; Setubal, J.C.; Vasconcellos, S.P. *PLoS One* **2019**, *14*, e0215396. DOI: 10.1371/journal.pone.0215396
29. Silva-Jiménez, H.; Araujo-Palomares, C.L.; Macias-Zamora, J.V.; Ramírez-Álvarez, N.; García-Lara, B.; Corrales-Escobosa, A.R. *Journal of the Mexican Chemical Society* **2018**, *62*, 214. DOI: 10.29356/jmcs.v62i2.411
30. Lovecka, P.; Pacovska, I.; Stursa, P.; Vrchotova, B.; Kochankova, L.; Demnerova, K. *New biotechnology* **2015**, *32*, 26. DOI: 10.1016/j.nbt.2014.07.003
31. Júnior, P.S.P.C.; Cardoso, F.P.; Martins, A.D.; Buttrós, V.H.T.; Pasqual, M.; Dias, D.R.; Schwan, R.F.; Dória, J. *Microbiological research* **2020**, *241*, 126585. DOI: 10.1016/j.micres.2020.126585
32. Muthuri, C.; Nyambura, N.; Njeri, V.; Tani, A.; Wangari, M. *Afr. J. Microbiol. Res* **2012**, *6*, 6414. DOI: 10.5897/AJMR12.1112
33. Pramanik, K.; Mitra, S.; Sarkar, A.; Soren, T.; Maiti, T.K. *Environmental Science and Pollution Research* **2017**, *24*, 24419. DOI: 10.1007/s11356-017-0033-z
34. Costerousse, B.; Schönholzer-Mauclaire, L.; Frossard, E.; Thonar, C. *Applied and environmental microbiology* **2018**, *84*, e01715. DOI: 10.1128/AEM.01715-17
35. Sarkar, A.; Pramanik, K.; Mitra, S.; Soren, T.; Maiti, T.K. *Journal of plant physiology* **2018**, *231*, 434. DOI: 10.1016/j.jplph.2018.10.010
36. Kajiwarra, H. *Journal of microbiological methods* **2016**, *120*, 1. DOI: 10.1016/j.mimet.2015.08.014
37. Sawada, H.; Horita, H.; Misawa, T.; Takikawa, Y. *Journal of general plant pathology* **2019**, *85*, 413. DOI: 10.1007/s10327-019-00869-3
38. Wang, Y.; Zhou, Q.; Li, B.; Liu, B.; Wu, G.; Ibrahim, M.; Xie, G.; Li, H.; Sun, G. *BMC microbiology* **2012**, *12*, 1. DOI: 10.1186/1471-2180-12-182
39. Ge, M.; Li, B.; Wang, L.; Tao, Z.; Mao, S.; Wang, Y.; Xie, G.; Sun, G. *Spectrochimica Acta Part A: Molecular and Biomolecular Spectroscopy* **2014**, *133*, 730. DOI: 10.1016/j.saa.2014.06.056
40. Illikoud, N.; Rossero, A.; Chauvet, R.; Courcoux, P.; Pilet, M.-F.; Charrier, T.; Jaffrès, E.; Zagorec, M. *Food microbiology* **2019**, *81*, 22. DOI: 10.1016/j.fm.2018.01.015
41. Zhang, D.; Palmer, J.; Teh, K.H.; Flint, S. *Lwt* **2020**, *134*, 110165. DOI: 10.1016/j.lwt.2020.110165

42. Sala-Comorera, L.; Caudet-Segarra, L.; Galofré, B.; Lucena, F.; Blanch, A.R.; García-Aljaro, C. *International Journal of Food Microbiology* **2020**, 334, 108850. DOI: 10.1016/j.ijfoodmicro.2020.108850
43. Niestepski, S.; Harnisz, M.; Korzeniewska, E.; Osińska, A. **2019**. Isolation of anaerobic bacteria of the *Bacteroides fragilis* group from environmental samples. In *E3S Web of Conferences*: EDP Sciences. 00058. DOI: 10.1051/e3sconf/201910000058
44. Furlan, J.P.R.; Pitondo-Silva, A.; Braz, V.S.; Gallo, I.F.L.; Stehling, E.G. *World Journal of Microbiology and Biotechnology* **2019**, 35, 1. DOI: 10.1007/s11274 -019-2614-0
45. Vicenzi, F.J.; Pilonetto, M.; Souza, H.A.P.H.d.M.d.; Palmeiro, J.K.; Riedi, C.A.; Rosario-Filho, N.A.; Dalla-Costa, L.M. *Memórias do Instituto Oswaldo Cruz* **2016**, 111, 37. DOI: 10.1590/0074-02760150314
46. Fehlberg, L.C.C.; Andrade, L.H.S.; Assis, D.M.; Pereira, R.H.V.; Gales, A.C.; Marques, E.A. *Diagnostic microbiology and infectious disease* **2013**, 77, 126. DOI: 10.1016/j.diagmicrobio.2013.06.011
47. Pinar-Méndez, A.; Fernández, S.; Baquero, D.; Vilaró, C.; Galofré, B.; González, S.; Rodrigo-Torres, L.; Arahal, D.R.; Macián, M.C.; Ruvira, M.A. *Water Research* **2021**, 203, 117543. DOI: 10.1016/j.watres.2021.117543

Combining the Power of Advanced Proteome-wide Sample Preparation Methods and Mass Spectrometry for defining the RNA-Protein Interactions

Tong Liu¹, Chaoshuang Xia², Xianyu Li^{1,3*}, and Hongjun Yang^{1*}

¹Beijing Key Laboratory of Traditional Chinese Medicine Basic Research on Prevention and Treatment for Major Diseases, Experimental Research Center, China Academy of Chinese Medical Sciences, Beijing, 100010, China

²Key Laboratory of Synthetic and Natural Function Molecule Chemistry of Ministry of Education, College of Chemistry and Materials Science, Northwest University, Xi'an 710069, China

³State key Laboratory of innovative Natural Medicine and TCM Injection, Jiangxi Qingfeng Pharmaceutical Co.,Ltd.

Received December 6, 2022; Revised December 23, 2022; Accepted December 23, 2022

First published on the web December 31, 2022; DOI: 10.5478/MSL.2022.13.4.115

Abstract : Emerging evidence has shown that RNA-binding proteins (RBPs) dynamically regulate all aspects of RNA in cells and involve in major biological processes of RNA, including splicing, modification, transport, transcription and degradation. RBPs, as powerful and versatile regulatory molecule, are essential to maintain cellular homeostasis. Perturbation of RNA-protein interactions and aberration of RBPs function is associated with diverse diseases, such as cancer, autoimmune disease, and neurological disorders. Therefore, it is crucial to systematically investigate the RNA-binding proteome for understanding interactions of RNA with proteins. Thanks to the development of the mass spectrometry, a variety of proteome-wide methods have been explored to define comprehensively RNA-protein interactions in recent years and thereby contributed to speeding up the study of RNA biology. In this review, we systematically described these methods and summarized the advantages and disadvantages of each method.

Keywords : proteomics, mass spectrometry, RNA-binding proteins, enrichment, RNA-protein interactions

Introduction

As delivery intermediate of genetic information in biological systems, RNA usually interacts with proteins, which are called RBPs, to form dynamic ribonucleoprotein complexes (RNPs) for implementing crucial biological functions.¹ RBPs widely participate in various biological processes of post-transcriptional gene regulation (PTGR), and also regulate every stage of the lifetime of RNA, from transcription, translation and through to decay.² As one salient example, pre-mRNA is regulated by mRNA binding proteins (mRBPs) to form mature mRNA through splicing, 5' end capping and 3' end processing.³ The mature

mRNA is exported to cytoplasm by specific mRBPs assistance for translation.^{4,5} Degradation of mRNA also requires a large number of mRBPs. Cumulative evidence has also shown that long non-coding RNA (lncRNA) may regulate biological processes such as chromatin modification, and apoptosis.^{6,7} In a word, the RBPs may regulate RNA modifications, localization, translation, and stability. Reciprocally, the corresponding RNAs can also affect functions and localization of RBPs.⁸ To date, a variety of RBPs have been investigated in eukaryotic cell. Individual RNA-protein interactions can form an intricate network to regulate complicated cellular processes. Of course, the broader research has uncovered that the deficiency or aberration of RBPs is closely involved in the occurrence and development of numerous diseases,^{9,10} including metabolic disorders, autoimmune disease, neurological disorders and cancer.¹¹⁻¹⁴ Considering the importance of their functions, numerous studies are paying special attention to the comprehensive identification and precise quantification of RBPs. However, it is still challenging to study their interactions with RNAs due to the low stoichiometry of RBPs, the ubiquity of RNase which can easily degrade the RNA and the immense complexity of RNA-protein interactions network. Therefore, it is of great significance to design an unbiased and effectively method for large-scale identification of

Open Access

*Reprint requests to Xianyu Li, Hongjun Yang

<https://orcid.org/0000-0001-9625-8476>

<https://orcid.org/0000-0001-5501-3288>

E-mail: phd_xianyuli@foxmail.com, hongjun0420@vip.sina.com

All the content in Mass Spectrometry Letters (MSL) is Open Access, meaning it is accessible online to everyone, without fee and authors' permission. All MSL content is published and distributed under the terms of the Creative Commons Attribution License (<http://creativecommons.org/licenses/by/3.0/>). Under this license, authors reserve the copyright for their content; however, they permit anyone to unrestrictedly use, distribute, and reproduce the content in any medium as far as the original authors and source are cited. For any reuse, redistribution, or reproduction of a work, users must clarify the license terms under which the work was produced.

RBPs. The initial research was confined to an RNA of interest and focused on the binding proteins, or a protein of interest and RNA that associate with it.¹⁵⁻¹⁷ These methods that aimed to single biomolecule of interest may omit the dynamic interaction from molecular networks. Compared with RNA-sequencing, the study of RBPs is more challenging due to low abundance and lack of amplification.¹⁸ Benefitting from the development of mass spectrometry, recent years have seen the emergence of numerous methods aimed at investigating the RNA-binding proteome systemically. Because each method has some strengths and drawbacks, it is necessary to choose optimal methods according to relevant research question. In this review, we systematically summarized methods for studying RNA-protein interactions on proteome-wide scale based on different principles recent years and provided a selection for scientists to address a particular biological question.

The poly(A)-based technologies

Based on the principle of complementary base pairing of Watson-Crick, RNA and directly bound proteins could be captured through hybridization of the poly(A) tails of RNA and oligo(dT) beads. That opened up the systematic identification of RBPs. The first widely accepted technology was reported Castello et.al in 2012,¹⁹ referred to as RNA-interactome capture (RIC). In this method, RNAs and proteins that directly bound were firstly “frozen” by widely used UV-crosslinking *in vivo*. As shown in Figure 1, cells were lysed under denaturing conditions, and the sequential RNA-protein complexes were enriched by oligo(dT) beads. The proteins were released by RNase treatment after several stringent washing. Following protease treatment, mass spectrometry-based proteomics was used to identify high confidence RBPs. Besides, RNAs from RNPs were released by proteinase K treatment and analyzed via high-throughput sequencing. Applied to HeLa cells, Castello et

al.¹⁹ discovered 860 RBPs by RIC coupled with mass spectrometry, including 300 novel RBPs. Using RIC and mass spectrometric analysis, ~800 RBPs were identified in HEK293 cells by Baltz et.al, many of which were unknown RBPs previously.²⁰ RIC yielded numerous RBPs from various biological origins, including several human cell lines,²¹⁻²³ mouse cell lines,^{11,24,25} *Saccharomyces cerevisiae*^{26,27} and *Caenorhabditis elegans*,²⁷ *Leishmania donovani*,²⁸ *Plasmodium falciparum*,²⁹ *Trypanosoma brucei*,³⁰ *Arabidopsis thaliana*,^{31,32} *Drosophila*^{33,34} and zebrafish.³⁵ Hentze et al.³⁶ summarized all published RNA interactomes into RBPs supersets according to different source. It greatly enriched the RBPs item. It is worth mentioning that metabolic enzymes, which play key functional roles in biological systems, were also identified as RBPs. For example, a high proportion of metabolic enzymes involved in glycolytic pathway were identified as RBPs in the human hepatocyte HuH7 cell.²⁷ Likewise, the RBPs that reported in the HL-1 cardiomyocyte cell included many mitochondrial metabolic enzymes involved in the tricarboxylic acid cycle, fatty acid oxidation and so on.¹¹ Hentze³⁷ laboratory presented alternative method, called enhanced RNA Interactome Capture (eRIC), which mainly used Locked Nucleic Acid (LNA)-modified capture probe instead of oligo(dT) beads. Applying the Jurkat cells, 683 and 588 RBPs were characterized from eRIC and RIC, respectively. Compared to the RIC, eRIC has notably advantages, such as excellent specificity, greater sensitivity and lower contamination from rRNA and DNA. Castello et al.³⁸ developed a comparative RNA Interactome Capture (cRIC) by combining stable isotopic labeling by amino acids in cell culture (SILAC)-based mass spectrometry, which could study the dynamic of the RBPs upon the virus infection. As a result, 794 proteins were identified in total, 91% of which were reported to be RBPs in eukaryotic cells. Moreover, 247 RBPs changed their binding activity after infected virus. It revealed that virus infection could

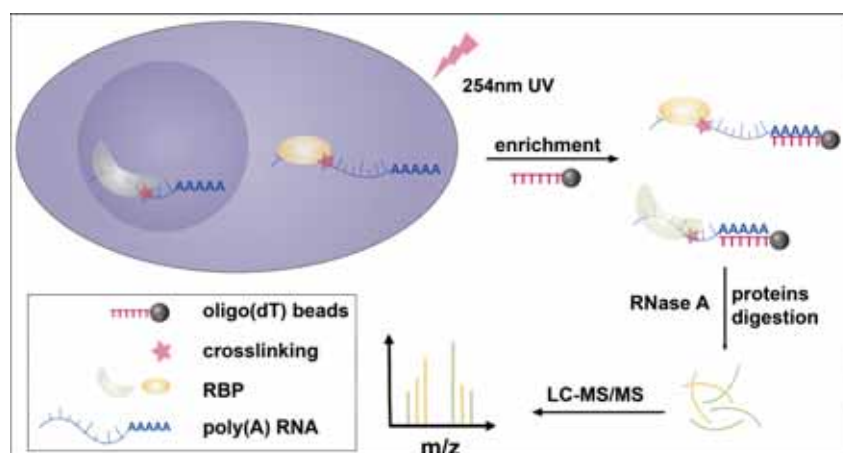


Figure 1. Schematic representation of the RNA-interactome capture. Only the significant steps are shown.

rearrange the cellular RBPs to regulate the life cycle of virus. They also used cRIC tandem quantitative mass spectrometry to systematically and comprehensively discovered the cellular RBPs that responded to severe acute respiratory syndrome coronavirus 2 (SARS-CoV-2) infection.³⁹ In their work, they uncovered that the cellular RBPs could be remodeled upon the SARS-CoV-2 infection. The RNA metabolic pathways were profoundly affected. They also described viral RNA interactome capture (vRIC) and revealed dozens of cellular RBPs and six viral RBPs that directly interacted with viral RNA. Furthermore, available antiviral drugs targeting host RBPs were identified as being capability of inhibiting infection against the SARS-CoV-2. It demonstrated that the RBPs have enormous potential for antiviral therapies.

Notably, most RBPs comprise one or multiple well-known RNA-binding domains (RBDs), where they interact with target RNA.⁴⁰ With the in-depth study, however, researchers noticed that many novel RBPs are lacking canonical RBDs. Meanwhile, the mutations of RBDs could be the cause of numerous monogenic diseases.⁴¹ Consequently, much attention was devoted to identifying the regions of RBPs interaction with RNA. As shown in Figure 2, in order to depict an atlas of RNA-binding sites in a proteome-wide manner, Castello et al.^{42,43} developed RBDmap-based approach, which combined UV cross-linking, oligo(dT) capture, controlled proteolysis and mass spectrometry to discover high-confidence RNA-binding sites on a proteome-wide scale. In brief, the RNA–protein complexes were primarily purified with the aforementioned RIC. After elution, the RBPs were partial digested and separated by a second round of oligo(dT) purification yielding two classes of peptides: (1) peptides released into the supernatant and (2) peptides remain bound to RNA. Subsequently, peptides remain bound to RNA were further subjected to proteolysis generating two types of peptides, including the peptides still covalently bound to the RNA, referred to X-link, and its neighboring peptides (N-link). It was difficult to

characterize X-link due to various mass shift resulting from residual nucleotides, while N-link could be easily identified by mass spectrometry and search algorithms. Most importantly, the RNA-binding region of RBPs, namely RBDpep, composed of X-link peptides and N-link peptides. The RNA-binding sites were detected through analysis of the RNA-bound and released fractions by mass spectrometry-based quantitative proteomics. Ultimately, they identified 1174 RNA-binding sites derived from 529 RBPs in HeLa cells. Plus, RBDmap has also proven its utility in HL-1 cardiomyocytes, for which RBDmap dissected the 568 RNA-binding regions of 368 murine proteins by mass spectrometry.

Overall, with the development and application of mass spectrometry, the advent of RNA interactome capture not only opened up the opportunities to system-wide identification of RBPs but also supported for the comprehensive study of RNA-protein interaction. Moreover, the discovery of novel RBPs with lack of classical RBD but closely relate to biological function implicated that the potential roles of RBPs need to be investigated in depth urgently.³⁶ Nevertheless, the poly(A)-based technologies are only limited to RBPs that bound poly(A) RNA. It is not suitable for unearthing the nonpoly(A) RNAs, including most ncRNAs and organisms without poly(A) RNA such as bacteria and many archaea.⁴⁴ Where proteins interacting with mRNA are of interest, the poly(A)-based technologies are recommendable.

The nucleotide analogs-based methods

Further efforts to extend into the nonpoly(A) RNA bound proteome had focused on methods that were used to nucleotide analogs tandem with click chemistry to capture proteins bound to nascent RNA, regardless of the polyadenylation state of RNA. Two more promising methods were published in different cells and systems. Bao et al.⁴⁵ presented an RNA interactome using click chemistry (RICK) method, which enabled to identify a wide range of RNA bound proteome. As illustrated in

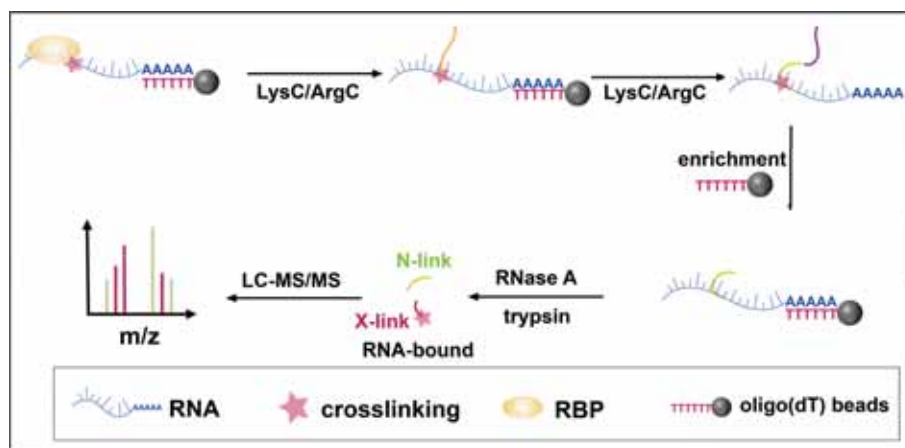


Figure 2. Schematic diagram for RBDmap. Only the significant steps are shown.

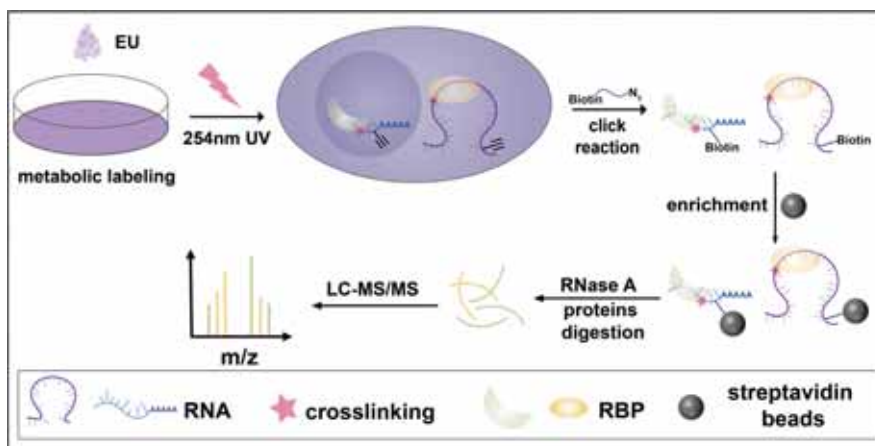


Figure 3. Schematic illustration of the nucleotide analogs-based methods. Only the significant steps are shown.

Figure 3, they exploited an alkynyl uridine analog, 5-ethynyluridine (EU), to label the newly transcribed RNA in living cells, followed by *in vivo* fixed the RNA-proteins with 254 nm UV light. Combined with click chemistry, the alkynyl could react with the azide-biotin to gain biotinylated RNA. Subsequent biotinylated RNA and covalently cross-linked proteins were captured via streptavidin beads. The resulting isolated RBPs were characterized and quantified by mass spectrometry. Consequently, a high-confidence RNA-binding proteomes containing 720 proteins and 518 proteins were identified from HeLa cells and mouse embryonic stem cells (mESCs), respectively. Contemporary, Chen's lab⁴⁶ introduced the same procedure, but used a photoactivatable uridine analog 4-thiouridine (4SU) by 365-nm UV light to cross-link RNA-proteins instead of 254nm light directly. This unbiased method was termed click chemistry-assisted RNA interactome capture (CARIC) and yielded 597 proteins constituting HeLa cells RNA interactome with the help of mass spectrometry. These two methods that were designed to profile RBPs by mass spectrometer rely on the alkynyl uridine analog-assisted click chemistry.

Overall, the combination of mass spectrometric methods and nucleotide analogs-based methods overcomes the limitations of the poly(A)-based technologies. CARIC and RICK were not restricted to the analysis of RBPs that associated with polyadenylated RNA, but could extend to the proteomic profiling interacting with all types of RNA. In addition, it might facilitate an in-depth interrogation of the complex regulatory mechanisms of the ncRNA bound proteins. Unfortunately, the nucleotide analogs-based methods embed artificially introduced nucleotide analogues into newly synthesized RNA through transcription. Therefore, the method is aimed at the analysis of newly transcribed RNA-bound proteins during process of cell culture, which mainly have the following two defects. Firstly, metabolic labeling may interfere with cellular physiological processes, such as

the inhibition of rRNA synthesis, nucleolar stress response,⁴⁷ and decreased cell viability.^{44,48} Secondly, bias may be introduced due to ignoring RNA that is already present. For studies targeting at nascent RNA-binding proteins, the nucleotide analogs-based methods may be a better choice.

The phase separation-based strategies

Phase separation has advanced the field by offering strategy that can be used for isolating RNA and proteins. The rationale of strategy is that RNA can repartition to the upper aqueous phase in the acidic guanidinium thiocyanate/phenol/chloroform (also called Trizol), while proteins remain in the lower organic phase.⁴⁹ Owing to the opposing physicochemical properties of the RNA and proteins, RNA-protein complexes would be concentrated at the interphase. Exploiting the phase separation offered a promising novel direction for the field of comprehensive identification of RNA-protein interactions. Therefore, three teams successively published effective strategies, named Orthogonal Organic Phase Separation (OOPS)⁵⁰ and Protein-Crosslinked RNA Extraction (XRNAX)⁵¹ as well as Phenol Toluol Extraction (PTex)⁵², that repurposed phase separation to enrich the cellular RNA-binding proteomes from the interface layer and catalog them with mass spectrometric analysis (Figure 4). Indeed, the crude RNA-protein complexes were obtained at the interface using Trizol in OOPS and XRNAX. The OOPS strategy undergone three consecutive rounds of phase separation to purify RNA-protein complexes. The RBPs migrated from the interface to the organic phase followed by RNase treatment. Benefit of high-throughput mass spectrometry, OOPS resulted in 1267 RNA-binding proteomes for U2OS cells, 1410 RNA-binding proteomes for HEK293 cells, and 1165 RNA-binding proteomes for MCF10A cells by mass spectrometry-based proteomics analysis, of which 759 proteins were shared by three human cell lines. Notably,

OOPS was used to obtain 364 RBPs of *E. coli*, including new discovered sRNA binding protein (ProQ)⁵³. It was the first systematically retrieved the RBPs from prokaryotes. By performing a single Trizol phase separation, XRNAX was able to produce crude RNA-protein complexes that were then subjected to limited protease digestion, resulting in RNA crosslinked to peptides. Reliable RBPs separation was achieved through an additional silica-based columns purification prior to mass spectrometric analysis. Applied to MCF7, HeLa and HEK293 cell lines, XRNAX yielded 1207, 1239 and 1357 high-confidence RBPs from three cell lines respectively. They discovered 858 RBPs shared among the three cell lines. Furthermore, the dynamics of RNA-proteins interactions was explored during arsenite stress using XRNAX incorporated an additional silica enrichment and mass spectrometric analysis. In terms of the results, most RBPs did not change the interaction with RNA, whereas several proteins represented remarkable decline their RNA-binding capacity under arsenite stress. Coincidentally, Hentze et al.⁵⁴ introduced a rapid strategy to enrich RNA-proteins, known as complex capture (2C). The principle on the basis of the strategy is that the nucleic acid can selectively retain to silica matrix columns. Based on this, the cross-linked RNA-proteins can also retain to the silica columns compared with non-cross-linked proteins⁵⁵. The following year Shchepachev et al.⁵⁶ described total RNA-associated protein purification (TRAPP) strategy which mainly based on recovery of all cross-linked RNA-proteins on silica beads. The described strategy entailed the extraction of cross-linked RNA-proteins under acidic condition and in-gel trypsin digestion of RBPs, followed by liquid chromatography-mass spectrometric analysis. They used yeast and *E. coli* for proof-of-principle experiments and discovered more novel RBPs. Although this strategy has broad applicability for RBPome characterization, the silica-based methods suffer from low recovery from silica gel columns. PTex described an alternative strategy that utilized a neutral mixture of

phenol: toluol to shift RNA, proteins and cross-linked RNPs into the aqueous phase, while the DNA and lipids were distributed to the interface. The aqueous phase was subsequently recovered and extracted twice using acidic phenol. On this condition, the RNPs were migrated to the interface, away from RNA in the upper aqueous layer and proteins in the lower organic layer. Eventually, the interface was subjected to precipitate using ethanol to highly enrich the cross-linked RNPs. The purified RNPs could be protease digestion and directly analysis by liquid chromatography-mass spectrometry. By applying this strategy, 3037 RBPs were significantly enriched from HEK293 cells.

Proximity labeling (PL) is a widely applicable tool for deciphering of molecular interactions in subcellular organelles and compartments of interest with nanometer-scale spatial resolution.⁵⁷ It would be an important step to a better separating subcellular region in complex cells. PL also integrated with RNA-proteins enrichment strategy to profile RNA-protein interactions in different subcellular regions. Qin et al.⁵⁸ have extensive experience in subcellular molecular interactions using PL. In particular, they turned attention to decipher of the RNA-protein interactions in spatially and temporally resolution. They developed a method that peroxidase-catalyzed PL combined with phase separation (APEX-PS) to categorize RBPs from specific subcellular regions (Figure 5a). By combining APEX-PS with mass spectrometry, they generated several RBPs datasets for nuclear, nucleolar, and outer mitochondrial membrane (OMM). Moreover, they mined novel RBPs function from outer mitochondrial membrane and confirmed the localization of OMM SYNJ2BP after puromycin treatment. Similarity, Chen's group⁵⁹ reported a strategy that used subcellular fractionation, acidic guanidinium-thiocyanate-phenol-chloroform biphasic extraction, and quantitative mass spectrometry to enrich RBPs from specific subcellular organelles (Figure 5b). 1775 and 2245 RBPs were uncovered by this strategy from the cell

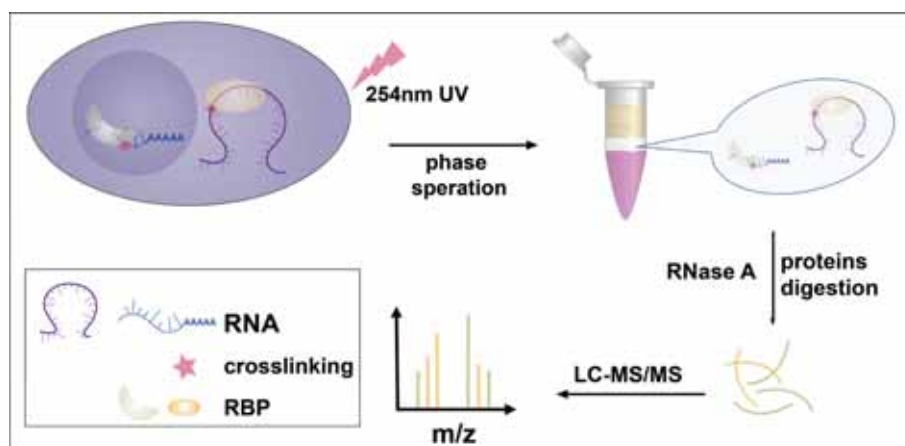


Figure 4. Schematic overview of the phase separation-based strategies. Only the significant steps are shown.

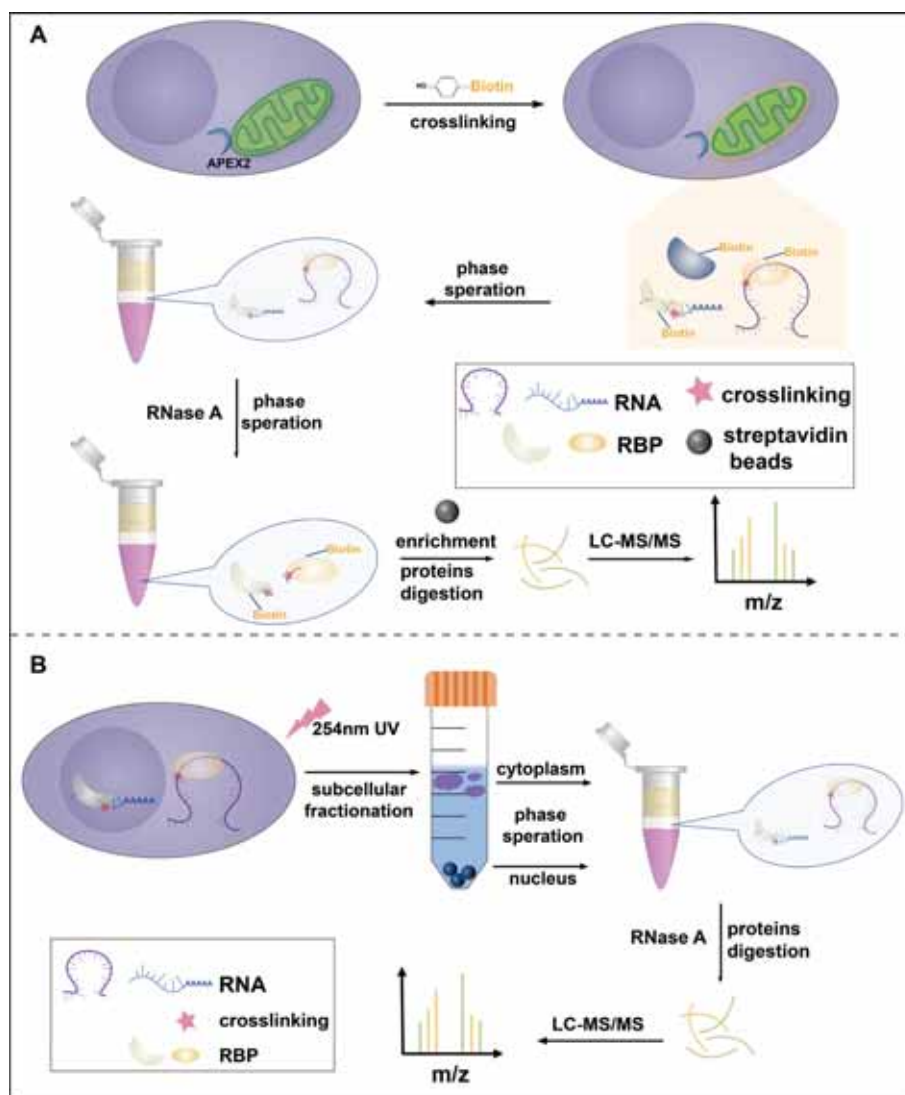


Figure 5. a. Schematic of APEX-PS. Only the significant steps are shown; b. the workflow for enrichment of nucleus and cytoplasm RNA-binding proteins. Only the significant steps are shown.

nucleus and cytoplasm, respectively. Further analysis discovered 403 unique RBPs from cell nucleus and 873 unique RBPs from cell cytoplasm. Among the all RBPs datasets not only contained a large number of known RBPs, but also revealed 614 RBPs that have never been reported previously. Systematically classified the RBPs subcellular localizations and provided an extra information about latent biological functions. In order to verify the novel identified RBPs, they characterized 2157 RNA binding interfaces originate from 892 RBPs using the modified RBDmap method. It could elucidate complex binding structural regarding the RNA-protein interactions.

Compared with poly(A)-based technologies, the phase separation-based strategies eliminated the focus on poly(A) RNA and based entirely on inherent physicochemical

properties of RNA and proteins. It mainly lied in the difference of the solubility between RNA, proteins and RNA-protein complexes. Meanwhile, phase separation-based strategies held enormous potential towards characterizing the prokaryotes RBPs from a system-wide perspective and thereby facilitated a better mining of RBPs biology functions with RNA-proteins interactions in prokaryotes. This strategy requires less than 1% of the cells needed by previous RBPs-enrich methods. OOPS and XRNAS are valuable approaches that manipulated simply and rapidly. Problematically, since glycoproteins and RNA-protein complexes have the same solubility, glycoproteins cannot be distinguished using phase separation-based strategies, creating a problem of glycoprotein contamination.

The chemical labeling-based approaches

Intense research have unearthed numerous RNA crosslinkers that used to connect interacting of RNA to each other, such as methylene blue and psoralen.⁶⁰ Among them, psoralen is a class of planar and ternary heterocyclic compounds that can form stable covalent bonds with pyrimidine bases (especially thymine and uracil) through cycloaddition reaction.⁶¹ The reasoning is that psoralen first intercalated into the pyrimidine bases after enter cells. Then the cycloaddition reaction was occurred by long wavelength ultraviolet irradiation (320–410 nm) to crosslink RNA and psoralen with covalent bonds.⁶² This photoactivation reaction could be used to efficient and unbiased capture of RNA, study of RNA interactions could be addressed, opening new opportunities to understand RNA biological functions on a genome-wide scale.

Exploiting the high reactivity of psoralen with uracil under 365 nm UV irradiation, Qin's lab synthesized a psoralen probe (PP) and developed a new PP-based RBPs identifying approach.⁶³ (As shown in Figure 6a) The PP could tag the nucleic acid and capture the nucleic acid-proteins complex in cells, followed by eluting enriched RBPs by treatment with RNase A. Subsequently, the product was digested with trypsin and characterized by quantitative mass spectrometry after stable isotopic dimethyl labelling. Applying this approach, the authors revealed a total of 2986 RBPs in HeLa cells, which covered ~70% of RBPs originated from HeLa cells reported by previous works. It also included 782 low abundant candidate RBPs. Meanwhile, 178 metabolic enzymes widely involved in metabolic pathways, which were discovered in candidate RBPs. Furthermore, the

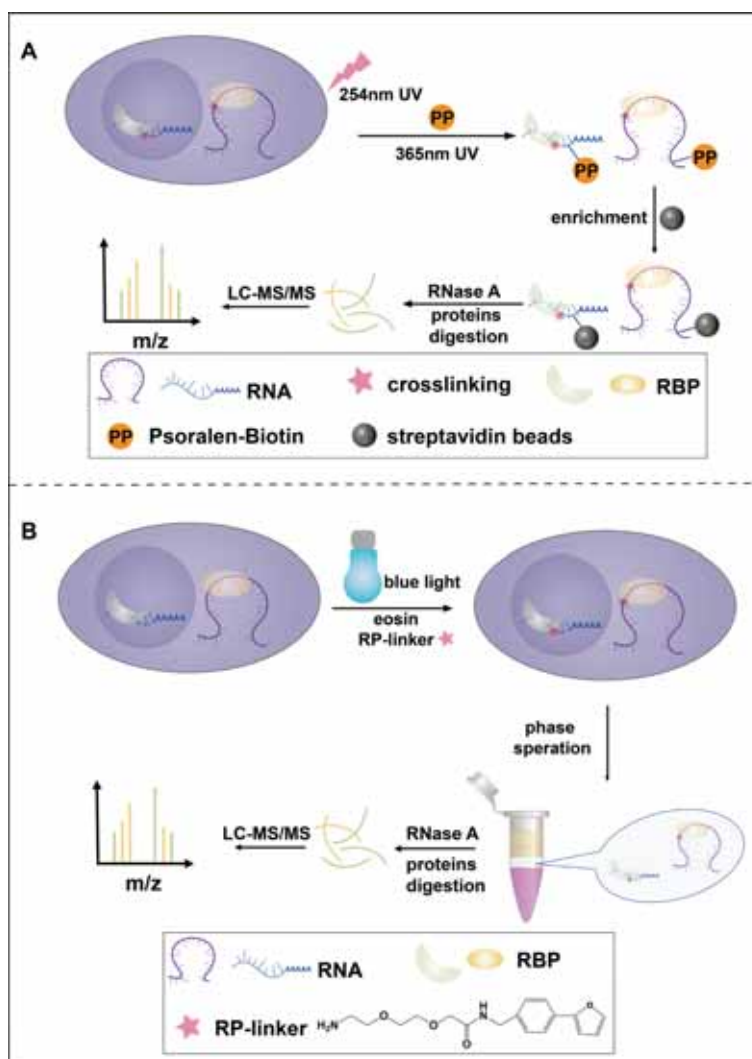


Figure 6. a. Schematic representation of the PP-based approach. Only the significant steps are shown; b. Experimental scheme of the PhotoCAX-MS. Only the significant steps are shown.

authors employed PP-based approach to investigate a large-scale dynamic of RNA-proteins interactions upon Actinomycin D-stimulation. As a result, the distribution map of RBPs with different decreasing/decay rates in RNPs was obtained. More importantly, it also provided a new high-throughput way to evaluate candidate RBPs. Additionally, PP-based approach can be combined with other methods to achieve more comprehensive and extensive coverage of RNA-binding proteome.

Zou et al.⁶⁴ designed a dual-functional photocatalytic RNA-protein crosslinker (RP-linker) which could be adopted for in-situ labelling and efficient crosslinking of RNA-protein complexes under blue light-triggered photocatalyst. Besides, they reported a comprehensive profiling of RNA-protein interaction approach by integrating photocatalytic crosslinking with phase separation and mass spectrometry, termed as “PhotoCAX-MS”, as shown in Figure 6b. The RP-linker was composed of a furan group and amine group for labelling RNAs and connecting RBPs, respectively. Thus, RNA-protein complexes were covalent linked by RP-linker upon photocatalytic conditions in cultured human HEK293 cells. And then the crosslinked RNA-protein complexes were enriched by phase separation for subsequent mass spectrometric analysis. With this approach, they identified 2044 RBPs from HEK293 cells. The PhotoCAX-MS could further yield novel insights concerning the dynamics remodeling of RNA-protein interactions in macrophage cells upon LPS-assisted and SILAC labelling. 1926 proteins were identified by liquid chromatography-tandem mass spectrometry, 1299 of which were shared in three independent biological replicates. Further analysis revealed 11 up-regulated RNA-binding proteins and 12 down-regulated RNA-binding proteins. Noticeably, the PhotoCAX-MS was also applied to dig the proteins directly binding with the 5' untranslated regions of SARS-CoV-2 RNA. A total of 193 RBPs were discovered by liquid chromatography-tandem mass spectrometry. Further analysis emerged the potential biological function of host RBPs in the SARS-CoV-2 infections.

In conclusion, the chemical labeling-based approaches greatly improved the specificity of RBPs enrichment and provided an ideal platform for in-depth RNA-protein interaction research. Of course, these approaches are still unbiased which can map all kind of RNA bound proteins. Although tremendous progress has been made for chemical labelling-based approaches to map all kind of RNA bound proteins, these approaches are still far from reaching the level of integration sufficient to address bioanalytical challenges. For example, PP-based methods tend to favor more abundant non-coding RNA-binding proteins and thus may inhibit the identification of mRNA-binding proteins. Due to the use of phase separation, RBPs with glycosylation may not be successfully recognized by PhotoCAX-MS.

Conclusions and perspectives

Recent efforts opened up new opportunities to study RNA-protein interactions and expanded the methods to characterize RNA-binding proteome with high-throughput mass spectrometry. We reviewed here experimental large-scale methods for RNA-protein complexes enrichment, with the characteristics of each method. Researchers can design a suitable method for specific issue. Considering different enrichment mechanisms, these methods can complement each other in some aspects. Taking advantage of these methods, it is promising to achieve more comprehensive and extensive coverage of RNA binding proteome, and thereby laying the foundation for the in-depth study of RNA-protein interactions. Nevertheless, given the fact that UV light that used to covalent crosslink RNA-protein complexes has poor penetrability, the application of these methods is confined to cultured cells (generally monolayer cells), fly and *Arabidopsis thaliana*, as well as bacteria. It is also worth noting that the current methods are not compatible with the identification of RNA-binding proteome from mammal tissue. To overcome this limitation, it is necessary to develop more crosslinking methods, such as new chemical crosslinkers, for replacing UV crosslinking in the fix of RNA-proteins complexes in future. In addition, proper control conditions and stringent screening cut-off RBPs should be carefully considered. The specific and precision of RNA-binding proteome can provide more confident data to support further biological study. The field of mass spectrometry-based proteomics is rapidly expanding and creating more convenience for comprehensive studying biological functions. It can be expected to open a new way to investigate RNA-binding proteome for understanding interaction of RNA with proteins by combining the advantages of proteome-wide sample preparation methods and mass spectrometry.

Acknowledgements

We are grateful for financial support from the Fundamental Research Funds for the Central Public Welfare Research Institutes (ZZ13-YQ-080) Scientific and technological innovation project of China Academy of Chinese Medical Sciences (CI2021B017, CI2021A05032, XTCX2021001).

Conflict of interest statement

There are no conflicts no declare.

Reference

- Gerstberger, S.; Hafner, M.; Tuschl, T. *Nature Reviews Genetics* **2014**, *15*, 829. DOI: 10.1038/nrg3813.
- Nair, L.; Chung, H.; Basu, U. *Nature Reviews Molecular Cell Biology* **2020**, *21*, 123. DOI: 10.1038/s41580-019-

- 0209-0.
3. Dreyfuss, G.; Kim, V.N.; Kataoka, N. *Nature Reviews Molecular Cell Biology* **2002**, 3, 195. DOI: 10.1038/nrm760.
 4. Koehler, A.; Hurt, E. *Nature Reviews Molecular Cell Biology* **2007**, 8, 761. DOI: 10.1038/nrm2255.
 5. Sonenberg, N.; Hinnebusch, A.G. *Cell* **2009**, 136, 731. DOI: 10.1016/j.cell.2009.01.042.
 6. Chen, R.; Liu, Y.; Zhuang, H.; Yang, B.; Hei, K.; Xiao, M.; Hou, C.; Gao, H.; Zhang, X.; Jia, C.; Li, L.; Li, Y.; Zhang, N. *Nucleic Acids Res.* **2017**, 45, 9947. DOI: 10.1093/nar/gkx600.
 7. Cooper, T.A.; Wan, L.; Dreyfuss, G. *Cell* **2009**, 136, 777. DOI: 10.1016/j.cell.2009.02.011.
 8. Huang, A.; Zheng, H.; Wu, Z.; Chen, M.; Huang, Y. *Theranostics* **2020**, 10, 3503. DOI: 10.7150/thno.42174.
 9. Jankowsky, E.; Harris, M.E. *Nature Reviews Molecular Cell Biology* **2015**, 16, 533. DOI: 10.1038/nrm4032.
 10. Gebauer, F.; Schwarzl, T.; Valcarcel, J.; Hentze, M.W. *Nature Reviews Genetics* **2021**, 22, 185. DOI: 10.1038/s41576-020-00302-y.
 11. Liao, Y.; Castello, A.; Fischer, B.; Leicht, S.; Foehr, S.; Frese, C.K.; Ragan, C.; Kurscheid, S.; Pagler, E.; Yang, H.; Krijgsveld, J.; Hentze, M.W.; Preiss, T. *Cell Reports* **2016**, 16, 1456. DOI: 10.1016/j.celrep.2016.06.084.
 12. Jazurek, M.; Ciesiolka, A.; Starega-Roslan, J.; Bilinska, K.; Krzyzosiak, W.J. *Nucleic Acids Res.* **2016**, 44, 9050. DOI: 10.1093/nar/gkw803.
 13. Pereira, B.; Billaud, M.; Almeida, R. *Trends In Cancer* **2017**, 3, 506. DOI: 10.1016/j.trecan.2017.05.003.
 14. Castello, A.; Fischer, B.; Hentze, M.W.; Preiss, T. *Trends Genet.* **2013**, 29, 318. DOI: 10.1016/j.tig.2013.01.004.
 15. Ramanathan, M.; Porter, D.F.; Khavari, P.A. *Nat. Methods* **2019**, 16, 225. DOI: 10.1038/s41592-019-0330-1.
 16. McHugh, C.A.; Russell, P.; Guttman, M. *Genome Biol.* **2014**, 15, 203. DOI: 10.1186/gb4152.
 17. Koenig, J.; Zarnack, K.; Luscombe, N.M.; Ule, J. *Nature Reviews Genetics* **2012**, 13, 77. DOI: 10.1038/nrg3141.
 18. Nechay, M.; Kleiner, R.E. *Curr. Opin. Chem. Biol.* **2020**, 54, 37. DOI: 10.1016/j.cbpa.2019.11.002.
 19. Castello, A.; Fischer, B.; Eichelbaum, K.; Horos, R.; Beckmann, B.M.; Strein, C.; Davey, N.E.; Humphreys, D.T.; Preiss, T.; Steinmetz, L.M.; Krijgsveld, J.; Hentze, M.W. *Cell* **2012**, 149, 1393. DOI: 10.1016/j.cell.2012.04.031.
 20. Baltz, A.G.; Munschauer, M.; Schwanhaeusser, B.; Vasile, A.; Murakawa, Y.; Schueler, M.; Youngs, N.; Penfold-Brown, D.; Drew, K.; Milek, M.; Wyler, E.; Bonneau, R.; Selbach, M.; Dieterich, C.; Landthaler, M. *Mol. Cell* **2012**, 46, 674. DOI: 10.1016/j.molcel.2012.05.021.
 21. Beckmann, B.M.; Horos, R.; Fischer, B.; Castello, A.; Eichelbaum, K.; Alleaume, A.-M.; Schwarzl, T.; Curk, T.; Foehr, S.; Huber, W.; Krijgsveld, J.; Hentze, M.W. *Nature Communications* **2015**, 6, 1. DOI: 10.1038/ncomms10127.
 22. Conrad, T.; Albrecht, A.-S.; Costa, V.R.d.M.; Sauer, S.; Meierhofer, D.; Orom, U.A. *Nature Communications* **2016**, 7, 1. DOI: 10.1038/ncomms11212.
 23. Kramer, K.; Sachsenberg, T.; Beckmann, B.M.; Qamar, S.; Boon, K.-L.; Hentze, M.W.; Kohlbacher, O.; Urlaub, H. *Nat. Methods* **2014**, 11, 1064. DOI: 10.1038/nmeth.3092.
 24. Kwon, S.C.; Yi, H.; Eichelbaum, K.; Foehr, S.; Fischer, B.; You, K.T.; Castello, A.; Krijgsveld, J.; Hentze, M.W.; Kim, V.N. *Nat. Struct. Mol. Biol.* **2013**, 20, 1122. DOI: 10.1038/nsmb.2638.
 25. Liepelt, A.; Naarmann-de Vries, I.S.; Simons, N.; Eichelbaum, K.; Foehr, S.; Archer, S.K.; Castello, A.; Usadel, B.; Krijgsveld, J.; Preiss, T.; Marx, G.; Hentze, M.W.; Ostareck, D.H.; Ostareck-Lederer, A. *Mol. Cell. Proteomics* **2016**, 15, 2699. DOI: 10.1074/mcp.M115.056564.
 26. Mitchell, S.F.; Jain, S.; She, M.; Parker, R. *Nat. Struct. Mol. Biol.* **2013**, 20, 127. DOI: 10.1038/nsmb.2468.
 27. Matia-Gonzalez, A.M.; Laing, E.E.; Gerber, A.P. *Nat. Struct. Mol. Biol.* **2015**, 22, 1027. DOI: 10.1038/nsmb.3128.
 28. Nandan, D.; Thomas, S.A.; Nguyen, A.; Moon, K.-M.; Foster, L.J.; Reiner, N.E. *PLoS One* **2017**, 12, e0170068. DOI: 10.1371/journal.pone.0170068.
 29. Bunnik, E.M.; Batugedara, G.; Saraf, A.; Prudhomme, J.; Florens, L.; Le Roch, K.G. *Genome Biol.* **2016**, 17, 1. DOI: 10.1186/s13059-016-1014-0.
 30. Lueong, S.; Merce, C.; Fischer, B.; Hoheisel, J.D.; Erben, E.D. *Mol. Microbiol.* **2016**, 100, 457. DOI: 10.1111/mmi.13328.
 31. Reichel, M.; Liao, Y.; Rettel, M.; Ragan, C.; Evers, M.; Alleaume, A.-M.; Horos, R.; Hentze, M.W.; Preiss, T.; Millar, A.A. *Plant Cell* **2016**, 28, 2435. DOI: 10.1105/tpc.16.00562.
 32. Marondedze, C.; Thomas, L.; Serrano, N.L.; Lilley, K.S.; Gehring, C. *Sci. Rep.* **2016**, 6, 1. DOI: 10.1038/srep29766.
 33. Sysoev, V.O.; Fischer, B.; Frese, C.K.; Gupta, I.; Krijgsveld, J.; Hentze, M.W.; Castello, A.; Ephrussi, A. *Nature Communications* **2016**, 7, 1. DOI: 10.1038/ncomms12128.
 34. Wessels, H.-H.; Imami, K.; Baltz, A.G.; Kolinski, M.; Beldovskaya, A.; Selbach, M.; Small, S.; Ohler, U.; Landthaler, M. *Genome Res.* **2016**, 26, 1000. DOI: 10.1101/gr.200386.115.
 35. Despic, V.; Dejung, M.; Gu, M.; Krishnan, J.; Zhang, J.; Herzel, L.; Straube, K.; Gerstein, M.B.; Butter, F.; Neugebauer, K.M. *Genome Res.* **2017**, 27, 1184. DOI: 10.1101/gr.215954.116.
 36. Hentze, M.W.; Castello, A.; Schwarzl, T.; Preiss, T. *Nature Reviews Molecular Cell Biology* **2018**, 19, 327. DOI: 10.1038/nrm.2017.130.
 37. Perez-Perri, J.I.; Rogell, B.; Schwarzl, T.; Stein, F.; Zhou, Y.; Rettel, M.; Brosig, A.; Hentze, M.W. *Nature Communications* **2018**, 9, 1. DOI: 10.1038/s41467-018-

- 06557-8.
38. Garcia-Moreno, M.; Noerenberg, M.; Ni, S.; Jarvelin, A.I.; Gonzalez-Almela, E.; Lenz, C.E.; Bach-Pages, M.; Cox, V.; Avolio, R.; Davis, T.; Hester, S.; Sohler, T.J.M.; Li, B.; Heikel, G.; Michlewski, G.; Sanz, M.A.; Carrasco, L.; Ricci, E.P.; Pelechano, V.; Davis, I.; Fischer, B.; Mohammed, S.; Castello, A. *Mol. Cell* **2019**, *74*, 196. DOI: 10.1016/j.molcel.2019.01.017.
 39. Kamel, W.; Noerenberg, M.; Cerikan, B.; Chen, H.; Ja, A.I.; Kammoun, M.; Lee, J.Y.; Shuai, N.; Garcia-Moreno, M.; Andrejeva, A.; Deery, M.J.; Johnson, N.; Neufeldt, C.J.; Cortese, M.; Knight, M.L.; Lilley, K.S.; Martinez, J.; Davis, I.; Bartenschlager, R.; Mohammed, S.; Castello, A. *Mol. Cell* **2021**, *81*, 2851. DOI: 10.1016/j.molcel.2021.05.023.
 40. Benhalevy, D.; Anastasakis, D.G.; Hafner, M. *Nat. Methods* **2018**, *15*, 1074. DOI: 10.1038/s41592-018-0220-y.
 41. Sun, W.; Wang, N.; Liu, H.; Yu, B.; Jin, L.; Ren, X.; Shen, Y.; Wang, L. *Nat. Chem.* **2022**. DOI: 10.1038/s41557-022-01038-4.
 42. Castello, A.; Frese, C.K.; Fischer, B.; Jarvelin, A.I.; Horos, R.; Alleaume, A.-M.; Foehr, S.; Curk, T.; Krijgsveld, J.; Hentze, M.W. *Nat. Protoc.* **2017**, *12*, 2447. DOI: 10.1038/nprot.2017.106.
 43. Castello, A.; Fischer, B.; Frese, C.K.; Horos, R.; Alleaume, A.-M.; Foehr, S.; Curk, T.; Krijgsveld, J.; Hentze, M.W. *Mol. Cell* **2016**, *63*, 696. DOI: 10.1016/j.molcel.2016.06.029.
 44. Smith, T.; Villanueva, E.; Queiroz, R.M.L.; Dawson, C.S.; Elzek, M.; Urdaneta, E.C.; Willis, A.E.; Beckmann, B.M.; Krijgsveld, J.; Lilley, K.S. *Curr. Opin. Chem. Biol.* **2020**, *54*, 70. DOI: 10.1016/j.cbpa.2020.01.009.
 45. Bao, X.; Guo, X.; Yin, M.; Tariq, M.; Lai, Y.; Kanwal, S.; Zhou, J.; Li, N.; Lv, Y.; Pulido-Quetglas, C.; Wang, X.; Ji, L.; Khan, M.J.; Zhu, X.; Luo, Z.; Shao, C.; Lim, D.-H.; Liu, X.; Li, N.; Wang, W.; He, M.; Liu, Y.-L.; Ward, C.; Wang, T.; Zhang, G.; Wang, D.; Yang, J.; Chen, Y.; Zhang, C.; Jauch, R.; Yang, Y.-G.; Wang, Y.; Qin, B.; Anko, M.-L.; Hutchins, A.P.; Sun, H.; Wang, H.; Fu, X.-D.; Zhang, B.; Esteban, M.A. *Nat. Methods* **2018**, *15*, 213. DOI: 10.1038/nmeth.4595.
 46. Huang, R.; Han, M.; Meng, L.; Chen, X. *Proc. Natl. Acad. Sci. U. S. A.* **2018**, *115*, E3879. DOI: 10.1073/pnas.1718406115.
 47. Burger, K.; Muehl, B.; Kellner, M.; Rohmoser, M.; Gruber-Eber, A.; Windhager, L.; Friedel, C.C.; Doelken, L.; Eick, D. *RNA Biol.* **2013**, *10*, 1623. DOI: 10.4161/rna.26214.
 48. Tani, H.; Akimitsu, N. *RNA Biol.* **2012**, *9*, 1233. DOI: 10.4161/rna.22036.
 49. Chomczynski, P.; Sacchi, N. *Nat. Protoc.* **2006**, *1*, 581. DOI: 10.1038/nprot.2006.83.
 50. Queiroz, R.M.L.; Smith, T.; Villanueva, E.; Marti-Solano, M.; Monti, M.; Pizzinga, M.; Mirea, D.-M.; Ramakrishna, M.; Harvey, R.F.; Dezi, V.; Thomas, G.H.; Willis, A.E.; Lilley, K.S. *Nat. Biotechnol.* **2019**, *37*, 169. DOI: 10.1038/s41587-018-0001-2.
 51. Trendel, J.; Schwarzl, T.; Horos, R.; Prakash, A.; Bateman, A.; Hentze, M.W.; Krijgsveld, J. *Cell* **2019**, *176*, 391. DOI: 10.1016/j.cell.2018.11.004.
 52. Urdaneta, E.C.; Vieira-Vieira, C.H.; Hick, T.; Wessels, H.-H.; Figini, D.; Moschall, R.; Medenbach, J.; Ohler, U.; Granneman, S.; Selbach, M.; Beckmann, B.M. *Nature Communications* **2019**, *10*, 1. DOI: 10.1038/s41467-019-08942-3.
 53. Smirnov, A.; Foerstner, K.U.; Holmqvist, E.; Otto, A.; Guenster, R.; Becher, D.; Reinhardt, R.; Vogel, J. *Proc. Natl. Acad. Sci. U. S. A.* **2016**, *113*, 11591. DOI: 10.1073/pnas.1609981113.
 54. Asencio, C.; Chatterjee, A.; Hentze, M.W. *Life Science Alliance* **2018**, *1*, e201800088. DOI: 10.26508/lsa.201800088.
 55. Koo, K.; Foegeding, P.M.; Swaisgood, H.E. *Biotechnol. Tech.* **1998**, *12*, 549. DOI: 10.1023/a:1008859632378.
 56. Shchepachev, V.; Bresson, S.; Spanos, C.; Petfalski, E.; Fischer, L.; Rappsilber, J.; Tollervy, D. *Mol. Syst. Biol.* **2019**, *15*, e8689. DOI: 10.15252/msb.20188689.
 57. Qin, W.; Cho, K.F.; Cavanagh, P.E.; Ting, A.Y. *Nat. Methods* **2021**, *18*, 133. DOI: 10.1038/s41592-020-01010-5.
 58. Qin, W.; Myers, S.A.; Carey, D.K.; Carr, S.A.; Ting, A.Y. *Nature Communications* **2021**, *12*, 1. DOI: 10.1038/s41467-021-25259-2.
 59. Yan, S.; Zhao, D.; Wang, C.; Wang, H.; Guan, X.; Gao, Y.; Zhang, X.; Zhang, N.; Chen, R. *Anal. Chim. Acta* **2021**, *1168*, 338609. DOI: 10.1016/j.aca.2021.338609.
 60. Harris, M.E.; Christian, E.L. 2009. RNA Crosslinking methods. In *Methods In Enzymology, Vol 468: Biophysical, Chemical, And Functional Probes Of Rna Structure, Interactions And Folding, Pt A*. D. Herschalag, editor. 127.
 61. Zhang, Y.; Chan, P.P.Y.; Herr, A.E. *Angewandte Chemie-International Edition* **2018**, *57*, 2357. DOI: 10.1002/anie.201711441.
 62. Aw, J.G.A.; Shen, Y.; Wilm, A.; Sun, M.; Lim, X.N.; Boon, K.-L.; Tapsin, S.; Chan, Y.-S.; Tan, C.-P.; Sim, A.Y.L.; Zhang, T.; Susanto, T.T.; Fu, Z.; Nagarajan, N.; Wan, Y. *Mol. Cell* **2016**, *62*, 603. DOI: 10.1016/j.molcel.2016.04.028.
 63. Zhang, Z.; Liu, T.; Dong, H.; Li, J.; Sun, H.; Qian, X.; Qin, W. *Nucleic Acids Res.* **2021**, *49*, e65. DOI: 10.1093/nar/gkab156.
 64. Luo, H.; Tang, W.; Liu, H.; Zeng, X.; Ngai, W.S.C.; Gao, R.; Li, H.; Li, R.; Zheng, H.; Guo, J.; Qin, F.; Wang, G.; Li, K.; Fan, X.; Zou, P.; Chen, P.R. *Angewandte Chemie-International Edition* **2022**, *61*, e202202008. DOI: 10.1002/anie.202202008.

Headspace GC-MS Analysis of Spring Blossom Fragrance at Chungnam National University Daedeok Campus

Yeonwoo Choi^{1†}, Sanghyun Lee^{2†}, Young-Mi Kim³, Huu-Quang Nguyen¹, Jeongkwon Kim¹, and Jaebeom Lee^{1,3*}

¹Department of Chemistry, Chungnam National University, Daejeon, 34134, Republic of Korea

²Department of Biology, Chungnam National University, Daejeon, 34134, Republic of Korea

³Department of Chemical Engineering and Applied Chemistry, Chungnam National University, Daejeon, 34134, Republic of Korea

Received September 28, 2022, Revised October 11, 2022, Accepted October 12, 2022

First published on the web December 31, 2022; DOI: 10.5478/MSL.2022.13.4.125

Abstract : There are many types of spring blossoms on the Daedeok campus of Chungnam National University (CNU) at the area of 1,600,000 square meters. As an assignment for the class of Analytical Chemistry I for second-year undergraduate students, 2021, flower petals collected from various floral groups (*Korean azalea*, *Korean forsythia*, *Dilatata lilac*, *Lilytree*, *Lily magnolia*, and *Prunus yedoensis*) were analyzed using headspace extraction coupled to gas chromatography-mass spectrometry (HS-GC-MS) to study the aromatic profiles and fragrance compounds of each sample group. Various types of compounds associated with the aroma profiles were detected, including saturated alcohols and aldehydes (ethanol, 1-hexanol, and nonanal), terpenes (limonene, pinene, and ocimene), and aromatic compounds (benzyl alcohol, benzaldehyde). The different contribution of these compounds for each floral type was visualized using statistical tools and classification models based on principal component analysis with high reliability ($R^2 = 0.824$, $Q^2 = 0.616$). These results showed that HS-GC-MS with statistical analysis is a powerful method to characterize the volatile aromatic profile of biological specimens.

Keywords : fragrance compound, headspace extraction, GCMS, spring blossoms, principal component analysis

Introduction

Various types of spring blossoms appear on the Daedeok campus of Chungnam National University (CNU) at an area of 1,600,000 m², in particular, Korean azalea (*Rhododendron schlippenbachii*), Korean forsythia (*Forsythia koreana*), Dilatata lilac (*Syringa oblata subsp. dilatata*), Lilytree (*Magnolia demudata*), Lily magnolia (*Magnolia liliiflora*), and Prunus cherry blossom (*Prunus yedoensis*). A special project in the class of Analytical Chemistry I for second-year students in the 2021 Spring semester was performed to analyze the aroma and aromatic contents of these spring

flowers at the CNU campus using headspace extraction coupled to gas chromatography-mass spectrometry (HS-GC-MS) and to identify the compounds that cause each flower to have a specific scent. In the class of Analytical Chemistry I, students learned about the general concepts of the analytical process, chemical measurements, statistics for experimental errors, quality assurance and calibration methods. Conventionally, qualitative and quantitative analysis methods were taught mainly with course materials (textbooks, lecture materials, etc.), and the corresponding experimental courses were designed based on these provided understandings. Unfortunately, experimental courses for second-year students had been suffering from an unexpected status due to the COVID-19 pandemic since 2020. All in-person classes had been closed for more than a year and substituted with on-line broadcasting alternatives. Therefore, this project was designed to have students experience experimental processes and methods for instrumental analysis, in specific, chromatography and mass spectrometry, in the analysis of practical specimens.

Aroma is usually composed of a complex mixture of various volatile organic compounds (VOCs), including amino acid-derived compounds, lipid-derived compounds, phenolic derivatives, mono- and sesquiterpenes.¹⁻⁴ Since a sense of smell is a physiological reaction caused by a

Open Access

†Both contributed equally.

*Reprint requests to Jaebeom Lee

<https://orcid.org/0000-0002-4563-2883>

E-mail: nanoleelab@cnu.ac.kr

All the content in Mass Spectrometry Letters (MSL) is Open Access, meaning it is accessible online to everyone, without fee and authors' permission. All MSL content is published and distributed under the terms of the Creative Commons Attribution License (<http://creativecommons.org/licenses/by/3.0/>). Under this license, authors reserve the copyright for their content; however, they permit anyone to unrestrictedly use, distribute, and reproduce the content in any medium as far as the original authors and source are cited. For any reuse, redistribution, or reproduction of a work, users must clarify the license terms under which the work was produced.

chemical stimulus, the molecules must be significantly light enough (<300 Da) to travel to the olfactory system via airborne.⁵ Therefore, gas chromatography (GC) coupled with mass spectrometric (MS) detector is often regarded as a powerful tool for aroma compound analysis, being a technological combination of the separation power of GC with the detection and quantification capability of MS. While flame ionization detector (FID) is more reliable and sensitive for quantitative analysis, the qualitative identification power of MS could provide robust and dynamic identification of chemical composition in samples with unknown or sophisticated background matrices, such as biological specimens. Furthermore, headspace (HS) extraction is an optimal method for volatile compound analysis, in which the volatile analytes could be extracted and isolated from the contaminants in the sample matrix. Methods based on HS-GC-MS can reduce the number of sample preparation steps required prior to analysis, as well as enable automation and programmed qualitative and quantitative analysis of biological samples.^{6,7}

In this study, the petal samples of 6 different species of spring blossoms were carefully collected at 16 locations on the campus. All students were divided into small groups to collect the samples. The samples were pre-treated and analyzed by HS-GC-MS with the special assistance of the Core-Facility center at the Department of Chemistry, CNU. Statistical analysis was performed to understand the relationship between the identified volatile compounds to

the aroma profile, and a classification model based on the GC-MS data was established to evaluate and visualize the aroma profiles according to each floral group.

Experimental details

Sample collection and Pre-treatment

A total of 62 undergraduate students in the two Analytical Chemistry I classes have participated in this project (Table S1). They were divided into 16 groups to collect the petal samples. All floral samples (*Korean azalea*, *Korean Forsythia*, *Dilatata Lilac*, *Lilytree* (aka., *Yulan magnolia*), *Lily Magnolia*, and *Prunus Yedoensis*) were collected from blooming flowers on the rooted plants before browning (Table S2). These samples were picked in April, 2021 across different sites on CNU Daedeok campus (Figure 1) and the exact picking time is different depending on the flowering time of each plant. The pistil, stamen, and leaves of the flowers were completely removed, and the petal samples were stored in a respective transparent close-tight Ziploc plastic bag at -20°C before analysis.

HS extraction conditions

The volatile organic compound profiles from the flower samples were extracted and injected into the GC-MS instrument using an automated static HS sampler (Agilent 7697A, Santa Clara, CA) at the CNU Chemistry Core Facility. The oven temperature was set at 100°C, the loop

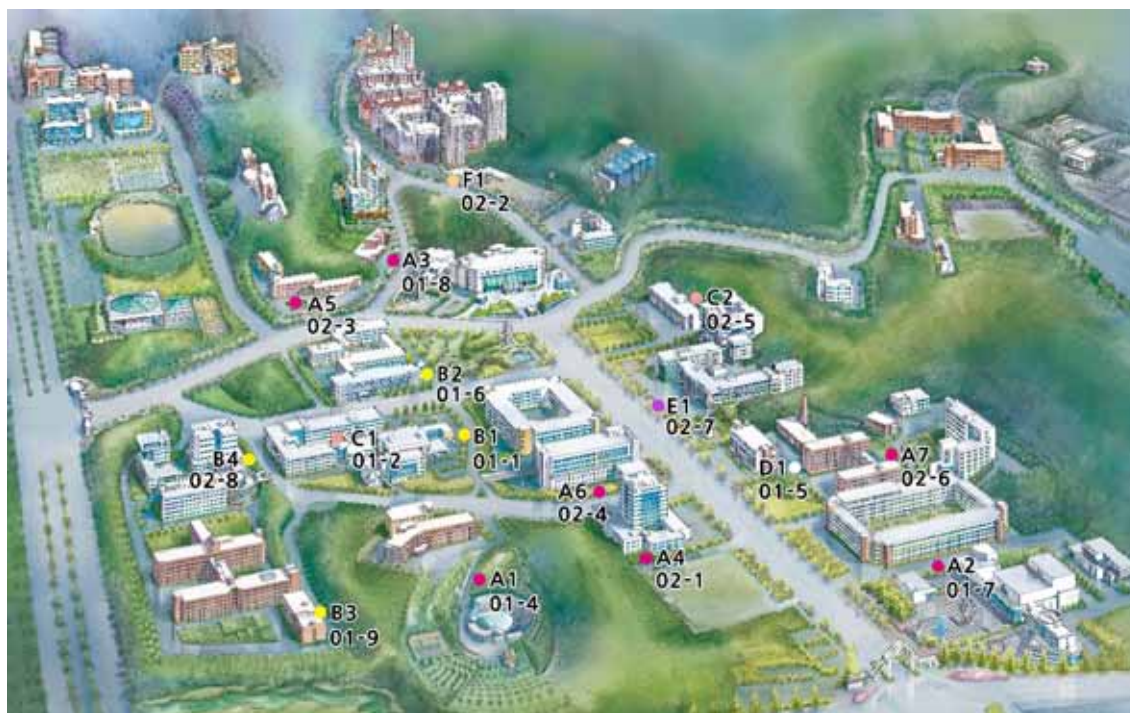


Figure 1. The CNU campus map indicating the places where flowers were collected. The student team numbers are also indicated on the map.

temperature was set at 110°C, and the transfer line was set at 120°C. Homogenized petal sample (1 g) was added to a 20 mL HS crimp vial with silicon septa, and equilibrated at 100°C for 15 min. The equilibrated sample was pressurized to 3 psi prior to injection by a fill flow of 50 mL·min⁻¹, and the injection time was 0.5 min.

GC-MS Analysis

The extracted volatile constituents from the pre-treated sample were analyzed by GC-MS (Agilent 6890N gas chromatograph with a 5975B mass analyzer) equipped with a VF-WAXms column (30 m × 0.25 mm × 0.5 μm) filled with low-bleed polyethylene glycol (PEG) stationary phase. The inlet was kept at 200°C in split injection mode (10:1 ratio), and the total flow rate was set at 13.6 mL·min⁻¹. The oven temperature was programmed as follows: initial column temperature was set at 50°C for 2 min, then increased to 200°C at a rate of 10°C·min⁻¹ and held at this temperature for 5 min (total running time 22 min). Ionization of analyte compounds was performed in positive electron ionization mode (EI+), in which 70 eV of ionization energy was acquired using built-in gain control. The MS source temperature was set at 230°C, MS Quad at 150°C, and the solvent delay was set to 2.5 min. The mass spectrometer was operated in scanning mode (*m/z* 40 to 359.0) with a scanning interval of 0.1 Da. Analyte compounds were identified using library search with NIST17 database, and the cut-off criteria for positive matches were set at 50% identification confidence.

Data pretreatment and analysis

The peak areas were integrated to calculate the peak area percentage (PA%) value which is related to the composition information of each compound in a sample. The PA% from each compound for each sample was calculated separately, and then averaged between each floral group to find the correlation between the compound profile and floral groups. For the multivariate data analysis, the raw chromatographic data (from RT= 2.6 min to 22 min, interval: 0.005 min) from each sample were used. Principle component analysis model was built using the SIMCA-P 11 program (Umetrics, Umea, Sweden), in which the log₁₀ transformation of the abundance from each data point was performed for normalization of the chromatographic data.

Results and discussions

HS-GC-MS chromatogram profiles of the spring blossom samples

Representative chromatograms of the HS-GC-MS analysis are shown in Figure 2. The volatile compounds identified by HS-GC-MS of each floral sample were quantified using the percentage peak area method, in which the PA% value was calculated using the integrated area of each compound divided by the total peak area of all compounds in the MS

scan mode. This calculation is based on the mass balance model, in which the chemical concentration of a component is expressed as the linear sum of products of its abundance and contribution. It should be noted that while this method is simple and suitable for broad identification and quantification of unknown or complex samples, the quantitation accuracy is limited due to the differences in ionization efficiency of different compound types toward the MS detector. As observed on the GC-MS chromatogram of the petal samples by each floral group (Figure S1-S3), the identified compounds and their relative amounts in each sample varied depending on the location, which could be related to the differences in the growing environment and the blossoming state of each individual plant. However, larger sample size and time-domain monitoring should be performed to obtain a statistically viable conclusion of these effects on the volatile compound profile in each group. In summary, a total of 114 volatile compounds were observed in the spring blossom flowers samples, in which 34 compounds (29.8%) were found in at least half of the samples collected. Distinctively, homology series and isomers of straight-chain saturated and unsaturated alkanes, alcohols, and aldehydes were identified with high amounts specifically in some floral groups. Therefore, the categorization of these compounds and their amount could assist in establishing the aroma profile of spring blossom samples. A Venn diagram of the identified compounds according to each floral group was described in Figure 3a. In all sample groups, 10 compounds were commonly found and identified as tetrahydrofuran (THF), aldehyde compounds (2-methyl butanal, 3-methyl butanal, hexanal, nonanal, and benzaldehyde), sulcatone (6-methyl-5-hepten-2-one), and terpenes (α -pinene, trans- β -ocimene, and γ -terpinene). Furthermore, 11 other compounds were detected in at least 4 floral groups. These compounds mostly come from certain plant metabolization processes and define the odorous profile of flowers, which are replicated and utilized in various commercial products as antibacterial agents and perfumes.⁸⁻¹⁰

Classification and comparison of volatile component profiles between each floral group

Statistical analyses were performed on the highly contributed chemical compound and compound groups between the five floral groups, in which the two magnolia samples were merged into one group, to further understand the differences between the volatile compound profile in each group. Firstly, the amount of benzaldehyde (RT = 12.362 min) was remarkably high in the sample of *Prunus yedoensis*, at 66.7% of the total VOC amount, while being less than 10% in the other floral groups, including *azalea* (9.6%), *Dilatata lilac* (2.1%), *forsythia* (1.0%) and *Magnolias* (0.57%). Possessing a strong sweet scent, benzaldehyde is formed under the enzymatic hydrolysis of amygdalin, a naturally occurring glycoside found in seeds and flowers of almonds, peaches or cherries. Previous

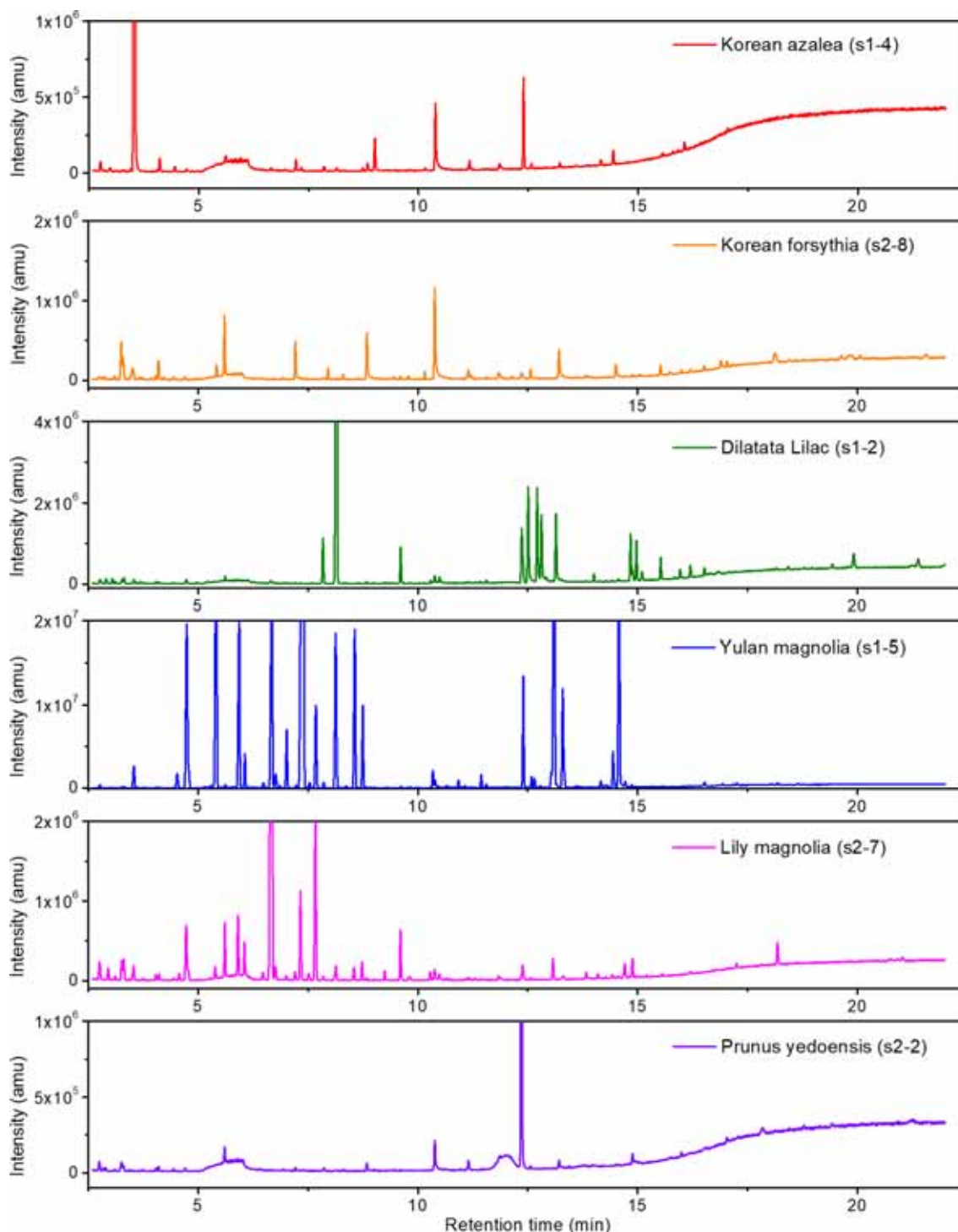


Figure 2. Representative HS-GC-MS chromatograms of the petal samples from 6 floral sources collected in this study.

reports also indicated the presence of high amount of benzaldehyde in cherry leaves or blossoms.^{11,12} On the other hand, lilac aldehydes and lilac alcohol were found predominantly in *Dilatata lilac*, which averaged 8.2% of

the total volatile contents in its samples.

Straight-chain saturated alkanes (C₁₀-C₁₆) were identified solely in *Korean forsythia* samples, in which their composition contribution was averaged at 6.34±0.73% of the total peak

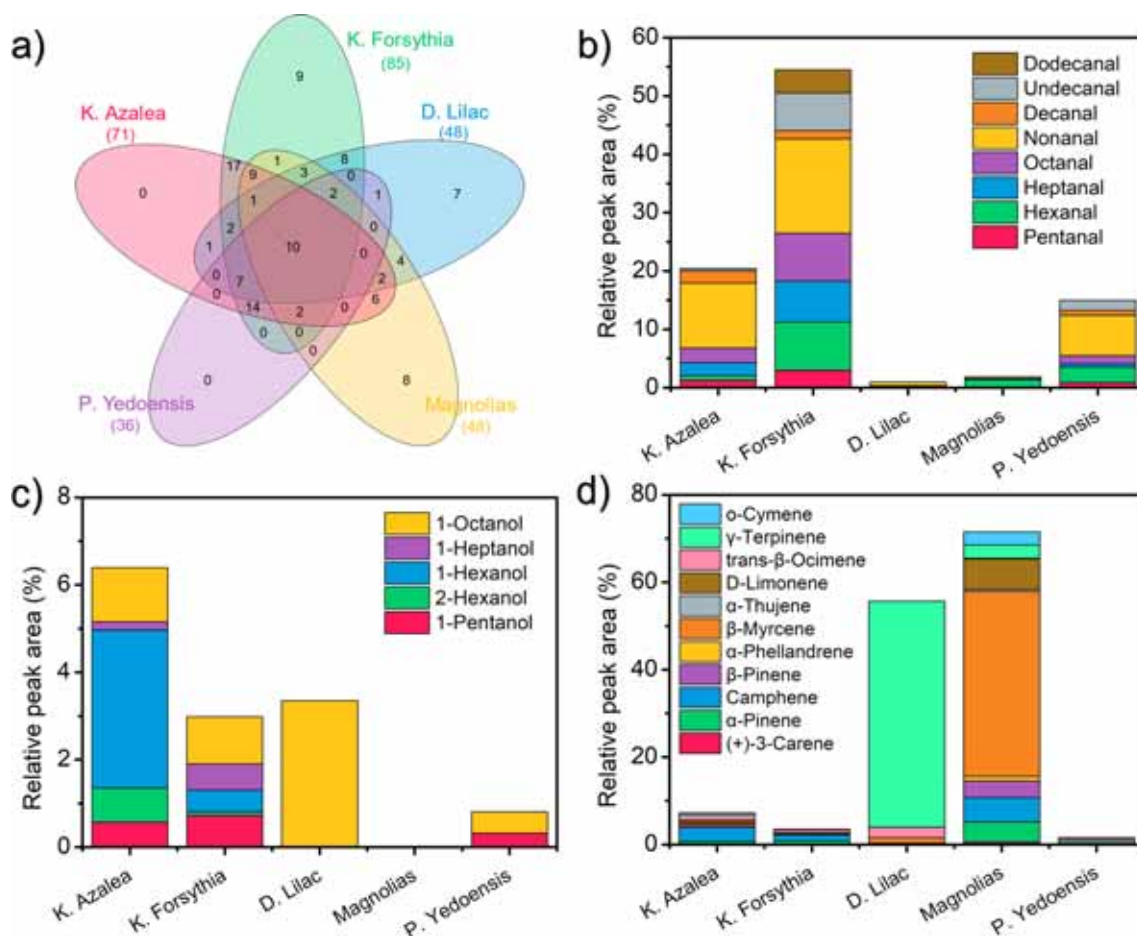


Figure 3. Statistical analysis on the volatile compound profile of the spring blossom samples. (a) Venn diagram showing the overlapping between the volatile content analyzed by HS-GC-MS of the floral groups, (b-d) Direct comparison of the relative peak area (%) of the identified compound groups: (b) saturated fatty aldehydes, (c) saturated alkanols, and (d) terpene and terpenoid compounds, according to each floral group.

area. On the other hand, the other blossom groups showed only insignificant traces of these compounds in the volatile phase analyzed. The yellow-colored blossom, often called “golden bell”, is one of the affluent flowers in early Spring throughout the Korean peninsula. Forsythia trees are usually grown in scrubs and roadside on the CNU campus, and its blossoms frequently come in close vicinity of road surfaces and nearby motor vehicles. Therefore, we suggest that n-alkanes found in the forsythia samples were associated with the contamination from the exhaust gas of internal combustion engines. Meanwhile, saturated fatty aldehydes (SFAs), especially nonanal ($C_9H_{18}O$) were found in the volatile phase of all flower samples (Figure 3b). The C_5 - C_{11} homology of SFAs was found in *Prunus yedoensis* and *Korean azalea* samples, which account for 15.0 and 20.5% of the total volatile contents, respectively. Furthermore, the volatile contents of *Korean forsythia* samples contained up to 54.5% of C_5 - C_{12} straight-chain saturated aldehydes,

which is the highest in this category. SFAs such as octanal and nonanal are highly fragrant compounds associated as the key odorants of various flowers and plants, such as rose orange¹³ or tea tree¹⁴, which could be responsible for the fruity and rosy odor of *forsythia* and *azalea* blossoms.

Saturated and short-chain alcohols such as ethanol and C_5 - C_8 alkanols were found to be the major volatile components in *Korean azalea* samples. Floral nectars, especially in *azalea* and *dandelion* blossoms, usually contain *Saccharomyces* yeasts which could convert glucose and galactose into ethanol. Among all collected samples, the ethanol contents in *azalea* samples peaked at 42.0%, followed by *Dilatata lilac* and *forsythia* samples at 16.5 and 10.5%, respectively. Furthermore, the distribution of short-chain alcohols ranged from C_5 to C_8 according to each floral group were described in Figure 3c. C_5 - C_8 alkanols contributed a total of 6.4% of the relative VOCs content in the *azalea* group, in which 1-hexanol was the

main compound (3.6%). In comparison, 1-octanol was solely detected in *Dilatata lilac* samples at 3.4%. Finally, the presence of different terpene and terpenoid compounds in floral blossom samples (Figure 3d) was discovered as one of the key components to define the aromatic profiles. γ -terpinene (RT = 8.142 min) was found to be highest in *Dilatata lilac* samples (51.7%), followed by *magnolias* (3.1%), while their content in the other floral groups ranged below 1%. Contrastingly, β -myrcene (RT = 6.654 min) was found as the major terpenoid compound in *magnolia* samples. Furthermore, other compounds such as 3-carene, α - and β -pinene, camphene, D-limonene and α -cymene were identified at various amounts in all the floral groups. Therefore, significantly different patterns in the distribution of aldehydes and alcohol compounds in the HS-GC-MS results could assist in defining and identifying the aromatic profile of each floral type.

Multivariate statistical analysis for classification of flowers from aroma profile

Statistical data analysis techniques, specifically multivariate data analysis methods such as principal component analysis (PCA) and partial least-squares discriminant analysis (PLS-DA) were vastly employed to characterize and differentiate the aroma profiles obtained from HS GC-MS data.^{15,16} These powerful tools allow swift and robust visualization of the trends and patterns in complex datasets obtained from advanced instrumental analysis techniques.¹⁷⁻¹⁹ In this study, the raw chromatographic data obtained from HS GC-MS analysis of the collected flower samples were processed using PCA to classify their aroma profiles based on their biological origins. Three major botany groups in this study (*Korean forsythia*, *Korean azalea*, and *Dilatata lilac*) were selected for the analysis, but the floral groups containing only a single sample were excluded (*Lilytree*, *Lily magnolia*,

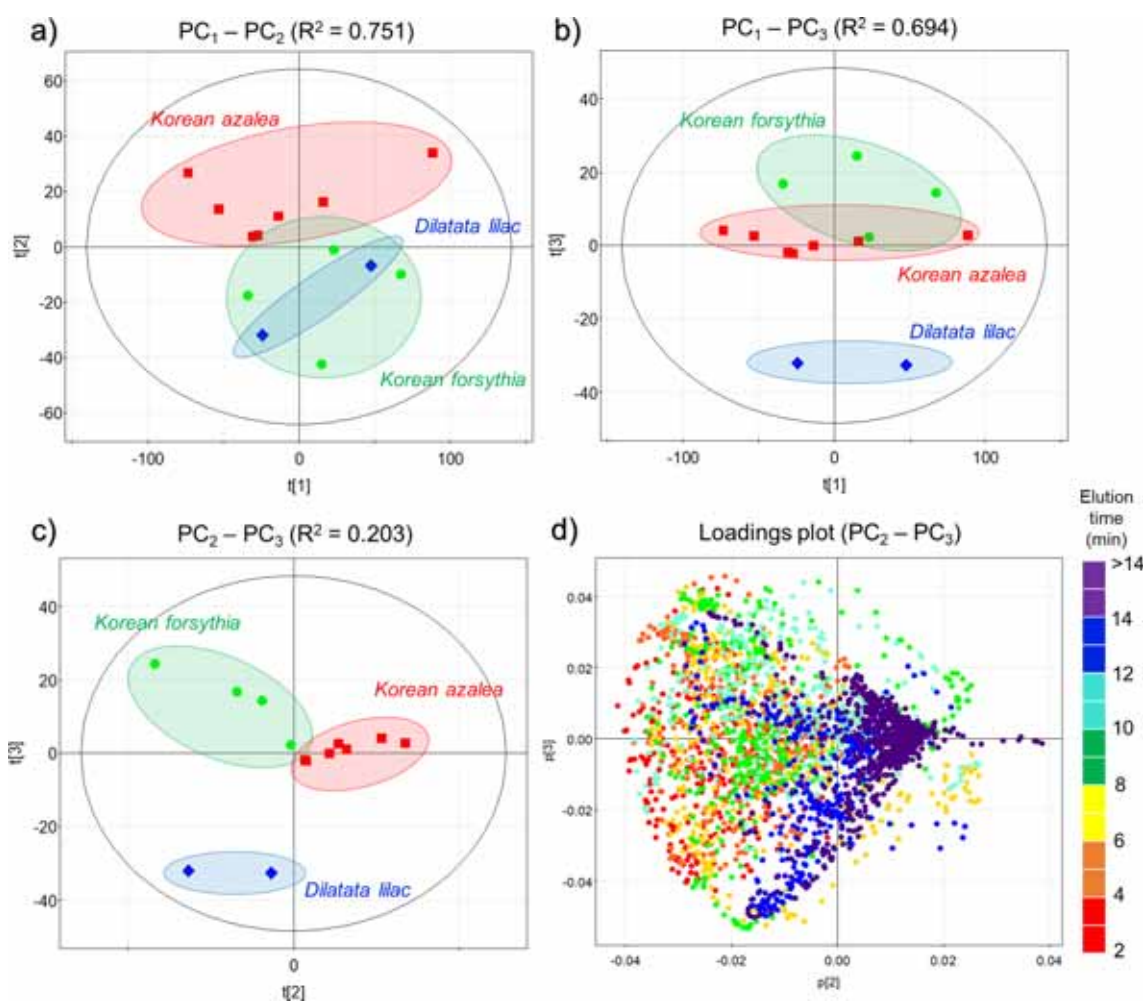


Figure 4. PCA analysis of the GC-MS data, showing the classification of the aroma profile according to the major flower sample groups: (a-c) score plot of the first 3 principal components (PCs) covering 82% of the total variance, and (d) loading plot of the PC₂-PC₃ pair, colored according to the elution time in GC-MS.

Prunus yedoensis).

A classification model comprised of 3 principal components (PCs) was able to explain up to 82% of the total variance, including R^2 ($PC_1 = 0.584$, $PC_2 = 0.140$, $PC_3 = 0.087$). The number of PCs was selected so that most of the characteristics of the original data were described while avoiding overfitting the model. The 2D score plots of each pair of components (Figure 4a-c) show that complete separation between the *Korean azalea* and other groups was achieved using the first two PCs, while the additional figures of the third component PC_3 could provide the differentiation between the GC-MS data from *Dilatata lilac* from the other floral groups. Interestingly, the score plot of PC_2 versus PC_3 showed a complete separation of the three groups despite the low amount of variance covered. The corresponding loading plot of the PC_2/PC_3 pair (Figure 4d) reveals the contribution of the aroma profile to the observed group separation. As observed in this plot, signal intensities from highly volatile, low molecular molecules (elution time < 6 min) were located at the low end of PC_2 which contributes to the location of *Korean forsythia* and *Dilatata lilac* groups, while the intensities from high boiling point molecules (elution time > 14 min) were highly associated to the location of *Korean azalea* samples. Furthermore, a complete separation of the three floral groups was observed in the 3-D score plot of the model (Figure S4), and the partial separation of elution time points into different layers in the 3-D space was also noted on the loading plot with three components as well. Therefore, it can be deduced that the major differences in the aroma profile of the three floral groups are based on the proportion of the high-volatility molecules (straight-chain alcohols and aldehydes) compared to the low-volatility molecules (branched alcohols and aromatic derivatives). These results show that HS-GC-MS analysis combined with statistical data analysis is a powerful tool to study and characterize the fragrance compounds of blossoms, which is useful for many applications such as perfume or personal care products.

Conclusions

With the collaboration of 62 undergraduate students in the Analytical Chemistry I class, floral petals from Korean Azalea, Korean Forsythia, Dilatata Lilac, Lilytree, Lily Magnolia, and Prunus Yedoensis were collected in April 2021 at CNU Daedeok campus. The flower samples were pre-treated and chromatographically separated to identify the fragrance compounds using HS-GC-MS. From the analysis, major volatile and aromatic compounds were identified, and these proportions were different according to the flower species. These analytical data may probably be useful for further metabolic and plant physiological analysis of landscape trees and fragrance effect depending on the botanical origin and environmental variances.

Furthermore, multivariate statistical analysis using the PCA method showed remarkable differentiation between floral origins based on the raw data of HS-GC-MS analysis, which may be largely useful for many industrial applications such as perfume or personal care products.

Acknowledgments

This research was supported by Chungnam National University (2020-2021).

References

- Rubiolo, P.; Sgorbini, B.; Liberto, E.; Cordero, C.; Bicchi, C. *Flavour Fragr. J.* **2010**, *25*, 282-290. DOI: 10.1002/ffj.1984
- Tomás-Barberán, F.A.; Robins, R.J. 1997. Phytochemistry of fruit and vegetables. In *International Symposium of Phytochemistry of Fruit and Vegetables (1995: Murcia, Spain)*: Clarendon Press.
- Schwab, W.; Davidovich-Rikanati, R.; Lewinsohn, E. *The plant journal* **2008**, *54*, 712. DOI: 10.1111/j.1365-313X.2008.03446.x
- Seymour, G.B.; Taylor, J.E.; Tucker, G.A. *Biochemistry of fruit ripening*, Springer Science & Business Media. UK, **2012**.
- Buck, L.; Axel, R. *Cell* **1991**, *65*, 175. DOI: 10.1016/0092-8674(91)90418-X
- Hyun, H.B.; Boo, K.H.; Kang, H.R.; Kim Cho, S. *Journal of Applied Biological Chemistry* **2015**, *58*, 175. <http://dx.doi.org/10.3839/jabc.2015.028>
- Robards, K.; Robards, K.; Haddad, P.R.; Jackson, P.; Jackson, P.; Haddad, P.A. *Principles and practice of modern chromatographic methods*, Academic Press. US, **1994**.
- Li, X.-l.; Sun, Z.-y.; Li, J.-y.; Fan, Z.-q.; Yin, H.-f. *Food Science* **2012**, *2012*, 16. <https://www.spkx.net.cn/EN/Y2012/V33/I16/130>
- Oh, S.-M.; Chun, J.-H.; Lee, M.-K.; Kim, J.-B.; Kim, S.-J. *Korean Journal of Agricultural Science* **2017**, *44*, 104. DOI: 10.7744/kjoas.20170012
- Yao, K.; Ma, H.; Huang, M.; Zhao, H.; Zhao, J.; Li, Y.; Dou, S.; Zhan, Y. *ACS Appl. Nano Mater.* **2019**, *2*, 5512. DOI: 10.1021/acsanm.9b01097.
- Ito, T.; Kumazawa, K. *Biosci., Biotechnol., Biochem.* **1995**, *59*, 1944. DOI: 10.1271/bbb.59.1944.
- Huang, X.-Q.; Li, R.; Fu, J.; Dudareva, N. *Nature Communications* **2022**, *13*, 1352. DOI: 10.1038/s41467-022-28978-2.
- Yousif, S.I.; Bayram, M.; Kesen, S. *Journal of Food Quality* **2018**, *2018*, 8564086. DOI: 10.1155/2018/8564086.
- Kang, S.; Yan, H.; Zhu, Y.; Liu, X.; Lv, H.-P.; Zhang, Y.; Dai, W.-D.; Guo, L.; Tan, J.-F.; Peng, Q.-H.; Lin, Z. *Food Research International* **2019**, *121*, 73. DOI: 10.1016/j.foodres.2019.03.009.

15. Maeztu, L.; Sanz, C.; Andueza, S.; Paz De Peña, M.; Bello, J.; Cid, C. *J. Agric. Food Chem.* **2001**, *49*, 5437. DOI: 10.1021/jf0107959.
16. Wadood, S.A.; Boli, G.; Xiaowen, Z.; Raza, A.; Yimin, W. *J. Mass Spectrom.* **2020**, *55*, e4453. DOI: 10.1002/jms.4453.
17. Rajalahti, T.; Kvalheim, O.M. *Int. J. Pharm.* **2011**, *417*, 280. DOI: 10.1016/j.ijpharm.2011.02.019.
18. Nguyen, H.-Q.; Lee, D.; Kim, Y.; Bang, G.; Cho, K.; Lee, Y.-S.; Yeon, J.E.; Lubman, D.M.; Kim, J. *Journal of Proteomics* **2021**, *245*, 104278. DOI: 10.1016/j.jprot.2021.104278.
19. Abid, A.; Zhang, M.J.; Bagaria, V.K.; Zou, J. *Nature Communications* **2018**, *9*, 2134. DOI: 10.1038/s41467-018-04608-8.

The Advanced Analytical Method Through the Quantitative Comparative Study of Taurine in Feed Using LC-MS/MS

Yeong Jun Seon[†], Hyung Ju Seo[†], Jiye Yoon, Hyunjeong Cho, Sunghie Hong, Seung Hwa Lee*, and Tae Woong Na*

Experiment Research Institute, National Agricultural Products Quality Management Service, 141, Yongjeon-ro, Gimcheon-si, Gyeongsangbuk-do, 39660, Korea

Received October 8, 2022, Revised November 7, 2022, Accepted November 21, 2022

First published on the web December 31, 2022; DOI: 10.5478/MSL.2022.13.4.133

Abstract : Taurine is a type of sulfur-containing amino acid having a sulfate functional group, that is biosynthesized from cysteine. It is mainly distributed in high concentrations in animal tissues and is known to have various effects such as osmotic pressure control, calcium control, anti-inflammatory, antioxidant, and hepatocellular protection. Also, taurine deficiency causes a variety of symptoms, including visual impairment. In particular, in the case of cats, taurine is not biosynthesized and must be supplied through food, so it is classified as an essential amino acid. In this study, an analysis method using mass spectrometry was developed instead of the commonly used derivatization method to quickly, environmentally, and precisely analyze taurine in various animal feeds. The developed analytical method showed good linearity ($R^2 > 0.99$), accuracy (81.97-105.78%), and precision (0.07-12.37%). In addition, the developed method was further verified through quantitative comparison with the derivatization method. This developed method was used in the determination of taurine in 20 animal feed samples obtained from South Korea. The levels of taurine found ranged from 81.53 to 6,743.53 mg/kg. The developed analysis method will be used for the detection and quantification of taurine in domestic feed.

Keywords : taurine, feed, LC-MS/MS, amino acid analyzer, comparative study

Introduction

Amino acids are components of proteins and are essential for animal growth and maintenance of physiological functions. There are about 20 kinds of amino acids that make up proteins, and they are classified into essential amino acids and non-essential amino acids. Essential amino acids are amino acids that must be supplied from the outside to sustain animal life and include lysine, leucine, methionine, phenylalanine, taurine, threonine, tryptophan, and valine.¹⁻³ Among them, taurine (β -amino ethane sulfonic acid) is a type of sulfur-containing amino acid having a structure in which an amino group is bonded to β -carbon

and a sulfate group is bonded to α -carbon.^{4,5} Taurine is biosynthesized from cysteine and mainly distributed in high concentrations in animal tissues (muscle, heart, brain, retina).^{2,6} The physiological action of taurine is known to have various effects such as cell proliferation, osmotic pressure regulation, calcium regulation, glucose metabolism promotion, nerve excitability regulation, anti-inflammatory, antioxidant, and hepatocellular protection.⁷⁻¹²

Amino acids in the feed are used as supplements added to feed to increase their utility. The addition of taurine to high-fat diets can improve serum total cholesterol and triglyceride levels without affecting the productivity of laying hens,¹³ and in the case of finishing pigs has shown that it increased growth and decreased serum and liver total cholesterol levels.¹⁴ In particular, in the case of cats, taurine cannot be biosynthesized and must be supplied through food, so it is classified as an essential amino acid. The minimum taurine content required for adult cats in pet food is set at 25 mg/100 kcal for dry food and 50 mg/100 kcal for wet food.¹⁵ Currently, taurine is classified as a supplementary feed in the domestic feed management law, and it is mainly used by adding it to the feeds of animals that need taurine, such as cats.¹⁶ Although there is no registration standard for taurine, an analysis method that can accurately quantify trace amounts of taurine contained in the feed ingredient and compound feed is needed to prevent taurine deficiency and excess.

A representative analysis method for analyzing taurine in feed is the Association of Official Analytical Chemists

Open Access

[†]Both authors contributed equally to this work.

*Reprint requests to Seung Hwa Lee, Tae Woong Na

<https://orcid.org/0000-0003-4828-8819>

<https://orcid.org/0000-0003-4003-083X>

E-mail: shlee96@korea.kr, naratw@korea.kr

All the content in Mass Spectrometry Letters (MSL) is Open Access, meaning it is accessible online to everyone, without fee and authors' permission. All MSL content is published and distributed under the terms of the Creative Commons Attribution License (<http://creativecommons.org/licenses/by/3.0/>). Under this license, authors reserve the copyright for their content; however, they permit anyone to unrestrictedly use, distribute, and reproduce the content in any medium as far as the original authors and source are cited. For any reuse, redistribution, or reproduction of a work, users must clarify the license terms under which the work was produced.

(AOAC) official method, which is an internationally recognized analysis method. In this analysis method, taurine is quantified in feed using LC-FLD through fluorescence derivatization after hydrolysis with hydrochloric acid and reaction with dansyl chloride.¹⁷ Several studies have been conducted to quantify taurine in sports drinks and dairy products based on AOAC internationally recognized analytical methods.¹⁸⁻²¹ Amino acids including taurine have an amino group (-NH₂) and a carboxyl group (-COOH) structure, and since absorption does not occur in the ultraviolet and visible light regions, the fluorescence derivatization process is absolutely necessary.²²⁻²⁴

Disadvantages of such an analysis method are that it takes a lot of time for sample preparation such as hydrolysis and derivatization, and LC-FLD analysis through derivatization is not suitable for accurate quantitative analysis because of its relatively low analytical sensitivity compared to LC-MS/MS. In addition, since the concentration of taurine is relatively low compared to other amino acids, the above pretreatment method to liberate all amino acids may be affected by other amino acids when taurine is separated from the column. Therefore, in this study, an analysis method using ultrasonic extraction and mass spectrometry that can analyze taurine without such a derivatization process was developed. In order to confirm the extraction efficiency of the developed method and the accuracy and precision of the instrumental analysis, a comparative experiment with the derivatization method based on the AOAC method was performed. Comparative experiments were performed using certified reference materials (CRM). It was confirmed that the analytical method developed through the comparative experiment between the analytical methods had no significant difference from the existing analytical method in quantifying taurine, and then the validity was confirmed within and between laboratories. Taurine analysis was performed on 20 feed samples using the finally developed analysis method.

Experimental

Chemicals and reagents

Taurine (99%) used as a standard material was a high-purity reagent from Sigma-Aldrich (St. Louis, MO, USA). Distilled water was prepared using a Milli-Q Direct 8 model manufactured by Merck Millipore (MA, USA). As for methanol, Merck (Darmstadt, Germany) product was used as HPLC grade, and formic acid (98%) was used by Thermo Fisher Scientific (Waltham, USA). Ammonium acetate (NH₄CH₃CO₂) used for solvent and extraction was manufactured by Thermo Fisher Scientific (Waltham, USA), and a syringe filter (Whatman, Maidstone, UK) for filtering the sample was 13 mm made of PTFE (polytetrafluoroethylene), 0.2 μm size was used. Hydrochloric acid was EP-S grade, manufactured by Chemitop (Korea), and Ethanol, manufactured by Merck (Darmstadt, Germany) was used as HPLC grade. The mobile phase solvent is buffer aqueous solution No. 05112 of KANTO Chemical (Tokyo, Japan). Buffer for protein hydrolysate PH-1 (Sodium citrate dihydrate 0.62%, Sodium chloride 0.56%, Citric acid monohydrate 1.97%, Ethanol

10.20%, β-Thiodiglycol 0.55%, 25% Brij-35 0.40%, n-Octanoic acid 0.01%, pH 3.3), ninhydrin reagent Reagent (R) 1 (Propylene glycol monomethyl ether 979 mL, Ninhydrin 39 g, Sodium borohydride 81 mg), Reagent (R) 2 (Distilled water 336 mL, Lithium acetate dihydrate) 204 g, Glacial acetic acid 123 mL, Propylene glycol monomethyl ether 401 mL) was purchased using a Ninhydrin Coloring Solution Kit from FUJIFILM Wako Pure Chemical (Osaka, Japan).

Linearity and calibration curve

The standard preparation for LC-MS/MS analysis is as follows. Taurine was dissolved in 10 mM ammonium acetate to prepare a standard stock solution at a concentration of 1,000 mg/L. To prepare a calibration solution for quantitative analysis, a standard solution was mixed with an untreated sample extract in a ratio of 9:1 to prepare a concentration of 20, 50, 100, 200, 500, 1,000, and 2,000 μg/L. The preparation of standard materials for the amino acid analyzer is as follows. Taurine was dissolved in 10 mM ammonium acetate to prepare a standard stock solution at a concentration of 1,250 mg/L. For quantitative analysis, standard solutions were prepared with 10 mM ammonium acetate at concentrations of 1,250, 2,500, 6,250, and 12,500 μg/L.

Sample preparation

For the untreated samples to verify the validity of the taurine analysis conditions, a compound feed for growing pigs and pets and a soybean ingredient feed were selected. In addition, experiments were conducted using SRM (NIST 3290) and pet dog food as samples to investigate the quantitative ability of the taurine analytical method.

Ultrasonic extraction method for LC-MS/MS

0.5 g of the homogenized sample was precisely weighed and placed in a 50 mL centrifuge tube, 50 mL of a 10 mM aqueous ammonium acetate was added, followed by ultrasonic extraction for 30 min, followed by centrifugation at 4°C, 4,000 g for 10 min. The extracted sample solution was filtered with a 0.2 μm (PTFE, Whatman Inc., Maidstone, UK) syringe filter, and then used as the sample solution.

Derivatization analysis method for amino acid analyzer

0.2 g of the homogenized sample into a 50 mL centrifuge tube, add 20 mL of 6 M HCl, and then hydrolyze at 110°C for 20 hours. After cooling the sample solution to room temperature, put it in a 100 mL volumetric flask and add water to adjust the total volume to 100 mL. Take 1 mL of supernatant, concentrate, and then re-dissolve in 10 mM aqueous ammonium acetate.¹⁷ The extracted sample solution was filtered with a 0.2 μm (PTFE, Whatman Inc., Maidstone, UK) syringe filter, and then used as the sample solution.

LC-MS/MS analysis

LC-MS/MS 8060 manufactured by Shimadzu (Tokyo, Japan) was used, and Hypersil Gold C18 (5 μm, 4.6 × 150 mm) was chosen as the analytical column. The flow rate was 0.5 mL/min. The injection volume was 5 μL and the

Table 1. Multiple reaction monitoring (MRM) conditions for taurine.

Compound	Precursor ion		Product ion					
	m/z	Q1 pre bias (V) ^{a)}	Quantitative ion			Qualitative ion		
			m/z	CE (V)	Q3 pre bias (V) ^{b)}	m/z	CE (V) ^{c)}	Q3 pre bias (V)
Taurine	124.2	-13	80.1	22	11	124.2	2	12

^{a)} Voltage promotes the ionization of the precursor ion.

^{b)} Voltage promotes the ionization of the product ion.

^{c)} Collision energy.

Table 2. Amino acid automatic analyzer L-8900 gradient conditions for taurine.

Time (min)	%B1 ^{a)}	Flow (mL/min)	%R1 ^{b)}	%R2 ^{c)}	%R3 ^{d)}	Flow (mL/min)
0.0	100	0.400	55	45	0	0.350
3.2	100	0.400	55	45	0	0.350
3.3	100	0.400	0	0	100	0.350
6.2	100	0.400	0	0	100	0.350
6.3	100	0.400	55	45	0	0.350
23.2	100	0.400	55	45	0	0.350

^{a)} Water solution contains following substances; Sodium citrate dihydrate 0.62%, sodium chloride 0.56%, citric acid monohydrate 1.97%, ethanol 10.20%, β -thiodiglycol 0.55%, Brij-35 (dissolve 25 g into 100 mL of distilled water.) 0.40%, and n-octanoic acid 0.01%, pH 3.3.

^{b)} Propylene glycol monomethyl ether 979 mL, ninhydrin 39 g, and sodium borohydride 81 mg.

^{c)} Distilled water 336 mL, lithium acetate dihydrate 204 g, glacial acetic acid 123 mL, and propylene glycol monomethyl ether 401 mL.

^{d)} Water solution contains 50 mL ethanol.

temperature was maintained at 40°C. The mobile phase is water containing 50 mM ammonium acetate as mobile phase A, and methanol containing 0.1% formic acid as mobile phase B. The gradient elution method was optimized. 0 min 97%(A) 3%(B), 5 min 97%(A) 3%(B), 6 min 3%(A) 97%(B), 7.5 min 3%(A) 97%(B), 8.5 min 97%(A) 3%(B), 12 min 97%(A) 3%(B). For detailed conditions of the mass spectrometer, the negative ion mode of the electrospray ionization (ESI) method was used, and the interface temperature 300°C, DL temperature 250°C, nebulizing gas 3 L/min, heating gas 10 L/min, drying gas 10 L/min. Multiple monitoring mode (MRM) conditions were established as shown in Table 1.

Amino acid analyzer analysis

Amino acid analyzer AAA L-8900 from Hitachi (Tokyo, Japan) was used, and the analysis column was chosen Hitachi ion exchange resin 855-4506 (Na type, 4.6 × 60 mm). The reaction column was Hitachi reaction column 852-3540 (4.6 × 60 mm). The flow rates of 0.4 mL/min (pump 1), 0.35 mL/min (pump 2), and injection volume were 20 μ L. The analysis column temperature was 57°C, and the reactor temperature was maintained at 135°C. The gradient conditions of the mobile phase are shown in Table 2.

Validation

The validity of the established analytical method was

verified according to the guidelines of the Ministry of Food and Drug Safety (MFDS): selectivity, linearity, accuracy, and precision.²⁵ To check the linearity, a matrix matched calibration standard solution was prepared so as to be 20–2,000 μ g/L, and the coefficient of correlation (R^2) of the calibration curve was obtained. In order to confirm the accuracy and precision of the analysis method, a recovery rate experiment was performed by adding a standard solution to the untreated sample. The recovery rate was repeated three times at LOQ, 2LOQ, and 5LOQ concentrations, respectively, to calculate the accuracy and relative standard deviation (%RSD, relative standard deviation). The LOQ of the analytical method was selected as the lowest concentration that satisfies the recovery criteria according to the validation guidelines of SANTE/12682/2019.²⁶ For more precise validation, cross-validation between laboratories was performed. The matrix effects were calculated by comparing the slope of the calibration curve of the taurine standard prepared by dissolving in a pure solvent and the slope of the calibration curve of the matrix-matched standard, respectively, using the following formula.

$$\text{Matrix effect(\%)} = \left(\frac{\text{Slope of calibration curve in matrix}}{\text{Slope of calibration curve in solvent}} - 1 \right) \times 100$$

Results and discussion

LC-MS/MS condition

The optimal multiple reaction monitoring (MRM) was established in the negative ion mode of electrospray ionization (ESI). Precursor ions were identified in full scan mode, and product ions were selected in consideration of the ratio of each ion. Among them, m/z 80.5, the product ion with the best sensitivity, was selected as the quantitation ion, and the ion showing the next highest sensitivity, m/z 124.2, was selected as the confirmation ion (Table 1).

Selectivity and linearity

For linearity evaluation, seven standard solution concentrations ranging from 20 to 2,000 $\mu\text{g/L}$ in matrix extracts were

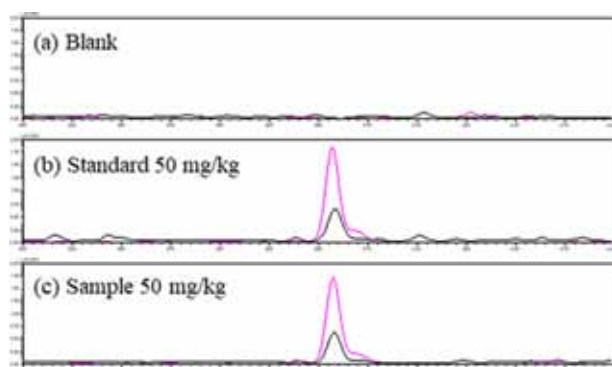


Figure 1. Representative chromatogram of (a) blank sample, (b) standard 50 mg/kg, and (c) sample 50 mg/kg.

analyzed to determine the linearity. In general, the coefficient of determination (R^2) was higher than 0.99 in all matrices, indicating suitable linearity. And as a result of analyzing the samples without treatment of the single feed and the compound feed by establishing the MRM conditions, high selectivity and resolution were confirmed (Figure 1).

Matrix effect

As a result of confirming the matrix effect on the pig, dog, and soybean feed used for validation, pig feed (-35.61%), dog feed (-44.31%), and soybean feed (-43.98%) were shown. In all samples, the signal of the analyte showed a tendency to decrease (suppression), and the matrix effect was within -50%. Therefore, it was confirmed that the application of matrix matched calibration is necessary for accurate quantification.

LOQ, precision, and accuracy

The limit of quantitation of the analytical method was selected as 10 mg/kg, which is the lowest stock concentration at which the recovery result satisfies the criteria for validation guidelines of SANTE/12682/2019.²⁶ In order to evaluate the accuracy and precision of the developed analysis method, breeding pigs, pet dog compound feed, and soybean ingredient feed were used. The recovery rate experiment was repeated three times with LOQ, 2LOQ, and 5LOQ concentrations, respectively. As a result, the accuracy and precision were 81.97–105.78 % and 0.07–12.37 %, confirming that the recommended standard was satisfied (Table 3).

Method comparison

The established analytical method is a simplified method

Table 3. LOQ, accuracy, and precision of taurine in feed ingredient (soybean) and compound feeds (pig and dog).

Analyte	LOQ (mg/kg)	Recovery Conc. ^{a)} (mg/kg)	Accuracy (Precision, %)					
			Intra-Lab ($n = 3$)			Inter-Lab ($n = 3$)		
			FI ^{b)} (soybean)	CF ^{c)} (pig)	CF (dog)	FI (soybean)	CF (pig)	CF (dog)
Taurine	10	10	83.39 (12.37)	95.98 (6.80)	105.78 (1.47)	98.15 (0.07)	94.30 (0.45)	87.90 (8.37)
		20	88.87 (8.26)	91.20 (7.54)	102.41 (6.82)	95.70 (1.63)	95.85 (1.70)	91.85 (2.08)
		50	81.97 (5.77)	88.92 (2.16)	102.20 (1.45)	92.95 (3.88)	91.75 (1.62)	94.15 (0.23)

^{a)} In the case of dog compound feed, taurine was detected in all blank samples, and the recovery concentration was adjusted to 20, 50, and 100 mg/kg.

^{b)} Feed ingredient.

^{c)} Compound feed.

Table 4. Comparison of quantitative values (%) and % RSD of taurine in CRM and real samples according to extraction method and analysis instrument.

Extraction method / Instrument	CRM ^{a)}		Real sample	
	Hydrolysis Extraction	Ultrasonic Extraction	Hydrolysis Extraction	Ultrasonic Extraction
Amino acid analyzer	0.19 (0.78)	0.19 (19.57)	0.19 (0.88)	0.21 (18.02)
LC-MS/MS	0.20 (9.94)	0.23 (10.27)	0.21 (4.80)	0.23 (8.34)

^{a)} The taurine content of the certified standard material was 0.24%.

Table 5. Content levels of taurine in 20 feed samples in South Korea.

Sample	No. of samples	Minimum (mg/kg)	Median (mg/kg)	Maximum (mg/kg)	Recommend level ^{a)} (mg/kg)
Cat feed	10	1,059.11	1,625.58	6,743.53	1,000
Dog feed	10	81.53	349.43	2,008.69	-

^{a)} Official Publication for taurine levels in dog and cat feed according to Association of American Feed Control Officials (AAFCO).

of the commonly used taurine pretreatment method, and since LC-MS/MS, which is different analytical equipment from the existing analytical method, was used, an experiment was performed to compare it with the existing amino acid analyzer. Therefore, we compared the results using LC-MS/MS and an automatic amino acid analyzer (Hitachi L-8900) for the sample solutions extracted with taurine by the conventional extraction method through HCl hydrolysis and the established extraction method. As a result, when ultrasonic extraction and LC-MS/MS were used, the results were closest to the quantitative value of CRM (Table 4).

Real sample analysis

The established method was applied in the determination of taurine in 20 pet feed samples obtained in various regions of South Korea. The presence of a positive sample was confirmed by comparing the retention time and product ion ratio obtained with the calibration standards. Taurine was detected at levels from 81.53 to 6,743.53 mg/kg in 20 feed samples (Table 5). According to the Association of American Feed Control Officials (AAFCO) official publication, recommend level of taurine in cat feed is defined as 1,000 mg/kg¹⁵. In this study, all cat feeds were found to be present in taurine at levels between 1,059.11 and 6,743.53 mg/kg and observed above the AAFCO recommended level of 1,000 mg/kg. It was confirmed that the developed method is capable of quantification and qualification of the taurine in animal feeds by ultrasonic extraction without the derivatization process, which is a traditional extraction method.

Conclusions

As a result of comparing the new analysis method for taurine analysis in feed with the existing general analysis method, it was confirmed that extraction was possible only with simple ultrasonic extraction without the existing derivatization process. Accordingly, it is expected that the time and cost of taurine analysis in feed can be greatly reduced. In addition, it is expected that a trace amount of taurine in the compound feed can be confirmed more accurately and precisely by checking the sensitivity and resolution more precisely than the existing equipment through the advancement of the analysis equipment. As can be seen from the monitoring results for real samples, it was confirmed that a small amount of taurine was detected. In conclusion, through this study, the analysis method related to the analysis of taurine in feed has been further advanced, and it is expected that more precise and accurate analysis will be possible through this study.

Acknowledgments

This research did not receive external financial support.

References

1. Carter, H.E. *Ann N Y Acad Sci* **1979**, 325, 236. DOI: 10.1111/j.1749-6632.1979.tb14138.x.
2. Ripps, H.; Shen, W. *Mol Vis* **2012**, 18, 2673.
3. Mitsuhashi, S. *Curr Opin Biotechnol* **2014**, 26, 38. DOI: 10.1016/j.copbio.2013.08.020.
4. Jong, C.J.; Sandal, P.; Schaffer, S.W. *Molecules* **2021**, 26, 4913. DOI: 10.3390/molecules26164913.
5. Brosnan, J.T.; Brosnan, M.E. *J Nutr* **2006**, 136, 1636S. DOI: 10.1093/jn/136.6.1636S.
6. De Luca, A.; Pierno, S.; Camerino, D.C. *J Transl Med* **2015**, 13, 243. DOI: 10.1186/s12967-015-0610-1.
7. Schaffer, S.; Kim, H.W. *Biomol Ther (Seoul)* **2018**, 26, 225. DOI: 10.4062/biomolther.2017.251.
8. Rafiee, Z.; Garcia-Serrano, A.M.; Duarte, J.M.N. *Nutrients* **2022**, 14, 1292. DOI: 10.3390/nu14061292.
9. Salze, G.P.; Davis, D.A. *Aquaculture* **2015**, 437, 215. DOI: 10.1016/j.aquaculture.2014.12.006.
10. Yoon, J.A.; Choi, K.-S.; Shin, K.-O. *The Korean Journal of Food And Nutrition* **2015**, 28, 404. DOI: 10.9799/ksfan.2015.28.3.404.
11. Yoon, J.A.; Shin, K.-O.; Choi, K.-S. *The Korean Journal of Food And Nutrition* **2015**, 28, 880. DOI: 10.9799/ksfan.2015.28.5.880.
12. Kim, S.-K.; Shin, M.-G.; Lee, B.-I. *Journal of Fisheries and Marine Sciences Education* **2020**, 32, 944. DOI: 10.13000/jfmse.2020.8.32.4.944.
13. Han, H.L.; Zhang, J.F.; Yan, E.F.; Shen, M.M.; Wu, J.M.; Gan, Z.D.; Wei, C.H.; Zhang, L.L.; Wang, T. *Poult Sci* **2020**, 99, 5707. DOI: 10.1016/j.psj.2020.07.020.
14. Yokogoshi, H.; Oda, H. *Amino Acids* **2002**, 23, 433. DOI: 10.1007/s00726-002-0211-1.
15. Association of American Feed Control Officials, USA. AAFCO Methods for substantiating nutritional adequacy of dog and cat foods.; See https://www.aafco.org/Portals/0/SiteContent/Regulatory/Committees/PetFood/Reports/Pet_Food_Report_2013_Midyear-Proposed_Revisions_to_AAFCO_Nutrient_Profiles.pdf.
16. Ministry of agriculture, food and rural affairs, South Korea. Standards and specifications for feed, etc.; See <https://www.law.go.kr/LSW/admRulLInfoP.do?admRulSeq=2100000068609>.
17. George, W.; Latimer, J. *Official methods of analysis of*

- AOAC international 20th edition*, AOAC international, Rockville, **2016**.
18. Vochyanova, B.; Opekar, F.; Tuma, P. *Electrophoresis* **2014**, 35, 1660. DOI: 10.1002/elps.201300480.
 19. Chae, H.; Jeong, O.-M.; Her, M.; Kang, J. *Journal of the Preventive Veterinary Medicine* **2021**, 45, 166. DOI: 10.13041/jpvm.2021.45.4.166.
 20. Ricciutelli, M.; Caprioli, G.; Cortese, M.; Lombardozi, A.; Strano, M.; Vittori, S.; Sagratini, G. *J Chromatogr A* **2014**, 1364, 303. DOI: 10.1016/j.chroma.2014.08.083.
 21. Manzi, P.; Pizzoferrato, L. *Int J Food Sci Nutr* **2013**, 64, 112. DOI: 10.3109/09637486.2012.704906.
 22. Gatti, R.; Gioia, M.G.; Andreatta, P.; Pentassuglia, G. *J Pharm Biomed Anal* **2004**, 35, 339. DOI: 10.1016/S0731-7085(03)00584-3.
 23. Hou, S.; He, H.; Zhang, W.; Xie, H.; Zhang, X. *Talanta* **2009**, 80, 440. DOI: 10.1016/j.talanta.2009.07.013.
 24. Uekusa, S.; Onozato, M.; Sakamoto, T.; Umino, M.; Ichiba, H.; Okoshi, K.; Fukushima, T. *Molecules* **2021**, 26, 3498. DOI: 10.3390/molecules26123498.
 25. Ministry of food and drug safety, South Korea, Guidelines for the standard procedure for preparing test methods for food, etc.; See https://www.mfds.go.kr/brd/m_1060/view.do?seq=12920&srchFr=&srchTo=&srchWord=&srchTp=&itm_seq_1=0&itm_seq_2=0&multi_itm_seq=0&company_cd=&company_nm=&page=69.
 26. European union reference laboratory, European commission, SANTE/12682/2019 Analytical quality control and method validation procedures for pesticide residues analysis in food and feed.; See https://www.eurl-pesticides.eu/userfiles/file/EurlALL/AqcGuidance_SANTE_2019_12682.pdf.

Relative Quantification of Glycans by Metabolic Isotope Labeling with Isotope Glucose in *Aspergillus niger*

Soo-Hyun Choi[†], Ye-Eun Cho[†], Do-Hyun Kim, Jin-il Kim, Jihee Yun, Jae-Yoon Jo, and Jae-Min Lim*

Department of Chemistry, Changwon National University, 20 Changwondaehak-ro, Uichang-gu, Changwon 51140, Republic of Korea

Received November 27, 2022, Revised December 12, 2022, Accepted December 14, 2022

First published on the web December 31, 2022; DOI: 10.5478/MSL.2022.13.4.139

Abstract : Protein glycosylation is a common post-translational modification by non-template-based biosynthesis. In fungal biotechnology, which has great applications in pharmaceuticals and industries, the importance of research on fungal glycoproteins and glycans is accelerating. In particular, the importance of quantitative analysis of fungal glycans is emerging in research on the production of filamentous fungal proteins by genetic modification. Reliable mass spectrometry-based techniques for quantitative glycomics have evolved into chemical, enzymatic, and metabolic stable isotope labeling methods. In this study, we intend to expand quantitative glycomics by metabolic isotope labeling of glycans in *Aspergillus niger*, a filamentous fungus model, by the MILPIG method. We demonstrate that incubation of filamentous fungi in a culture medium with carbon-13 labeled glucose ($1\text{-}^{13}\text{C}_1$) efficiently incorporates carbon-13 into N-linked glycans. In addition, for quantitative validation of this method, light and heavy glycans are mixed 1:1 to show the performance of quantitative analysis of various N-linked glycans simultaneously. We have successfully quantified fungal glycans by MILPIG and expect it to be widely applicable to glycan expression levels under various biological conditions in fungi.

Keywords : *Aspergillus niger*, Glycans, Glycosylation, Metabolic labeling, Isotopic glucose, Quantitative glycomics, MILPIG, Mass spectrometry

Introduction

Protein glycosylation is a common post-translational modification by a non-templated dynamic process.^{1,2} Glycans of glycoproteins play a crucial role in cellular responses to external stimuli, growth, and differentiation, and abnormal glycan composition is directly linked to various diseases.³ Current use of glycoprotein biomarkers in the clinical setting is usually based on the protein level, but complex and highly dynamic protein decorators such as glycosylation require continuous developments of analytical strategies. As analytical approaches for glycoproteins and glycans, mass spectrometry has contributed greatly to

understanding the physiological and pathological processes regulated by glycans and overcoming the challenges of quantitative analysis posed by the complexity of glycoconjugates.^{4,5}

Most strategies for relative quantitative glycomics have been achieved with isotopic labeling of glycans through the incorporation of stable D, ^{13}C , ^{15}N , and ^{18}O isotopes. Chemical *in vitro* labeling of glycans includes permethylation of glycans by isotope-labeled⁶ or isobaric iodomethane^{7,8} and reductive amination by isotope-labeled⁹ or isobaric tag^{10,11} with an amine group as a nucleophile. As enzymatic *in vitro* labeling strategies for glycans, methods by labeling ^{18}O at the reducing end of glycans through hydrolysis of ^{18}O -water with glycosidase were introduced.^{12,13} Methods for relative quantification of N-linked glycans utilizing transglycosylation of Endo-M with isotopically labeled acceptors have also been proposed.¹⁴⁻¹⁶

In addition to the chemical and enzymatic approaches, metabolic isotope labeling strategies of glycans with isotope-labeled monomer building blocks (glutamine or glucose) have been introduced as viable alternatives. IDAWG, isotopic detection of amino sugars using glutamine, is a pioneering report on the feasibility of metabolic incorporation for relative quantification in cell culture.^{17,18} This idea was expanded into a strategy to comprehensively quantify glycomes as the metabolic incorporation of isotopes into glycans.

Open Access

[†]These authors contributed equally to this work.

*Reprint requests to Jae-Min Lim

<https://orcid.org/0000-0002-7153-0194>

E-mail: jmlim@changwon.ac.kr

All the content in Mass Spectrometry Letters (MSL) is Open Access, meaning it is accessible online to everyone, without fee and authors' permission. All MSL content is published and distributed under the terms of the Creative Commons Attribution License (<http://creativecommons.org/licenses/by/3.0/>). Under this license, authors reserve the copyright for their content; however, they permit anyone to unrestrictedly use, distribute, and reproduce the content in any medium as far as the original authors and source are cited. For any reuse, redistribution, or reproduction of a work, users must clarify the license terms under which the work was produced.

MILPIG (metabolic isotope labeling of polysaccharides with isotopic glucose) was devised as a metabolic labeling strategy for glycans by adding isotopically labeled glucose ($1\text{-}^{13}\text{C}_1$) to a glucose-free medium in rice (*Oryza sativa*) cell culture.¹⁹ A follow-up study further demonstrated the quantification of high-mannose *N*-linked glycans with a small number of aminosugars and linear *O*-Man glycans without aminosugars through baker's yeast (*Saccharomyces cerevisiae*) culture for the construction of an isotope labeling model system.²⁰

In this study, the MILPIG method is used as a model for *Aspergillus niger*, the most versatile filamentous fungal platform strain, to explore the feasibility of isotope labeling and quantitative analysis of fungal glycans.^{21,22} It is noteworthy that the study of glycoproteins and glycans of fungi is considerably accelerated in fungal biotechnology, which is of great importance in pharmaceutical and industrial research.²³⁻²⁵ In particular, the importance of quantitative analysis of fungal glycans is emerging in the study of the overproduction of filamentous-fungal enzymes and glycosylation pathways by genetic modification.²⁶⁻²⁸

The biosynthesis of isotopically labeled glycan and quantitative analysis of glycan were performed in fungal culture conditions with isotopically labeled glucose ($1\text{-}^{13}\text{C}_1$) by the MILPIG method. We demonstrated that fungal *N*-linked glycans have mass differences between light and heavy glycans, depending on the number of sugars in the glycan. Based on this, a comparative quantitative analysis method was provided by obtaining a mass spectrum of a 1:1 mixture of light and heavy glycans for quantitative glycomics. From the experimental investigation with filamentous fungi, MILPIG was shown to yield excellent relative quantification of glycans by providing sufficient mass differences that increase with the number of sugars in the glycan.

Experimental

Materials and Chemicals

Peptide: *N*-glycosidase F (PNGase F) was purchased from New England BioLabs (Ipswich, MA, USA). $1\text{-}^{13}\text{C}_1$ glucose (98% - 99%) was purchased from Cambridge Isotope Laboratories (Tewksbury, MA, USA). 4-(2-Hydroxyethyl)piperazine-1-ethanesulfonic acid (HEPES) and sodium metabisulfite ($\text{Na}_2\text{S}_2\text{O}_5$) were purchased from Alfa Aesar (Haverhill, MA, USA). All other reagents and materials such as yeast nitrogen base (YNB), potato dextrose agar (PDA), d-glucose, trypsin, chymotrypsin, acetic acid (AcOH), methyl iodide (CH_3I), ammonium bicarbonate (NH_4HCO_3), dimethyl sulfoxide (DMSO), anhydrous DMSO, methanol (MeOH), anhydrous MeOH, chloroform, HPLC grade water, dichloromethane (DCM), isopropanol, sodium hydroxide (NaOH), acetonitrile (ACN), acetone, ethylenediaminetetraacetic acid (EDTA), sodium dodecyl sulfate (SDS), polyvinylpyrrolidone (PVPP), Discovery® DSC-18 SPE tube (solid-phase

extraction C18 column), respectively were purchased from Sigma-Aldrich (St. Louis, MO).

Fungiculture and Protein Extraction

The isolated *Aspergillus niger* was cultured on a potato dextrose agar plate at 26°C in darkness. The fungus spores were inoculated in the potato dextrose agar medium at 28°C and incubated in a shaking incubator at 28°C for 5 days of activation. To prepare fungal culture media according to the experimental conditions, yeast nitrogen base (67 mg) and d-glucose or $1\text{-}^{13}\text{C}_1$ glucose (50 mg or indicated amount) were dissolved with 10 mL of distilled water in 15 mL conical tube and autoclaved at 121°C for 15 min. The activated fungal spores were inoculated in conditional culture media and incubated in a shaking incubator at 28°C for 14 days or otherwise specified duration.

On the day of harvest, the fungal biomass was recovered through centrifugation and the fungi were washed three times with 3 mL of distilled water. For the glycan quantitative experiment, normal glucose and $1\text{-}^{13}\text{C}_1$ glucose-labeled fungi were mixed in equal proportion after harvest for subsequent analytical procedures. The fungal sample was transferred to a mortar, frozen with liquid nitrogen, and then finely ground and homogenized. The homogenized fungal sample was transferred to a conical tube and resuspended in 5 mL of 50 mM HEPES (pH 7.5) buffer containing 20 mM sodium metabisulfite, 5 mM EDTA, 0.1% (w/v) SDS, and 1.7% polyvinylpyrrolidone to extract fungal proteins. The sample was vortexed for 5 min at room temperature and centrifuged at $5,000 \times g$ for 15 min at 4°C. The supernatant was recovered and subjected to acetone precipitation three times at 4°C for 3 hours to remove contaminants. The pellet was collected by centrifugation and dried by a vacuum concentrator. The dried pellet was weighed and stored at -20°C until analysis.

Preparation of *N*-linked Glycans

Equal amounts of protein pellets (2.0 mg) were resuspended in 300 μL of 40 mM NH_4HCO_3 by sonication followed by boiling at 100°C for 2 min. After cooling to room temperature, 25 μL of trypsin stock (2 mg/mL in 40 mM NH_4HCO_3) was added. The samples were incubated overnight (18 h) at 37°C and boiled at 100°C for 5 min to deactivate proteases. The digested samples were loaded onto an equilibrated C18 extraction column, washed with 1 mL of 5% AcOH three times, and then eluted stepwise using 1 mL of 20% isopropanol in 5% AcOH, 40% isopropanol in 5% AcOH, and 100% isopropanol. The resulting glycopeptides were dried in a vacuum concentrator, resuspended with 29 μL of $1 \times$ PNGase F reaction buffer and 1 μL PNGase F (500 U), and incubated for 18 h at 37°C. The released glycan mixture was reconstituted in 5% AcOH and loaded onto an equilibrated C18 extraction column. *N*-linked oligosaccharides were

eluted by 1 mL of 5% AcOH three times and dried by the vacuum concentrator for subsequent permethylation.

Permethylation of Glycans

To facilitate the analysis of oligosaccharides by mass spectrometry, released oligosaccharide mixtures were permethylated as described previously.⁸ Briefly, glycans were resuspended in 200 μ L of anhydrous dimethyl sulfoxide and 250 μ L of freshly prepared dehydrated NaOH/DMSO reagent (mixture of 50% NaOH in 2 mL of anhydrous DMSO). After sonication and vortexing under the nitrogen gas, 100 μ L of CH₃I was added and the mixtures were vortexed vigorously for 5 min. 2 mL of distilled water was added to the samples and the excess CH₃I was removed by bubbling with a nitrogen stream. 2 mL of dichloromethane was added. After vigorous mixing and phase separation by centrifugation, the upper aqueous layer was removed and discarded. The nonpolar organic phase was then extracted 4 times with distilled water. Dichloromethane was evaporated on the heating module at 45°C with a mild nitrogen stream and the permethylated glycans were stored at -20°C until analysis.

Analysis of Glycans by Mass Spectrometry

For glycome analysis via direct infusion nanospray MS, permethylated glycans were dissolved by combining 15 μ L of the isotopically mixed sample in 100% methanol plus 35 μ L of 1 mM NaOH in 80% methanol. They were infused directly into a Q ExactiveTM Plus Orbitrap mass spectrometer (Thermo Fisher Scientific, USA) using a Nanospray FlexTM ion source with a fused-silica emitter (360 \times 75 \times 30 μ m, SilicaTipTM, New Objective) at 2.2 kV capillary voltage, 220°C capillary temperature, and a syringe flow rate of 0.8 μ L/min. The full FTMS spectra of *N*-linked glycans, typically recorded at 70,000 resolution in positive ion and profile mode, were collected at 500–2,000 *m/z* for 30 s with 5 microscans and 150 ms maximum injection time. The MS/MS spectra following higher energy collision dissociation (HCD) for structural information were obtained at 40% normalized collision energy for *N*-linked glycans.

Data Analysis

Mass spectra of glycan samples were interpreted manually and glycan structures were built graphically using GlycoWorkbench glycoinformatics tools.²⁹ The area of each isotope peak was integrated and the area of the glycan peak for comparative quantification was calculated as the sum of the peak areas obtained from the isotope envelope and the error according to the purity of the isotope labeled glucose was corrected. The relative abundance ratio of the 1:1 mixture was defined as the peak area ratio between normal glycans and isotopically labeled glycans.

Results and Discussion

Incorporation of Isotopic (1-¹³C₁) Glucose into Glycans

Glucose is the most important energy source for all living organisms and an indispensable precursor for glycan biosynthesis through the hexosamine biosynthetic pathway (HBP) in protein glycosylation. Therefore, in the MILPIG strategy as shown in Figure 1, isotopically labeled glucose in fungal culture media containing 1-¹³C₁ glucose is converted to the isotopically labeled UDP-*N*-acetylglucosamine (UDP-GlcNAc), a nucleotide sugar donor, which is important for protein glycosylation. Isotope-labeled UDP-GlcNAc is utilized in the biosynthesis of glycans and finally leads to the synthesis of isotope-labeled glycoproteins.

Considering that intracellular glucose flux is essential for cellular glycoconjugate biosynthesis, quantitative glycomics were established from the biosynthesis of isotopically labeled glycans with isotopically labeled glucose as shown in Figure 2. Here, we applied *Aspergillus niger* as a model system to the MILPIG method of fungi and conducted a study to evaluate the labeling efficiency of isotope-labeled glycans and the feasibility of quantitative glycomics.

Isotopically Labeled Glycans in Fungi by MILPIG

In our initial experimental design, we labeled fungi for 14 days with 7.5 mg/mL of normal (light) or with 1-¹³C₁ isotopic (heavy) glucose and then isolated *N*-linked glycans from glycoproteins. To reliably quantitate the

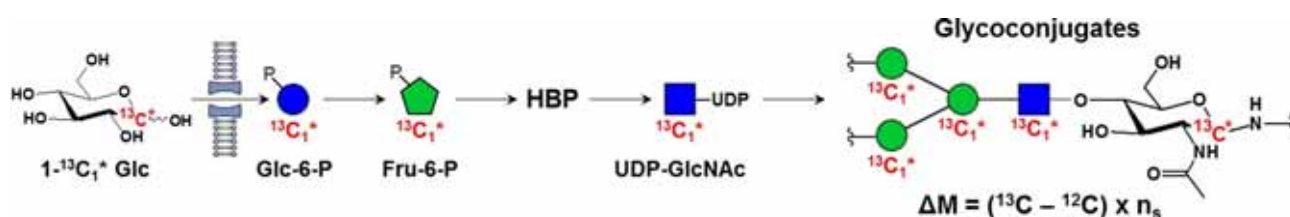


Figure 1. Biosynthetic pathway of isotopically labeled glycans by MILPIG method in fungi. Isotope labeling of glycoconjugates through the hexosamine biosynthetic pathway (HBP). An asterisk denotes an isotopically labeled species. ΔM is the mass difference between normal and isotopically labeled glycans by the sum of the number of sugars (n_s) in the glycans. The glycan structures are drawn based on the Consortium of Functional Glycomics Nomenclature Committee convention.²⁹

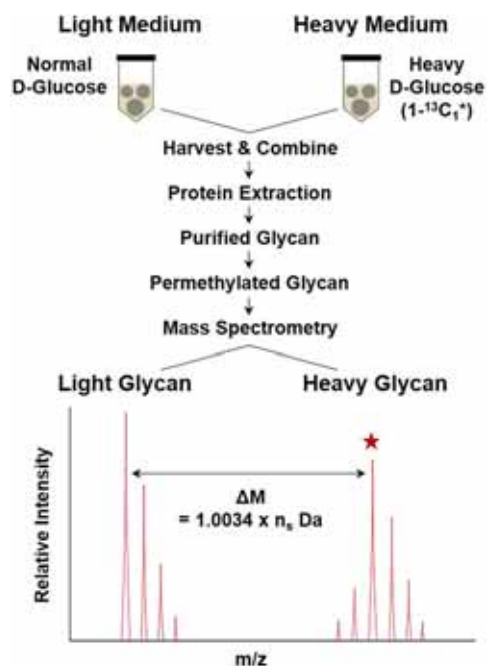


Figure 2. Schematic of the MILPIG strategy for relative quantification of glycans in fungi.

incorporation of $1\text{-}^{13}\text{C}_1$ glucose into the *N*-linked glycans, released glycans were permethylated prior to mass spectrometry-based analysis.

Glycan synthesis of filamentous fungi reported in the literature generally follows the high mannose pathway, and as shown in Figure 3, mass spectra of high mannose *N*-linked glycans from $\text{Man}_8\text{GlcNAc}_2$ (Man8) to $\text{Glc}_3\text{Man}_8\text{GlcNAc}_2$ (Glc3Man9) were obtained. In particular, the full spectrum of heavy *N*-linked glycans isolated from fungi cultured in the presence of isotopically labeled glucose is shown. The increase in the mass of isotopically labeled glycans is correlated with the total number of sugars in their corresponding structures and the charge state.

Comparing the monoisotopic peaks of high mannose *N*-linked glycan structures obtained from the fungi grown in normal or $1\text{-}^{13}\text{C}_1$ glucose reveal increases in mass ranging from m/z 5.0170 to 7.0213 Da, complying with their sugar ring numbers as well as their doubly charge status. It is noteworthy that the $^{13}\text{C}_1$ -incorporation is universal added to all carbohydrate rings, including both Man and GlcNAc.

Collectively, we demonstrated that MILPIG applied to fungi can be effectively applied to simultaneously isotope labeling and quantify *N*-linked glycans released from their glycoproteins.

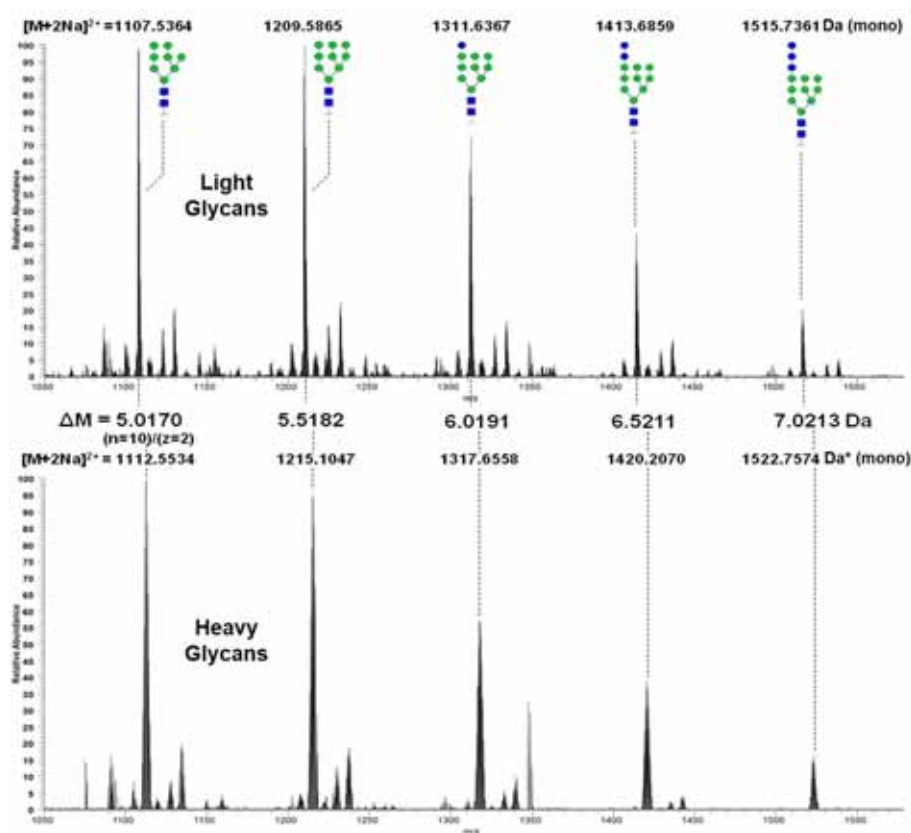


Figure 3. Full mass spectra of the light and heavy *N*-linked glycans released from fungi grown in either normal (light) or $1\text{-}^{13}\text{C}_1$ (heavy) glucose. ΔM is the mass difference according to the number of sugar (n)/charge state (z).

Mass Shift and Isotope Distribution of Light and Heavy Glycans

Isotope labeling efficiency in *in vivo* metabolic labeling determines the success of quantitative mass spectrometry. Sufficient mass shift and proper isotope distribution in the mass spectrum between light and heavy are particularly important for quantitative analysis of large biomolecules such as *N*-linked glycans.

In the yeast model experiment of MILPIG, over-incorporation of isotope carbon of glycan was observed by glucose depletion and incubation time. Therefore, in this study, fungi were cultured for 7.5 mg/mL and 14 days, respectively, considering the relatively high glucose concentration and slow growth rate, and Figure 4 shows the light and heavy mass spectrum of a representative Glc2Man9 *N*-linked glycan.

The full spectrum of the glycan mixture containing the

light and heavy glycan pairs showed the masses of m/z 1413.6806 (mono) and m/z 1420.2019 (mono) by sodiated divalent adducts $[M + 2Na]^{2+}$, as shown in the respective spectrum shown in Figure 3. The mass shift is 6.5 Da in the 13 sugar and charge states of the glycan, showing a sufficient mass difference without mass interference between the last over-incorporation peak (dotted arrow) of the light glycan and the first under-incorporation peak (dotted arrow) of the heavy glycan.

Describing the isotopic envelope of glycans, the isotopic envelope range of light glycans shows 2.5 Da from monoisotopic mass, whereas that of heavy glycans shows a relatively broad isotopic cluster of 5.5 Da. This observation can be summarized as showing a broad isotope envelope due to under- and over-incorporation centered on monoisotopic mass as ^{13}C recycling occurs frequently due to increased incubation time according to the growth rate of fungi.

As a result, although under- and over-incorporation due to the purity of isotope glucose and gluconeogenesis occurs, the sufficient mass difference between light and heavy glycans shows the advantage of quantitative glycomics without interference of mass spectrum peaks.

Relative Quantification of *N*-linked Glycans in Fungi

To provide MILPIG-based quantitative glycomics of fungi, we mixed equal amounts of normal and metabolically labeled fungal samples in culture media with light or heavy glucose. The glycans were then released from the purified glycoproteins with PNGase F, permethylated, and analyzed by mass spectrometry. A full MS spectrum of *N*-linked glycan mixtures containing both light and heavy glycan pairs for Man8, Man9, Glc1Man9, Glc2Man9, and Glc3Man9 is shown in Figure 5. As all of them are ionized as sodiated divalent adducts, each of glycan pairs exhibits

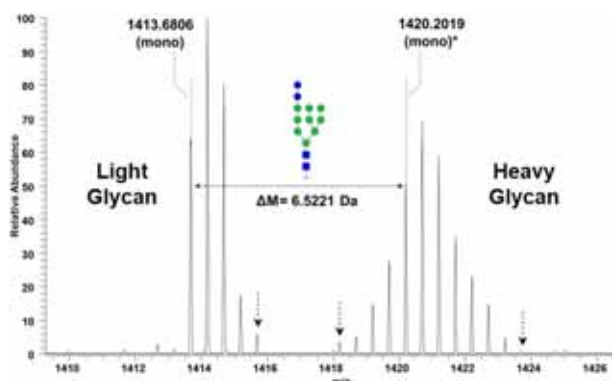


Figure 4. Mass shift and isotope distribution of light and heavy Glc2Man9 *N*-linked glycans in a 1:1 mixture of fungi grown in light and heavy culture media. The mass difference is 6.5 Da in the number of 13 sugars and $[M + 2Na]^{2+}$.

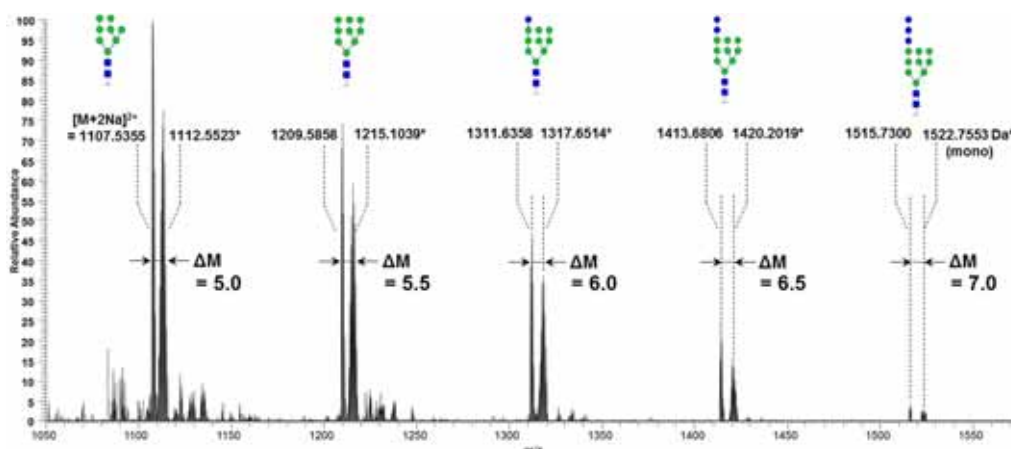
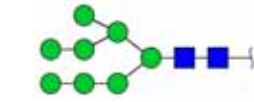
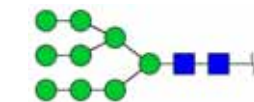
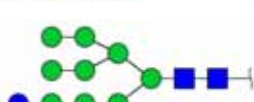


Figure 5. Full mass spectrum of *N*-linked glycans measured as a 1:1 mixture of normal (light) glycans and isotope-labeled (heavy) glycans in fungi. ΔM denotes the mass difference according to the number of sugar/charge state.

Table 1. Relative area ratios for a 1:1 mixture of light and heavy *N*-linked glycans in fungi

No.	Structure	Number of Sugars	Measured $[M + 2Na]^{2+}$ (mono)		ΔM	Ratio of Areas ^a (¹² C/ ¹³ C)
			Light (¹² C)	Heavy (¹³ C)		
1		10	1107.5355	1112.5523	5.0168	0.76 ± 0.04
2		11	1209.5858	1215.1039	5.5181	0.91 ± 0.01
3		12	1311.6358	1317.6514	6.0156	0.85 ± 0.03
4		13	1413.6806	1420.2019	6.5213	1.06 ± 0.01
5		14	1515.7300	1522.7553	7.0253	1.03 ± 0.02

^aThe values represent the mean ± standard deviation (SD) for biological triplicates.

their characteristic mass differences of 5.0, 5.5, 6.0, 6.5, and 7.0 Da.

The full mass spectrum shows that the higher the molecular weight, the lower the peak intensity is due to the difference in ionization efficiency and glycan expression. However, light and heavy glycan pairs show a decrease at the same rate, providing quantitative information. In general, it can be seen that the peak patterns of glycan pairs are offset from each other in area comparison of the mass peaks of glycan pairs because the peaks of heavy glycans are low and the isotope clusters are wide compared to light glycans. By enlarging the isotopic envelope pairs of light and heavy glycans as shown in Figure 4, relative quantification of glycans can be obtained from the peak area of each isotope pair without overlapping between the glycan pairs with sufficient mass increments.

To obtain quantitative information, we tabulated the ratio of the area of each isotope pair to the five glycans as shown in Table 1. The theoretical area ratio of light and heavy glycans was 1, whereas the area ratio of experimental results obtained an average of 0.92 in light/heavy, indicating that the expression of heavy glycans was relatively high. However, Man8, Man9, and Glc1Man9 glycans have relatively large peak areas, so errors due to high concentrations are relatively large, whereas Glc2Man9 and Glc3Man9 glycans provide accurate ratios at appropriate concentrations. These results support the excellent performance of the MILPIG method for quantitative glycomics in fungi with high isotope labeling efficiency.

Conclusions

Various qualitative and quantitative analysis techniques of glycans by mass spectrometry have contributed significantly to the biological information and biomarker discovery of glycoproteins. Quantitative analysis of glycans has generally evolved into methods for labeling isotope tags or isotopic elements by chemical or enzymatic *in vitro* reactions for mass spectrometry.

In addition, metabolic isotope labeling strategies of glycans have been proposed, and isotope-labeled glycans are biosynthesized by glycosylation machinery by supplying isotope-labeled biomolecules mainly needed on HBP in cell culture. By the IDAWG and MILPIG methods, the biosynthesis of isotope-labeled glycans in murine embryonic stem cells using isotope-labeled glutamine and in rice and yeast using isotope-labeled glucose were respectively demonstrated, and quantitative glycomics by mass spectrometry were established.

It is noteworthy that the study of glycoproteins and glycans of fungi is greatly accelerated in fungal biotechnology, which is of great importance in pharmaceutical and industrial research. In particular, the importance of quantitative analysis of fungal glycans is emerging in the study of overproduction of filamentous-fungal enzymes and glycosylation pathways by genetic modification. For this reason, in this study, using *Aspergillus niger* as a model system, the biosynthesis of isotope-labeled glycans and quantitative analysis of glycans in the culture conditions of isotope-labeled glucose are provided.

We showed that the fungal *N*-linked glycans by MILPIG method provide a mass difference between light glycans and heavy glycans according to the number of sugars in the glycan. It was shown that the isotopically labeled glycan provides a sufficient mass shift compared to the normal glycan, resulting in effective separation without mass overlapping interference. Based on this, a comparative quantitative analysis method was provided by obtaining mass spectrum of a 1:1 mixture of light and heavy glycans for quantitative glycomics. From the experimental investigation, it was shown that the MILPIG method can be applied to the quantitative analysis of glycans through successful isotope labeling of glycans in fungal culture systems.

Acknowledgments

This research was supported by Changwon National University in 2021-2022.

References

1. Reily, C.; Stewart, T. J.; Renfrow, M.B.; Novak, J. *Nat. Rev. Nephrol.* **2019**, 15(6), 346-366. DOI: 10.1038/s41581-019-0129-4.
2. Spiro, R.G. *Glycobiology* **2002**, 12(4), 43R-56R. DOI: 10.1093/glycob/12.4.43r.
3. Scherpenzeel, M.V.; Willems, E.; Lefeber, D.J. *Glycoconj. J.* **2016**, 33, 345-358. DOI: 10.1007/s10719-015-9639-x.
4. Delafield, D.G.; Li, L. *Mol. Cell Proteomics* **2021**, 20, 100054. DOI: 10.1074/mcp.R120.002095.
5. Yun, J.; Jo, J.-Y.; Tuomivaara, S.T.; Lim, J.-M. *Microchem. J.* **2021**, 170, 106655. DOI: 10.1016/j.microc.2021.106655.
6. Manilla, G.A.; Warren, N.L.; Abney, T.; Atwood III, J.A.; Azadi, P.; York, W.S.; Pierce, M.; Orlando, R. *Glycobiology* **2007**, 17, 677-687. DOI: 10.1093/glycob/cwm033.
7. Atwood III, J.A.; Cheng, L.; Manilla, G.A.; Warren, N.L.; York, W.S.; Orlando, R. *J. Proteome Res.* **2008**, 7, 367-374. DOI: 10.1021/pr070476i.
8. Dong, X.; Peng, W.; Yu, C.Y.; Zhou, S.; Donohoo, K.B.; Tang, H.; Mechref, Y. *Anal. Chem.* **2019**, 91(18), 11794-11802. DOI: 10.1021/acs.analchem.9b02411.
9. Xia, B.; Feasley, C.L.; Sachdev, G.P.; Smith, D.F.; Cummings, R.D. *Anal. Biochem.* **2009**, 387, 162-170. DOI: 10.1016/j.ab.2009.01.028.
10. Yang, S.; Yuan, W.; Yang, W.; Zhou, J.; Harlan, R.; Edwards, J.; Li, S.; Zhang, H. *Anal. Chem.* **2013**, 85, 8188-8195. DOI: 10.1021/ac401226d.
11. Zhou, S.; Hu, Y.; Veillon, L.; Snovidá, S. I.; Rogers, J. C.; Saba, J.; Mechref, Y. *Anal. Chem.* **2016**, 88, 7515-7522. DOI: 10.1021/acs.analchem.6b00465.
12. Zhang, W.; Wang, H.; Tang, H.; Yang, P. *Anal. Chem.* **2011**, 83, 4975-4981. DOI: 10.1021/ac200753e.
13. Tao, S.; Orlando, R. *J. Biomol. Tech.* **2014**, 25, 111-117. DOI: 10.7171/jbt.14-2504-003.
14. Jeong, S.H.; Lim, J.-M. *Bull. Korean Chem.* **2020**, 41, 1056-1059. DOI: 10.1002/bkcs.12120.
15. Yoo, J.Y.; Ko, K.S.; Seo, H.-K.; Park, S.; Fanata, W.I.D.; Harmoko, R.; Ramasamy, N.K.; Thulasinathan, T.; Mengiste, T.; Lim, J.-M.; Lee, S.Y.; Lee, K.O. *J. Biol. Chem.* **2015**, 290(27), 16560-16572. DOI: 10.1074/jbc.M115.653162.
16. Shi, Q.; Hashimoto, R.; Otsubo, T.; Ikeda, K.; Todoroki, K.; Mizuno, H.; Jin, D.; Toyo'oka, T.; Jiang, Z.; Min, J.Z. *J. Pharm. Biomed. Anal.* **2018**, 149, 365-373. DOI: 10.1016/j.jpba.2017.11.032.
17. Orlando, R.; Lim, J.-M.; Atwood III, J.A.; Angel, P.M.; Fang, M.; Aoki, K.; Alvarez-Manilla, G.; Moremen, K.W.; York, W.S.; Tiemeyer, M.; Pierce, M.; Dalton, S.; Wells, L. *J. Proteome Res.* **2009**, 8, 3816-3823. DOI: 10.1021/pr8010028.
18. Fang, M.; Lim, J.M.; Wells, L. *Curr. Protoc. Chem. Biol.* **2010**, 2, 55-69. DOI: 10.1002/9780470559277.ch090207.
19. Seo, H.K.; Fanata, W.I.D.; Kim, S.J.; Park, S.H.; Lee, Y.I.; Lee, K.O.; Lim, J.-M. *Bull. Korean Chem. Soc.* **2016**, 37(9), 1518-1521. DOI: 10.1002/bkcs.10877.
20. Kim, J.Y.; Joo, W.H.; Shin, D.S.; Lee, Y.I.; Teo, C.F.; Lim, J.M. *Anal. Biochem.* **2021**, 621, 114152. DOI: 10.1016/j.ab.2021.114152.
21. Cairns, T.C.; Nai, C.; Meyer, V. *Fungal Biol. Biotechnol.* **2018**, 5, 13. DOI: 10.1186/s40694-018-0054-5.
22. Meyer, V. et al. *Fungal Biol. Biotechnol.* **2020**, 7, 5. DOI: 10.1186/s40694-020-00095-z.
23. Barreto-Bergter, E.; Figueiredo, R.T. *Front. Cell. Infect. Microbiol.* **2014**, 4, 145. DOI: 10.3389/fcimb.2014.00145.
24. Maras, M.; van Die, I.; Contreras, R.; van den Hondel, C.A.M.J.J. *Glycoconj. J.* **1999**, 16, 99-107. DOI: 10.1023/a:1026436424881.
25. Kainz, E.; Gallmetzer, A.; Hatzl, C.; Nett, J.H.; Li, H.; Schinko, T.; Pachlinger, R.; Berger, H.; Reyes-Dominguez, Y.; Bernreiter, A.; Gerngross, T.; Wildt, S.; Strauss, J. *Appl. Environ. Microbiol.* **2008**, 74(4), 1076-1086. DOI: 10.1128/AEM.01058-07.
26. Deshpande, N.; Wilkins, M.R.; Packer, N.; Nevalainen, H. *Glycobiology* **2008**, 18(8), 626-637. DOI: 10.1093/glycob/cwn044.
27. Hui1, J.P.M.; White, T.C.; Thibault, P. *Glycobiology* **2002**, 12(12), 837-849. DOI: 10.1093/glycob/cwf089.
28. Stals, I.; Sandra, K.; Geysens, S.; Contreras, R.; Van Beeumen, J.; Claeysens, M. *Glycobiology* **2004**, 14(8), 713-724. DOI: 10.1093/glycob/cwh080.
29. Ceroni, A.; Maass, K.; Geyer, H.; Geyer, R.; Dell A.; Haslam, S.M. *J. Proteome Res.* **2008**, 7, 1650-1659. DOI: 10.1021/pr7008252.

A Sensitive, Efficient, and Cost-Effective Method to Determine Rotigotine in Rat Plasma Using Liquid-Liquid Extraction (LLE) and LC-MRM

Ji Seong Kim^{1†}, Yong Jin Jang^{1†}, Jin Hee Kim¹, Jin Hwan Kim¹, Jae Hee Seo¹, Il-Ho Park², Myung Joo Kang^{1*}, and Yong Seok Choi^{1*}

¹College of Pharmacy, Dankook University, Cheonan, Chungnam 31116, South Korea

²College of Pharmacy, Sahmyook University, Seoul 01795, South Korea

Received December 12, 2022, Revised December 20, 2022, Accepted December 20, 2022

First published on the web December 31, 2022; DOI: 10.5478/MSL.2022.13.4.146

Abstract : Rotigotine (RTG) is a non-ergot dopamine agonist used to manage the early stage of Parkinson's disease (PD) as transdermal patch. However, the poor medication compliance of PD patients and skin issues related with repeated applications of RTG patches lead to the search for alternative formulations and it also requires appropriate analytical methods for their *in vivo* evaluation. Thus, here, a sensitive, efficient, and cost-effective method to determine RTG in rat plasma using liquid-liquid extraction (LLE) and multiple reaction monitoring was developed. The use of 20 μ L of rat plasma for sample treatment, 8-OH-DPAT as the internal standard, and methyl *tert*-butyl ether as the LLE solvent in the present method gives it advantages over previous methods for the analysis of RTG in biological samples. The good analytical performance of the developed method was confirmed in specificity, linearity (the coefficient of determination ≥ 0.999 within 0.1-100 ng/mL), sensitivity (the lower limit of quantitation at 0.1 ng/mL), accuracy (81.00–115.05%), precision ($\leq 10.75\%$), and recovery (81.00-104.48%) by following the FDA guidelines. Finally, the applicability test of the validated method to the *in vivo* evaluation of a RTG formulation showed that the present method is the only method which can be accurately applied to that longer than 24 hours, critical for the development of formulations with reduced dosing frequencies. Therefore, the present method could contribute to the development of new RTG formulations helpful to people suffering from PD.

Keywords : rotigotine, multiple reaction monitoring, liquid-liquid extraction, rat plasma, pharmacokinetics

Introduction

Rotigotine (RTG, Figure 1A) is a non-ergot dopamine agonist used to manage the early stage of Parkinson's disease (PD).¹ Due to its poor oral bioavailability (1%) by the extensive first-pass hepatic clearance and nonpolar characteristics (logP of 5.17), its formulation in the market is limited to transdermal patch which shows advantages like the relatively long dosing interval (once a day) and the reduction of motor adverse effects including dyskinesia,

motor fluctuations, and resting tremor.² However, the poor medication compliance of PD patients and skin issues, such as erythema, pruritus, and dermatitis, related with repeated applications of RTG patches lead to the search for alternative formulations with reduced dosing frequencies.³ Thus, to facilitate the development of new RTG formulations, appropriate analytical methods for their *in vivo* evaluation are needed.

Recently, liquid chromatography and multiple reaction monitoring assay (LC-MRM), a considerably specific and sensitive technique which belongs to liquid chromatography and tandem mass spectrometry (LC-MS/MS) is commonly chosen for drug analyses and it has been widely used for the *in vivo* evaluation of RTG formulations, too.⁴⁻⁶ In the case of sample treatment, also important due to its preventive effect to signal suppression among co-eluting compounds from an LC column in LC-MS/MS, protein precipitation and liquid-liquid extraction (LLE) have been generally employed for the determination of RTG in biological samples.⁷⁻⁹ However, protein precipitation, mainly removing proteins from a sample, may not be effective to solve the suppression effect of nonpolar analytes like RTG to keep the quantitative property of the method.¹⁰ Until now, Sha *et al.*'s method to determine RTG in rat plasma using LLE and LC-MRM

Open Access

[†]Both authors contributed equally to this work.

*Reprint requests to Yong Seok Choi, Myung Joo Kang

<https://orcid.org/0000-0001-6740-3160>

<https://orcid.org/0000-0001-8878-2972>

E-mail: analysc@dankook.ac.kr, kangmj@dankook.ac.kr

All the content in Mass Spectrometry Letters (MSL) is Open Access, meaning it is accessible online to everyone, without fee and authors' permission. All MSL content is published and distributed under the terms of the Creative Commons Attribution License (<http://creativecommons.org/licenses/by/3.0/>). Under this license, authors reserve the copyright for their content; however, they permit anyone to unrestrictedly use, distribute, and reproduce the content in any medium as far as the original authors and source are cited. For any reuse, redistribution, or reproduction of a work, users must clarify the license terms under which the work was produced.

seems to be the most acceptable in the community, there are still some margins to be improved.⁸ First, while its lower limit of quantitation (LLOQ, 0.2 ng/mL) is lower than others, it may not be sensitive enough for longer-period pharmacokinetic studies.⁸ Also, the demand of relatively large volume of plasma (50 μ L) and high cost brought by the use of a stable isotope RTG (RTG-d₃) as an internal standard (IS) are additional drawbacks.⁸

Thus, here, a sensitive, efficient, and cost-effective method to determine RTG in rat plasma using LLE and LC-MRM was developed. The use of 20 μ L of rat plasma for sample treatment, 8-OH-DPAT (CAS number: 78950-78-4) as the IS, and methyl *tert*-butyl ether (MTBE) as the LLE solvent in the present method gives it advantages over previous methods for the analysis of RTG in biological samples. The developed method was validated in various parameters according to FDA guidelines and its applicability to longer-period pharmacokinetic studies was also confirmed.

Experimental

Chemicals and reagents

RTG ($\geq 99.0\%$), 8-OH-DPAT ($\geq 99.0\%$) used as the IS, ammonium formate (LC-MS grade), and formic acid were purchased from Sigma Aldrich (St. Louis, MO, USA). Acetonitrile for HPLC, MTBE, and water were obtained from J. T. Baker (Phillipsburg, NJ, USA).

Preparation of standard solutions

To prepare stock solutions, RTG and the IS were both dissolved at 1 mg/mL in acetonitrile. The RTG stock solution was diluted with acetonitrile to 160 ng/mL (the RTG working solution), and the extraction solvent was prepared by the dilution of the IS stock solution with MTBE to 200 ng/mL. All stock solutions and working solutions including the extraction solvent were stored at -27°C, until use.

Liquid-liquid extraction (LLE)

An aliquot (20 mL) of rat plasma was mixed with 500 μ L of the extraction solvent including the IS using a vortex mixer for a minute. After centrifugation of the mixture at 12,000 \times g for 10 minutes, the whole top layer (the extraction solvent layer) was transferred to a micro-centrifuge tube. Then, the solution taken was dried at room temperature under nitrogen stream, and the resulting residue was reconstituted in 100 μ L of acetonitrile. The final solution was centrifuged at 12,000 \times g for 10 minutes, and a part of its supernatant was analyzed by LC-MS/MS. A matrix-matched standard (MMS) and a standard-spiked sample (SSS) were prepared by adding an appropriate volume of the RTG working solution into the final LLE extract obtained from blank rat plasma and into blank rat plasma prior to the LLE steps, respectively. For the present

study, SSSs were employed as QC samples (0.1, 0.3, 40, and 80 ng/mL for LLOQ, low QC (LQC), middle QC (MQC) and high QC (HQC), respectively). Also, MMSs (0.1, 2, 10, 25, 50, and 100 ng/mL) were used for building calibration curves.

Liquid chromatography and tandem mass spectrometry (LC-MS/MS)

For LC-MRM, a Shimadzu Nexera UPLC system (Tokyo, Japan) and a Shimadzu LCMS 8060 triple quadrupole mass spectrometer were interfaced through electrospray ionization (ESI) in positive ion mode. For LC separation, a Waters Atlantis HILIC Silica column (2.1 \times 150 mm, 3 mm, Santa Clara, CA, USA) and the isocratic mobile phase condition (the volumetric ratio of 2 mmol/L of an aqueous ammonium formate solution including 0.1% (v/v) formic acid (MP A) to acetonitrile including 0.1% (v/v) formic acid (MP B), 15:85) were used. A sample was separated at the flow rate of 0.25 mL/min for eight minutes, and the autosampler and the column oven were kept at 4 and 40°C, respectively. For ESI, source parameters were set as follows: nebulizing gas flow at 2 L/min, heating gas flow at 10 L/min, drying gas flow at 10 L/min, interface temperature at 300°C, DL temperature at 250°C, and heating block temperature at 400°C. In the case of MRM, three MRM transitions per compound were monitored: one with the highest sensitivity was the screening transition used for the quantitation and the others were the confirmatory transitions for the target identity confirmation. In the case of RTG, 316.1 *m/z* (precursor ion) / 147.3 *m/z* (product ion) / -24 V (collision energy), 316.1 *m/z* / 77.1 *m/z* / -73 V, and 316.1 *m/z* / 107.1 *m/z* / -64 V were the screening transition, the confirmatory transition 1, and the confirmatory transition 2, respectively. In addition, the screening transition of 248.1 *m/z* / 147.1 *m/z* / -23 V, the confirmatory transition 1 of 248.1 *m/z* / 91.2 *m/z* / -42 V, and the confirmatory transition 2 of 248.1 *m/z* / 102.1 *m/z* / -17 V were applied for the IS. All mass spectrometry data were acquired and analyzed using Lab Solutions (version 5.93, Shimadzu). For quantitation, three pre-requirements (all three transition peaks should have the same retention time; the signal to noise ratio (S/N) of the screening transition peak should be higher than 10; all confirmatory transition peaks should have the S/N values higher than 3) were checked. When all they were satisfied, a screening transition peak area ratio of RTG to the IS was calculated and used for quantitation.

Application to pharmacokinetic study in rats

The validated LC-MS/MS method was employed to determine the plasma concentration-time profile of RTG, following topical application of a RTG microemulsion formula. The animal study was carried out after the approval of the Institutional Animal Care and Use Committee (IACUC) of Dankook University (DKU-22-

045, Cheonan, South Korea). Seven-week-old male Sprague-Dawley rats (200 ± 20 g) acquired from Samtako Bio Korea (Gyeonggi-do, South Korea) were kept under controlled environmental conditions ($23 \pm 1^\circ\text{C}$, 12 h day/12 h night) with free access to standard food and water. After 3 days of acclimatization period, the hair in the dorsal region was shaved and then RTG-loaded microemulsion hydrogel consisted of 2% (w/v) RTG was topically administered at 2 mg/kg as RTG.¹¹ At predetermined time, the rat blood samples (approximately 0.2 mL) were collected in heparinized 1.5 mL polythene tubes from the jugular vein. The collected blood was centrifuged at 13,000 rpm for 10 minutes and the resulting plasma was taken and kept in a deep freezer at -80°C until its treatment using LLE. Pharmacokinetic parameters of RTG, such as the maximum drug concentration in plasma (C_{\max}), time to reach C_{\max} (T_{\max}), area under the curve for drug concentration in plasma-time (AUC), and elimination half-life ($T_{1/2}$), were calculated from the pharmacokinetic profile, using a WinNonlin[®] version 5.2 program (Pharsight Co., Mountain View, CA).

Results and discussion

Method development

Liquid chromatography and multiple reaction monitoring

For the present study, 8-OH-DPAT (Figure 1B), whose chemical structure is similar with that of RTG, was selected as the IS. Since 8-OH-DPAT is much cheaper than stable isotope ^3H -labeled RTG s such as RTG- d_3 , the present method has cost advantage.⁸ $[\text{M}+\text{H}]^+$ ions (316.1 m/z and 248.1 m/z for RTG and the IS, respectively) were chosen as precursor ions. Product ions for MRM were chosen from product ion scan (PIS) results of individual precursor ions. The strongest fragment ions (147.3 m/z and 147.1 m/z for RTG and the IS, respectively) were chosen for quantitation. As confirmatory transitions for identity confirmation, the second and third strongest intensities (77.1 and 107.1 m/z for RTG and 91.2 and 102.1 m/z for the IS) were selected. In the case of separation, a HILIC silica column and the isocratic mobile phase condition (the volumetric ratio of MP A to MP B, 15:85) were used for the efficient separation of components including RTG and the IS with less suppression effect within eight minutes. While RTG is non-polar, it is

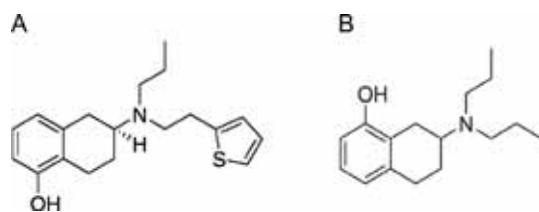


Figure 1. Chemical structures of rotigotine (A) and 8-OH-DPAT (B)

a base due to its tertiary amine bound to three electron donating groups. It means that if the pH of its solution is kept much lower than the pKa value of its mono-protonated conjugate acid (about 10), it mainly exists as its conjugate acid form whose relative polarity is higher than that of its free form. Thus, at the mobile phase condition of the present method (about pH 3), majority of RTGs are kept as mono-protonated RTG cations which may have attraction with deprotonated free silanol groups at the surface of silica packing materials as well as retainability in polar liquid stationary phase film of the HILIC silica column.

Sample preparation

For the development of highly sensitive and simple sample preparation steps which can be applied to rat plasma, LLE was chosen in the present study.¹⁰ Some organic solvents including MTBE, ethyl ether, and their mixtures were compared to find the optimal extraction solvent for RTG. Since MTBE showed much higher recovery of RTG ($103.89 \pm 4.13\%$, $n=3$) from a SSS (0.1 ng/mL of RTG) than others (63.57 ± 6.82 , 68.72 ± 6.56 , 75.44 ± 6.23 , and $82.22 \pm 5.39\%$ from ethyl ether, the mixture of 70% v/v of ethyl ether and 30% v/v MTBE, the mixture of 50% v/v of ethyl ether and 50% v/v MTBE, and the mixture of 30% v/v of ethyl ether and 70% v/v MTBE, respectively, $n=3$), MTBE was selected as the LLE solvent in the present study. The volume of rat plasma required for the sample preparation was decided to 20 mL, the minimal volume which showed precise and linear results from comparison experiments of various plasma volumes (data not shown). To the best of our knowledge, the present sample preparation method is the most efficient one in the aspect of the volume of rat plasma demanded to determine RTG in it (20 mL in the present method vs. 50 mL in Sha *et al.*'s method, the previously most efficient one) and it may be explained by the better extraction of RTG by MTBE.⁸ Also, the deposit of contaminants originated from rat plasma on the curtain plate of the mass spectrometer by continuous analyses of prepared samples was checked and there was not any significant sign of contamination in the system.

Method validation

The present method was validated in specificity, linearity, sensitivity, accuracy, precision, and recovery according to the FDA guidelines.¹² First, the specificity of this method was confirmed by comparison between blank rat plasma and the LLOQ sample (Figure 2). In the chromatogram from the LLOQ sample, RTG and the IS peaks were identified at about 4.8 and 5.1 minutes, respectively, but both were not observed from the blank plasma analyses. Also, the good linearity (the coefficient of determination, $r^2 \geq 0.998$) of the method was confirmed over the concentration range between 0.1 and 100 ng/mL, ($n=6$, Table 1). Third,

Determination of Rotigotine in Rat Plasma Using LLE and LC-MRM

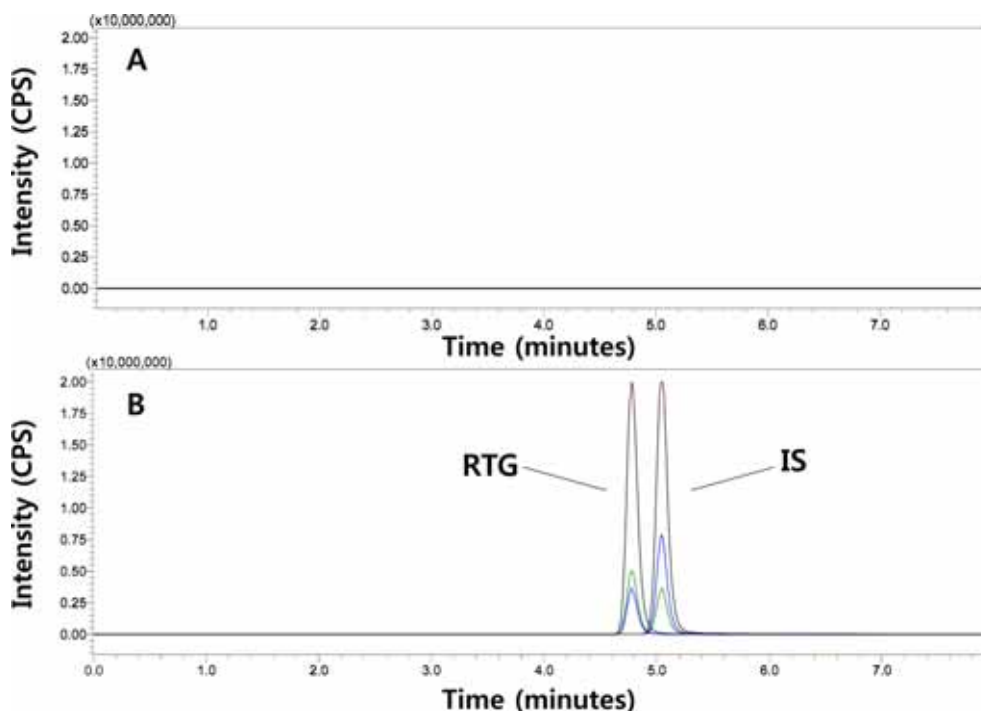


Figure 2. Multiple reaction monitoring chromatograms of blank rat plasma (A) and rat plasma including 50 ng/mL of RTG and IS (B). RTG and IS stand for rotigotine and 8-OH-DPAT, respectively.

accuracy and precision estimated from all QC sample results were good enough to satisfy the criteria of FDA guidelines: the intra-day accuracy between 83.48 and 115.05%; the inter-day accuracy between 81.00 and 113.50%; the intra-day precision, not more than 7.43%;

Table 1. Information from the calibration curves of rotigotine in rat plasma (n = 6)

Concentration range (ng/mL)	Slope	y-Intercept	R ²
	Mean ± SD	Mean ± SD	
0.1 - 100	0.0247 ± 0.0019	0.0003 ± 0.0002	≥ 0.999

inter-day precision, not more than 10.75% (Table 2). Finally, good recovery (the percentage of the RTG screening transition peak area of a QC sample to that of its counter MMS with the same RTG concentration) between 81.00 and 104.48% was observed (Table 2). Based on all validation results, LLOQ, the lowest concentration showing good accuracy, precision, and recovery within the linear dynamic range was confirmed as 0.1 ng/mL and it is proven to be the most sensitive method to determine RTG in rat plasma (0.1 ng/mL in the present method vs. 0.2 ng/mL in Sha *et al.*'s method, the previously most sensitive one).⁸ The more improved sensitivity of the present method than those of previous ones may be

Table 2. Accuracy, precision, and recovery confirmed by LC-MRM analyses of rotigotine (RTG) in rat plasma (n = 6)

Types	Nominal concentration of RTG (ng/mL)	Calculated concentration of RTG (ng/mL)	Accuracy (%)	Precision (%)	Recovery (mean ± standard deviation, %)
Intra-day	0.1	0.11±0.01	111.91	4.20	98.45 ± 4.50
	0.3	0.28±0.02	93.89	7.43	93.65 ± 7.98
	40	34.34±0.85	85.84	2.11	85.53 ± 2.11
	80	74.10±2.62	92.63	3.27	95.53 ± 3.37
Inter-day	0.1	0.11±0.01	112.56	10.75	96.09 ± 4.13
	0.3	0.28±0.02	93.73	7.13	93.84 ± 6.04
	40	34.57±1.11	86.42	2.78	85.43 ± 2.72
	80	71.78±3.13	89.73	3.91	91.76 ± 4.31

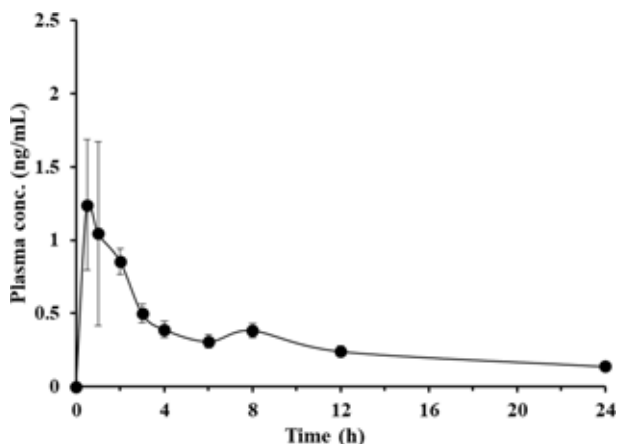


Figure 3. Plasma concentration-time profile of rotigotine (RTG) following topical application of RTG loaded microemulsion hydrogel in normal rats (2 mg/kg as RTG). Data represent mean \pm standard deviation (n = 4).

Table 3. Pharmacokinetic parameters of rotigotine (RTG) following topical application of RTG -loaded microemulsion hydrogel in normal rats (2 mg/kg as RTG)

Parameter	Mean \pm Standard deviation (n=4)
AUC _(0-24 h) (ng·h/mL)	7.60 \pm 1.43
AUC _(0-∞) (ng·h/mL)	10.84 \pm 3.63
C _{max} (ng/mL)	1.96 \pm 0.78
T _{max} (h)	1.00 \pm 0.71
T _{1/2} (h)	9.69 \pm 4.51

explained by the better extraction of RTG by MTBE, the LLE solvent.

Pharmacokinetic profile of RTG following topical application in rats

The plasma concentration-time profile of RTG after topical application is depicted in Figure 3. Additionally, the relevant pharmacokinetic parameters such as AUC, C_{max}, T_{max}, and elimination T_{1/2} calculated from the pharmacokinetic profiles are represented in Table 3. After topical administration, the level of RTG in plasma increased rapidly and reached C_{max} (1.96 ng/mL) after an hour (T_{max}). Afterward, the drug concentration in plasma gradually decreased over 24 hours, with the extended elimination T_{1/2} of 9.98 \pm 3.95 hours. The AUC_(0-24 h) and AUC_(0-∞) values of RTG, an indicator of the extent of drug absorption, were determined to 7.60 and 10.84 ng·h/mL, respectively. The plasma concentration of RTG after 24 hours of post-dosing was determined to 0.137 ng/mL, which was about 1.37-fold higher than LLOQ (0.1 ng/mL) of the currently established method. It strongly suggests that the present method with LLOQ at 0.1 ng/mL is the only method which can be accurately applied to the *in vivo* evaluation of RTG formulation

longer than 24 hours, critical for the development of formulations with reduced dosing frequencies.³

Conclusions

A sensitive, efficient, and cost-effective method to determine RTG in rat plasma using LLE and MRM was developed. The use of 20 μ L of rat plasma for sample treatment, 8-OH-DPAT as the IS, and MTBE as the LLE solvent in the present method gives it advantages over previous methods for the analysis of RTG in biological samples. The developed method was validated in various parameters including specificity, linearity, sensitivity, accuracy, precision, and recovery by following the FDA guidelines. Finally, the applicability test of the validated method to the *in vivo* evaluation of a RTG formulation showed that the present method with LLOQ at 0.1 ng/mL is the only method which can be accurately applied to that longer than 24 hours, critical for the development of formulations with reduced dosing frequencies. Since the present study resulted the most sensitive as well as efficient method to determine RTG in rat plasma, it could contribute to the development of new RTG formulations helpful to people suffering from PD.

References

1. Reynolds, N. A.; Wellington, K.; Easthope, S. E. *CMS drugs*. **2005**, 19, 973, doi.org/10.2165/00023210-200519110-00006
2. Choudhury, H.; Zakaria, N. F. B.; Tilang, P. A. B.; Tzeyung, A. S.; Pandey, M.; Chatterjee, B.; Alhakamy, N. A.; Bhattamishra, S. K.; Kesharwani, P.; Gorain, B.; Md. S. *J. Drug Delivery Sci. Technol.* **2019**, 54, 101301, doi.org/10.1016/j.jddst.2019.101301
3. Md, S.; Karim, S.; Saker, S. R.; Gie, O. A.; Hooi, L. C.; Yee, P. H.; Kang, A. W.; Zhe, C. K.; Ian, N.; Aldawsari, H. M.; Hosny, K. M.; Alhakamy, N. A. *Curr. Pharm. Des.* **2020**, 26, 2222, doi.org/10.2174/1381612826666200316154300
4. Elshoff, J. P.; Braun, M.; Andrea, J. O.; Middle, M.; Cawello, W. *Clin. Ther.* **2012**, 34, 966, doi.org/10.1016/j.clinthera.2012.02.008
5. Cawello, W.; Wolff, H. M.; Meuling, W. J. A.; Horstmann, R.; Braun, M. *Clin. Pharmacokinet.* **2007**, 46, 851, doi.org/10.2165/00003088-200746100-00003
6. Kujirai, H.; Itaya, S.; Ono, Y.; Takahashi, M.; Inaba, A.; Shimo, Y.; Hattori, N.; Orimo, S. *Parkinson's disease*. **2020**, 2020, 5892163, doi.org/10.1155/2020/5892163
7. Mohamed, S.; Riva, R.; Contin, M. *Biomed. Chromatogr.* **2017**, 31, e3944, doi.org/10.1002/bmc.3944
8. Sha, C.; Han, J.; Zhao, F.; Shao, X.; Yang, H.; Wang, L.; Yu, F.; Liu, W.; Li, Y. *J. Pharm. Biomed. Anal.* **2017**, 146, 24, doi.org/10.1016/j.jpba.2017.07.018
9. Bai, J.; Xie, L. Y.; Yang, L.; Wang, R.-Q.; Chen, X.; Hu, S. *J. Chromatogr. B: Anal. Technol. Biomed. Life Sci.*

Determination of Rotigotine in Rat Plasma Using LLE and LC-MRM

- 2021, 1178, 7, doi.org/10.1016/j.jchromb.2021.122583
10. Kim, D. Y.; Lee, H. C.; Jang, Y. J.; Kim, J. H.; Lee, H. R.; Kang, M. J.; Choi, Y. S. *Mass Spectrom. Lett.* **2020**, 11, 71, doi.org/10.5478/MSL.2020.11.4.71
11. Wang, Z.; Mu, H.-J.; Zhang, X.-M.; Ma, P.-K.; Lian, S.-N.; Zhang, F.-P.; Chu, S.-Y.; Zhang, W.-W.; Wang, A.-P.; Wang, W.-Y.; Sun, K.-X.; *Int. J. Nanomed.* **2015**, 2015, 633, doi.org/10.2147/IJN.S74079
12. Food and Drug Administration. *Bioanalytical method validation: guidance for industry FDA-2013-D-1020*. **2018**.; See <https://www.fda.gov/files/drugs/published/Bioanalytical-Method-Validation-Guidance-for-Industry.pdf>.

Inhibitory Effects of Dietary Schisandra Supplements on CYP3A Activity in Human Liver Microsomes

Bae-Gon Kang, Eun-Ji Park, So-Young Park, and Kwang-Hyeon Liu*

BK21 FOUR Community-Based Intelligent Novel Drug Discovery Education Unit, College of Pharmacy and Research Institute of Pharmaceutical Sciences, Kyungpook National University; Daegu 41566, Korea

Received November 9, 2022, Revised December 13, 2022, Accepted December 21, 2022

First published on the web December 31, 2022; DOI: 10.5478/MSL.2022.13.4.152

Abstract : *Schisandra chinensis* and its fruits have been used as a traditional herbal medicine to treat liver dysfunction, fatigue, and chronic coughs. Several *in vitro* and *in vivo* studies suggested that dibenzocyclooctadiene lignans present in *Schisandra* fruits strongly inhibit CYP3A4 activity. However, reports on the inhibitory potential of dietary *Schisandra* supplements against CYP3A activity are limited despite their increasing consumption as dietary supplements. In this study, we evaluated the CYP3A-inhibitory potential of four dietary *Schisandra* supplements in human liver microsomes. At a concentration of 0.05 mg/mL, *Schisandra* supplements from Nature's Way, Swanson, Planetary Herbals, and Only Natural inhibited CYP3A activity by 93.9, 70.8, 33.6, and 24.8%, respectively. Nature's Way, which exhibited the strongest inhibition against CYP3A, had the highest contents of gomisins B and C, which potently inhibit CYP3A activity. The *in vivo* pharmacokinetics of this product should be examined to determine whether the clinical relevance of inhibiting CYP3A activity by dietary *Schisandra* supplementation.

Keywords : CYP3A, Inhibition, Lignan, *Schisandra* supplements

Introduction

The concomitant administration of dietary botanical supplements and prescribed drugs has increased worldwide. For example, approximately 18–20% of adults in the United States consume prescribed drugs concurrently with dietary supplements.¹ The concomitant use of dietary supplements and drugs may result in pharmacokinetic herb-drug interactions (HMDI) causing increased toxicity or decreased efficacy.²

Several medicinal herbs reportedly cause HMDI, including echinacea, ginseng, milk thistle, and St John's wort.³ As a well-known example, consumption of St John's wort reduces the oral bioavailability of co-administered drugs, including cyclosporine, tacrolimus, and simvastatin by inducing CYP3A enzymes, eventually leading to insufficient drug effects.⁴ Co-administration with

grapefruit juice also increases the oral bioavailability of drugs, such as calcium channel blockers and HMG-CoA reductase inhibitors, which function as CYP3A substrates and inhibit CYP3A enzymes.⁵

Cytochrome P450 (P450) 3A enzymes are considered the most important human P450 owing to their high relative abundance in the liver and intestine and their involvement in the metabolism of over 50% of marketed drugs.⁶ Therefore, evaluating the inhibitory effects of drug candidates or traditional herbal medicines against CYP3A enzymes is essential for developing new drugs. *Schisandra chinensis* Bailon and its fruits, known as omija, wuweizi, and gomishi in Korea, China, and Japan, respectively, have been used in herbal medicine to treat liver dysfunction, chronic coughs, and fatigue.⁷ Several *in vitro* studies have suggested that dibenzocyclooctadiene lignans present in omija strongly inhibit CYP3A4 activity in a time-dependent manner.^{8,9} A recent *in vivo* study also suggested that gomisins A, a type of omija lignan, participates in the pharmacokinetic interaction of cyclophosphamide by blocking CYP3A-mediated bioactivation, thus reducing chloroacetaldehyde production and playing a role in the chemopreventive activity of omija against cyclophosphamide toxicity.¹⁰

Owing to various pharmacological activities of *Schisandra*, its market is expected to grow with a compound annual growth rate (CAGR) of 7.56% during 2022–2029 (<https://www.datamintelligence.com/research-report/schisandra-market>). To date, reports on the inhibitory effect of dietary *Schisandra* supplements on CYP3A activity are limited.

Open Access

*Reprint requests to Kwang-Hyeon Liu
<https://orcid.org/0000-0002-3285-5594>
E-mail: dstlkh@knu.ac.kr

All the content in Mass Spectrometry Letters (MSL) is Open Access, meaning it is accessible online to everyone, without fee and authors' permission. All MSL content is published and distributed under the terms of the Creative Commons Attribution License (<http://creativecommons.org/licenses/by/3.0/>). Under this license, authors reserve the copyright for their content; however, they permit anyone to unrestrictedly use, distribute, and reproduce the content in any medium as far as the original authors and source are cited. For any reuse, redistribution, or reproduction of a work, users must clarify the license terms under which the work was produced.

Therefore, we evaluate the potential of four representative dietary Schisandra supplements to inhibit CYP3A-mediated midazolam 1'-hydroxylase activity in human liver microsomes (HLMs). We also compare the difference in the CYP3A inhibitory potential of dietary Schisandra supplements from different manufacturers by analysing the omija lignan content.

Experimental

Materials

Gomisin A ($\geq 98\%$), gomisin C ($>98\%$), schisandrin (98%), deoxyschisandrin ($\geq 98\%$), and wuweizisu C ($\geq 98\%$) (Figure 1) were purchased from Sigma-Aldrich (St. Louis, MO, USA). Gomisin B (95%) (Figure 1) and midazolam were purchased from Toronto Research Chemicals (Toronto, ON, Canada). Gomisin N ($>99\%$) (Figure 1) was obtained from CoreSciences (Seoul, Korea). Pooled HLMs (XTreme 200, H2630, mixed gender) were supplied by XenoTech (Lenexa, KS, USA). All the other solvents used were of LC-MS grade (Fisher Scientific Co., Pittsburgh, PA, USA).

Samples of dietary Schisandra supplements

Dietary Schisandra supplements were obtained from local commercial sources or online shopping malls. Available information is presented in Table 1. Samples were stored at 4°C until further use. Dietary Schisandra supplement stock solutions (2.5 mg/mL) were prepared in 50% methanol.

Inhibitory effects of dietary Schisandra supplements against CYP 3A enzyme

The inhibitory potential of dietary *Schisandra* supplements on CYP3A activity was evaluated using our previously developed method, with slight modifications.⁹ Briefly, microsomal incubation mixtures containing 0.1 M phosphate buffer (pH 7.4), pooled HLMs (0.25 mg/mL), midazolam as a CYP3A probe substrate (0.1 mM), and dietary Schisandra supplement samples (0.05 mg/mL) were pre-incubated (37°C, 5 min). Subsequently, the NADPH generating system was added and further incubated for 10 min. After quenching the incubated samples with cold acetonitrile, the samples were centrifuged. Aliquots of the supernatants were analyzed using liquid chromatography-tandem mass spectrometry (LC-MS/MS).⁹

LC-MS/MS analysis

1'-Hydroxymidazolam was separated on a Kinetex XB-C18 column (100 × 2.1 mm, 2.6 μm, Phenomenex, Torrance, CA, USA) and analyzed using a Shimadzu LC-MS 8060 system (Shimadzu, Kyoto, Japan). The mobile phase consisted of water containing 0.1% formic acid (A) and acetonitrile containing 0.1% formic acid (B). The elution conditions for the analysis of 1'-hydroxymidazolam were set as 8% B for 0–0.5 min, 8%→60% B for 0.5–5 min, 60% B for 5–6 min, 60%→8% B for 6–6.1 min, and 8% B for 6.1–9 min.⁹ The mass transition and collision energy (CE) used for the quantitation of 1'-hydroxymidazolam were m/z 342 → 203 and 28 eV, respectively.

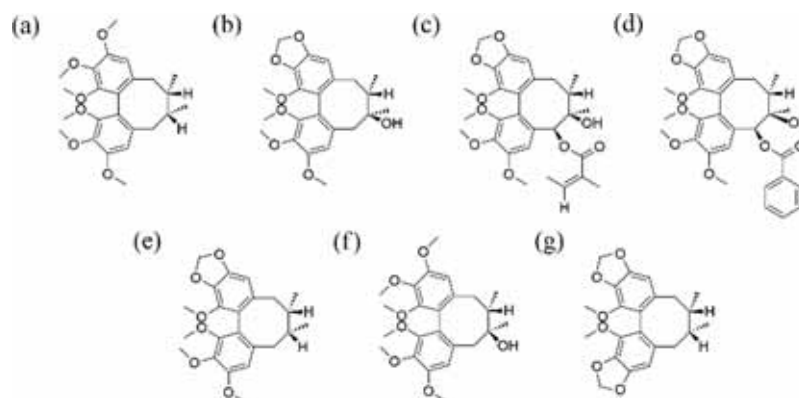


Figure 1. Chemical structures of the seven schisandra lignans: (a) deoxyschisandrin; (b) gomisin A; (c) gomisin B; (d) gomisin C; (e) gomisin N; (f) schisandrin; and (g) wuweizisu C.

Table 1. Available information about the commercial dietary Schisandra supplements used in this study.

Maker	Trade name	Herbal supplement	Amount per serving
Nature's Way	Schisandra Fruit	Schisandra	1,160 mg
Only Natural	Schizandra Extract	Schisandra extract	500 mg
Planetary Herbals	Schisandra Adrenal Complex	Schisandra fruit	1,420 mg
Swanson	Schizandra Berries	Schisandra berry	525 mg

Quantitative analysis of dibenzocyclooctadiene lignans in dietary Schisandra supplements

Dibenzocyclooctadiene lignans in dietary Schisandra supplements were analyzed using a LC-MS/MS method developed by our group.¹¹ Seven lignans were separated on a Kinetex C18 column (100 × 2.1 mm, 2.6 μm). The mass transitions used for quantitation of gomisin A, gomisin B, gomisin C, gomisin N, deoxyschisandrin, wuweizisu C, and schisandrin were m/z 417 → 399 (CE 20 eV), m/z 537 → 415 (CE 25 eV), m/z 554 → 415 (CE 20 eV), m/z 401 → 300 (CE 25 eV), m/z 417 → 316 (CE 25 eV), m/z 385 → 285 (CE 25 eV), and m/z 433 → 415 (CE 25 eV), respectively. The lower limits of quantification for gomisin A, gomisin B, gomisin C, gomisin N, deoxyschisandrin, wuweizisu C, and schisandrin were 0.05, 0.005, 0.005, 0.005, 0.005, 0.01, and 0.005 mg/mL, respectively. The inter-assay precision values for all analytes were less than 15.0%.

Results and Discussion

We observed that Schisandra lignan components potently inhibited the CYP3A enzyme, resulting in metabolic drug interactions. Gomisin B and gomisin C, with methylenedioxyphenyl and bulky groups at position 6, most strongly inhibited CYP3A metabolism, with IC_{50} values as low as 0.19–0.62 mM, which was much lower than those of the other P450s.^{9,12} In addition, lignans having one methylenedioxyphenyl group, such as gomisin A, B, C, and N, potently inhibit the CYP3A enzyme in a time- and NADPH-dependent manner through the metabolite-intermediate complexes.⁸ Wuzhi capsule, a commercially available Chinese medicine composed of Schisandra extracts, increased plasma concentrations of tacrolimus in combination with tacrolimus in patients who underwent liver transplantation.¹³

Over 20 traditional herbal medicines composed of Schisandra extracts have been documented in the Pharmacopoeia of Korea (<https://www.law.go.kr/LSW/admRulLsInfoP.do?admRulSeq=200000021929>). With the increasing consumption of dietary supplements, evaluating their potential to cause HMDIs is crucial. However, reports on the potential of dietary Schisandra supplements to inhibit CYP3A activity are limited. Therefore, we evaluated the CYP3A-inhibitory potential of four dietary Schisandra supplements using HLMs. The addition of commercial dietary Schisandra supplements inhibited microsomal CYP3A-mediated midazolam 1'-hydroxylase activity. The inhibitory potential against CYP3A enzyme followed the order: 'Nature's Way > Swanson > Planetary Herbals ≅ Only Natural (Figure 2).' At a concentration of 0.05 mg/mL, extracts of Schisandra supplement from Nature's Way inhibited CYP3A activity by 93.9%.

Four dietary Schisandra supplements exhibited different CYP3A inhibition potentials. Phytochemical investigations

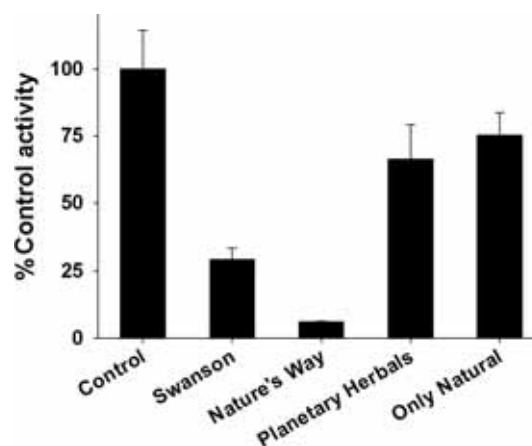


Figure 2. Inhibition of human CYP3A-mediated midazolam 1'-hydroxylation activity by commercial dietary Schisandra supplements. Human liver microsomes (0.25 mg/mL) were incubated with 0.1 mM midazolam and dietary Schisandra supplements (0.05 mg/mL). Data shown are averages of triplicate experiments ($n=3$).

have showed that dibenzocyclooctadiene lignan contents are quite different according to the variety of Schisandra, cultivation area, and cultivation time. For example, the gomisin C contents in Schisandra chinensis were ca. 20-fold higher than those in Schisandra sphenanthera.¹⁴ In addition, in the same varieties of Schisandra chinensis, the contents of the 10 lignans varied widely among the samples from different districts.¹⁴ Thus, we analyzed the major omija lignan components (gomisin A, gomisin B, gomisin C, gomisin N, deoxyschisandrin, schisandrin, and wuweizisu C) in each product using LC-MS/MS¹¹ to elucidate the differences in the CYP3A inhibition potential of the four products (Figure 3). The mean correlation coefficient (r^2) of the calibration curves were over 0.984. The limit of quantification for gomisin A, gomisin B, gomisin C, gomisin N, deoxyschisandrin, schisandrin, and wuweizisu C were 50, 5, 5, 5, 5, 5, and 10 ng/mL, respectively. Information on the contents of seven omija lignans in dietary Schisandra supplements is presented in Table 2.

We previously reported that gomisin B and gomisin C strongly inhibit CYP3A-mediated midazolam 1'-hydroxylation activity, with IC_{50} values of 0.42 and 0.30 mM, respectively.⁹ The inhibitory effect of gomisin A, gomisin N, deoxyschisandrin, schisandrin, and wuweizisu C on CYP3A activity was 7.4-fold lower than that of gomisin B and gomisin C.^{9,15} Nature's Way, which exhibited the strongest inhibitory effect on CYP3A, had the highest contents of gomisin B and gomisin C (Figure 4), which had the strongest inhibitory potential against CYP3A activity. Swanson, which had the second highest gomisin B and gomisin C contents, inhibited the CYP3A activity second. Planetary Herbals and Only Natural, which had a

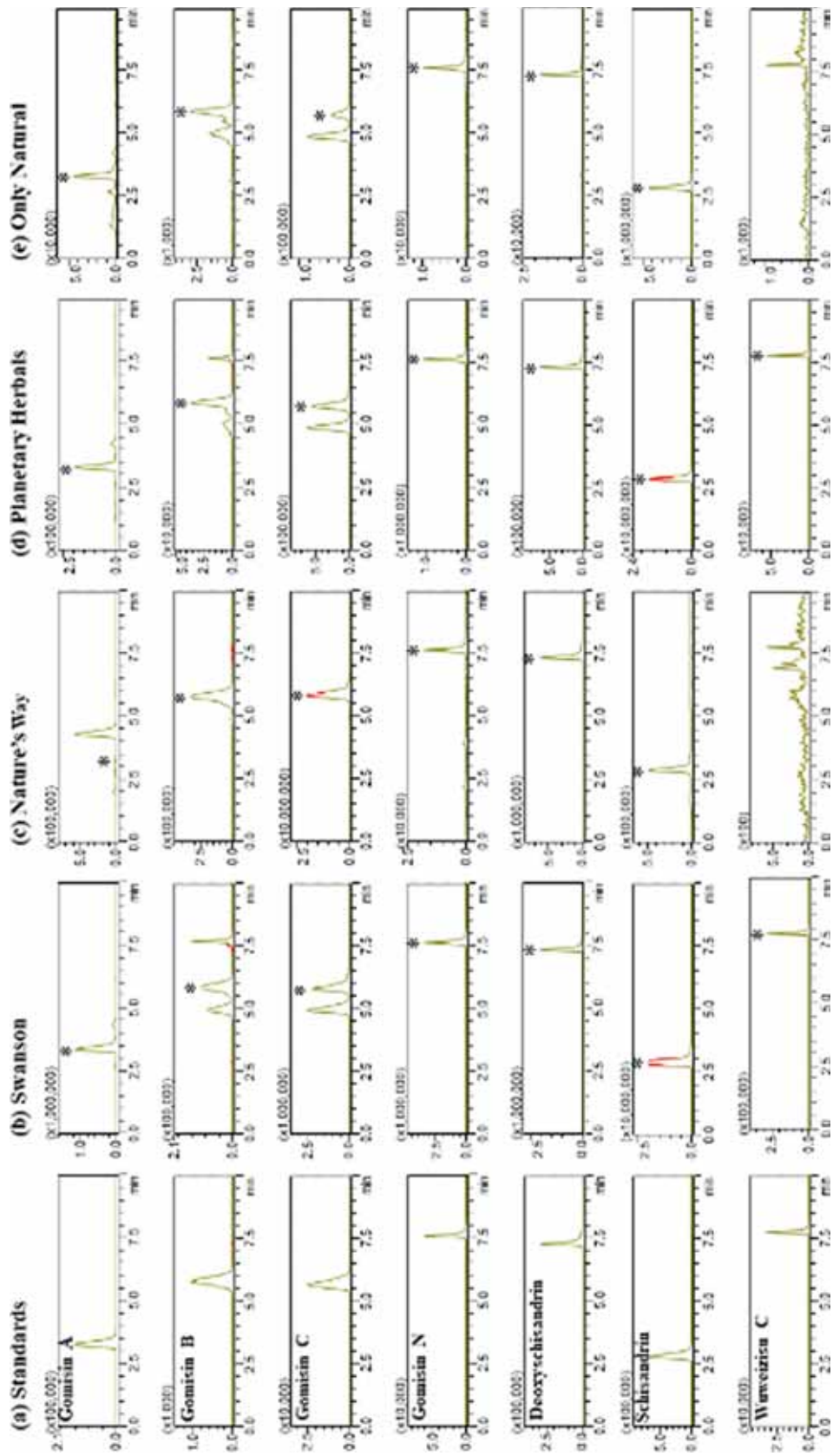
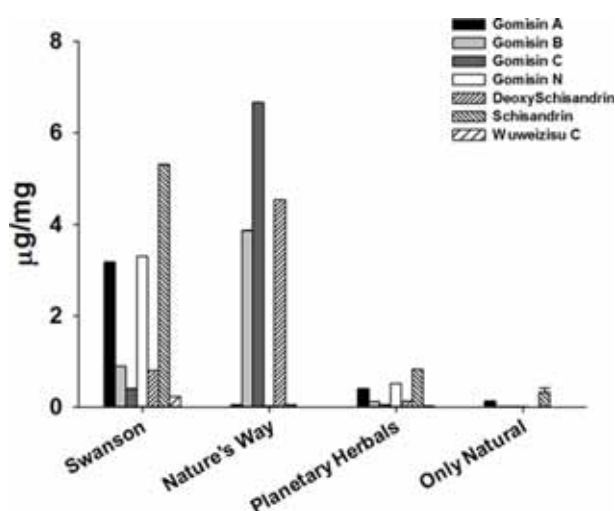


Figure 3. Representative selected reaction monitoring chromatograms of seven dibenzocyclooctadiene lignan standards (a) and dietary Schisandra supplements extracts from Swanson (b), Nature's Way (c), Planetary Herbals (d), and Only Natural (e). Gomisin A (3.25 min), gomisin B (5.79 min), gomisin C (5.64 min), gomisin N (7.58 min), deoxyshisandrin (7.26 min), schisandrin (2.83 min), and wuweizisu C (7.74 min) were monitored in positive electrospray ionization mode.

Table 2. Contents of seven dibenzocyclooctadiene lignans in four dietary Schisandra supplements ($n=3$).

Lignans Sample	Contents ($\mu\text{g}/\text{mg}$ samples)						
	Gomisin A	Gomisin B	Gomisin C	Gomisin N	Deoxyschisandrin	Schisandrin	Wuweizisu C
Swanson	3.167 \pm 0.009	0.900 \pm 0.002	0.400 \pm 0.002	3.300 \pm 0.006	0.800 \pm 0.001	5.300 \pm 0.014	0.233 \pm 0.001
Nature's Way	0.050 \pm 0.013	3.867 \pm 0.002	6.667 \pm 0.002	0.020 \pm 0.004	4.533 \pm 0.001	0.050 \pm 0.009	ND*
Planetary Herbals	0.405 \pm 0.006	0.129 \pm 0.001	0.061 \pm 0.001	0.515 \pm 0.004	0.132 \pm 0.001	0.825 \pm 0.003	0.029 \pm 0.001
Only Natural	0.120 \pm 0.012	0.010 \pm 0.002	0.010 \pm 0.002	0.010 \pm 0.001	0.004 \pm 0.001	0.330 \pm 0.089	ND*

ND*: not detected

**Figure 4.** Contents of seven dibenzocyclooctadiene lignans in four dietary Schisandra supplements, measured by liquid chromatography-tandem mass spectrometry. Data shown are averages of triplicate experiments ($n=3$).

substantially low content of the seven lignans, had negligible inhibitory effects against the CYP3A enzyme.

Schisandra extracts reportedly altered the pharmacokinetics of CYP3A substrate drugs.⁸ After oral administration (1.89 mg/kg) of cyclosporine A with co-administration of a Wuzhi tablet (containing 7.5 mg gomisin C/tablet; dose 250 mg/kg), the area under the curve and C_{\max} values of cyclosporin A were significantly increased by 293.1% and 84.1%, respectively.¹⁶ Furthermore, oral Wuzhi capsules (containing 11.25 mg deoxyschisandrin/capsule) significantly increased the oral bioavailability of tacrolimus through CYP3A inhibition in healthy individuals.¹⁷ Dietary Schisandra supplements from Nature's Way contained 4.48 mg gomisin B, 7.74 mg gomisin C, and 5.26 mg deoxyschisandrin per servings, which are similar to the contents in Wuzhi tablets (7.5 mg gomisin C/tablet) and capsules (11.25 mg deoxyschisandrin/capsule). Therefore, Nature's Way supplements might potentially cause HMDI with drugs predominantly metabolized by the CYP3A enzyme *in vivo*.

Conclusions

In conclusion, we evaluated the CYP3A inhibitory potential of four dietary Schisandra supplements in human liver microsomes. Dietary supplement from Nature's Way strongly inhibited CYP3A-mediated midazolam 1'-hydroxylase activity. This product contained high levels of gomisin B and gomisin C, which exhibited the strongest inhibitory potential against CYP3A activity. *In vivo* studies investigating the pharmacokinetic interactions between dietary supplement from Nature's Way and CYP3A substrates are required to determine the clinical relevance of these interactions.

Acknowledgements

This research was supported by Kyungpook National University Research Fund, 2021.

References

- Bent, S. *J Gen Intern Med* **2008**, 23, 854. DOI: 10.1007/s11606-008-0632-y.
- Gurley, B.J.; Fifer, E.K.; Gardner, Z. *Planta Med* **2012**, 78, 1490. DOI: 10.1055/s-0031-1298331.
- Gurley, B.J.; Swain, A.; Hubbard, M.A.; Williams, D.K.; Barone, G.; Hartsfield, F.; Tong, Y.; Carrier, D.J.; Cheboyina, S.; Battu, S.K. *Mol Nutr Food Res* **2008**, 52, 755. DOI: 10.1002/mnfr.200600300.
- Nowack, R. *Nephrology (Carlton)* **2008**, 13, 337. DOI: 10.1111/j.1440-1797.2008.00940.x.
- Howell, S.M.; Krivda, S.J. *Cutis* **2008**, 81, 467.
- Thummel, K.E.; Wilkinson, G.R. *Annu Rev Pharmacol Toxicol* **1998**, 38, 389. DOI: 10.1146/annurev.pharmtox.38.1.389.
- Yang, K.; Qiu, J.; Huang, Z.; Yu, Z.; Wang, W.; Hu, H.; You, Y. *J Ethnopharmacol* **2022**, 284, 114759. DOI: 10.1016/j.jep.2021.114759.
- Zhang, F.; Zhai, J.; Weng, N.; Gao, J.; Yin, J.; Chen, W. *Front Pharmacol* **2022**, 13, 816036. DOI: 10.3389/fphar.2022.816036.
- Seo, H.J.; Ji, S.B.; Kim, S.E.; Lee, G.M.; Park, S.Y.; Wu, Z.; Jang, D.S.; Liu, K.H. *Pharmaceutics* **2021**, 13. DOI: 10.3390/pharmaceutics13030371.

Inhibitory Effects of Dietary Schisandra Supplements on CYP3A Activity in Human Liver Microsomes

10. Zhai, J.; Zhang, F.; Gao, S.; Chen, L.; Feng, G.; Yin, J.; Chen, W. *Molecules* **2017**, *22*. DOI: 10.3390/molecules22081298.
11. Seo, H., Ji, S., Kim, S., Lee, G., Moon, S., Jang, D. S., & Liu, K. (2020). *Mass Spectrometry Letters*, *11*(2), 30-35, DOI: 10.5478/MSL.2020.11.2.3.
12. Iwata, H.; Tezuka, Y.; Kadota, S.; Hiratsuka, A.; Watabe, T. *Drug Metab Dispos* **2004**, *32*, 1351. DOI: 10.1124/dmd.104.000646.
13. Kou, K.; Sun, X.; Li, M.; Li, T.; Hu, Y.; Li, S.; Lv, G. *J Clin Pharm Ther* **2022**, *47*, 200. DOI: 10.1111/jcpt.13533.
14. Lu, Y.; Chen, D.F. *J Chromatogr A* **2009**, *1216*, 1980. DOI: 10.1016/j.chroma.2008.09.070.
15. Li, W.L.; Xin, H.W.; Su, M.W.; Xiong, L. *Methods Find Exp Clin Pharmacol* **2010**, *32*, 163. DOI: 10.1358/mf.2010.32.3.1434161.
16. Xue, X.P.; Qin, X.L.; Xu, C.; Zhong, G.P.; Wang, Y.; Huang, M.; Bi, H.C. *Phytother Res* **2013**, *27*, 1255. DOI: 10.1002/ptr.4849.
17. Xin, H.W.; Wu, X.C.; Li, Q.; Yu, A.R.; Zhu, M.; Shen, Y.; Su, D.; Xiong, L. *Br J Clin Pharmacol* **2007**, *64*, 469. DOI: 10.1111/j.1365-2125.2007.02922.

Simultaneous Liquid Chromatography Tandem Mass Spectrometric Determination of 35 Prohibited Substances in Equine Plasma for Doping Control

Young Beom Kwak¹, Jundong Yu^{1*}, and Hye Hyun Yoo^{2*}

¹Korea Racing Authority, Gwachon, Republic of Korea

²College of Pharmacy, Hanyang University, Ansan, Republic of Korea

Received December 4, 2022, Revised December 21, 2022, Accepted December 23, 2022

First published on the web December 31, 2022; DOI: 10.5478/MSL.2022.13.4.158

Abstract : Many therapeutic class drugs such as beta-blocker, corticosteroids, NSAIDs, etc are prohibited substances in the horse racing industry. Liquid chromatography-tandem mass spectrometry (LC-MS/MS) technology makes it possible to isolate drugs from interference, enables various drug analyses in complex biological samples due to its sensitive sensitivity, and has been successfully applied to doping control. In this paper, we describe a rapid and sensitive method based on solid-phase extraction (SPE) using solid phase cartridge and LC-MS/MS to screen for different class's 35 drug targets in equine plasma. Plasma samples were pretreated by SPE with the NEXUS cartridge consisted non-polar carbon resin and minimum buffer solvent. Chromatographic separation of the analytes was performed on ACQUITY HSS C18 column (2.1 × 150 mm, 1.8 μm). The elution gradient was conducted with 5 mM ammonium formate (pH 3.0) in distilled water and 0.1% formic acid in acetonitrile at a flow rate of 0.25 mL/min. The selected reaction monitoring (SRM) mode was used for drug screening with multiple transitions in the positive ionization mode. The specificity, limit of detection, recovery, and stability was evaluated for validation. The method was found to be sensitive and reproducible for drug screening. The method was applied to plasma sample analysis for the proficiency test from the Association of Racing Chemist.

Keywords : Doping control, Equine plasma, LC-MS/MS

Introduction

Many therapeutic class drugs such as beta-blocker, corticosteroids, and NSAIDs, etc are prohibited substances in horse racing as specified in Article 6 of the International Agreement on Breeding, Racing and Wagering¹ published by the International Federation of Horseracing Authorities (IFHA) and in human sports in the World Anti-Doping Agency (WADA) Prohibited List,² respectively.

The screening of drugs in doping control is critical for sports fairness and horse welfare.³⁻⁴ Drug testing methods have evolved over a long period. The method for the

detection of drugs in biological samples before the 1970s started with the use of gas chromatography-mass spectrometry (GC-MS).⁵ Currently, liquid chromatography-mass spectrometry (LC-MS) is the most widely used method for doping testing in sports. The LC-MS method allowed the analysis of thermally labile substances with a wide range of molecular weights faster and with better sensitivity.⁶⁻⁸ A recent trend has emerged in doping control for animal and human sports, utilizing tandem mass spectrometry for drug detection due to significant technological improvements in selectivity, sensitivity, and robustness in tandem mass spectrometry.⁹⁻¹² The coupling of liquid chromatography and tandem mass spectrometry (LC-MS/MS) has also made it possible to screen drugs in complex biological fluids. In LC-MS/MS, mass filtering can separate the effective signals of the target drug from interferences to improve detection ability. Theoretically, most drugs of less than 1000 Da could be analyzed in a single analytical run.

In many years, the analysis of plasma has become increasingly popular for doping control purposes because sample collection is easier and has less analytical matrix effect and variation than urine, relatively. In blood analysis, the parent drug in blood can usually be used as an analysis target, but in urine, drug metabolites may be used as the main analysis target, so it is often difficult to obtain

Open Access

*Reprint requests to Jundong Yu, Hye Hyun Yoo

<https://orcid.org/0000-0002-8948-021X>

<https://orcid.org/0000-0001-8282-852X>

E-mail: jundong@kra.co.kr, yooohh@hanyang.ac.kr

All the content in Mass Spectrometry Letters (MSL) is Open Access, meaning it is accessible online to everyone, without fee and authors' permission. All MSL content is published and distributed under the terms of the Creative Commons Attribution License (<http://creativecommons.org/licenses/by/3.0/>). Under this license, authors reserve the copyright for their content; however, they permit anyone to unrestrictedly use, distribute, and reproduce the content in any medium as far as the original authors and source are cited. For any reuse, redistribution, or reproduction of a work, users must clarify the license terms under which the work was produced.

reference standards for analysis.¹² However, the blood concentration is very low, so the use of a sensitive instrument is essential.

In this paper, we describe a rapid and sensitive method based on solid-phase extraction (SPE) using a solid-phase cartridge consisting of non-polar carbon resin and LC-MS/MS to screen for different class's 35 drug targets in equine plasma. Method validation parameters including specificity, sensitivity, extraction recovery, and stability are evaluated. The method was applied to plasma sample analysis for the proficiency test from the Association of Racing Chemist (AORC).

Materials and methods

Materials

Acepromazine maleate, atenolol, amitriptyline hydrochloride, betamethasone, chlorpromazine hydrochloride, dexamethasone, diclofenac sodium, flunixin meglumine, ketamine, ketoprofen, lidocaine, meloxicam, mepivacaine hydrochloride, methyl-prednisolone, pentazocine, pseudoephedrine hydrochloride, reserpine, salbutamol, stanzolol and triamcinolone acetonide were purchased from USP (Rockville, MD, USA). Boldenone, nandrolone, and testosterone were purchased from Steraloids (Newport, RI, USA). Clenbuterol hydrochloride, ephedrine, firocoxib, flumethasone, fluphenazine hydrochloride, methocarbamol, nordiazepam, piroxicam, sildenafil citrate, terbutaline hemisulfate salt, phenacetin and ammonium formate were purchased from Sigma-Aldrich (St. Louis, MO, USA). Detomidine hydrochloride was obtained from Santa Cruz Biotechnology (Santa Cruz, CA, USA). HPLC-grade acetonitrile (ACN), HPLC-grade distilled water (DW), and methanol (MeOH) were purchased from J.T. Baker (Phillipsburg, NJ, USA). Formic acid (FA), hexane, and ammonium hydroxide (NH₄OH) were purchased from Junsei Chem (ChouKuu, Japan). ABS ELUT Nexus cartridges (60 mg/3 mL) were purchased from Agilent Technologies (Les Ulis, France).

Instrumentation

Chromatographic separation and ESI conditions were followed based on the previously published author's paper.⁸ Chromatographic separation of the analytes was performed using the Sciex Exion UHPLC system on ACQUITY HSS C18 column (2.1 × 150 mm, 1.8 μm). The elution gradient was conducted with 5 mM ammonium formate (pH 3.0) in DW (mobile phase A) and 0.1% FA in acetonitrile (mobile phase B) at a flow rate of 0.25 mL/min, 10% mobile phase B for 1 min, 10–40% mobile phase B for 2 min, 40%–95% mobile phase B for 4.5 min, 95% mobile phase B for 0.5 min, 10% mobile phase B for 0.1 min, and 10% mobile phase B for 3.5 min. The injection volume was 5 μL. Tandem mass (MS/MS) analysis was performed on AB Sciex QTRAP 6500 (Toronto, Canada). The ionization was performed in the positive mode using the Turbo Ionspray source at a temperature of 550°C. The

ion spray voltage was 5500 V. Selected reaction monitoring (SRM) for detection was used with 150 s set for the detection window. The transitions optimized for 35 analytes and ISTD were summarized in Table 1. Data processing and handling were performed by MultiQuant 3.0.2 and Analyst 1.6 software.

Preparation of stock and working solutions

The stock solutions of analytes and internal standard (ISTD) were independently prepared by weighing the suitable quantity of reference material at a concentration of 1000 μg/mL in MeOH. The working solutions were prepared by dilution of the stock solution with MeOH. The stock solutions and working solutions were kept at -20°C.

Sample preparation

The equine blood sample in a heparin tube was centrifuged for 10 minutes at 3000 rpm and the plasma supernatant was separated. A solid phase extraction was conducted on Nexus (3 mL, 60 mg) cartridge. The ISTD (10 μg/mL, 20 μL) was added to the plasma sample (2 mL). Then the plasma sample was adjusted to pH 9 or higher by adding 1 mL of 2% NH₄OH. The sample (3 mL) was loaded onto the cartridge. The cartridge was washed using 3 mL of DW and 3 mL of hexane, dried for 3 minutes, washed with MeOH (3 mL), and dried again for two minutes. Analytes were eluted using 3 mL of MeOH. The solvent was evaporated under nitrogen at 50°C. The residue was finally vortexed with LC initial solvent (50 μL) and transferred into a vial.

Method validation

The specificity, limit of detection (LOD), recovery, and stability were measured for analytical method validation.

Specificity

Specificity was tested by checking for possible interfering peaks in SRM for analytes and the ISTD from blank plasma samples of 20 different origins

LOD and recovery

LOD was estimated based on a signal-to-noise ratio of (S/N) at least three measured peak to peak ($n = 10$). The recovery of analytes was measured by spiking the standard solution of analytes at 50 ng/mL ($n = 5$).

Stability

Stability tests of analytes were performed at a concentration level of 50 ng/mL. The stability tests were conducted at 25°C for 1 day and 7 days and at -4°C for 1 day and 7 days. ($n = 5$ each).

Application

The developed method for each analyte was applied to plasma samples for the proficiency test from AORC.¹³

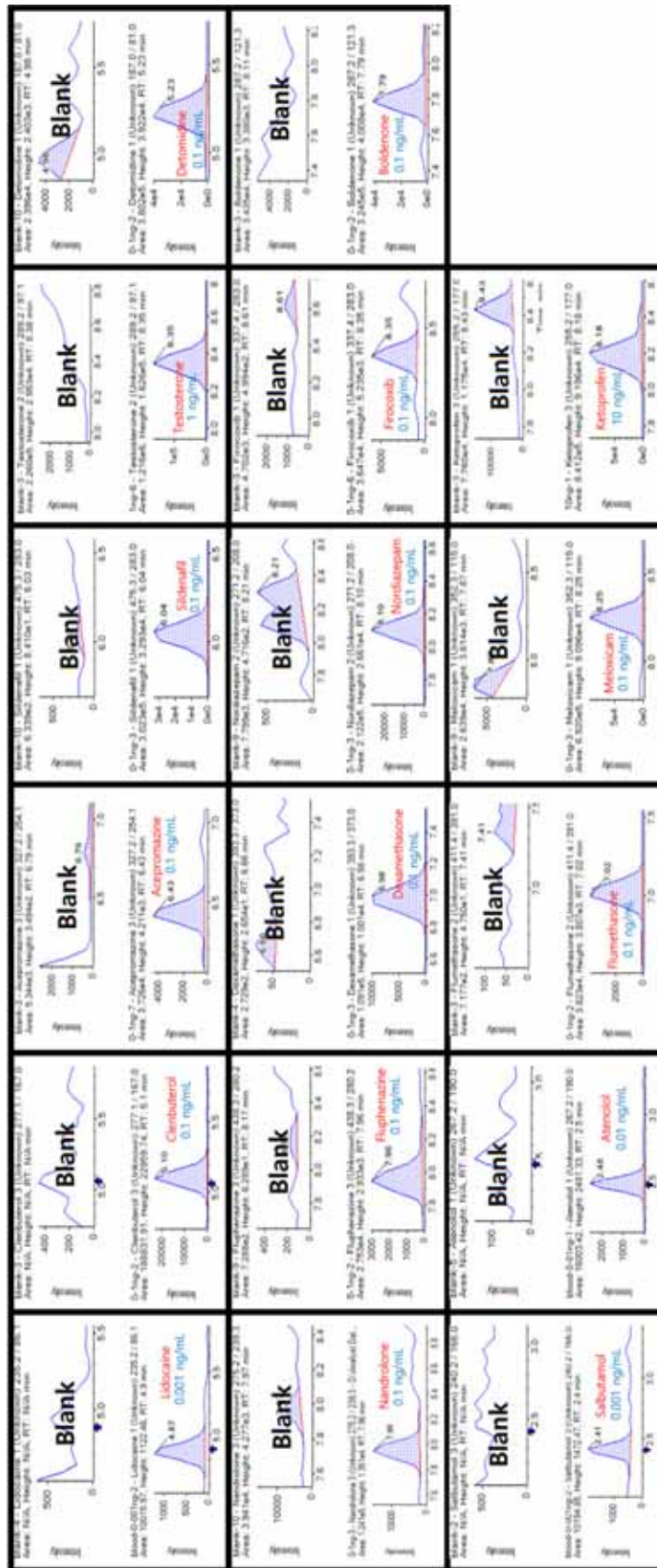


Figure 1. (continued)

Results and Discussion

Solid-phase extraction

The extraction procedure from plasma was simple and straightforward that based on a non-polar retention mechanism with no pre-conditioning required and minimum buffer solvent used to cover more than 30 analytes in different drug classes including tranquilizers, beta-blockers, corticosteroids, etc. The SPE protocol was the improved approach compared to previous WCX cartridge extraction which was complicated using many buffers to screen for varieties of drugs with LC-MS/MS in the author's laboratory. Plasma samples are fast and simply extracted using single solvents (DW, hexane, MeOH) in the process other than using a basic solvent to adjust the pH of the sample at the first step.

Chromatography and spectrometry

SRM conditions for analyte analysis were optimized by infusing reference standard solutions dissolved in MeOH directly into the mass spectrometer under declustering potential (DP), entrance potential (EP), collision energy (CE), and collision cell exit potential (CXP). All analytes stably produced protonated ions in the positive mode. All analytes which were performed by chromatographic separation on an HSS C18 column with acidic base LC mobile solvents showed good peak shapes. The elution time for analytes was within 9.5 min (Figure 1 and Table 1).

Specificity

The specificity was determined with different origin plasma samples ($n = 20$). The significant interference at the

Table 1. Mass spectrometry parameters and retention times for the 36 substances. The DP, EP, CE, and CXP were optimized for SRM transitions.

Name	Therapeutic classification	Polarity	Precursor ion (m/z)	Product ion (m/z)	DP (V)	EP (V)	CE (V)	CXP (V)	RT (min)
Acepromazine	Tranquilizer	+	327.2	254.1	80	10	35	11	6.43
				86.1	80	10	35	11	
Atenolol	β -Blocker	+	267.2	190.0	60	10	27	11	2.48
				145.0	60	10	40	11	
Amitriptyline	Antidepressant	+	278.3	218.0	60	10	35	11	7.21
				191	60	10	35	11	
Betamethasone	Corticosteroids	+	393.4	355.0	45	10	18	11	6.99
				373.0	45	10	13	11	
Boldenone	Anabolic steroid	+	287.2	121.3	65	10	35	11	7.79
				135.0	65	10	20	11	
Chlorpromazine	Tranquilizer	+	319.2	58.0	60	10	55	11	7.38
				86.0	60	10	30	11	
Clenbuterol	Bronchodilator	+	277.1	167.0	40	10	35	11	5.10
				259.0	40	10	17	11	
Detomidine	Sedative	+	187.0	81.0	81	10	29	11	5.23
				373.0	45	10	13	11	
Dexamethasone	Corticosteroids	+	393.3	355.0	45	10	18	11	6.98
				193.2	100	10	44	11	
Diazepam	Anxiolytic	+	285.1	154.1	100	10	38	11	8.82
				214.1	80	10	50	11	
Diclofenac	NSAID	+	296.0	250.0	80	10	20	11	9.17
				115.1	70	10	36	11	
Ephedrine	Sympathomimetic	+	166.0	148.0	70	10	15	11	4.17
				283.0	65	10	14	11	
Firocoxib	NSAID	+	337.4	237.0	65	10	21	11	8.35
				279.0	75	10	32	11	
Flunixin	NSAID	+	297.3	264.0	75	10	45	11	8.86
				391.0	50	10	13	11	
Flumethasone	Corticosteroids	+	411.4	371.0	50	10	16	11	7.02

Table 1. Continued.

Name	Therapeutic classification	Polarity	Precursor ion (m/z)	Product ion (m/z)	DP (V)	EP (V)	CE (V)	CXP (V)	RT (min)
Fluphenazine	Antipsychotic	+	438.3	280.2	20	10	40	11	7.96
				171.1	20	10	34	11	
Ketamine	Anesthetic	+	238.1	125.0	75	10	46	11	4.80
				220.2	75	10	20	11	
Ketoprofen	NSAID	+	255.2	177.0	70	10	26	11	8.18
				209.0	70	10	21	11	
Lidocaine	Local analgesic	+	235.2	86.1	100	10	30	11	4.87
				58.0	100	10	51	11	
Meloxicam	NSAID	+	352.3	115.0	55	10	25	11	8.25
				141.0	55	10	21	11	
Mepivacaine	Local anesthetic	+	247.2	98.0	80	10	35	11	4.84
				70.0	80	10	50	11	
Methocarbamol	Skeletal muscle relaxant	+	424.2	118.0	55	10	14	11	5.35
				199.0	55	10	13	11	
Methylprednisolone	Corticosteroids	+	375.2	161.1	60	10	23	11	6.87
				185.4	60	10	30	11	
Nandrolone	Anabolic steroid	+	275.2	239.3	80	10	20	11	7.96
				257.3	80	10	20	11	
Nordiazepam	Anxiolytic	+	271.2	208.0	70	10	40	11	8.10
				140.0	70	10	40	11	
Pentazocine	Opioid analgesic	+	286.2	218.2	80	10	27	11	5.54
				173.2	80	10	38	11	
Piroxicam	NSAID	+	332.2	95.0	50	10	22	11	7.49
				121.0	50	10	29	11	
Pseudoephedrine	Sympathomimetic	+	166.1	148.0	30	10	15	11	4.17
				133.0	30	10	28	11	
Reserpine	Antihypertensive	+	609.3	195.1	100	10	38	11	7.34
				397.1	100	10	47	11	
Salbutamol	β -agonists	+	240.2	166.0	35	10	20	11	2.41
				222.0	35	10	15	11	
Sildenafil	Vasodilator	+	475.3	283.0	90	10	52	11	6.04
				311.0	90	10	40	11	
Stanozolol	Anabolic steroids	+	329.3	121.1	60	10	45	11	8.55
				95.1	60	10	45	11	
Terbutaline	Bronchodilator	+	226.2	125.0	50	10	33	11	2.36
				152.0	50	10	22	11	
Testosterone	Anabolic steroid	+	289.2	97.1	80	10	35	11	8.35
				109.1	80	10	35	11	
Triamcinolone acetonide	Corticosteroids	+	435.3	415.0	50	10	15	11	7.39
				339.0	50	10	20	11	
Phenacetine (ISTD)	-	+	180.0	110.0	80	10	28	11	6.05

retention times of the transitions was not observed. A suspicious sample could be further evaluated through

follow-up analysis using multiple SRMs (Table 1).

LOD and recovery

All target analytes were consistently detectable in spiked samples. The LODs listed in Figure 1 and Table 2 were measured by the lowest concentrations evaluated at an S/N ratio of greater than 3:1 in the SRM chromatogram. The LODs for the different analytes were between 0.001 and 10 ng/mL with over 31% of the analytes having LODs at or

below 0.01 ng/mL, and over 92% at or below 0.1 ng/mL. The LOD of ketoprofen was measured relatively high at 10 ng/mL. These results show the improved sensitivity for 21 analytes (atenolol, amitriptyline, boldenone, dexamethasone, diazepam, firocoxib, flumethasone, fluphenazine, ketamine, lidocaine, mepivacaine, methylprednisolone, nandrolone, nordiazepam, piroxicam, pseudoephedrine, reserpine,

Table 2. Method validation results: limit of detection (LOD), recovery, and stability.

Name	LOD (ng/mL) (<i>n</i> = 10)	Recovery (%) (<i>n</i> = 5)	Stability (%) (<i>n</i> = 5)			
			25°C		-4°C	
			1day	7day	1day	7day
Acepromazine	0.1	56.9±14.1	107.7	112.8	108.0	105.3
Atenolol	0.01	83.8±5.2	102.0	100.3	107.5	105.3
Amitriptyline	0.1	64.7±16.2	104.3	105.2	100.7	140.9
Betamethasone	0.1	95.4±16.1	91.6	103.8	97.2	100.2
Boldenone	0.1	75.4±11.6	101.2	103.1	98.5	102.1
Chlorpromazine	0.01	44.4±14.2	106.4	105.7	99.9	106.4
Clenbuterol	0.1	84.9±8.1	101.5	108.4	106.3	98.5
Detomidine	0.1	78.6±17.3	104.9	107.7	107.1	103.5
Dexamethasone	0.1	91.0±14.8	106.1	110.8	108.5	103.8
Diazepam	0.1	50.7±7.3	101.0	108.2	109.1	95.3
Diclofenac	0.1	21.3±11.5	100.6	99.4	101.2	97.8
Ephedrine	0.01	55.4±3.7	101.0	103.1	105.5	106.6
Firocoxib	0.1	74.6±7.6	100.2	95.5	97.8	100.6
Flunixin	0.1	31.1±4.6	102.2	103.2	99.9	103.9
Flumethasone	0.1	85.1±14.2	105.9	107.3	104.7	107.3
Fluphenazine	0.1	18.4±14.9	107.7	110.0	101.0	105.3
Ketamine	0.01	70.6±9.0	104.0	98.0	102.0	102.5
Ketoprofen	10	23.4±7.3	92.5	110.6	103.9	106.4
Lidocaine	0.001	81.0±8.2	98.7	101.9	104.1	109.5
Meloxicam	0.1	46.8±4.9	109.0	102.2	105.9	98.9
Mepivacaine	0.001	100.4±6.4	97.4	100.3	106.3	103.0
Methocarbamol	0.1	88.9±14.1	103.3	100.4	107.1	103.2
Methylprednisolone	0.1	74.6±11.6	109.5	107.7	104.7	108.2
Nandrolone	0.1	62.7±9.9	100.2	98.5	99.8	99.7
Nordiazepam	0.1	69.4±9.8	101.2	104.6	109.1	108.0
Pentazocine	0.001	68.0±14.4	102.5	100.8	104.6	104.4
Piroxicam	0.01	49.3±6.9	100.9	104.0	109.1	98.6
Pseudoephedrine	0.01	56.3±3.7	93.0	102.0	101.6	107.0
Reserpine	0.1	20.5±10.3	103.7	103.2	103.9	94.1
Salbutamol	0.001	50.4±3.0	108.1	101.1	105.3	109.8
Sildenafil	0.1	77.4±8.4	99.5	100.5	100.4	97.5
Stanozolol	1	59.0±15.0	97.5	98.4	100.8	100.1
Terbutaline	0.01	44.9±3.2	105.1	109.2	97.1	107.5
Testosterone	1	68.9±7.0	100.2	99.4	97.4	98.6
Triamcinolone acetonide	0.1	85.1±14.3	106.6	108.6	103.2	105.2

Table 3. Drug analysis results in proficiency plasma drug test from AORC. The minimum concentrations spiked in blank plasma for the proficiency test were acepromazine (1 ng/mL), dexamethasone (0.2 ng/mL), methylprednisolone (0.1 ng/mL), and testosterone (0.5 ng/mL), respectively.

Sample number	Detected analytes
Plasma 16-A	Dexamethasone, methylprednisolone
Plasma 16-B	Blank
Plasma 16-C	Acepromazine, testosterone

salbutamol, sildenafil, terbutaline, triamcinolone acetonide) in a short LC run time compared to the previous method.¹² The mean extraction recovery of analytes was between 18.4% to 100.4% with a maximum RSD of 17.3%. The result means that most of the analytes were well recovered from plasma after SPE with the nexus cartridge. The analytes with low recoveries below 50 % showed sensitive LODs below 10 ng/mL (Table 2).

Stability

Spiked plasma samples were stable for 7 days at 25°C and -4°C. These results mean that the analytes are stable during all analytical procedures. The data obtained are shown in Table 2.

Application

The developed method was applied to the analysis of plasma samples with a proficient plasma drug test from AORC. Three plasma test samples were analyzed, one sample was blank, and dexamethasone, methylprednisolone, acepromazine, flufenamic acid, and testosterone were detected in other two samples (Table 3).

Conclusion

In conclusion, a sensitive, rapid, and simple method for the analysis of 35 prohibited drugs in equine plasma was developed. Significant interference from the matrices was not observed. The LODs for the plasma method ranged from 0.001 ng/mL to 10 ng/mL and the mean recovery was between 18.4% to 100.4% with a maximum RSD of 17.3%. The plasma samples were stable for 7 days at 25°C and -4°C. The method was successfully applied to plasma sample analysis for the proficiency test from AORC.

Conflicts of interest

The authors declare no conflict of interest.

Acknowledgments

The authors wish to thank Mr. Taek Soo Kim for technical advice.

References

- International Federation of Horseracing Authorities. Article 6 of the International Agreement on Breeding, Racing, and Wagering. <https://www.ifhaonline.org/resources/2018Agreement.pdf>. Accessed 27 Nov 2022.
- World Anti-Doping Agency. 2022, WORLD ANTI-DOPING CODE INTERNATIONAL STANDARD PROHIBITED LIST. https://www.wada-ama.org/sites/default/files/resources/files/2022list_final_en.pdf. Accessed 27 Nov 2022.
- P. L. Toutain. *Handb Exp Pharmacol.* **2010**, DOI: 10.1007/978-3-642-10324-7_13
- J. K. Wong.; T. S. Wan. *Vet J.* **2014**, 200, DOI: 10.1016/j.tvjl.2014.01.006
- D. Thieme.; P. Hemmersbach. *Handb Exp Pharmacol.* **2010**, 195, DOI: 10.1007/978-3-540-79088-4_1
- N. H. Yu.; E. N. M. Ho.; F. P. W. Tang.; T. S. M. Wan.; A. S. Y. Wong. *J Chromatogr A.* **2008**, 1189, 1-2, DOI: 10.1016/j.chroma.2007.11.022
- T. Sobolevsky.; B. Ahrens.; *Drug Test Anal.* **2020**, 13, 2, DOI: 10.1002/dta.2917
- Kwak, Y. B.; Yu, J.; Yoo, H. H. . *Drug Test Anal.* **2022**, DOI: 10.1002/dta.3271
- J. Sim.; B. Cho.; M. Park.; J. Rhee.; S. In.; S. J. Choe.; *Anal Toxicol.* **2020**, 44, 2, DOI: 10.1093/jat/bkz002
- G. Balcells.; O. J. Pozo.; A. Esquivel.; A. Kotronoulas.; J. Joglar.; J. Segura.; R. Ventura. *J Chromatogr A.* **2015**, 1389, DOI: j.chroma.2015.02.022
- M. Timms.; N. Hall.; V. Levina.; J. Vine.; R. Steel. *Drug Test Anal.* **2014**, 6, 10, DOI: 10.1002/dta.1624
- E. N. Ho.; W. H. Kwok.; A. S. Wong.; T. S. Wan. *Drug Test Anal.* **2013**, 5, 7, DOI: 10.1002/dta.1395
- Association of Racing Chemist. AORC PROFICIENCY TESTING DRUG LISTS. <https://www.aorc-online.org/members/documents/aorc-proficiency-testing-drug-lists>. Accessed 27 Nov 2022.

Comparative Analysis of the Phyto-compounds Present in the Control and Experimental Peels of *Musa paradisiaca* used for the Remediation of Chromium Contaminated Water

Vidhya Kaniyappan^{1*}, Regina Mary Rathinasamy¹, and Job Gopinath Manivanan²

¹PG and Research Department of Zoology, Auxilium College (Autonomous), Vellore – 632006, T.N, India

²PG and Research Department of Zoology, Voorhees College, Vellore – 632001, T.N, India

Received November 13, 2022, Revised December 27, 2022, Accepted December 31, 2022

First published on the web December 31, 2022; DOI: 10.5478/MSL.2022.13.4.166

Abstract : Banana peels are also widely used as bio-adsorbent in the removal of chemicals contaminants and heavy metals from water and soil. GC-MS plays an essential role in the phytochemical analysis and chemo taxonomic studies of medicinal plants containing biologically active components. Intrinsically, with the use of the flame ionization detector and the electron capture detector which have very high sensitivities, Gas chromatography can quantitatively determine materials present at very low concentrations and most important application is in pollution studies. In the present study banana peels were used as bio-adsorbent to remediate the heavy metal contaminated water taken from three different stations located around the industrial belts of Ranipet, Tamilnadu, India. The AAS analysis of the samples shows a decrement of chromium concentration of 98.93%, 96.16% and 96.5% in Station 1, 2 and 3 respectively which proves the efficiency of the powdered peels of *Musa paradisiaca*. The GC-MS analysis of the control and treated peels of *Musa paradisiaca* reveals the presence of phytochemicals like Acetic Acid, 1-Methylethyl Ester, DL-Glyceraldehyde Dimer, N-Hexadecanoic Acid, 3-Decyn-2-Ol, 26-Hydroxy, Cholesterol, Ergost-25-Ene-3,5,6,12-Tetrol, (3.Beta.,5.Alpha.,6.Beta.,12.Beta.), 1-Methylene-2b-Hydroxymethyl-3, and 3-Dimethyl-4b-(3-Methylbut-2-Enyl)-Cyclohexane in the control banana peels. The banana peels which were used for the treatment reveals the changes and alteration of the phytochemicals. It is concluded that the alteration in phytochemicals of the experimental banana peels were due to adsorption of chromium heavy metal from the sample.

Keywords : Bio-adsorbent, Banana peels, GCMS, AAS, Phytochemicals, Heavy metals, Chromium.

Introduction

The non-nutrient plant chemical compounds and bioactive compounds are referred to as phytochemicals.¹⁻³ Applications of phytochemicals have expanded recently, particularly in the fields of nutraceuticals and functional foods.⁴ The importance of phytochemicals for health is highlighted by Asif *et al.*⁵ One of the most significant crops in the world estimated at 72.5 million metric tonnes of bananas are produced globally, of which India contributes 21.77 million metric tonnes.⁶ The fruit peels from this variety that are thrown away make up 18 to 33%

Open Access

*Reprint requests to Vidhya Kaniyappan

<https://orcid.org/0000-0002-5155-9571>

E-mail: yonigrace@gmail.com

All the content in Mass Spectrometry Letters (MSL) is Open Access, meaning it is accessible online to everyone, without fee and authors' permission. All MSL content is published and distributed under the terms of the Creative Commons Attribution License (<http://creativecommons.org/licenses/by/3.0/>). Under this license, authors reserve the copyright for their content; however, they permit anyone to unrestrictedly use, distribute, and reproduce the content in any medium as far as the original authors and source are cited. For any reuse, redistribution, or reproduction of a work, users must clarify the license terms under which the work was produced.

of the total fruit peel waste. The banana peels are rich in potassium, phosphorus, magnesium, and calcium as well as 52 other chemical components and nutritional goods.⁷ In comparison to the fruit's pulp, banana peels are rich in chemical components that are valued for their anti-fungal and antibacterial activities.^{8,9} The biotechnological manufacture of protein from banana peel waste also produces ethanol, alpha-amylase, and cellulose.¹⁰ According to Kanazawa *et al.*,¹¹ banana peels include a variety of phytochemicals and phytonutrient components, primarily antioxidants. These include anthocyanins, delphinine, catecholamines, beta-carotene, and alpha-carotene.¹¹ In recent years GC-MS studies have been increasingly applied for the analysis of medicinal plants as this technique has proved to be a valuable method for the analysis of non-polar components and volatile essential oil, fatty acids, lipids, and alkaloids.¹²⁻¹⁴ A key use of GC-MS is the monitoring of environmental contaminants. Equipment for GCMS has become less expensive while significantly improving in reliability. In the current study, the effectiveness of using banana peels to remediate chromium-contaminated wastewater was evaluated. The amount of chromium present in the contaminated water before and after the treatment using banana peels were evaluated by using Atomic Absorption

Spectroscopy (AAS) method. Using the GC-MS technique, the Phyto-compound changes in the experimental *Musa paradisiaca* peels were compared to the control.

Experimental

Study Area

Ranipet is located at 12.56 degree Northern latitude and 79.20 Eastern longitudes and is 93 km west of Chennai, it is geographically 25 km away from the northeast of Vellore. Tamil Nadu Chromate Chemicals Limited (Plate 1) is an industry located in the Chennai-Bangalore national highway NH4 near the Ranipet Industrial area, Ranipet District. Topographically the area is sloping towards the south and southeast side which is towards Puliyanankannu and further down to the Palar river. The Palar which is one of the major drinking water sources is running from west to east and is located 4.5 km down the streamline of the site.¹⁵ Tamil Nadu Pollution Control Board (Tamil Nadu Pollution Control Board, unpublished report, 1996) estimated that ~150,000 tons of solid chromium waste accumulated over two decades of plant operation has been stacked in the open yard (stack height varies from 4 to 5 m) on 3.5 ha of land within the Tamil Nadu Chromate and Chemicals Limited (TCCL) premises, Ranipet, Tamil Nadu, India (Plate 1a). The chemicals from that raw ore were getting leached out by rainwater and seeping into the groundwater and affecting the quality of the groundwater.¹⁶ Samples were collected from Station 1 (Stagnant water inside the TCCL), Station 2 (Run off water from the TCCL) and Station 3 (Stagnant water outside the TCCL), Ranipet, TN, India. (Plate 1b).

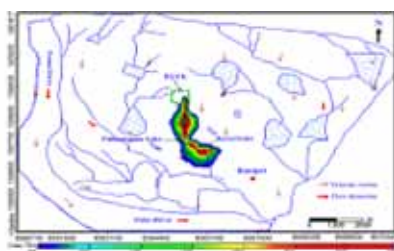


Plate 1. TCCL Topography



Plate 1a. TCCL - Ore Dump Site



Plate 1b. Sample Collection

Preparation of Bio-Adsorbent and Treatment Process

The peels of *Musa paradisiaca* were removed and washed thoroughly in distilled water to remove the external

dirt. The peels were cut into small pieces (Plate 2) and dried under the hot sun for 3 days (Plate 3).¹⁷ Then the dried peels were washed thoroughly in an orbital shaker and dried in a hot air oven for 2 hr at 80°C to remove the moist content. Then the dried peels were powdered blending them in a blender and sieved using 250 microns sieve (Plate 4, 5).¹⁸ Eight grams of powdered peels of *Musa paradisiaca* (Plate 17) were added to 100 mL of Sample 1, 2, and 3 and mixed well using a magnetic stirrer. The treatment setup (Plate 6) was left for 24 hr at room temperature and constant pH.^{19,20} The filtrate was dried and subjected to GC-MS analysis. (Plate 7). The treated water sample was subjected to AAS analysis for determining the adsorption efficiency of the bio-adsorbent and to evaluate the chromium concentration.²¹ AAS is an analytical technique used to determine the concentration of metal ions in a sample.



Plate 2. Fresh Peels of *Mp*



Plate 3. Dried Peels of *Mp*



Plate 4. Powdered Peels of *Mp*



Plate 5. 250 micron Sieve



Plate 6. Treatment setup



Plate 7. Filtration

Preparation of Methanol Extract

The control and the experimental filtrate of the treated banana peel powder was evaporated to dryness and 10 g of powdered peels were dissolved in 100 mL of 100% methanol (CH_3OH) and stirred well using a magnetic stirrer for 3 hours and left overnight. Extracts (50 mL) were then transferred to clean vessels, evaporated to dryness, and dissolved in dimethyl sulfoxide to yield a final concentration of approximately 10 mg/mL and subjected for GC-MS analysis.²²

Table 1. Adsorption Efficiency of Powdered Peels of *Musa paradisiaca* on Heavy Metal Chromium by AAS Method.

Sample	Conc. of Cr (mg/L) before remediation	Conc. of Cr (mg/L) after treatment	Mean adsorption	df	t value	Significance p value
Station 1 Stagnant water inside the TCCL	701.311	7.437 ± 0.3791 (98.93)	0.0288	5	48.053	0.000
Station 2 Run off water from the TCCL	782.047	29.958 ± 0.5315 (96.16)	0.1159	5	138.043	0.000
Station 3 Stagnant water outside the TCCL	849.569	29.629 ± 0.3716 (96.51)	0.1146	5	195.308	0.000

Values in parenthesis () indicates % change over control

Values are Mean, ± SD of 6 individual observation

Significant at $p < 0.005$

GC-MS analysis

GC-MS analysis from the methanol extract of banana peels was carried out in the instrument Perkin Elmer GC Clarus 680, Mass spec Clarus 600 (EI), using the software Turbo Mass ver 5.4.2 and NIST – 2008 library year. The identification of the chemical components was influenced by their GC retention time, percentage composition (area %), and retention indices. The interpretation and identification of their mass spectra were confirmed by the mass spectral incorporated library. The identification was further confirmed by comparing it with the database of the spectrum of known components stored in the GC MS NIST (2008) library.²³ The GC-MS was performed at SIF Laboratory, VIT, Vellore, TN, India.

Result

Table 1 shows the results of the Atomic Absorption Spectroscopy (AAS) analysis performed to estimate the concentration of chromium present in the untreated and treated water samples. 6 individual samples were taken from each Station and experiment was carried out. Mean Value, ± SD and percentage change over control and student t test were done using SPSS version 26. Station 1 shows an initial chromium concentration as 701.311 mg/L. After the treatment, it is estimated as 7.437 mg/L of chromium concentration. Station 2 shows an initial chromium concentration as 782.047 mg/L. After the treatment, it is estimated as 29.958 mg/L of chromium concentration. Station 3 shows an initial chromium concentration as 849.569 mg/L. After the treatment, it is estimated as 29.629 mg/L of chromium concentration.

The exploration of phytochemical screening with methanol extract of *Musa paradisiaca* peels by GCMS is tabulated in Table 2 which reveals the presence of acetic

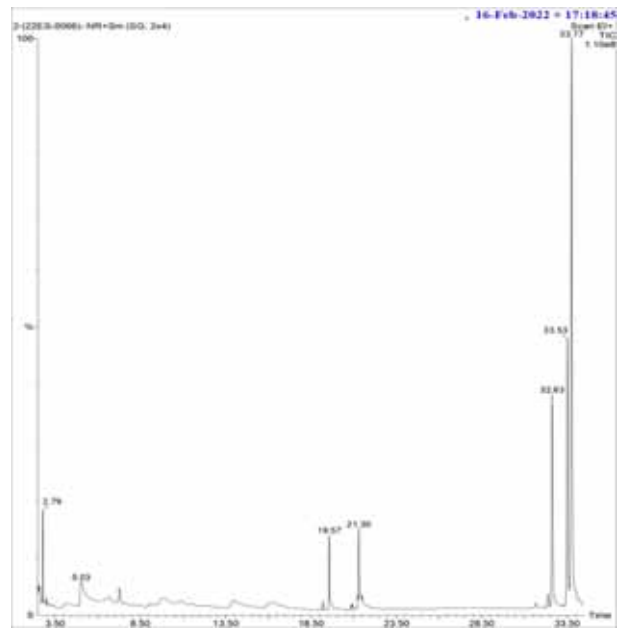
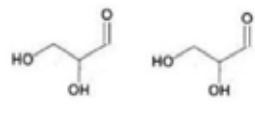
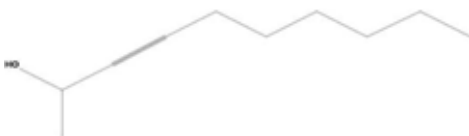
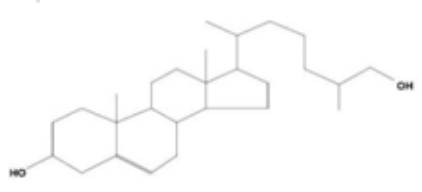
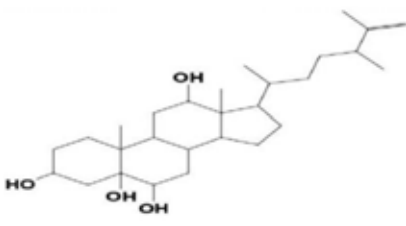
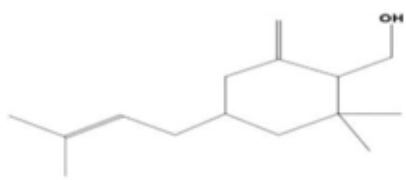


Figure 1. Chromatogram Obtained from the GC-MS with the Extract of Control peels of *Musa paradisiaca*

acid 1-methyl ethyl ester having molecular formula $C_5H_{10}O_2$ with 2.799 min of retention time, DL-Glyceraldehyde dimer having molecular formula $C_6H_{12}O_6$ with 5.039 min of retention time, N-hexadecenoic acid having molecular formula $C_{16}H_{32}O_2$ with 19.570 min of retention time. N-hexadecenoic acid is also called palmitic acid with molecular formula $C_{16}H_{32}O_2$ and 19.570 min retention time. Other compounds include 3-den-2-of having molecular formula $C_{10}H_{18}O$ with 21.2296 min retention time, 2-6-hydroxy cholesterol having a molecular

Table 2. The Phyto-compounds identified by GC-MS in Methanol Extract of Control Peels of *Musa paradisiaca*

S. No	RT	Compound name	Molecular Formula	Molecular weight	Structure
1	2.799	Acetic Acid, 1-Methylethyl Ester	C ₅ H ₁₀ O ₂	102	
2	5.039	D1-Glyceraldehyde Dimer	C ₅ H ₁₀ O ₂	180	
3	19.570	N-Hexadecanoic Acid	C ₁₆ H ₃₂ O ₂	256	
4	21.296	3-Decyn-2-ol	C ₁₀ H ₁₈ O	154	
5	32.626	26-Hydroxy Cholesterol	C ₂₇ H ₄₆ O ₂	402	
6	33.526	Ergost-25-Ene- 3,5,6,12,-Tetrol, (3.Beta.,5.A1pha.,6.B eta.,12.Beta.)-	C ₁₅ H ₂₄ O	220	
7	33.776	1-Methylene-2b Hydroxymethyl-3, 3-Dimethyl-4b-(3- Methylbut-2-Enyl)- Cyclohexane	C ₁₅ H ₂₆ O	222	

formula C₂₇H₄₆O₂ with 32.626 min retention time, Ergost-25-ene-3,5,6,12 Tetrol having molecular formula C₁₅H₂₄O with 33.526 min as retention time and 1-methylene 2b-hydroxy methyl- 3,3-dimethyl-4b cyclohexane having molecular formula C₁₅H₂₆O with 33.776 min retention time. Figure 1 shows a GC-MS Chromatogram of methanol extracts of control peels of *Musa paradisiaca*. The chromatogram shows the RT taken by the analytes to pass through the column and reach the mass spectrometer.

Table 3 shows the main compounds identified by GC-MS in the methanol extract of treated peels of *Musa paradisiaca* in Sample 1 (Treated Peels from Station 1) with five compounds. The bioactive components with their retention time (RT), names of the compounds, and molecular structure of the compound are tabulated. The analysis reveals Undecanoic acid (22.59%), Hexadecanal (39.58%), 4, 22-Stigmastadiene-3-one, 2R-Acetoxyethyl-

1 (26.84%), 3,3-Trimethyl-4T-(3-Methyl-2-Buten-1-yl)-1t-Cyclohexanol (27.02%) and 9, 19-Cycloergost-24(28)-EN-3-ol, 4,14-dimethyl-acetate (3.beta., 4.alpha.)- (100%). Figure 2 shows the Chromatogram of GC-MS analysis of methanol extract of treated peels of *Musa paradisiaca* in Sample 1, at RT 19.910 has 10.457 area%, RT 21.391 has 18.322 area%, RT 27.569 has 12.425 area%, RT 28.039 has 12.508 area% and RT 28.164 has 46.288 area%.

Table 4 shows the main compounds identified by GC-MS in the methanol extract of treated peels of *Musa paradisiaca* in Sample 2 (Treated Peels from Station 2) were eleven compounds. The analysis reveals 4h-pyran-4-one,2,3-dihydro-3,5-dihydroxy-6-methyl- (62.39%), Methane carbothiolic acid (50.82%), 2-Amino-octadec-7-ene-1,3-diol butaneboronate (41.46%), Hydroperoxide,1-methylpentyl (21.96%), 2,3-anhydro-d-galactosan (41.30%), 2,3-anhydro-d-galactosan (41.30%), 3-dimethylsilyloxytridecane (78.63%),

Table 3. The Phyto-compounds identified by GC-MS in Methanol Extract of Treated Peels of *Musa paradisiaca* in Sample 1

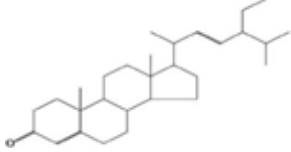
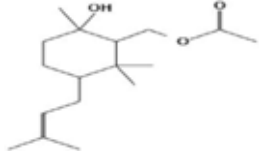
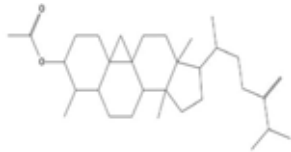
S. No	RT	Compound name	Molecular Formula	Molecular weight	Structure
1	19.910	Undecanoic acid	C ₁₁ H ₂₂ O ₂	186	
2	21.391	Hexadecana	C ₁₆ H ₃₂ O	240	
3	27.569	4,22-Stigmastadiene-3-one	C ₂₉ H ₄₆ O	410	
4	28.039	2R-Acetoxyethyl-1,3,3-Trimethyl-4T-(3-Methyl-2-Buten-1-yl)-Cyclohexanol	C ₁₇ H ₃₀ O ₃	282	
5	28.164	9,19-Cycloergost-24(28)-EN-3-ol, 4,14-dimethyl-acetate (3.beta.,4.alpha.)-	C ₃₂ H ₅₂ O ₂	468	

Table 4. The Phyto-compounds identified by GC-MS in Methanol Extract of Treated Peels of *Musa paradisiaca* in Sample 2

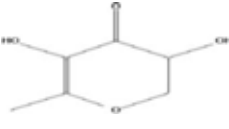
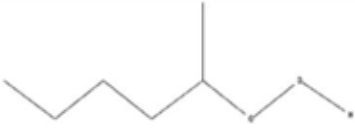
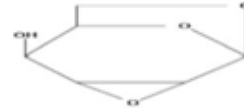
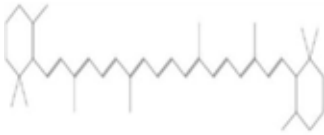
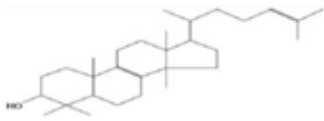
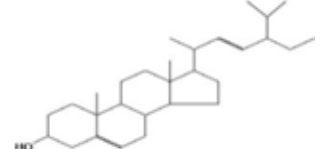
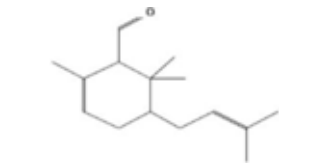
S. No	RT	Compound name	Molecular Formula	Molecular weight	Structure
1	14.613	4h-pyran-4-one,2,3-dihydro-3,5-dihydroxy-6-methyl-	C ₆ H ₈ O ₄	144	
2	16.494	Methane carbothiolic acid	C ₂ H ₄ OS	76	
3	18.270	2-Amino-octadec-7-ene-1,3-diol butaneboronate	C ₂₂ H ₄₄ O ₂ NB	365	
4	19.260	Hydoroperoxide,1-methyl-pentyl	C ₆ H ₁₄ O ₂	118	
5	20.181	2,3-anhydro-d-galactosan	C ₆ H ₈ O ₄	114	
6	21.766				

Table 4. Continued

S. No	RT	Compound name	Molecular Formula	Molecular weight	Structure
7	25.052	3-dimethylsilyloxytridecane	C ₁₅ H ₃₄ OSi	258	
8	27.659	.Beta.carotene	C ₄₀ H ₅₆	536	
9	27.744	Lanosterol	C ₃₀ H ₅₀ O	426	
10	28.254	Stigmasterol	C ₂₉ H ₄₈ O	412	
11	28.434	1-formyl-2,2,6-trimethyl-3-cis-(3-methylbut-2-enyl)-5-cyclohexene	C ₁₅ H ₂₄ O	220	

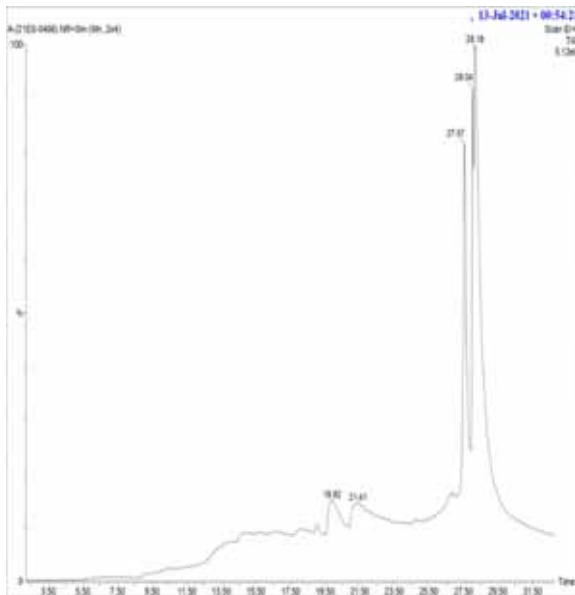


Figure 2. Chromatogram Obtained from the GC-MS with the Extract of Control peels of *Musa paradisiaca* Treated in Sample 1

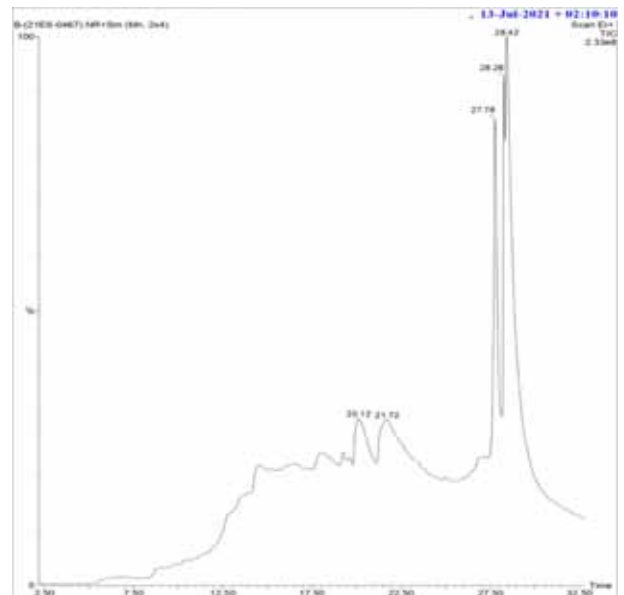


Figure 3. Chromatogram Obtained from the GC-MS with the Extract of Control peels of *Musa paradisiaca* Treated in Sample 2

Beta carotene (23.02%), Lanosterol (36.28%), Stigmasterol (20.90%) and 1-formyl-2,2,6-trimethyl-3-cis-(3-methylbut-2-enyl)-5-cyclohexene (100%). Figure 3 GC-MS Chromatogram

of methanol extracts of treated peels *Musa paradisiaca* in Sample 2 showing the peak retention times and the peak heights.

Table 5. The Phyto-compounds identified by GC-MS in Methanol Extract of Treated Peels of *Musa paradisiaca* in Sample 3

S. No	RT	Compound name	Molecular Formula	Molecular weight	Structure
1	27.649	9,19-Cycloergost-24 (28)-En-3-Ol,4,14-Dimethyl-,Acetate,(3.Beta.,4.Alpha.,5.Alpha)	C ₃₂ H ₅₂ O ₂	468	
2	27.764	4,5-Secocholest-6-En-4-Oic Acid,5-Oxo	C ₂₇ H ₄₄ O ₃	416	
3	28.239	22-Stigmasten-3-One	C ₂₉ H ₄₈ O	412	
4	28.414	2-Methyl-3-(3-Methyl-But-2-Enyl)-2-(4-Methyl-Pent-3-Enyl)-Oxetane	C ₁₅ H ₂₆ O	222	

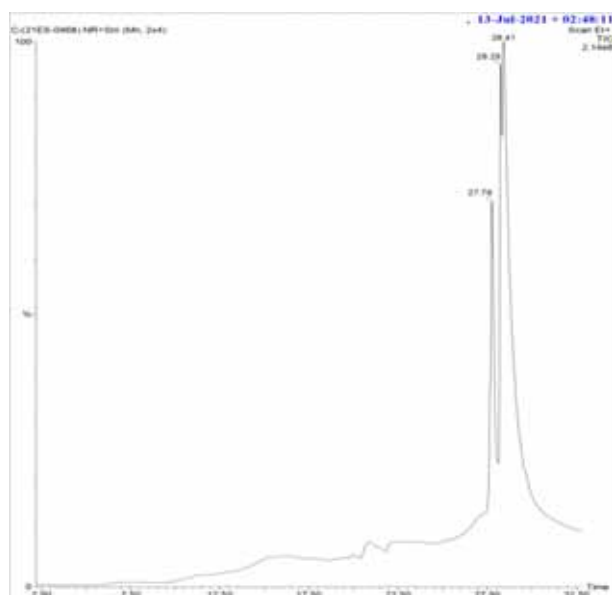
**Figure 4.** Chromatogram Obtained from the GC-MS with the Extract of Control peels of *Musa paradisiaca* Treated in Sample 3

Table 5 shows the main compounds identified by GC-MS in the methanol extract of treated peels of *Musa paradisiaca* in Sample 3 (Treated Peels from Station 3) with five compounds. The analysis reveals 9,19-cycloergost – 24

(28)-en-3-ol,4,14-dimethyl-acetate, (3.beta.,4.alpha.,5.alpha) (22.59%), 4,5-secocholest-6-en-4-oic acid,5-oxo (39.58%), 22-stigmasten-3-one (26.84%), 2-methyl-3-(3-methyl-but-2-enyl)-2-(4-methyl-pent-3-enyl)-oxetane (27.02%). Figure 4 showed a GC-MS Chromatogram of methanol extracts of treated peels *Musa paradisiaca* in Sample 3 showing the peak retention times and the peak heights.

Discussion

Biowaste of plants is the source of potentially bioactive compounds which are useful in all areas. The biological and pharmacological properties are very vital and still many are unknown.²³ Effective use of peels of *Musa paradisiaca* for the remediation of chromium-contaminated water paves the way to reclaim the environment that is lost due to heavy metal pollution. The ASS result shows there was a decrement in chromium concentration in Samples 1, 2, and 3 which proves the efficiency of the powdered peels of *Musa paradisiaca*. The adsorption efficiency of the bio-adsorbent was 98.93%, 96.16%, and 96.5% in stations 1, 2, and 3 respectively. Methanol is the most commonly used extraction solvent due to its high polarity which could produce high extraction yields. Methanol usually enriches more hydrophilic molecules than hydrophobic molecules.²⁴ The exploration of phytochemical screening with methanol

extract of control *Musa paradisiaca* peels reveals the presence of Glyceraldehyde an aldotriose comprising propanal having hydroxy groups at the 2- and 3-positions. Most sugars found in nature are D-sugars, which are related to D glyceraldehyde, whilst most amino acids found in proteins belong to the L-stereochemical series related to L-glyceraldehyde.²⁵ Palmitic acid is a saturated fatty acid used in the production of soap and renovates the skin.²⁶ These are the organic compounds required for the normal growth and maintenance of life of animals, including humans, and are essential for the transformation of energy and regulation of the metabolism of structural units.²⁷

Acetic acid 1-methyl ethyl ester having molecular formula $C_5H_{10}O_2$ with 2.799 min of retention time in which the methyl esters are found to be an excellent solvents with low volatility and good solubility. They are widely used to replace mineral spirits in the textile, screen ink industry, and graphics arts industries. Their main benefits are low volatility and flammability, low toxicity, and environmental compatibility. They have also been used in paint removal products in both consumer and industrial applications. Methyl esters have also found applications in the removal and recovery of spilled crude oil and other petroleum products from both coastal and inland spill sites.²⁸ It has been reported that estragole has many biological effects including antioxidant and antimicrobial activities. The hexadecanoic acid ethyl ester can be an antioxidant, hypocholesterolemic, nematocide, pesticide,

and lubricant activities, and hemolytic 5 – alpha is a reductase inhibitor.²⁹ It is found that it has been used as an antioxidant in the oils and fats in lipid oxidation and also as an agent in foodstuffs and health functional ingredients in various foods and dietary supplements.

The exploration of phytochemical screening with methanol extract of *Musa paradisiaca* peels reveals the presence of 2-butanone, 4-(acetyloxy)- having molecular formula $C_6H_{10}O_3$ with 2.698 min of retention time, Benzene Aceto nitrile 4-hydroxy having molecular formula C_8H_7ON with 14.088 min of retention time, Beta.-d-glucopyranose, 1,6-anhydro- having molecular formula $C_6H_{10}O_5$ with 14.573 min of retention time, D-glycero-d-tallo-heptose having molecular formula $C_7H_{14}O_7$ with 15.829 min of retention time, 1,5,9-undecatriene, 2,6,10-trimethyl-, (z)- having molecular formula $C_{14}H_{24}$ with 17.985 min of retention time, N-hexadecanoic acid having molecular formula $C_{16}H_{32}O_2$ with 19.685 min of retention time, 9-hexadecenoic acid having molecular formula $C_{16}H_{30}O_2$ with 21.471 min of retention time, 2-Piperidinone, n-[4-bromo-n-butyl]- having molecular formula $C_9H_{16}ONBR$ with 21.661 min of retention time, Glucitol, 6-o-nonyl- having molecular formula $C_{15}H_{32}O_6$ with 24.602 min of retention time, 2-Tert-butyl-4,6-bis (3,5-di-tert-butyl-4-hydroxybenzyl) phenol having molecular formula $C_{40}H_{58}O_3$ with 29.805 min of retention time and 1-hexyl-2-nitrocyclohexane having molecular formula $C_{12}H_{23}O_2N$ with 32.256 min of retention time. However, in single metal solutions, ions with larger ionic

Table 6. Comparison of Phyto-compounds Present in the Control and Experimental Peels of *Musa paradisiaca* in Sample 1, 2, and 3 by GC-MS

S.No	RT	Compounds present in the Control peels	Compounds present in the Experimental Peels in Sample 1	Compounds present in the Experimental Peels in Sample 2	Compounds present in Experimental Peels in Sample 3
1	2.799	Acetic Acid, 1-Methyl-ethyl Ester	-	-	-
2	5.039	D1-Glyceraldehyde Dimer	-	-	-
3	14.613	-	-	4h-pyran-4-one,2,3-dihydro-3,5-dihydroxy-6-methyl	-
4	16.494	-	-	Methane carbothiolic acid	-
5	18.270	-	-	2-Amino-cotadec-7-ene-1,3-diol butaneboronate	-
6	19.260	-	-	Hydroperoxide, 1-methylpentyl	-
7	19.570	N-Hexadecanoic Acid	-	-	-
8	19.910	-	Undecanoic acid	-	-
9	20.181	-	-	2,3-anhydro-d-galactosan	-

Table 6. Continued

S.No	RT	Compounds present in the Control peels	Compounds present in the Experimental Peels in Sample 1	Compounds present in the Experimental Peels in Sample 2	Compounds present in Experimental Peels in Sample 3
10	21.296	3-Decyn-2-O1	-	-	-
11	21.391	-	Hexadecanal	-	-
12	21.766	-	-	2,3-anhydro-d-galactosan	-
13	25.052	-	-	3-dimethyl silyloxy-tridecane	-
14	27.569	-	4,22-Stigmastadiene-3-one	-	-
15	27.649	-	-	-	9,19-Cycloergost-24(28)-En-3-O1,4,14-Dimethyl-,Acetate,(3.Beta.,4.Alpha.,5.Alpha)
16	27.659	-	-	Beta.carotene	-
17	27.744	-	-	Lanosterol	-
18	27.764	-	-	-	4,5-Secocholest-6-En-4-Oic Acid,5-Oxo
19	28.039	-	2R-Acetoxyethyl-1,3,3-Trimethyl-4T-(3-Methyl-2-Buten-1-yl)-1t-Cyclohexanol	-	-
20	28.164	-	9, 19-Cycloergost-24(28)-EN-3-ol, 4,14-dimethyl-acetate (3.beta., 4.alpha.)-	-	-
21	28.239	-	-	-	22-Stigmasten-3-One-
22	28.254	-	-	Stigmasterol	-
23	28.414	-	-	-	2-Methyl-3-(3-Methyl-But-2-Enyl)-2-(4-Methyl-Pent-3-Enyl)-Oxetane
24	28.434	-	-	1-formyl-2,2,6-trimethyl-3cis-(3-methylbut-2-enyl)-5-cyclohexene	-
25	32.626	26-Hydroxy Cholesterol	-	-	-
26	33.526	Ergost-25-Ene-3,5,6,12-Tetrol, (3.Beta.,5.Alpha.,6.Beta., 12.Beta.)-	-	-	-
27	33.776	1-Methylene-2b-Hydroxymethyl-3,3-Dimethyl-4b-(3-Methyl-but-2-Enyl)-Cyclohexane	-	-	-

radii are better adsorbed than those with less ionic radii.³⁰ The banana peels which were used for the treatment reveal changes and alterations of the phytochemicals in all three experimental banana peels.

The alteration in the phytochemicals of the experimental banana peels was due to the adsorption of chemical contaminants from the sample. Further, while comparing the GC-MS analysis of the control and the experimental banana peels it is evidenced that the adsorption of chemical compounds was found effective, and binding the adsorbed chemicals, changing the chemical composition of phytochemicals which is tabulated in Table 6. The functional groups that were active in removing Chromium from water were the carboxylic and amine groups and the alterations in the phytochemicals were due to the adsorption of heavy metal chromium. The anionic ligands present on the cell wall such as carboxyl, amine, hydroxyl, carbonyl, sulfhydryl and phosphoryl groups immobilizes the metal ions³¹ and then uptake occurs³² which was evidenced.

Conclusion

Waste banana peels were used as a bio-adsorbent for the remediation of the chromium-contaminated wastewater collected from the industrial area of Ranipet District, TN, India and found to be very best, low cost and effective bio-adsorbent to remediate the heavy metal chromium. The compared results of control and experiment bio-adsorbent, peels of *Musa paradisiaca* showed the phytochemicals alterations due to the adsorption of chromium heavy metal from the sample which evidences the adsorption capacity of banana peels. This cost-effective, eco-friendly method could be used for the remediation of chromium-polluted water for the restoration of the polluted water bodies.

References

- Liu, R.H.; *Journal of Nutrition*. **2004**, 134 (12):3479-3485. DOI: 10.1093/jn/134.12.3479S
- Nweze, E.L.; Okafor, J.I.; Njoku O.; *Journal of Biological Research and Biotechnology*. **2004**, 2 (1): 34-46. DOI: 10.4314/br.v2i1.28540
- J. H. Doughari.; I. S Human.; S. Bennade and P. A. Ndakidemi.; *Journal of Medicinal Plants Research*. **2009**, 3(11): 839-848.
- Tiwari, B.K.; Brunton, N.P.; Brennan, C.; *Handbook of Plant food phytochemicals: sources, stability and extraction*. John Wiley and Sons, 1-4, **2013**.
- Asif Ahmed Kibri.; Kamrunnessa, Md.; Mahmudur Rahman.; Annanya Kar.; *Malaysian Journal of Halal Research Journal (MJHR)*. **2019**, 2(1). DOI: 10.2478/mjhr-2019-0005
- Anhwange, B.A.; T.J.Ugye.; D. Nyiaatagher.; *Electronic Journal of Environment, Agricultural and Food Chemistry*. **2009**, 8(6), 437-442.
- Kondo Satoru.; Kittikorn Monrudee.; Kanlayanarat Srichai.; *Postharvest Biology and Technology*. **2005**, 36, 309-318 DOI: 10.1016/j.postharvbio.2005.02.003
- Someya, S.; Yoshiki, Y.; Okubo, K.; *Food Chemistry*. **2002**, 79(3), 351-354.
- S. Suliman.; S.F. van Vuuren.; A.M. Viljoen.; *Letters in Applied Microbiology*. **2009**, 48(4), 440-446. DOI: 10.1111/j.1472-765X.2008.02548.x
- Zhang, P.; Whistler, R.L.; BeMiller, J.N.; Hamaker, B.R.; *Carbohydrate Polymers*. **2005**, 59(4), 443-458 DOI: 10.1016/j.carbpol.2004.10.014
- Kanazawa, K.; Sakakibara, H.; *Journal of Agricultural and Food Chemistry*. **2000**, 48(3), 844-848. DOI: 10.1021/jf9909860
- Hussein AO.; Mohammed GJ.; Hadi MY, Hameed IH.; *Journal of Pharmacognosy and Phytotherapy*. **2016**, 8(3), 49-59. DOI: 10.5897/JPP2015.0368
- Sosa AA.; Bagi SH.; Hameed IH.; *International Journal of Pharmacognosy and Phytochemical Research*. **2016**, 8(5), 109-126. DOI: 10.5897/JPP2015.0371
- Huda Jasmin M.Altameme.; Mohammed Yahya Hadi.; Imad Hadi Hameed.; *Journal of Pharmacognosy and Phytotherapy*. **2015**, 7(10), 238-252. DOI: 10.5897/JPP2015.0361
- Edwin, D. Thangam.; Nehru Kumar V.; Anitha Vasline Y.; *International Journal of Applied Engineering Research*. **2019**, 14(2), 342-347. Doi: 10.36478/jeasci.2019.342.347
- Nirmala, B. Suchetan.; P.A. Darshan; D. Sudha.; A.G. Lohith.; T.N. Suresh.; E. Mamtha.; *International Journal of Chem Tech Research*. **2004**, 5(1), 288-292.
- Deshmukh Prashant D.;Gajanan K. Khadse.; Vilas M. Shinde.; Pawankumar Labhassetwar.; **2017**, *Journal of Bioremediation and Biodegradation*. 8(03), 395. DOI: 10.4172/2155-6199.1000395.
- Priyanka Kumari.; **2017**, *International Research Journal of Engineering and Technology*. 4(6), 1404-1406.
- Renu Dubey.; J. Bajpai.; Anil Kumar Bajpai.; *Journal of Water Process Engineering*. **2015** (5) 83-94. DOI: 10.1016/j.jwpe.2015.01.004
- Moriya, M.; Ho, Y.H.; Grana, A.; Nguyen, L.; Alvarez, A., Jamil, R., Ackland, M.L.; Michalczyk, A.; Hamer, P.; Ramos, D.; Kim, S.; *American Journal of physiology-cell physiology*. **2012**, 295(3), C708-21.
- Malcolm, J. Brandt.; K. Michael Johnson.; Don, D. Ratnayaka.; *Twort's Water Supply book*. Seventh Edition, **2017**.
- Erica C. Larson.; Christopher D. Pond.; Prem P. Rai.; Teatulohi K. Matainaho.; Pius Piskaut.; Michael R. Franklin.; Louis R. Barrows.; *Evidence-Based Complementary and Alternative Medicine*. **2016**, 7869710. DOI: 10.1155/2016/7869710
- Muthukumaran Pakkirisamy.; Suresh Kumar Kalakandan.; Karthikeyen Ravichandran.; *Pharmacogn J*. **2017**, 9(6), 952-956. DOI: 10.5530/pj.2017.6.149
- Dieu-Hien Truong.; Dinh Hieu Nguyen.; Nhat Thuy

- AnhTa.; Anh VoBui.; Tuong Ha Do.; Hoang Chinh Nguyen.; *Journal of Food Quality*. **2019**, 8178294. DOI: 10.1155/2019/8178294
25. Nigel Aylward.; Neville Bofinger.; *Progress in Biological Chirality*. **2004**, 13-28
26. Oredo V.E.; E.D. Dikio.; *Ann. Appl. Sci.*, **2020**, 6 (1), 9-15
27. Traber M.G.; Atkinson,J.; *Free Radic Biol Med*. **2007**, 43, 4-15, DOI: 10.1016/j.freeradbiomed.2007.03.024
28. Bernie Y, Tao.; *Industrial Applications for Plant Oils and Lipids, Bioprocessing for Value-Added Products from Renewable Resources*. 1st Edition, Elsevier, **2007**. DOI: 10.1016/b978-044452114-9/50025-6
29. Jyotsna S. Waghmare.; Ankeeta H. Kurhade.; *European Journal of Experimental Biology*. **2014**, 4(5), 10-15
30. Igwe K. K.; Nwankwo P. O.; Otuokere I. E.; Ijioma S. N.; Amaku F.M.; *Journal of Research in Pharmaceutical Science*. **2015**, 2(11), 01-06
31. Volesky, B.; *Hydro Metallurgy*. **2003**, 71:179-190. DOI: 10.1016/S0304-386X(03)00155-5
32. Joo, J, H.; Hassan, SHA, Oh, SE.; *International Deterioration and Biodegradation*. **2010**, 64:734-741 DOI: 10.1016/j.ibiod.2010.08.007

Analysis of Amyloid Beta 1-16 (A β 16) Monomer and Dimer Using Electrospray Ionization Mass Spectrometry with Collision-Induced Dissociation

Kyoung Min Kim and Ho-Tae Kim*

Department of Chemistry and Bioscience, Kumoh National Institute of Technology, 61, Daehak-ro, Gumi, Gyeongbuk, 39177, Republic of Korea

Received December 2, 2022, Revised December 12, 2022, Accepted December 12, 2022

First published on the web December 31, 2022; DOI: 10.5478/MSL.2022.13.4.177

Abstract : The monomer and dimer structures of the amyloid fragment A β (1–16) sequence formed in H₂O were investigated using electrospray ionization mass spectrometry (MS) and tandem MS (MS/MS). A β 16 monomers and dimers were indicated by signals representing multiple proton adduct forms, [monomer+zH]ⁿ⁺ (=M^{z+}, z = charge state) and [dimer+zH]^{z+} (=D^{z+}), in the MS spectrum. Fragment ions of monomers and dimers were observed using collision-induced dissociation MS/MS. Peptide bond dissociation was mostly observed in the D1–D7 and V11–K16 regions of the MS/MS spectra for the monomer (or dimer), regardless of the monomer (or dimer) charge state. Both covalent and non-covalent bond dissociation processes were indicated by the MS/MS results for the dimers. During the non-covalent bond dissociation process, the D³⁺ dimer complex was separated into two components: the M¹⁺ and M²⁺ subunits. During the covalent bond dissociation of the D³⁺ dimer complex, the b and y fragment ions attached to the monomer, (M+b₁₀₋₁₅)^{z+} and (M+y₉₋₁₅)^{z+}, were thought to originate from the dissociation of the M²⁺ monomer component of the (M¹⁺+M²⁺) complex. Two different D³⁺ complex geometries exist; two distinguished interaction geometries resulting from interactions between the M¹⁺ monomer and two different regions of M²⁺ (the N-terminus and C-terminus) are proposed. Intricate fragmentation patterns were observed in the MS/MS spectrum of the D⁵⁺ complex. The complicated nature of the MS/MS spectrum is attributable to the coexistence of two D⁵⁺ configurations, (M¹⁺+M⁴⁺) and (M²⁺+M³⁺), in the A β 16 solution.

Keywords : A β 16, A β 16 dimer, collision-induced dissociation, mass spectrometry, MS/MS

Introduction

An understanding of protein misfolding is crucial to understanding the pathology of neurodegenerative diseases. One example of a misfolded protein is A β in Alzheimer's disease (AD).^{1,2} AD is characterized by the extracellular deposition of A β in the form of plaques and neurofibrillary tangles of the Tau protein in the brain.^{3,4} In the plaque deposition of A β , A β oligomers that formed in the early stage of A β aggregation are considered to be the most neurotoxic agents in AD.⁵⁻⁸ However, the structure and formation process of A β oligomers are not yet understood

clearly because of the metastable character of A β oligomers.⁹

Accordingly, oligomer formation processes have been studied using various experimental and theoretical methods including ion-mobility mass spectrometry,^{10,11} CD,^{12,13} NMR experiments^{14,15} and computer simulations.¹⁶⁻²⁰ The collision cross-sections and the percentage of β -strands or α -helix content of oligomers were reported to aid in understanding or inhibiting A β fibril formation process. One (residues 12–24), two (residues 12–24 and 30–42), or three (1–6, 12–24, and 30–42) active regions were reported as critical interaction areas in the A β 42 aggregation process.^{14,21-23} Several stable dimer conformations were also reported in a simulation study of A β oligomer.^{19,20}

Short A β fragments (A β 16–20, A β 35–40, A β 1–16, A β 17–42, and A β 1–28) have been studied to aid in understanding (or inhibiting) the A β aggregation process.²⁴⁻²⁸ However, the exact sequence of aggregation events and their role remain unclear. In particular, reports of the A β 16 fragment, which is regarded as a potential inhibitor^{29,30} of A β aggregation, are discrepant. Some studies^{31,32} reported that A β 16 fragments do not aggregate and reduce A β 16 cytotoxicity in neuronal cells, whereas other reports state that A β 16 aggregates and A β 16 oligomers are cytotoxic.^{26,33} These conflicting experimental results were obtained using

Open Access

*Reprint requests to Ho-Tae Kim
<https://orcid.org/0000-0002-1541-3081>
 E-mail: hotaekim@kumoh.ac.kr

All the content in Mass Spectrometry Letters (MSL) is Open Access, meaning it is accessible online to everyone, without fee and authors' permission. All MSL content is published and distributed under the terms of the Creative Commons Attribution License (<http://creativecommons.org/licenses/by/3.0/>). Under this license, authors reserve the copyright for their content; however, they permit anyone to unrestrictedly use, distribute, and reproduce the content in any medium as far as the original authors and source are cited. For any reuse, redistribution, or reproduction of a work, users must clarify the license terms under which the work was produced.

various experimental techniques. Metal (Ni, Cu, Zn, and Al, among others) ion-induced A β 16 aggregation was also studied to understand the reactivity and functional group activity of A β 16. The 10–16 residue region of A β appears to be an effective metal ion trapping unit.^{34,35} His6 and other carbonyl groups have also been reported as potential active regions for the metal ion binding unit.

In this study, we used collision-induced dissociation (CID) in conjunction with electrospray ionization (ESI)-mass spectrometry (MS) to obtain structural information on the A β 16 monomer and dimer. A β 16 dimer complexes were allowed to form in solution and were electrosprayed onto a quadrupole ion guide. ESI-MS was assumed to produce intact gas-phase dimer complex ions from the A β 16 dimer complex in solution. A low-energy CID-tandem MS (MS/MS) method was applied to investigate the fragment ion species and patterns of the multiply charged monomers and dimers of A β 16.

Experimental

The MS and MS/MS spectra for the A β 16 fragmentation pattern analysis were obtained using a Thermo Finnigan LTQ mass spectrometer (Thermo Fisher Scientific, Waltham, MA, USA), which is a linear ion trap mass spectrometer equipped with an atmospheric pressure ESI source.

MS conditions

A β 16 samples (in H₂O) were introduced to the ESI interface via a direct infusion method using a microsyringe pump (Hamilton, USA) at a flow rate of 1 mL/min. The CID-MS/MS experiments were conducted at capillary temperatures of 150°C, which resulted in the best signal-to-noise ratios for the MS/MS spectra. The positive ion MS

spectra were acquired over an m/z range of 100–2000 by averaging 1000–4000 scans. The MS/MS experimental conditions were as follows: ion-trap pressure, 1×10^{-5} Torr; activation time, 30 ms; injection time, 100–200 ms; and isolation width, 0.8–1.5 mass units. The parent A β 16 ions were individually and manually selected and subjected to CID. The collision energies were optimized for each MS/MS experiment to obtain sufficient signal-to-noise ratios.

Reagents

The A β 16 peptide, synthetic peptide (purity > 95%), amidated at the C-terminus (DAEFRHDSGYEVHHQK-NH₂, Peptron, Daejeon, Korea), and HPLC-grade H₂O (Merck Ltd., Korea) were used in the experiments. A β 16 peptides were dissolved in H₂O to prepare 150 μ M solutions. Solutions were prepared to achieve sufficient D⁵⁺ ion intensity in the CID-MS/MS experiments. The experiments were performed within 24 h of sample preparation.

Results and Discussion

MS Spectra

Under our ESI experimental conditions, the mass spectra of the A β 16 solutions indicated the presence of multiply charged monomers and oligomers (Figure 1). A β 16 monomers were observed at m/z 1953.9, 977.5, 652.0, and 489.2, ranging from 1+ to 4+ and [M+H⁺] to [M+4H⁺] as multiple proton adducts forms. The A β 16 peptide contains five basic residues (Arg5, His6, His13, His14, and Lys16) and an N-terminal position available for protonation. There are also four acidic residues (Asp1, Glu3, Asp7 and Glu11) in the A β 16 peptide. The M⁵⁺ peak at m/z 391.6 was not observed in the ESI-MS spectrum of the A β 16 solution (Figure 1). The M³⁺ monomer peak was observed with a

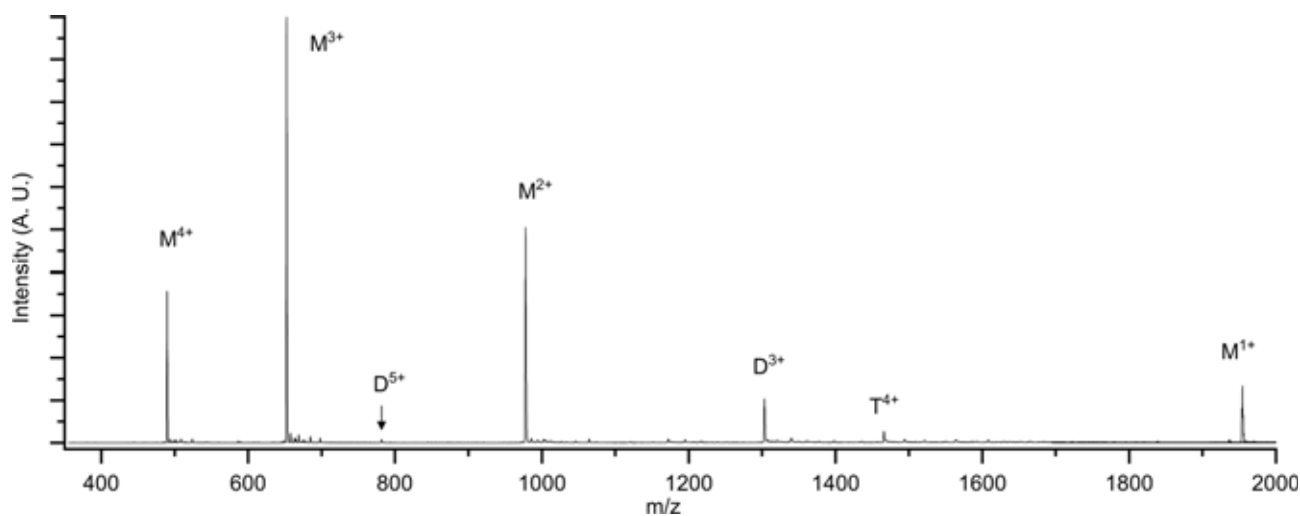


Figure 1. ESI-MS spectrum of A β 16 solution. Multiply charged monomers and oligomers are represented as M^{z+}, D^{z+}, and T^{z+} (M = monomer, D = dimer, T = trimer, and z = charge state).

high-intensity peak. For the oligomers, peaks were observed at m/z 1302.9, 782.2, and 1465.7, corresponding to D^{3+} , D^{5+} , and T^{4+} (T=trimer), respectively.

MS spectra of the A β 16 peptide have been reported in previous studies.³⁶⁻³⁸ Oligomer complexes were not observed in these spectra because of the A β 16 concentrations and experimental conditions. The positive charge state distribution of the A β 16 monomers (Figure 1) is consistent with that of the previously reported MS spectrum. The new observation of D^{3+} , D^{5+} , and T^{4+} complexes indicated the possibility of aggregation of the A β 16 peptides. The aggregation process of A β 16 might be different from that of A β protein because of the extra A β 17-42 peptide region. The configurations (up to trimer) and m/z values of the observed complexes are listed in the Supplementary Information Table S1.

MS/MS spectra of monomers

CID-MS/MS experiments were conducted to obtain structural information regarding the parent A β 16 monomer and dimer ions. The MS/MS spectra of A β 16 monomers are shown in Figure 2 and 3. The fragment ions were labeled with various colors and shapes based on the charge states and fragment ion species in Figure 2 and 3. The m/z values and assignments for the fragment ions in Figure 2 and 3 are presented in the Supplementary Information Table S2. These monomer MS/MS fragmentation patterns are useful for analyzing the dimer MS/MS spectrum,

according to the charge state. The similar fragment ions of M^{2+} , M^{3+} , and M^{4+} monomers have been reported under different experimental conditions (in CH₃OH:H₂O 97:3 solution).³⁶ The MS/MS fragment ion species shown in Figure 2 and 3 are similar to those of previously reported spectra. However, some fragment ions observed in this study have not been reported previously (including b_{13}^{3+} , b_{14}^{3+} , b_{15}^{3+} , shown in Figure 2b, y_{13}^{3+} , b_9^{2+} , shown in Figure 3a, and y_{14}^{3+} , shown in Figure 3b). In the MS/MS spectrum for A β 16 M^{1+} and M^{2+} (Figure 2), we observed high-intensity fragment ions at the peptide bonds of the N-terminus (D1–D7) and C-terminus (V11–K16) region. The peptide bond dissociation between D7 and S8, corresponding to the b_7 and y_9 ions, was also observed as another characteristic dissociation channel in the CID process of M^{1+} or M^{2+} parent ions. The dissociation process in the central region, residues S8–Y10, cannot be observed in the monomer spectra (Figure 2). However, we observed distinctive fragment ions, originating from the S8–Y10 central region, in the MS/MS spectrum of M^{3+} (Figure 3a). The (b_8^{2+} – b_{10}^{2+}) fragment ions were observed by a part of the (2+) b_u ion series peaks at $u = 7$ –15. The (2+) b_u ion series peaks at $u = 7$ –15, which were observed at high intensities, are the characteristic ion series observed in the MS/MS spectrum of M^{3+} (Figure 3a). These ion series were only observed in the MS/MS spectrum of M^{3+} among four monomer parent ions (M^{1+} – M^{4+}). The b or y fragment ions from the peptide bonds of the N-terminus and C-

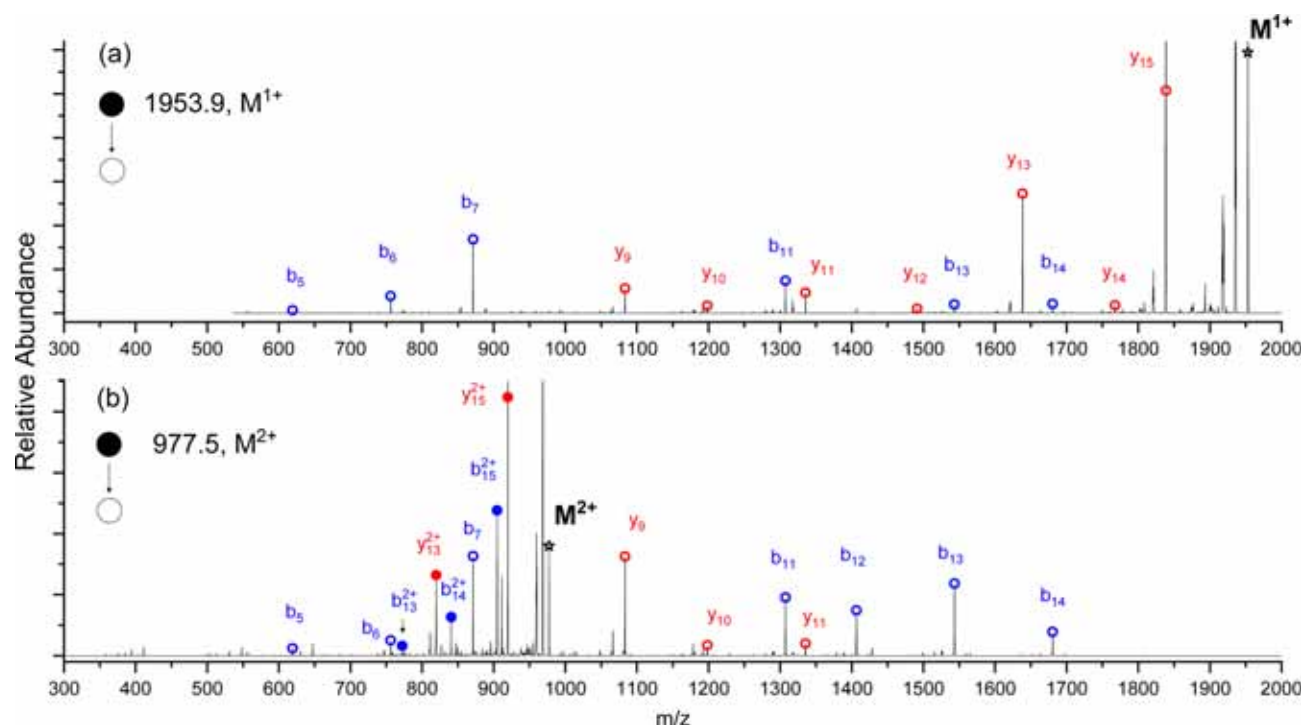


Figure 2. MS/MS spectra of monomers of A β 16 (a) M^{1+} and (b) M^{2+} . (1+) b fragment ions are indicated by blue empty circle and (1+) y fragment ions are indicated by red empty circle at top of peak. (2+) b and y fragment ions are indicated by filled circles.

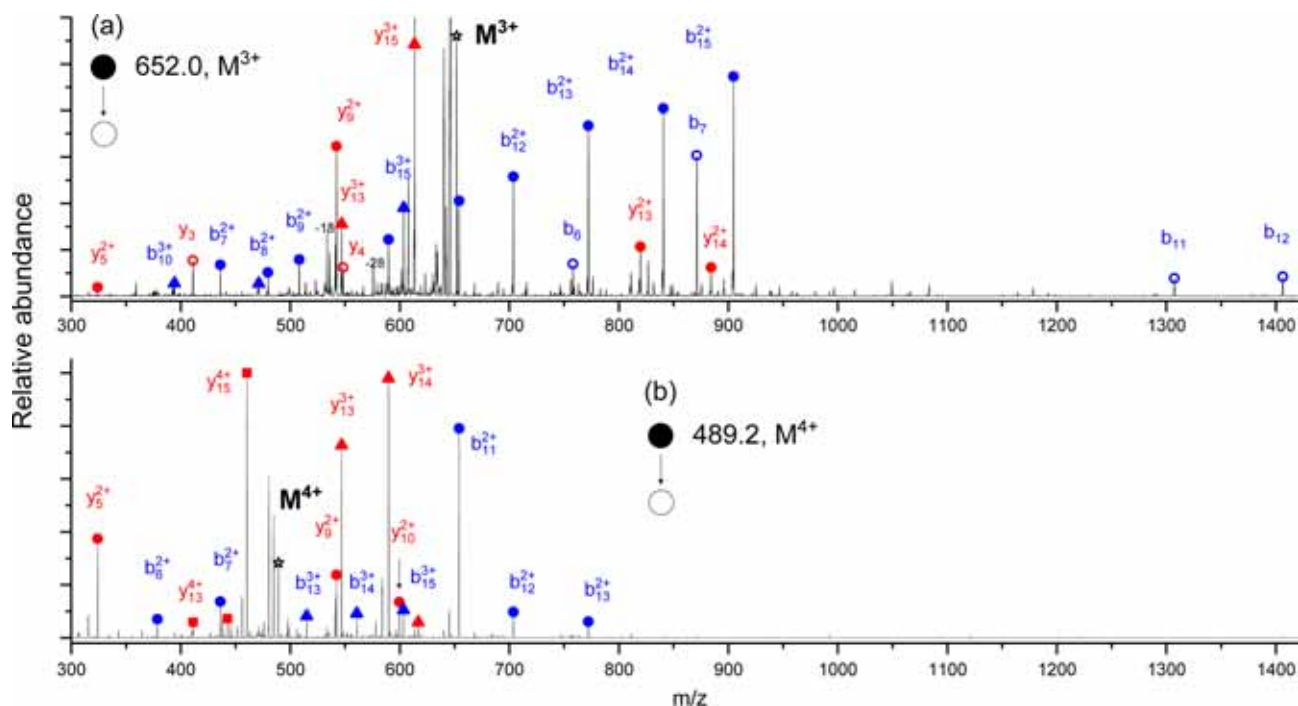


Figure 3. MS/MS spectra of (a) M^{3+} and (b) M^{4+} monomers. (1+) b fragment series peaks are indicated by empty blue circles and (1+) y fragment series peaks are indicated by empty red circles at top of peak. (2+) b and y fragment ions are indicated by filled circles, (3+) b and y fragment ions by filled triangles, and (4+) b and y fragment ions by filled squares at top of peak.

Table 1. Comparison of MS/MS fragment ions of A β 16 monomers and dimers. b and y ions were observed in MS/MS spectrum for monomers and b, y, (M+ b), and (M+ y) fragment ions were observed in MS/MS spectrum for dimers.

Parent ion	Observed MS/MS fragment ions		
	residue 1-7	residue 8-10	residue 11-16
M^{1+}	$b_5^{1+} - b_7^{1+} // y_{15}^{1+} - y_9^{1+}$		$b_{11}^{1+} - b_{14}^{1+}$
M^{2+}	$b_5^{1+} - b_7^{1+}$ $y_{11}^{1+} - y_9^{1+} // y_{15}^{2+} - y_{13}^{2+}$		$b_{11}^{1+} - b_{14}^{1+} // b_{13}^{2+} - b_{15}^{2+}$
M^{3+}	$b_5^{1+} - b_7^{1+}$ $b_7^{2+}, y_{14}^{2+}, y_{13}^{2+}$ y_{15}^{3+}, y_{13}^{3+}	$b_8^{2+} - b_{10}^{2+}$ b_{10}^{3+}	$b_{11}^{1+} - b_{12}^{1+} // y_4^{1+} - y_3^{1+}$ $\ll b_{11}^{2+} - b_{15}^{2+} \gg$ b_{12}^{3+}, b_{15}^{3+}
M^{4+}	$b_6^{2+} - b_7^{2+}$ $\langle y_{14}^{3+}, y_{13}^{3+} \rangle$ $y_{15}^{4+} - y_{13}^{4+}$		$b_{11}^{2+} - b_{13}^{2+}, y_5^{2+} - y_3^{2+}$ $b_{13}^{3+} - b_{15}^{3+}$
D^{3+}	$b_5^{1+} - b_7^{1+}$ $[M+y_{11}]^{2+} - [M+y_9]^{2+} // [M+y_{15}]^{3+} - [M+y_{13}]^{3+}$		$[M+b_{11}]^{2+} - [M+b_{14}]^{2+}$
D^{5+}	b_7^{1+} $[M+y_{11}]^{3+} - [M+y_9]^{3+}$ $\langle [M+y_{14}]^{4+}, [M+y_{13}]^{4+} \rangle$ $[M+y_{15}]^{5+} - [M+y_{13}]^{5+}$	$[M+b_{10}]^{5+}$	$b_{11}^{1+}, b_{12}^{1+} // b_{11}^{2+}, b_{12}^{2+} // y_4^{1+}$ $[M+b_{11}]^{3+} - [M+b_{13}]^{3+}$ $\ll [M+b_{11}]^{4+} - [M+b_{15}]^{4+} \gg$ $[M+b_{12}]^{5+}, [M+b_{15}]^{5+}$

terminus regions are also observed in Figure 3 with (+1) to (+4) charge states. The observed fragment ions are listed in Table 1.

MS/MS spectra of the dimers

Both covalent and non-covalent bond dissociation were indicated by the MS/MS spectra of the dimers (Figure 4).

D^{3+} complex presumably coexist in the A β 16 solution. The D^{3+} complex geometry shown in Scheme 1a is a likely candidate to explain the series ① or ③ fragment ion patterns, whereas the Scheme 1b geometry explains the series ② fragment ion patterns.

The Scheme 1b geometry of D^{3+} complex is not appropriate for explaining the singly charged b_5 – b_7 ions in ① pattern because the fragile R5–D7 region of M^{2+} is blocked by the attachment of M^{1+} , which inhibits the dissociation of the fragile R5–D7 region of M^{2+} . Judging from the common observation of singly or doubly charged b_5 – b_7 ions in the MS/MS spectra of M^{1+} – M^{4+} , the R5–D7 region is prone to dissociation in the A β 16 complex.

Therefore, it is deduced that the singly charged b_5 – b_7 ions in ① pattern were resulted from the Scheme 1a geometry of D^{3+} complex because there is no interaction between M^{1+} component and the fragile R5–D7 region of M^{2+} . The possible dissociation channels are indicated by arrows in Scheme 1. If the M^{1+} component is attached to the restricted D1–F4 region of M^{2+} in the Scheme 1b geometry, the singly charged b_5 – b_7 ions of ① pattern could be differently observed, resulted in the $[M^{1+}+b_5]$ – $[M^{1+}+b_7]$ attached ions. However, the attached fragment ions $[M^{1+}+b_5]$ – $[M^{1+}+b_7]$ were not observed in the D^{3+} MS/MS spectrum (Figure 4a).

Notably, fragment ion series ② in the D^{3+} MS/MS spectrum is low intensity. The intensities of the $[M+b_{11}]^{2+}$ – $[M+b_{14}]^{2+}$ and $[M+b_{14}]^{3+}$ – $[M+b_{15}]^{3+}$ monomer attached ions were significantly lower than those of (b_{11}^{1+} – b_{14}^{1+}) and (b_{14}^{2+} – b_{15}^{2+}), as shown in Figure 2b.

In fragment ion series of ③ pattern, the $[M+y_9]^{2+}$ ion is a counter ion to the b_7^{1+} fragment ion in the D7–S8 peptide bond dissociation process of the D^{3+} complex illustrated in Scheme 1a. The high intensities of the $[M+y_9]^{2+}$ and b_7^{1+} ions suggested that the D7–S8 peptide bond is one of the weak bonds in the D^{3+} complex of Scheme 1a, similar to how the D7–S8 peptide bond is one of the weak bonds in the M^{2+} monomer.

According to the difference in the intensities of ② and ③ patterns (Figure 4a), it is presumed that the complex formation efficiency of Scheme 1a geometry is better than that of Scheme 1b geometry. Consequently, we believe that the geometry proposed in Scheme 1a is the major species of D^{3+} complex in the A β 16 solution.

In the MS/MS spectrum of the D^{5+} complex (Figure 4b), intricate fragmentation patterns resulting from the covalent bond dissociation process were observed. Two characteristic fragmentation patterns are observed in Figure 4b, ④ $[(M^{1+})+(y_{13}^{3+})]^{4+}$ and $[(M^{1+})+(y_{14}^{3+})]^{4+}$ and ⑤ $[(M^{2+})+(b_{11}^{2+})]^{4+}$ – $[(M^{2+})+(b_{15}^{2+})]^{4+}$ fragment ions. The fragment ion series and intensities of ④ pattern or ⑤ pattern are consistent to those of the M^{4+} or M^{3+} spectrum (Figure 3) except (M^{1+}) or (M^{2+}) monomer attachment in the ④ and ⑤ fragment ions. Therefore, the fragment ions of ④ pattern were assigned to the fragments resulting from the

dissociation of the M^{4+} monomer component of the ($M^{1+}+M^{4+}$) dimer geometry and the fragment ions of ⑤ pattern were assigned to those resulting from the dissociation of the M^{3+} monomer component of the ($M^{2+}+M^{3+}$) dimer geometry.

The triply charged ⑥ $[M+y_{11}]^{3+}$ – $[M+y_9]^{3+}$ and $[M+b_{11}]^{3+}$ – $[M+b_{13}]^{3+}$ ion signals are commonly attributable to fragments resulting from the dissociation of the M^{4+} component in the ($M^{1+}+M^{4+}$) or M^{3+} component of the ($M^{2+}+M^{3+}$) dimer geometry.

However, the ⑦ (b_7^{1+} , b_{11}^{1+} , and b_{12}^{1+}) ion signals are attributable to the fragments resulting from the dissociation of the M^{3+} monomer component of the ($M^{2+}+M^{3+}$) dimer geometry. The (b_7^{1+} , b_{11}^{1+} , and b_{12}^{1+}) fragment ion signals were not observed in the MS/MS spectrum for M^{4+} (Figure 3b). The two proposed D^{3+} structures (Schemes 1a and 1b) are still applicable to the D^{5+} structures with different combinations of ($M^{1+}+M^{4+}$) or ($M^{2+}+M^{3+}$) dimer geometries. Judging from the similar intensities of the signals in ④ and ⑤ patterns, no geometric preference for either ($M^{1+}+M^{4+}$) or ($M^{2+}+M^{3+}$) configurations was indicated.

Conclusion

CID-MS/MS experiments were conducted to obtain structural information regarding of the A β 16 dimer complex. The D^{3+} complex is composed of two subunits, M^{1+} and M^{2+} . The Scheme 1a geometry of D^{3+} complex was expected to be more favorable than the Scheme 1b geometry. The b and y fragment ions attached to the monomer, ($M+b_{10-15}$) $^{2+}$ and ($M+y_{9-15}$) $^{2+}$, were believed to originate from the dissociation of the M^{2+} monomer component of the ($M^{1+}+M^{2+}$) dimer geometry. Intricate fragmentation patterns were observed in the MS/MS spectrum of the D^{5+} complexes. The complicated nature of the MS/MS spectrum is attributable to the coexistence of two D^{5+} configurations, ($M^{1+}+M^{4+}$) and ($M^{2+}+M^{3+}$), in the A β 16 solution.

Acknowledgments

This study was supported by the Research Fund of the Kumoh National Institute of Technology (202002270001).

Notes and references

Electronic Supplementary Information is available: [Details of any available supplementary information should be included here]. See DOI: xx.xxxx/xxxxx./

References

- Chiti, F.; Dobson, C. M. *Annu. Rev. Biochem.* **2006**, *75*, 333. DOI: 10.1146/annurev.biochem.75.101304.123901

2. Shankar, G. M.; Walsh, D. M. *Mol. Neurodegener.* **2009**, 4, 48. DOI:10.1186/1750-1326-4-48
3. Selkoe, D. J. *Physiol Rev.* **2001**, 81, 741. DOI: 10.1152/physrev.2001.81.2.741
4. Brunden, K. R.; Trojanowski, J. Q.; Lee, V. M.-Y. *Nat. Rev. Drug Discov.* **2009**, 8, 783. DOI: 10.1038/nrd2959.
5. Kirkitadze, M. D.; Bitan, G.; Teplow, D. B. *J. Neurosci. Res.* **2002**, 69, 567. DOI: 10.1002/jnr.10328
6. Klein, W. L.; Stine, W. B.; Teplow, D. B. *Neurobiol. Aging* **2004**, 25, 569. DOI: 10.1016/j.neurobiolaging.2004.02.010
7. Haass, C.; Selkoe, D. J. *Nat. Rev. Mol. Cell Biol.* **2007**, 8, 101. DOI: 10.1038/nrm2101
8. Sengupta, U.; Nilson, A. N.; Kaye, R. *EBioMedicine* **2016**, 6, 42. <http://dx.doi.org/10.1016/j.ebiom.2016.03.035>
9. Benilova, I.; Karran, E.; De Strooper, B. *Nat. Neurosci.* **2012**, 15, 349. DOI: 10.1038/nn.3028
10. Pujol-Pina, R.; Vilaprinyó-Pascual, S.; Mazzucato, R.; Arcella, A.; Vilaseca, M.; Orozco, M.; Carulla, N. *Scientific Reports* **2015**, 5, 14809. DOI: 10.1038/srep14809
11. Bernstein, S. L.; Dupuis, N. F.; Lazo, N. D.; Wyttenbach, T.; Condrón, M. M.; Bitan, G.; Teplow, D. B.; Shea, J.-E.; Ruotolo, B. T.; Robinson, C. V.; Bowers, M. T. *Nat. Chem.* **2009**, 1, 326. DOI: 10.1038/nchem.247
12. Kirkitadze, M. D.; Condrón, M. M.; Teplow, D. B. *J. Mol. Biol.* **2001**, 312, 1103. DOI: 10.1006/jmbi.2001.4970
13. Ono, K.; Condrón, M. M.; Teplow, D. B. *Proc. Natl. Acad. Sci. U.S.A.* **2009**, 106, 14745. DOI: 10.1073/pnas.0905127106
14. Petkova, A. T.; Yau, W.-M.; Tycko, R. *Biochemistry* **2006**, 45, 498. DOI: 10.1021/bi051952q
15. Paravastu, A. K.; Leapman, R. D.; Yau, W.-M.; Tycko, R. *Proc. Natl. Acad. Sci.* **2008**, 105, 18349. DOI: 10.1073/pnas.0806270105
16. Chong, S.-H.; Ham, S. *Phys. Chem. Chem. Phys.* **2012**, 14, 1573. DOI: 10.1039/c2cp23326f
17. Zhang, T.; Zhang, J.; Derreumaux, P.; Mu, Y. *J. Phys. Chem. B* **2013**, 117, 3993. DOI: 10.1021/jp312573y
18. Das, P.; Chacko, A. R.; Belfort, G. *ACS Chem. Neurosci.* **2017**, 8, 606. DOI: 10.1021/acscchemneuro.6b00357
19. Barz, B.; Liao, Q.; Strodel, B. *J. Am. Chem. Soc.* **2018**, 140, 319. DOI: 10.1021/jacs.7b10343
20. Zou, Y.; Qian, Z.; Chen, Y.; Qian H.; Wei, G.; Zhang, Q. *ACS Chem. Neurosci.* **2019**, 10, 1585. DOI: 10.1021/acscchemneuro.8b00537
21. Reinke, A. A.; Ung, P. M.; Quintero, J. J.; Carlson, H. A. & Gestwicki, J. E. *J. Am. Chem. Soc.* **2010**, 132, 17655. DOI: 10.1021/ja106291e
22. Ahmed, M.; Davis, J.; Aucoin, D.; Sato, T.; Ahuja, S.; Aimoto, S.; Elliott, J. I.; Van Nostrand, W. E.; Smith, S. O. *Nat. Struct. Mol. Biol.* **2010**, 17, 561. DOI: 10.1038/nsmbl.1799
23. Haupt, C.; Leppert, J.; Rçnicke, R.; Meinhardt, J.; Yadav, J. K. *Angew. Chem. Int. Ed. Engl.* **2012**, 51, 1576. DOI: 10.1002/anie.201105638
24. Castelletto, V.; Ryumin, P.; Cramer, R.; Hamley, I. W.; Taylor, M.; Allsop, D.; Reza, M.; Ruokolainen, J.; Arnold, T.; Hermida-Merino, D.; Garcia, C. I.; Leal, M. C.; Castaño, E. *Scientific Reports* **2017**, 7, 43637. DOI: 10.1038/srep43637
25. Berhanu, W. M.; Masunov, A. E. *J. Mol. Model* **2011**, 17, 2423. DOI: 10.1007/s00894-010-0912-4
26. M. Shabestari, M.; Plug, T.; Motazacker, M. M.; Meeuwenoord, N. J.; Filippov, D. V.; Meijers, J. C. M.; Huber, M. *Appl. Magn. Reson.* **2013**, 44, 1167. DOI: 10.1007/s00723-013-0469-3
27. Kuhn, A. J.; Abrams, B. S.; Knowlton, S.; Raskatov, J. A. *ACS Chem. Neurosci.* **2020**, 11, 1539. DOI: 10.1021/acscchemneuro.0c00160
28. Jiang, D.; Men, L.; Wang, J.; Zhang, Y.; Chickenyen, S.; Wang, Y.; Zhou, F. *Biochemistry* **2007**, 46, 9270. DOI: 10.1021/bi700508n
29. A. Awasthi, A.; Matsunaga, Y.; Yamada, T. *Exp. Neurol.* **2005**, 196, 282. DOI: 10.1016/j.expneurol.2005.08.001
30. Y. Matsunaga, Y.; Fujii, A.; Awasthi, A.; Yokotani, J.; Takakura, T.; Yamada, T.; *Regul. Pept.* **2004**, 120, 227. DOI: 10.1016/j.regpep.2004.03.013
31. Liao, M.Q.; Tzeng, Y.J.; Chang, L.Y.; Huang, H.B.; Lin, T.H.; Chyan, C.L.; Chen, Y.C. *FEBS Lett.* **2007**, 581, 1161. DOI: 10.1016/j.febslet.2007.02.026
32. Liu, R.; McAllister, C.; Lyubchenko, Y.; Sierks, M.R. *J. Neurosci. Res.* **2004**, 75, 162.
33. Du, X.T.; Wang, L.; Wang, Y.J.; Andreasen, M.; Zhan, D.W.; Feng, Y.; Li, M.; Zhao, M.; Otzen, D.; Xue, D.; Yang, Y.; Liu, R.T. *J. Alzheimer's Dis.* **2011**, 27, 401. DOI: 10.3233/JAD-2011-110476
34. Furlan, S.; Hureau, C.; Faller, P.; La Penna, G. *J Phys Chem B* **2010**, 114, 15119. DOI: 10.1021/jp102928h
35. Istrate, A. N.; Kozin, S. A.; Zhokhov, S. S.; Mantsyzov, A. B.; Kechko, O. I.; Pastore, A.; Makarov, A. A.; Polshakov, V. I. *Scientific Reports* **2016**, 6, 21734. DOI: 10.1038/srep21734
36. Zirah, S.; Rebuffat, S.; Kozin, S. A.; Debey, P.; Fournier, F.; Lesage, D.; Tabet, J.-C. *Int. J. Mass Spectrom.* **2003**, 228, 999. DOI: 10.1016/S1387-3806(03)00221-5
37. Ma, Q.-F.; Hu, J.; Wu, W.-H.; Liu, H.-D.; Du, J.-T.; Fu, Y.; Wu, Y.-W.; Lei, P.; Zhao, Y.-F.; Li, Y.-M. *Biopolymers*, **2006**, 83, 20. DOI: 10.1002/bip.20523
38. Li, J.; Lyu, W.; Rossetti, G.; Konijnenberg, A.; Natalello, A.; Ippoliti, E.; Orozco, M.; Sobott, F.; Grandori, R.; Carloni, P. *J. Phys. Chem. Lett.* **2017**, 8, 1105. DOI: 10.1021/acs.jpcclett.7b00127

Comparative Sample Preparation Methods for a Label-Free Proteomic Analysis

Thy N. C. Nguyen^{1†}, Jung Hyun Lee², Nayeon Kim³, Jae Rim Choi⁴, Hung M. Vu¹, and Min-Sik Kim^{1,5,6*}

¹Department of New Biology, DGIST, Daegu, 42988, Republic of Korea

²Department of Life Sciences, Kyungpook National University, Daegu, 41566, Republic of Korea

³Department of Biological Engineering, Konkuk University, Seoul, 05029, Republic of Korea

⁴Department of Biomedical Sciences, Dong-A University, Busan, 602760 Republic of Korea

⁵New Biology Research Center, DGIST, Daegu, 42988, Republic of Korea

⁶Center for Cell Fate Reprogramming and Control, DGIST, Daegu, 42988, Republic of Korea

Received December 2, 2022; Revised December 28, 2022; Accepted December 29, 2022

First published on the web December 31, 2022; DOI: 10.5478/MSL.2022.13.4.184

Mass spectrometry (MS) is the cutting-edge platform that propels biological and clinical research. MS-based bottom-up proteomics has expedited the characterization of signal transductions and aberrant proteomes of disease specimens through protein identification, protein-protein interaction discovery, and post-translational dynamics profiling. The typical pipeline of the bottom-up strategy for MS involves protein digestion prerequisite to peptide separation by liquid chromatography and data acquisition on a mass spectrometer.¹ The refinement of the sample processing is critical to fulfilling the quest for augmenting proteome coverage, robustness, and throughput, alongside the quantum leap of the instrument and computational analysis.

Enzymatic digestion of proteomes into peptides is a hallmark of bottom-up proteomics, influencing the quality of protein identification and quantitation. To deduce the optimal condition for protease activity, many studies have been conducted using different lysis reagents and buffers.²⁻⁵ The conventional in-solution digestion method using urea is the most feasible and cost-effective. Urea is a chaotropic denaturant that can disrupt intraprotein interactions, resulting in protein unfolding to facilitate trypsin accessibility. As a hydrophilic compound, urea can be

removed by reversed-phase liquid chromatography (RP-HPLC), hence its compatibility with mass spectrometry. However, carbamylation modification on proteins and peptides' amines caused by urea under heat hinders digestion sites.^{6,7} Sodium dodecyl sulfate (SDS) is an alternative to urea with more efficient solubilization of membrane proteins, but it can damage the RP-HPLC. Evidence and concerns were also raised regarding the ion suppression and poor spectra in electrospray ionization mass spectrometry, which resulted from residual SDS exceeding 0.01%.^{8,9} To resolve this, filter-aided sample preparation (FASP) was established to remove the ionic detergent by centrifugation and retain proteins above the molecular weight cut-off.^{3,5} Another imperative method is the in-gel digestion approach that utilizes size-based separation assisted by negatively charged protein-SDS complexes. Not only does it dissipate SDS during electrophoresis, but it also enhances the depth of proteome characterization by reducing sample complexity.^{10,11}

DataOn is a web-based resource established by Korea Institute of Science and Technology Information to improve re-analysis of registered data. In this protocol, we exemplified in-gel, in-solution and FASP digestion strategies. The demonstration videos entitled "Comparative sample preparation methods for label-free proteomic analysis (videos)" can be accessed at: <https://doi.org/10.22711/idr/966>, and through Supplementary Materials.

Open Access

*Reprint requests to Min-Sik Kim

<https://orcid.org/0000-0001-7317-5360>

E-mail: mkim@dgist.ac.kr

All the content in Mass Spectrometry Letters (MSL) is Open Access, meaning it is accessible online to everyone, without fee and authors' permission. All MSL content is published and distributed under the terms of the Creative Commons Attribution License (<http://creativecommons.org/licenses/by/3.0/>). Under this license, authors reserve the copyright for their content; however, they permit anyone to unrestrictedly use, distribute, and reproduce the content in any medium as far as the original authors and source are cited. For any reuse, redistribution, or reproduction of a work, users must clarify the license terms under which the work was produced.

Procedure

Cell lysis

Reagents

- Sodium dodecyl sulfate (SDS, Sigma)
- UltraPure™ Tris (Invitrogen)
- Hydrochloric acid (Sigma-Aldrich)
- Urea (ThermoScientific)
- HPLC water (J.T.Baker, ThermoScientific)

Reagent setup

Stock solution:

- √ 20% SDS (w/v) in HPLC water. Can be stored at room temperature for up to 1 year.
- *SDS is flammable, irritative to skin and eyes, and harmful if swallowed or inhaled. Handle with care and avoid inhalation.
- √ 1 M Tris in HPLC water and bring to pH 8.0 by adding HCl. Can be stored at room temperature for up to 1 year.
- *Hydrochloric acid is volatile and corrosive. It causes skin burns, eye damage, and respiratory irritation. Open the bottle in a fume hood or a well-ventilated area.

Working solution:

- √ 4% SDS (v/v) in 50 mM Tris-HCl (pH 8.0) and HPLC water.
- √ 8 M Urea in 50 mM Tris-HCl (pH 8.0) and HPLC water.

Apparatus

- Sonic dismembrator (Fisher Scientific)
 - Micro centrifuge (Smart R17 Plus, Hanil)
 - Eppendorf ThermoMixer C (Eppendorf)
 - HyperVAC speed vacuum (Gyrozen)
1. Wash adherent cells with 5 mL cold PBS before harvesting.
 2. Centrifuge cells at $1500 \times g$ for 5 minutes at 4°C . Remove the supernatant.
 3. Lyse approximately 1×10^5 to 10^6 cells in the presence of 200 μL 8 M urea, 50 mM Tris-HCl (pH 8.0) for in-solution digestion or 200 μL of 4% SDS, 50 mM Tris-HCl (pH 8.0) for in-gel and FASP digestion methods.
 4. Apply probe sonication with 10 seconds interval and 10% power to reduce the viscosity.
 5. Cool the samples on ice for 5 seconds.
 6. Repeat step 4 & 5 for three times.
 7. Heat samples at 95°C for 5 minutes.
*Note: Digestion with urea should not be boiled to prevent carbamylation of proteins.
 8. Centrifuge samples at $14\ 000 \times g$ for 15 minutes to collect proteins in the supernatant.
*Note: Samples can be stored at -80°C for the future process but freeze-thaw cycles should be avoided.

In-solution digestion

Reagents

- Dithiothreitol (DTT, Sigma)
- Iodoacetamide (IAA, Sigma)
- HPLC water (J.T.Baker, Thermo Scientific)
- Trifluoroacetic acid (TFA, Sigma-Aldrich)

- Ammonium bicarbonate (ABC, Sigma-Aldrich)
- PierceTM Trypsin protease, MS-grade (Thermo Scientific)

Reagent setup

Stock solution:

- √ 1 M DTT in HPLC water. Can be stored at -20°C for 1 year
- √ Prepare 10% TFA (v/v) by diluting with HPLC water in a Duran bottle. Can be stored at room temperature for up to 1 month.
- *TFA is volatile and corrosive. It causes skin burns, eye damage, and respiratory irritation. Open the bottle in a fume hood or a well-ventilated area.

Working solution:

- √ Prepare 100 mM DTT by diluting stock DTT in HPLC water.
- *DTT is susceptible to oxidation. Prepare freshly before use.
- √ Dissolve IAA in HPLC water to a final concentration of 200 mM.
- *IAA is unstable and light-sensitive. Prepare freshly before use and perform experiments in the dark.
- √ Prepare 50 mM ABC buffer (pH 7.8) by dissolving ABC in HPLC water.
- √ Reconstitute 20 μg of trypsin with 100 μL of 50 mM ABC (pH 7.8) to obtain a final concentration of 0.2 $\mu\text{g}/\mu\text{L}$.

Apparatus

- Eppendorf ThermoMixer C (Eppendorf)
1. Reduce the disulfide bonds of proteins with 22 μL of 100 mM DTT to a final concentration of 10 mM at 56°C for 30 minutes.
 2. Alkylate the sulfhydryl functional groups of proteins with 25 μL of 200 mM IAA to a final concentration of 20 mM. Cover samples in foil and incubate at room temperature for 30 minutes.
 3. Dilute samples with 2 mL of 50 mM ABC to decrease the urea concentration below 1 M.
 4. Incubate samples overnight at 37°C with sequencing-grade trypsin with 1:50 of an enzyme-to-protein ratio.
 5. Acidify samples with 20 μL of 10% TFA to quench trypsin activity.

FASP

Reagents

- Urea (Thermo Scientific)
- Triethylammonium bicarbonate buffer (TEAB, Merck)
- Dithiothreitol (DTT, Sigma)
- Iodoacetamide (IAA, Sigma)
- Trifluoroacetic acid (TFA, Sigma-Aldrich)
- HPLC water (J.T.Baker, Thermo Scientific)
- PierceTM Trypsin protease, MS-grade (Thermo Scientific)

Reagent setup

Stock solution:

- ✓ 1 M DTT in HPLC water. Can be stored at -20°C for 1 year.
- ✓ Prepare 10% TFA (v/v) by diluting with HPLC water in a Duran bottle. Can be stored at room temperature for up to 1 month.
*TFA is volatile and corrosive. It causes skin burns, eye damage, and respiratory irritation. Open the bottle in fume hood or in a well-ventilated area.

Working solution:

- ✓ Make 50 mM TEAB (v/v) (pH 8.0) in HPLC water.
- ✓ Prepare 8 M urea in 50 mM TEAB (pH 8.0) with HPLC water.
*Urea reaction with water is endothermic. However, increasing temperature decomposes urea to ammonia and isocyanic acid, so the reaction should be kept at room temperature. Urea crystal might be hard to be solubilized, mix vigorously by a magnetic stirrer if needed.
- ✓ Prepare 100 mM DTT by diluting stock DTT in HPLC water.
*DTT is susceptible to oxidation. Prepare freshly before use.
- ✓ Dissolve IAA in HPLC water to a final concentration of 200 mM (w/v).
*IAA is unstable and light-sensitive. Prepare freshly before use and perform the experiment in the dark.
- ✓ Reconstitute 20 µg of trypsin with 100 µL of 50 mM TEAB (pH 8.0) to obtain a final concentration of 0.2 µg/µL.

Apparatus

- 3kDa Amicon Ultra-0.5 centrifugal filter unit (Millipore, Merck)
- Micro centrifuge (Smart R17 Plus, Hanil)
- Eppendorf ThermoMixer C (Eppendorf)

1. Follow step 1 and 2 as in the in-solution digestion method.
2. Dilute samples with 8 mL of 8 M urea to decrease the concentration of SDS from 4% to less than 0.1%.
3. Transfer 300 µL of samples to a 3k-Da filter and centrifuge for 15 minutes at 14,000 × g. Discard the flow-through.
*Note: 15 mL Amicon filter can be used to accelerate the process.
4. Repeat step 3 until the remaining volume is finished.
5. Centrifuge the sample-containing filter with 200 µL of 8 M urea in 50 mM TEAB (pH 8.0) at 14,000 × g for 15 minutes.
6. Repeat step 5 for three times.
7. Exchange 8 M urea in 50 mM TEAB (pH 8.0) with 200 µL of 50 mM TEAB at 14 000 xg centrifugation

for 15 minutes.

8. Repeat step 7 for three times.
*Note: Approximately 100 µl of the sample will remain in the filter after centrifugation.
9. Recover the samples by placing the filter upside down in the collection tube and centrifuge at 1000 xg for 2 minutes.
10. Incubate samples overnight at 37°C with sequencing-grade trypsin (1:50 enzyme-to-protein ratio).
11. Acidify samples with 20 µL of 10% TFA to quench trypsin activity.

In-gel digestion

Reagents

- Ammonium bicarbonate (Sigma-Aldrich)
- Acetonitrile (ACN, J.T.Baker, Thermo Scientific)
- Dithiothreitol (Sigma)
- Iodoacetamide (IAA, Sigma)
- Pierce™ Trypsin protease, MS-grade (Thermo Scientific)
- SimplyBlue™ SafeStain (Invitrogen)

Reagent setup

Stock solution:

- ✓ 1 M DTT in HPLC water. Can be stored at -20°C for 1 year.
- ✓ 1 M ABC (pH 7.8) (w/v) in HPLC water. Can be stored at room temperature for up to 1 year.

Working solution:

- ✓ Prepare 50 mM ABC buffer (pH 7.8) by diluting stock 1 M ABC in HPLC water.
- ✓ Prepare the destaining buffer with the final concentration of 10 mM DTT and 50 mM ABC in 40% acetonitrile.
*DTT is susceptible to oxidation. Prepare freshly before use.
- ✓ Dissolve IAA in HPLC water to a final concentration of 200 mM. Further, dilute it 10-fold to obtain a final concentration of 20 mM.
*IAA is unstable and light-sensitive. Prepare freshly before use and perform the experiment in the dark.
- ✓ Reconstitute 20 µg of trypsin with 2mL of 50 mM ABC (pH 7.8) to obtain a final concentration of 0.01 µg/µL.
- ✓ Make harvest buffer containing 40% acetonitrile (v/v) and 0.1% formic acid (v/v) in HPLC water.

Apparatus

- Gel cutter (SPL Life Science)
 - Micro centrifuge (Smart R17 Plus, Hanil)
 - Eppendorf ThermoMixer C (Eppendorf)
1. After electrophoresis, stain the gel with SimplyBlue™ SafeStain solution according to manufacturer's protocol.

2. Excise the band of interest by an extraction tool and transfer it into a 1.5mL Eppendorf tube.
3. Dice the gel bands into smaller cubes with a pipette tip (approximately 1 mm³)
4. Cover the gel with 300 μ L of DTT-containing destaining buffer.
5. Shake the gel-filled tube at 900 rpm at room temperature for 10 minutes.
6. Remove the destaining solution and repeat steps 4 & 5 until there is no visible blue stain.
7. Fill the tube with 300 μ L of 20 mM IAA solution at room temperature for 30 minutes, then remove the excess solution.
8. Add 200 μ L of 100% acetonitrile to dehydrate the gel and change the buffer every 5 minutes until the gel pieces are rigid.
9. Remove acetonitrile and evaporate the remaining solution in the samples by speed vac.
10. Incubate sample with 100 μ L of 50 mM ABC buffer containing 1 μ g trypsin on ice until the white gel pieces become transparent.
11. Remove the excess trypsin, add the ABC buffer just cover gel pieces and incubate at 37°C overnight.
12. Transfer the ABC inside the gel-filled tube to a new 1.5 mL Eppendorf tube.
13. Add 200 μ L of harvest buffer into the gel tube and shake at 900rpm for 20 minutes.
14. Collecting the solution into the 1.5 mL tube of the previous step 12.
15. Repeat steps 13 and 14 for two more times.
16. Dry the collected peptide solution in the speed vac at 4°C overnight.

Discussion

Taken together, our protocol amalgamates the popular approaches for MS-based bottom-up proteomics, enabling their further application and evaluation to elucidate biological and pathophysiological questions. There is no universal protein preparation method for bottom-up proteomic research, albeit it is arguably the most critical process. Previously, we employed the complementary protein fractionation by SDS-PAGE and peptide fractionation by reversed-phase liquid chromatography to delineate a draft map of the human proteome, substantiating it as a powerful routine to reduce proteome's complexity.¹⁰ Of note, the inevitable pitfall of this method entails massive keratin contamination, incomplete peptide recovery, and incompatibility for high-throughput investigation.^{11,12} The alternative strategy, FASP, is touted to be conceptually promising for removing interfering chemicals by utilizing a spin filter and centrifugation. However, its inherent advantages are weighed down by sample loss and incomplete SDS elimination.^{2,5} We successfully applied the in-solution digestion method for identifying albumin modifications in

human serum and FASP for profiling the proteome of the autism spectrum disorder mice.^{13,14} In addition, buffers in this protocol (ABC, TEAB, and Tris-HCl) can be used interchangeably depending on the experimental goals. Thus far, the decision for the optimal approach is subject to the samples' nature and the ultimate purposes of the investigation.

Acknowledgments

This work was supported by the National Research Foundation of Korea (NRF) grant funded by the Ministry of Science, ICT & Future Planning (grant No. NRF-2022R1A2C2013377 and DGIST R&D program [22-CoE-BT-04]).

Supporting information

Supplementary Information is available at https://drive.google.com/file/d/1ELX6Rcg9UvBPzcvBNZiZtCNS2ppl-iCL/view?usp=share_link

References

1. Aebersold, R.; Mann, M. *Nature* **2003**, 422, 198. DOI: 10.1038/nature01511.
2. Erde, J.; Loo, R.R.; Loo, J.A. *J Proteome Res* **2014**, 13, 1885. DOI: 10.1021/pr4010019.
3. Manza, L.L.; Stamer, S.L.; Ham, A.J.; Codreanu, S.G.; Liebler, D.C. *Proteomics* **2005**, 5, 1742. DOI: 10.1002/pmic.200401063.
4. Weston, L.A.; Bauer, K.M.; Hummon, A.B. *Anal Methods* **2013**, 5. DOI: 10.1039/C3AY40853A.
5. Wisniewski, J.R.; Zougman, A.; Nagaraj, N.; Mann, M. *Nat Methods* **2009**, 6, 359. DOI: 10.1038/nmeth.1322.
6. Chen, E.I.; Cociorva, D.; Norris, J.L.; Yates, J.R., 3rd. *J Proteome Res* **2007**, 6, 2529. DOI: 10.1021/pr060682a.
7. Gordon, J.A.; Jencks, W.P. *Biochemistry* **1963**, 2, 47. DOI: 10.1021/bi00901a011.
8. Botelho, D.; Wall, M.J.; Vieira, D.B.; Fitzsimmons, S.; Liu, F.; Doucette, A. *J Proteome Res* **2010**, 9, 2863. DOI: 10.1021/pr900949p.
9. Ikonou, M.G.; Blades, A.T.; Kebarle, P. *Analytical Chemistry* **1990**, 62, 957. DOI: 10.1021/ac00208a012.
10. Kim, M.S.; Pinto, S.M.; Getnet, D.; Nirujogi, R.S.; Manda, S.S.; Chaerkady, R.; Madugundu, A.K.; Kelkar, D.S.; Isserlin, R.; Jain, S.; Thomas, J.K.; Muthusamy, B.; Leal-Rojas, P.; Kumar, P.; Sahasrabudhe, N.A.; Balakrishnan, L.; Advani, J.; George, B.; Renuse, S.; Selvan, L.D.; Patil, A.H.; Nanjappa, V.; Radhakrishnan, A.; Prasad, S.; Subbannayya, T.; Raju, R.; Kumar, M.; Sreenivasamurthy, S.K.; Marimuthu, A.; Sathe, G.J.; Chavan, S.; Datta, K.K.; Subbannayya, Y.; Sahu, A.; Yelamanchi, S.D.; Jayaram, S.; Rajagopalan, P.; Sharma, J.; Murthy, K.R.; Syed, N.; Goel, R.; Khan, A.A.; Ahmad,

- S.; Dey, G.; Mudgal, K.; Chatterjee, A.; Huang, T.C.; Zhong, J.; Wu, X.; Shaw, P.G.; Freed, D.; Zahari, M.S.; Mukherjee, K.K.; Shankar, S.; Mahadevan, A.; Lam, H.; Mitchell, C.J.; Shankar, S.K.; Satishchandra, P.; Schroeder, J.T.; Sirdeshmukh, R.; Maitra, A.; Leach, S.D.; Drake, C.G.; Halushka, M.K.; Prasad, T.S.; Hruban, R.H.; Kerr, C.L.; Bader, G.D.; Iacobuzio-Donahue, C.A.; Gowda, H.; Pandey, A. *Nature* **2014**, 509, 575. DOI: 10.1038/nature13302.
11. Shevchenko, A.; Tomas, H.; Havlis, J.; Olsen, J.V.; Mann, M. *Nat Protoc* **2006**, 1, 2856. DOI: 10.1038/nprot.2006.468.
12. Ruelcke, J.E.; Loo, D.; Hill, M.M. *J Proteomics* **2016**, 149, 3. DOI: 10.1016/j.jprot.2016.03.025.
13. Jang, W.E.; Park, J.H.; Park, G.; Bang, G.; Na, C.H.; Kim, J.Y.; Kim, K.-Y.; Kim, K.P.; Shin, C.Y.; An, J.-Y.; Lee, Y.-S.; Kim, M.-S. *Molecular Psychiatry* **2022**. DOI: 10.1038/s41380-022-01822-1.
14. Lee, J.H.; Jang, W.E.; Park, J.H.; Mohammad, H.B.; Lee, J.-Y.; Jeong, W.-H.; Kim, M.-S. **2022**, 43, 444. DOI: 10.1002/bkcs.12478.

Author Guidelines

Aims and Scope

Mass Spectrometry Letters publishes brief letters (maximum length of 4 pages), technical notes, articles, reviews, and tutorials on fundamental research and applications in all areas of mass spectrometry. The manuscripts can be either invited by the editors or submitted directly by authors to the journal editors. Mass Spectrometry Letters topical sections are diverse, covering ion chemistry in a broad sense; gas-phase thermodynamics or kinetics; theory and calculations related with mass spectrometry or ions in vacuum; ion-optics; analytical aspects of mass spectrometry; instrumentations; methodology developments; ionization methods; proteomics and its related research; metabolomics and its related research; bioinformatics; software developments; database development; biological research using mass spectrometry; pharmaceutical research by mass spectrometry; food sciences using mass spectrometry; forensic results using mass spectrometry; environmental mass spectrometry; inorganic mass spectrometry; chromatography-mass spectrometry; tandem mass spectrometry; small molecule research using mass spectrometry; TOF-SIMS, etc. The scope of Mass Spectrometry Letters is not limited to the above-mentioned areas, but includes ever-expanding areas related directly or indirectly to mass spectrometry. Criteria for publication are originality, urgency, and reportable values. Short preliminary or proof-of-concept results, which will be further detailed by the following submission to other journals, are recommended for submission.

The publication frequency

Mass Spectrometry Letters will be published at least four times a year; 31st March, 30th June, 30th September, 31st December every year are the scheduled publishing dates. The publication frequency is subjected to future change, which should be advised by the Editorial board meeting's decisions.

The publication charge

All the papers will be published for free without any payment of page charge or article processing charge and the access to the papers in Mass Spectrometry Letters is also free to the public in general through the homepage

of the journal. The publication cost will be covered by the Korean Society for Mass Spectrometry. The printed journal issue will be provided to the Korean Society for Mass Spectrometry members who have completed the annual membership fee payment.

The copyright

All MS Letters content is Open Access, meaning it is accessible online to everyone, without fee and authors' permission. All MS Letters content is published and distributed under the terms of the Creative Commons Attribution License ([Http://creativecommons.org/licenses/by/3.0/](http://creativecommons.org/licenses/by/3.0/)). Under this license, authors reserve the copyright for their content; however, they permit anyone to unrestrictedly use, distribute, and reproduce the content in any medium as far as the original authors and source are cited. For any reuse, redistribution, or reproduction of a work, users must clarify the license terms under which the work was produced.

Referee Reviews

Submitted manuscripts are subjected to review by at least 2 referees selected by the editors. The authors can recommend preferred potential reviewers with the names and e-mail addresses. Note that the editor retains the sole right to decide whether or not the suggested reviewers are used.

Conflict of interest

All authors are requested to disclose any actual or potential conflict of interest including any financial, personal or other relationships with other people or organizations within three years of beginning the submitted work that could inappropriately influence, or be perceived to influence, their work.

Submission declaration and verification

Submission of an article implies that the work described has not been published previously (except in the form of an abstract or as part of a published lecture or academic thesis), that it is not under consideration for publication elsewhere, that its publication is approved by all authors and tacitly or explicitly by the responsible

authorities where the work was carried out, and that, if accepted, it will not be published elsewhere in the same form, in English or in any other language, including electronically without the written consent of the copyright-holder. To verify originality, your article may be checked by the originality detection software.

Research/publication ethics and research/publication malpractice statement

For the policies on the research and publication ethics not stated in these instructions, international standards for editors and authors (<http://publicationethics.org/international-standards-editors-and-authors>) can be applied.

Language and language services

The manuscript should be prepared in good English (American or British usage is accepted, but not a mixture of these). English language proof-reading service is recommended before publication.

Submission

Submission to this journal proceeds totally online and you will be guided stepwise through the creation and uploading of your files.

Manuscript Types

Mass Spectrometry Letters publishes several types of articles: letter, technical note, article, review, and tutorial.

- **Review.** A comprehensive overview on a topic in mass spectrometry. There is no restriction in length.
- **Article.** A full-length article presenting important new research results. The length of the articles should not exceed ten printed pages.
- **Technical note.** A short description of a novel apparatus of technique. The length of technical notes should not exceed three printed pages.
- **Letter.** A short report on any subject in mass spectrometry, requiring urgency, timeliness, and scientific significance. The length of letters should not exceed four printed pages.
- **Tutorial.** A tutorial is an educational exposition covering recent trends and basic knowledge in mass spectrometry. There is no restriction in length

All manuscripts for publication in Mass Spectrometry Letters, except review and tutorial, should include Title, Authors, Abstract, Introduction, Experimental section, Results and Discussion, Conclusions, Acknowledgments, and References.

Preparation of Manuscripts

All the manuscripts for publication in Mass Spectrometry Letters should be prepared in English. Authors are strongly recommended to use the manuscript template (Manuscript Template) provided from the Mass Spectrometry Letters website.

1) Manuscript type

The type of a manuscript should be specified in the cover letter.

2) Title

The title should be concise and informative. Authors are strongly recommended to limit the title to 250 letters including space, and to avoid abbreviations and formulae wherever possible. A short running title consisting of less than 70 letters including space should be provided by authors.

3) Authors

List full names of all authors (given names first and surnames last) followed by the authors' affiliations and addresses where the actual work was carried out. Superscript numbers are labeled after the authors' names and in front of the appropriate affiliations. Specify current addresses, if necessary, as footnotes. Provide the full postal address of each affiliation including the country name. Corresponding author(s) should be indicated with asterisk symbols. The email address(es) of corresponding author(s) are additionally required in the manuscript.

4) Abstract

The abstract should not exceed 250 words. It should be a single paragraph which summarizes the content of the article.

5) Introduction

The introduction should state the purpose and the backgrounds of the work. It may include appropriate citations of previous works with brief summaries. Do not include or summarize current findings in this section.

6) Experimental section

Authors should provide details on experimental procedures including the model names, the manufactures of instruments, and reagents, so that the works are reproducible elsewhere by readers.

7) Results and discussion

Authors should provide the results of the work with clear and concise manners. Authors should discuss the significance of observations, measurements, or computations.

8) Conclusion

A brief summary should be provided in conclusions.

9) Acknowledgements

Provide a list of financial supports and individuals whom to be acknowledged.

10) References

Literatures to be cited should be numbered by order of appearance in the manuscript. The corresponding texts should be indicated with superscripted Arabic numbers (e.g., 1). The reference format must follow the examples provided below. Unpublished results are not allowed in the reference list with an exception of the literatures accepted for publication as “in press”.

<Journals>

Hong, E. S.; Yoon, H.-J.; Kim, B.; Yim, Y.-H.; So, H.-Y.; Shin, S. K. *J. Am. Soc. Mass Spectrom.* **2010**, 21, 1245, DOI: 10.1016/j.jasms.2010.03.035

<Books>

Bunker, P. R.; Jensen, P. *Molecular Symmetry and Spectroscopy*, 2nd ed.. NRC Research Press: Ottawa, 1998.

Zare, R. N. *Angular Momentum*, Wiley: New York, 1998.

<Software>

Werner, H. J.; Knowles, P. J.; Lindh, R.; Manby, F. R.; Schutz, M. MOLPRO, version 2006. 1., A package of ab initio Programs; See <http://www.molpro.net>.

<Proceedings>

Bensaude-Vincent, B. *The New Identity of Chemistry as Biomimetic and Nanoscience*; 6th International Conference on the History of Chemistry, Leuven (Belgium), August 28 - September 1, 2007, p 53.

11) Equations and math formulae

Equations and math formulae should be prepared by Microsoft Equation 3.0 (or a later version). All the equations and math formulae should be numbered by order of appearance in the manuscript with Arabic numbers.

12) Tables

Tables should be numbered by order of appearance in the manuscript with Arabic numbers. Each table should have a brief title. Footnotes may be placed, if necessary, to supplement the tables. Avoid vertical rules. The size of table should fit the MSL's page (16.5 cm × 22.5 cm).

13) Figures

Figures should be numbered by order of appearance in the manuscript with Arabic numbers. Each figure should have a brief title followed by a brief description, which consists of one or two sentences. Sub-numbering is possible with lowercase alphabets (e.g., a, b, etc.), if necessary. The resolution of a figure should be better than 600 dpi. JPEG (jpg, Joint Photographic Expert Group) format is recommended.

14) Units

SI units rather than conventional units should be used for reporting measures. Information regarding on SI units can be found at <https://www.nist.gov/pml/weights-and-measures/metric-si/si-units>.

